ISAS - INTERNATIONAL SCHOOL
FOR ADVANCED STUDIES

A STUDY OF INHOMOGENEITIES

IN COSMOLOGICAL MODELS WITH DARK MATTER

THROUGH LINEAR AND NON-LINEAR STAGES

Thesis submitted for the degree of

" Doctor Philosophiae "

CANDIDATE: SUPERVISOR:

R. Valdarnini   Prof. D. W. Sciama

Academic year 1983-84

I.S.A.S. - INTERNATIONAL SCHOOL FOR ADVANCED STUDIES

A STUDY OF INHOMOGENEITIES

IN COSMOLOGICAL MODELS WITH DARK MATTER

THROUGH LINEAR AND NON-LINEAR STAGES

Thesis submitted for the degree of

' Doctor Philosophiae '

CANDIDATE   SUPERVISOR

R. Valdarnini   Prof.D.W.Sciama

Academic year 1983-84

ACKNOWLEDGMENTS

CONTENTS

ABSTRACT

Among hot problems in cosmology and (high energy) astrophysics, the role

played by dark matter and its nature deserves a particular attention.

It is widely believed that dark matter has a key role in accounting for

the dynamics of gravitating systems over a wide range of mass scales.

The amount of dark matter needed to account for observational data seems

however to increase when going from small scales (e.g. star dynamics in

the solar neighborough) towards greater scales (galaxies, galaxy clusters,

etc.) .

In principle dark matter could be made either of ordinary baryonic matter

or of more exotic particles. In the former case, besides the problem of

explaining in which form this matter should exist in order neither to radia-

te nor to absorbe radiation, we face severe costraints coming from cosmo-

logical nucleosynthesis results. According to the most recent results of

Yang et al. (1984) the observed abudances of De, ^{3}He, T, ^{7}Li, etc. constraint

the baryonic density parameter Ω_B to be below 0.1 . Dynamical estimates

over galaxy cluster (or greater) scales, instead, seem to indicate that

the overall density parameter $\Omega \geq$ 0.3.

The possible existence of a non-baryonic dark matter component appears

therefore quite reasonable.

A number of possible candidates for it have been suggested.

In principle, massive neutrinos with mass of some tens of eV could solve

most present epoch dynamical problems.

Their role in the frame of the origin and evolution of inhomogeneities has however been widely debated in the literature,and it seems difficult to account for a number of cosmological evidences in the frame of cosmological models in which the sole components of dark matter are massive neutrinos. A careful analysis of the way in which this conclusion is attained will be performed also in this thesis.

An alternative possibility is that dark matter is made of other kinds of collisionless particles (X)with higher mass (m_X) and lower number density. A critical value for m_X is 1 KeV. It can be shown that, if $m_X \geqslant 1$ KeV, the smallest inhomogeneities surviving at the beginning of non-linar stages exceed a galactic mass. Galaxies will then rise from fragmentation of primaval fluctuations in non-linar collapse stages.

If, instead, $m_X \leqslant 1$ KeV, primeval inhomogeneities will involve less than a galactic mass. The former case fits the so-called ' pancake' scenario, the latter case fits the so-called ' hierarchical' clustering scenario.

In both cases the galactic mass scale should be singled out by the dynamics of dissipative phenomena. Of course, also the intermediate case $m_X \simeq 1$KeV, leading directly to inhomogeneities of galactic size should not be disgarded.

The existence of collisionless particles of various masses can fit different fundamental different schemes.

Supersymmetries lead to the expected existence of particles whose mass

should exceed 0.8 KeV (Goldberg 1983), but is likely to be much higher.

Right-handed massive neutrinos are an alternative possibilty. Recent reports

on the Moscow experiment seem to support their existence.

Further proposals range from axions (particles related to CP violations)

to exotic proposals like quark nuggets (Witten 1984).

Within the framework of X-dominated Universe the details of galaxy formation

theory and clustering are just beginning to be worked out.

In the first part of the thesis we deal with the linear evolutions of

adiabatic perturbations in a Universe dominated by dark matter made of X

particles with $m_X \simeq$ 1 KeV, or by a mixture of such X particles and massive

neutrinos (ν). Hereafter by X particles we shall intend particles whose

mass is $\simeq$ 1 KeV.

The second part of the thesis concerns N-body numerical experiments to si-

mulate the gravitational collapse of a protogalaxy in the presence of a dark

halo.

The first part comprises chapters I to III.

The first chapter is an introduction to the dark matter problem, stressing the

cosmological and astrophysical consequences arising if dark matter is made

of massive neutrinos or other massive collisionless quanta.

In the second chapter we present the results of numerical computations for

the linear evolution of adiabatic perturbations in a X-dominated Universe;

a comparison with results concerning ν - dominated models shows that the

final spectra are in better agremeent with the large scale clustering

features. The possibilty that dark matter is made of X and ν is also

debated. Even if massive neutrinos account for most of such mixture

($\simeq$ 75 %), the final spectra are drastically changed by the action of

X- particles. Moreover the mass scale over which non-linearity is achieved

first is strongly sensitive to the steepness of the initial spectrum.

In the third chapter the small scale fluctuations in the microwave (MW)

background radiation are computed in models dominated either by massive

neutrinos or X particles; ν -dominated models can be in conflict with

most recent limits (Uson and Wilkinson 1984) on small scale MW back-

ground fluctuations unless galaxies have formed at very recent epochs.

On the contrary X-dominated models find much less difficulty to fit MW

background data and the limits on the epoch of galaxy formation turn out

to be highly dependent on the steepness of the initial spectrum.

The second part comprises chapters IV to V.

The fourth chapter is a discussion of the present status of galaxy formation

theories at the beginning of non-linear stages in the presence of dark

matter. N-body numerical experiments, which have been performed to simula-

te the gravitational collapse of galaxies, are also debated.

In. the fifth chapter we present a series of results from N-body numerical

experiments, for the collapse of a protogalaxy with and withouth a dark

halo. Although the research on this point is still in progress, we have

completed a number of numerical simulations showing that elliptical gala-

xies should have collapsed by a large factor (in radius) as a consequences

of the potential wells due to the dark haloes.

I. THE DARK MATTER PROBLEM

I.1. Evidence and problems for dark matter

In recent years there has been a growing experimental evidence that

the Universe appears to be gravitationally dominated by a form of unseen

dark matter from spiral galaxies up to cluster super-cluster scales (Faber

and Gallagher 1979, hereafter FG).

For spiral galaxies the rotational curve V (R), which gives the

velocity of rotation versus distance R from the centre, appears to be

flat up to radii comparable to R_H and beyond (Rubin et al. 1978, Bosma

1981).

The unseen keplerian fall off in V (R) at large radii implies that

spiral galaxies are embedded in a halo of dark matter. The simplest

hypothesis is that the halo has spherical symmetry (although other

interpretations are possible, sec e.g. Bahcall et al. 1982); in such a

case V (R)$\simeq$const implies $\rho_{Halo} \propto R^{-2}$ and $M_{Halo} \propto R$.

If one defines a mass-to-light ratio, equal to one in solar units,

for spiral galaxies one has $\left(M/L_B\right) \simeq (5-15)h$ (FG).

where h is the Hubble constant in units of 100 $Km \, sec^{-1} M_{pc}^{-1}$.

This M/L ratio is only a conservative limit since the full extension

- - - - -

* R_H is the Holmberg radius at which the galaxy surface brightness
reaches 26.5 B mag/ squ arc sec.

of the flatness of the rotational curve is unknown and M/L refers to the Holmberg radius.

For elliptical galaxies the presence of dark matter is not yet firmly established and in respect to spiral galaxies the situation is much more complicated. The reason being that for these systems the rotation is negligible (Bertola and Capaccioli 1975, Illingworth 1977) and the mean rotational velocity is much less than the velocity dispersion σ .

If one refers only to the central regions the King (1972) model, which has a gaussian and isotropic velocity distribution with σ constant over the core region of radius r_c (at r_c the surface brightness drops to $\frac{1}{2}$ of its central value), gives $(M/L_B) \simeq (5-10)\, h$ (Faber and Jackson 1976, Schechter and Gunn 1979).

There are several cases in which σ is constant also out of the nucleus. Schechter and Gunn (1979), on a sample of 12 elliptical galaxies , found that σ is constant up to $r \simeq 6\, h^{-1} Kpc$.
In the isotropic velocity dispersion case the explanation is that M/L grows linearly with the radius (Efstathiou et al. 1980). There are several elliptical galaxies (Illingworth 1981) in which the velocity dispersion profile decreases with radius and they are consistent with an isotropic model and M/L constant.

The conclusion would be that at least in elliptical galaxies with

$\sigma \simeq$ const there is evidence of dark matter. However this conclusion must be taken with care: if the flattening of these systems is due to an anisotropic velocity dispersion, as in the Binney(1976) model, the σ profile could be determined by dynamical effects and not related to true gradients in M/L (Illingworth 1981).

Going on larger scales, the mass-to-light ratio seems to increase linearly with the considered scale (Rood 1981). Galaxy clusters are the largest systems for which M/L is known.

Using the virial theorem FG found $\left\langle M/L_B \right\rangle \simeq 290$, over a sample of seven clusters, with a range 165-800.

Such high values for M/L in clusters have been independently confirmed using the King model applied to the cluster central regions (Rood et al. 1972, Bahcall 1974, Van den Bergh 1977) and by dynamical models for the Coma cluster using N-body computer simulations (White 1976).

Together with spiral galaxies, clusters are the systems for which the experimental evidence for dark matter is particularly striking.

On mass scales below the galactic ones there are recent measurements of dark matter for dwarf galaxies (Faber and Lin 1983, Aaronson 1983), not yet confirmed (Cohen 1983), and in the solar neighbourhood (Bahcall 1984).

Since these measurements are of extreme theoretical importance in

deciding the true nature of dark matter, they will be discussed in detail in the following paragraphs.

From the mass-to-light ratio found for large clusters, it appears that dark matter dominates gravitationally the Universe on large scales ($R \geq 10 h^{-1} M_{pc}$) with respect to the 'visible' mass.

In estimating the mean matter density in the Universe the cosmological density parameter

$$\Omega = \rho / \rho_c \tag{1.1}$$

is defined, where ρ is the present mean matter density and $\rho_c = 3H^2 / 8\pi G$ is the critical density necessary to close the Universe.

There are two ways to estimate Ω : the first makes use of the cosmic virial theorem(Fall 1975; Davis, Geller and Hucra 1978; Peebles 1979), the other estimates Ω from the local anisotropies in the Hubble flow due to the collapse of the Local group towards the Local supercluster (White and Silk 1979, Davis et al. 1980).

In the first method the assumption of virial equilibrium on the considered scale yields a relation between the peculiar galaxy pair velocities and Ω ; in determining this relation the two point correlation function $\xi(r)$ * (Peebles 1980, hereafter LSS) is used, then the assumption is implicit that the light is a tracer of the mass

------

* Observationally it is found $\xi(r) = (r_0 / r)^{\gamma}$, with $\gamma = 1.77 \pm 0.04$, $r_0 = (5.4 \pm 0.3) h^{-1} M_{pc}$ on scales $0.1 h^{-1} M_{pc} \leq r \leq 10 h^{-1} M_{pc}$ (Davis and Peebles, 1983).

distribution. Typically one finds (Davis, Geller and Hucra 1978; Peebles 1979) $\Omega \simeq 0.2 - 0.3$, however the determination of Ω with the cosmic virial theorem is affected by the poor knowledge of $\xi(r)$ at $r \geq 10 \, M_{pc}$ (Gunn 1978).

In the second approach the motion of the Local group is supposed to be entirely determined from the Supercluster matter over density, i.e. our Local group is gravitationally collapsing toward the Supercluster.

This does not agree with the observed dipolar anisotropy in the cosmic background radiation (Smoot and Lubin 1979, Cheng et al. 1979), according to these measurements the motion of the Local group with respect to the CBR is of the order of $v \simeq (500 \pm 100) \, km\,sec^{-1}$, but the apex of the dipolar anisotropy is nearly 45° off the Virgo centre.

The direction of the dipolar anisotropy in the CBR can be reconciled with the previous hypotheses if one assumes that the SC collapse is non-spherical, with non-radial motions in the outer regions (White and Silk 1979). This hypothesis has been confirmed by Aaronson et al. (1980) who did not find appreciable anisotropies in the Hubble flow at a redshift $c\dot{z} \simeq 5000 \, km\,sec^{-1}$, i.e. the motion of the Local group is entirely determined by the gravitational action of the Supercluster.

From the Local group motion is found $\Omega \simeq 0.4 \pm 0.1$ (Davis et al.

1980). Using the standard big-bang model it is possible to set upper limits to the baryonic contribution to Ω trough the observed Helium and Deuterium abundances; Yang et al.(1984) found $0.01 \leq \Omega_b \leq 0.14$ In such a case it is still possible to explain dark matter in purely baryonic terms, but only in a low-Ω Universe ($\Omega \simeq 0.1$).

However there are several arguments which suggest that dark matter must be of non baryonic nature (Peebles 1979 α).

In the case of galactic haloes dark matter cannot be atomic hydrogen since in this case the 21 cm background would be too high, the needed surface density is about $160 \ M_\odot pc^{-2}$ which imply a column density $\simeq 10^{22} cm^{-2}$. a 100 times greater than the HI column density at the poles (Kerr 1965); dark matter cannot be ionized hydrogen since to avoid gravitational collapse over a free-fall time scale ($\simeq 10^8 yr$) the halo equilibrium temperature must be $T \simeq 5 \cdot 10^6 \ °K$, from the $E \leq 1 keV$ X-ray background the upper limit to the plasma density in the halo is $\simeq 10^{-3} cm^{-3}$ (Field 1972), a one hundred times less than that deduced for the halo through the rotational curve.

Obviously dark matter cannot be in the form of main sequence star which otherwise would have been seen in the solar neighborhood. Objects formed by heavy elements (comets, rockets) must not be too abundant with respect to hydrogen, further a halo made of metals implies a very low level of

contamination with disk stars, which seems implausible. Star remnants (white dwarfs, neutron stars, black holes) are probably excluded, when such objects are formed they would return a large amount of chemically evolved gas to the interstellar medium, which is not observed.

Another possibility is that dark matter is made of low-mass degenerate stars ($M \le 0.1 \, M_\odot$) or 'Jupiters'. For these objects the central temperature is not enough to have nuclear burning but they will be infrared sources since they are still cooling. Observations on the halo surface brightness for NGC4565 (Boughn et al. 1981) yield a lower limit to the mass-to-light ratio for the halo $M/L_K > 38 \, M_\odot/L_{\odot,K}$ in the K band, in this case the observations exclude the possibility of a halo made of 'Jupiters', unless the slope of the initial mass function is very steep (Hegyi 1984).

Although the nature of dark matter is still unknown a naive approach suggests that it must be of non-dissipative type since it appears to be much less clustered than baryons. In such a case it is also plausible for dark matter to be collisionless.

In recent years it has been proposed that dark matter is non-baryonic and made of neutrinos (or other elementary particles of supersymmetric type) with a non-zero rest mass.

Although the actual constraint on Ω does not allow the complete

ruling out of a baryonic explanation for dark matter, like Pop. III objects for example (Rees 1978, Carr 1980), in what follows we shall assume as a fundamental hypothesis that dark matter is of non-baryonic nature. Within this framework even primordial black holes are a possibility (Carr 1977), but only massive neutrinos or other weakly interacting massive collisionless quanta will be considered here.

I.2. Massive neutrinos

The experimental detection of non-zero rest mass for the electronic neutrino (Lyubimov et al. 1980), of the order of the tens of eV, has lead many authors to a revival of the old idea that dark matter is made of massive neutrinos (Gershtein and Zel'dovich 1966, Marx and Szalay 1972, Cowsik and McClelland 1972).

The experiment of Lyubimov as yet to be confirmed but massive neutrinos, or other weakly interacting massive particles, are equally interesting candidates for dark matter. These particles are non-baryonic and after their decoupling they behave in a collisionless way. From the preceding discussion we have seen that both of these properties are likely to be satisfied for dark matter.

Let us first examine the cosmological consequences of a non-zero

rest mass for neutrinos. Before their decoupling neutrinos are kept

in thermal equilibrium by weak interactions, their phase space distribution

was ($\hbar = k_B = c = 1$, the neutrino chemical potential is taken to

be zero)

$$\mathcal{g}_\gamma (p_\gamma) = \frac{1}{(2\pi)^3} \; \frac{1}{e^{E_\gamma/T_\gamma} + 1} \simeq \frac{1}{(2\pi)^3} \; \frac{1}{e^{p_\gamma/T_\gamma} + 1} \qquad (1.2)$$

at the onset of their decoupling, which happens at temperature $T_{\gamma d}$

$\simeq 3\,MeV$, neutrinos were ultrarelativistic and since both p_γ and

T_γ scale as $R^{-1}(t)$, where R(t) is the cosmic scale

factor, the distribution (1.2) can be equally applicable at the present

epoch, also if neutrinos are today nonrelativistic.

The neutrino temperature is related to the radiation one by $T_\gamma = (4/11)^{1/3} T_r$, because after they decouple neutrinos do not share in

the heating caused by $e^+\;e^-$ pair annihilation (Weinberg 1972).

Thus their present number density is

$$N_{\gamma_i} = \frac{4\pi g_{\gamma_i}}{(2\pi)^3} \; T_{\gamma_i}^3 \int_0^\infty \frac{x^2\,dx}{e^x + 1} \simeq 75\,g_{\gamma_i}\;cm^{-3} \qquad (1.3)$$

where g_{γ_i} is the total number of speen degree of freedom for the

neutrino species i (i = e, μ, τ) and $T_{r_0} = 2.7\,^{\circ}K$ is the

photon temperature today. With a summing of the various species we have

($\rho_r = N_{r_i}\, m_{r_i}$)

$$\Omega_r = \frac{\rho_r}{\rho_c} \simeq 5 \cdot 10^{-2}\, h^{-2}\, \sum_i m_{r_i}\, (eV) \qquad . \qquad (1.4)$$

For $\Omega_b \leq 0.1$ one has that the neutrino contribution to Ω is

dominant for (Schramm and Steigman 1981)

$$\sum m_r\, (eV) \geq 1.4\, eV \qquad ; \qquad (1.5)$$

from the lower limits to the age of the Universe t $_o$ and the relation

between t $_o$ and Ω (Weinberg 1972) it is possible to conclude

(Zel'dovich and Sunyaev 1980)

$$\sum m_r\, (eV) \leq (30 - 50)\, eV \qquad . \qquad (1.6)$$

If the sum of the neutrino masses would exceed this limit massive neutrinos

could still be a solution to the dark matter problem with a non-zero

cosmological constant, which is the hypothesis suggested by Zel'dovich

and Sunyaev (1980). This possibility will not be considered here.

From eq. (1.4) we see that massive neutrinos with rest mass of the order of tens of eV yield the density parameter Ω of order unity, in the same range of the observed one for dark matter. Thus, at least as a general order of magnitude argument, dark matter could be made of massive neutrinos. However any theory on the nature of dark matter must be linked in a crucial way with the formation of galaxies, since these objects are observed to be embedded in dark haloes and it is likely that these haloes have played an important role in the formation and subsequent evolution of galaxies.

Let us consider the impact of the massive neutrinos hypothesis on the galaxy formation theory. The evolution of neutrino density perturbations has been widely studied in the literature, both in the linear stages (Doroshkevich et al.1980, Bond et al. 1980, Wasserman 1981, Peebles 1982, Bond and Szaley 1983, Bonometto et al. 1984), and in the non linear ones (Mellot 1983, Centrella and Mellot 1983, Shapiro et al. 1983, Klypin and Shandarin 1983, Frenck et al. 1983).

Primeval neutrino density perturbations must be adiabatic since, before neutrino decoupling, each source of radiation density fluctuation distributes in the same way both radiation and neutrinos and after neutrino decoupling it is unlikely that neutrino density fluctuations would have been formed. After the decoupling the neutrinos are collisionless and

do not have pressure, but they have kinetic energy from their thermal motions. Substituting c_s^2 with $\langle v_\gamma^2 \rangle /3$ in the expression for the Jeans mass, where c_s is the sound velocity and $\langle v_\gamma^2 \rangle^{1/2}$ is the neutrino velocity dispersion, a neutrino Jeans mass $M_{J\gamma}$ can be calculated in the same way as for baryons (this is a very crude argument and must not be taken too seriously; in reality one must resort to a numerical solution of the relativistic Boltzmann equation for neutrinos, see appendix A.2 for more details). The condition $M > M_{J\gamma}$ still means that in the density perturbation $\delta_\gamma \equiv (\delta\rho/\rho)_\gamma$ the gravitational energy dominates and the perturbation collapses. An important difference of neutrinos with respect to baryons is that for $M < M_{J\gamma}$ neutrino density perturbations are erased owing to Landau damping. This happens because for $M < M_{J\gamma}$ the perturbation kinetic energy overtakes the gravitational one and the neutrino mean free path is large compared to the perturbation wavelength, so neutrinos freely escape from the perturbation and the overdensity is erased.

For neutrinos there is the important coincidence that they become non-relativistic at a redshift $z_{\gamma_{NR}} \simeq 4 \cdot 10^4 \, m_\gamma \, (eV) / 30 \, eV$ which is of the same order of the redshift $z_{eq} \simeq 10^4 \, \Omega \, h^2$ at which the Universe becomes matter dominated.

At $z > z_{\gamma_{NR}}$ it is $\langle v_\gamma^2 \rangle \simeq c^2$ and for $z < z_{\gamma_{NR}}$

it is $\langle v_\nu^2 \rangle \simeq T_\nu / m_\nu$, then it is found that

$$
\begin{cases}
M_{J\nu}\,(z > z_{\nu_{NR}}) \simeq 5 \cdot 10^{15} \left(\dfrac{1 + z_{eq}}{1 + z} \right)^{-3} \\[4ex]
M_{J\nu}\,(z < z_{\nu_{NR}}) \simeq 5 \cdot 10^{15} \left(\dfrac{1 + z}{1 + z_{eq}} \right)^{3/2} \left[\dfrac{32\,eV}{m_\nu c^2} \right]^{7/2} .
\end{cases} \tag{1.7}
$$

The eq.s (1.7) show that the only neutrino density perturbations which

survive the ν - derelativistization are those with $M_\nu \simeq M_{J\nu_{MAX}}$

$\simeq M_{J\nu}\,(z \simeq z_{\nu_{NR}}) \equiv M_{\nu_c} \simeq 10^{15}\,M_\odot$ (Bond et al. 1980,

Doroshkevich et al. 1980), i.e. a cluster supercluster scale.

In Fig. 1.1 the $M_{J\nu}$ behaviour is shown versus the redshift z,

together with the baryonic Jeans mass M_{Jb} and the horizon one.

It is usually assumed that the Fourier power spectrum of the primeval

density contrast is of the form $|\delta_k|^2 = k^n$, where k is the

comoving wave number of the perturbation with mass $M = \dfrac{\pi}{6}\,\rho \left(\dfrac{2\pi R(t)}{k} \right)^3$

and n is called spectral index. Then the r.m.s. neutrino density fluctuations

on mass scale M will have the following dependence

$$
\begin{cases}
\delta_\nu \propto M^{-\frac{1}{2} - \frac{n}{6}} & M \geq M_{\nu_c} \\[4ex]
\delta_\nu \simeq 0 & M \leq M_{\nu_c}
\end{cases} \tag{1.8}
$$

at $z < z_{\nu_{NR}}$. A safe assumption is that n > -3 , which means that
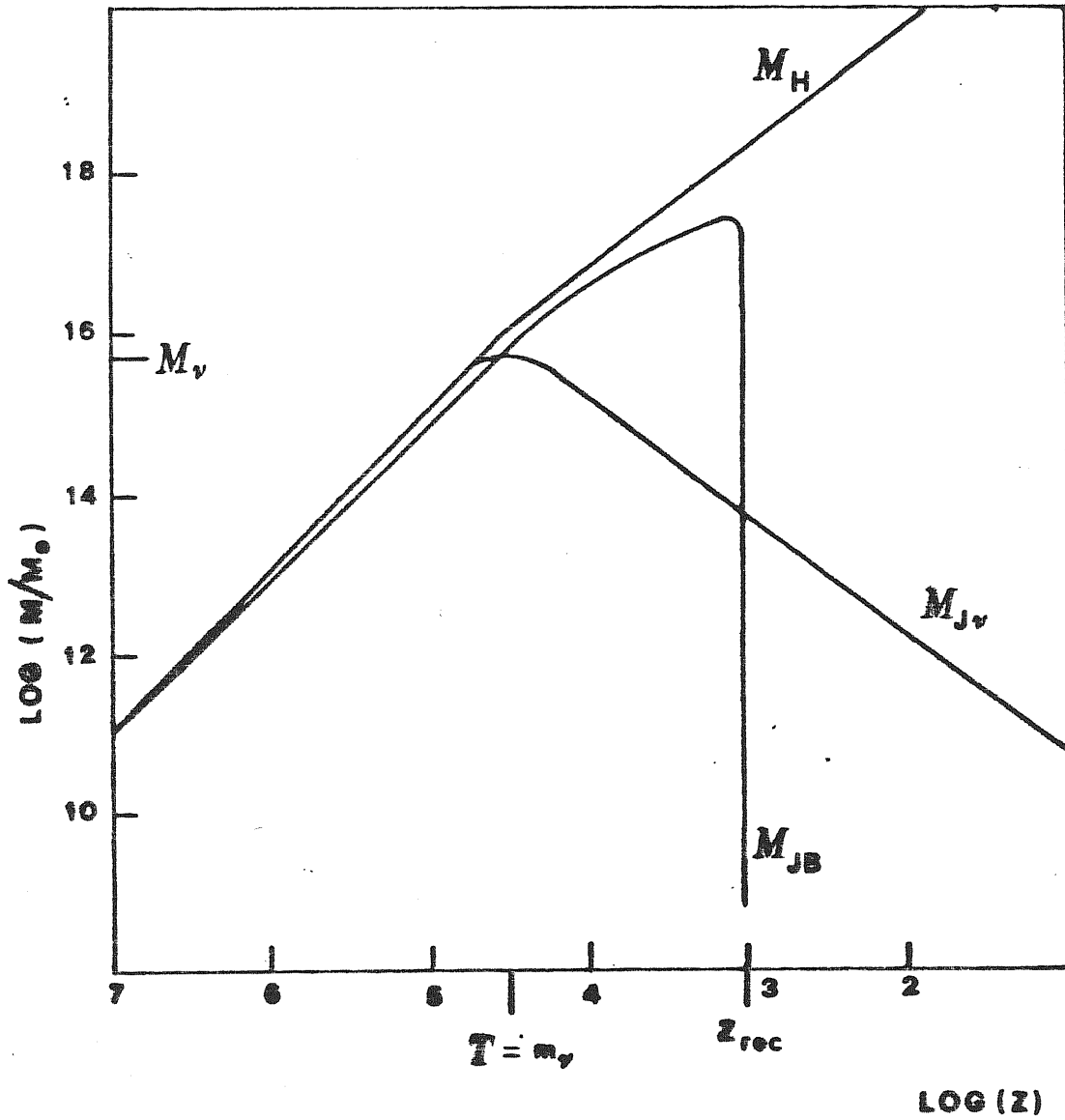
Fig. 1.1 Neutrino Jeans mass $M_{J\gamma}$ and baryonic Jeans mass M_{J_b} versus redshift z. M_H is the horizon mass. Here is Ω_b =0.03, Ω_γ =1.

the observed clustering decreases with increasing scales.

A n = 1 spectrum is theoretically favoured since it implies that density perturbation of different wavelengths will have the same amplitude when they come into the horizon, i.e. the primeval spectrum has not preffered scales (Zel'dovich 1972).

From eq. (1.8) we see that M_{r_c} is the first mass scale to undergo collapse and to reach the non-linear stage in a scenario involving massive neutrinos. Since the collapse proceeds in a cold environment small initial anisotropies in the geometry of the perturbation will be amplified at later stages and the collapse of the neutrino perturbation will be strongly flattened along one direction, as in the ordinary Zel'dovich (1970) pancake theory.

The growth of baryonic perturbations in a neutrino dominated Universe is strongly amplified after the recombination, with respect to a baryon dominated Universe, by the presence of neutrino perturbation potential wells. This implies that mass scales which are reaching non-linearity now ($M \simeq 10^{15} M_\odot$, corresponding to an angular scale $\theta \simeq 10'$) require smaller baryon perturbations at recombination, i.e. the small scale radiation fluctuations $\frac{\Delta T}{T}$ are expected to be smaller than in the baryonic case in a neutrino dominated Universe and below the observational upper limits $\frac{\Delta T}{T} < 3 \cdot 10^{-5}$ on angular scales $\theta \simeq 4'$ (Partridge 1980).

See chapter III for more details.

Furthermore an adiabatic theory for the formation of galaxies where the first scale to collapse is of the order of $10^{15} M_\odot$, provides a natural explanation for the existence of the large scale inhomogeneities observed in the galaxy distribution (Einasto et al. 1980, Kirshner et al. 1981).

In this scenario galaxies are formed after the collapse of the neutrino pancake through the cooling and fragmentation of the baryonic pancake.

A central point is if neutrinos can form the dark haloes of galaxies, since the neutrino velocity dispersion in the pancake will be of the order of $10^3 Km\ sec^{-1}$, which may be too great to allow neutrinos to collapse over galactic scales. A constraint on the neutrino mass from the scale of the collapsed system can be worked out from phase space considerations (Tremaine and Gunn 1979, hereafter TG).

At the onset of neutrino decoupling the maximum value of the fine grained phase space neutrino distribution was $g_r / 2 h^3$, from the Liouville theorem this maximum has been conserved, so the coarse grained phase space density for the collapsed system cannot exceed this limit.

Assuming a Maxwellian velocity distribution for the collapsed system TG found

$$m_\nu \geq 10^2 \left(\frac{100 \, Km \, sec^{-1}}{\sigma} \right)^{1/4} \left(\frac{1 \, Kpc}{r_c} \right)^{1/2} eV \quad , \qquad (1.9)$$

here σ is the velocity dispersion and r_c the core radius of the collapsed system. For $\sigma \simeq 200 \, Km \, sec^{-1}$ and $r_c \simeq 20 \, Kpc$ one finds $m_\nu \geq 20 \, eV$.

If the neutrino mass is of the order of tens of eV eq. (1.9) becomes an equality for a galactic system, which simply means that neutrinos which collapse over these scales cannot undergo phase-mixing, i.e. they must be rather cold. In a one dimensional numerical simulation Mellott (1983) has shown that about 12% of neutrinos inside the pancake have a low velocity dispersion ($\simeq 10^2 \, Km \, sec^{-1}$), with a small amount of phase-mixing, and are able to collapse over galactic scales. This point requires some care:in a realistic tridimensional simulation it is likely that neutrinos acquire large transversal velocities in collapsing onto the system, which would imply strong phase-mixing for the neutrino distribution itself.

The neutrino scenario provides us a natural explanation for the observed trend in M/L, which increases with the considered scale, since more neutrinos will be caught inside deeper potential wells.

However S. Faber (1982) has stressed how the M/M_{lum} ratio is

physically more meaningful, where $M_{\ell um}$ is the total baryonic mass for the considered system. In this case $M/M_{\ell um}$ is found to be constant over a wide range of scales, $M/M_{\ell um} \simeq 10 - 15$, from spiral galaxies up to cluster scales. For large clusters the difference betwee $M/M_{\ell um}$ and M/L_B is due to the different stellar populations in elliptical galaxies in clusters plus the contribution to $M_{\ell um}$ from X-ray emitting gas. If these measurements should be confirmed, a $M/M_{\ell um}$ constant over a large range of scales would favour the hypothesis that galaxies with their dark haloes have been formed earlier and that clusters have followed later in a collisionless way by means of gravitational clustering of the galaxies themselves. In this case the increase of $M/M_{\ell um}$ with the considered scale will be much less than in a neutrino model for dark matter.

The neutrino scenario suffers serious problems both on small scales (below the galactic ones) and on large cluster scales. The recent experimental evidence for dark matter over dwarf galaxy scales (Faber and Lin 1983, Aaronson 1983) from eq. (1.9) implies a neutrino mass $m_\nu \simeq 500$ eV. This does not agree with the upper limits to m_ν from eq. (1.6), unless $\Omega_\nu > 2$, which seems implausible (Gott et al. 1974).

These measurements for dwarf galaxies are not been confirmed (Cohen 1983), but a positive detection of dark matter would definitively rule out

neutrinos as sole dark matter constituents.

On large scales numerical experiments (Centrella and Mellott 1983, Frenk et al. 1983) indicate that the slope of the two point correlation function $\xi(r)$ has a time dependent steepness. But only if non-linear evolution is started in a restricted redshift interval, can an agreement with observations be possible.

Another point which weakens ν models for dark matter is a comparison between the large scale (R $\simeq$ 50 Mpc) matter velocities and the theoretical ones (Kaiser 1983) for these regions the collapse is still in the linear phase and the observed velocities ($\simeq$ 100 Kmsec^{-1}) imply that large scale structures have reached the non-linear stage at small redshift, $z_{h\ell} \simeq$ 1, in contrast with the idea that galaxy formations are subsequent to the pancake ones and associated with the QSO distribution in z, around z $\simeq$ 3-5.

For these reasons in the literature the hypothesis has been considered of other weakly interacting massive quanta as possible constituents of dark matter. Their general properties will be outlined in the next paragraph.

I.3. Other particles

The developments of supersymmetric theories have suggested the

hypothesis that the Universe is gravitationally dominated by neutral weakly interacting particles, more massive than neutrinos. These particles might be super-symmetric partners of known particles - photinos (Cabibbo et al. 1981), gravitinos (Pagel et al. 1982); other possibilities are right-handed neutrinos (Olive and Turner 1982) or axions (Preskill et al. 1983). Among these particles the mass of the lightest of them, probably a photino, might be as low as some KeV (Ellis et al 1984). For other particles their mass seems to lie in the GeV range. Axions are the most considered in the framework of this approach.

In what follows we shall label X the generic particle with mass in the KeV range, and we shall often refer to it as a photino, while we shall indicate as A those particles which are much more massive $(m_A \simeq GeV)$.

X particles interact more weakly then neutrinos and they decouple earlier. Then they do not share in the heating caused by the annihilation of the various species after their decoupling ($\pi^{\pm}, \pi^{o}, \mu^{\pm}, e^{\pm}$) and today the X temperature is much less than radiation one. Even if m_X is large with respect to the neutrino mass ($m_X \simeq KeV$) the X density parameter $\Omega_X \propto n_X T_X^3$ is still of order unity.

The same argument is applied to A particles, with the difference that A decouple when they are nonrelativistic and a Boltzmaniann factor $e^{-m_A/T}$ appears in the calculation of their present number density.

In such a case m_A might well be in the GeV range without there being problems for the value of Ω ($\Omega_A \simeq 1$).

An important difference of X particles with respect to neutrinos is that they become non-relativistic before the Universe becomes matter dominated. The growth of X density perturbations which enter the horizon at a redshift $z_H > z_{eq}$ is suppressed by the radiation which still dominates the energy density (Bond et al.1982, Blumenthal et al.1982).

A rough calculation suggests that X density perturbations δ_x with mass range $M_{x_c} \leqslant M \leqslant M_{eq}$ (M_{eq} is the horizon mass at z_{eq} and M_{x_c} is the critical damping scale for X particles) will be flattened by a factor $M^{2/3}$ (a numerical treatment for the time evolution of δ_x shows that this flattening is not very strong, see chapter II for more details). M_{x_c} is found to be (Bond et al.1982) $M_{x_c} \simeq m_{pe}^3 \, m_x^{-2} \simeq 10^{12} (m_x / KeV)^{-2} M_\odot$, here m_{pe} is the Planck mass.

At $t \ll t_{eq}$ the mass spectrum for these type of particles will be

$$
\begin{cases}
\delta_x \propto M^{-\frac{1}{2} - \frac{h}{6}} & M \geqslant M_{eq} \\[2em]
\delta_x \propto M^{-(h-1)/6} & M_{x_c} \leqslant M \leqslant M_{eq} \\[2em]
\delta_x \simeq 0 & M \leqslant M_{x_c}
\end{cases}
\tag{1.10}
$$

for $-3 < n < 1$ the spectrum increases with the considered scale, reaches a peak at M_{eq} and then falls off. In such a case clusters will collapse first. For $n \geqslant 1$ non-linearity is achieved first on galactic scales, and large scale structures will form later through non-dissipative gravitational clustering, as in the White and Rees (1978) theory. An argument often quoted in favour of an X-dominated Universe is the presence of dark matter in dwarf galaxies (Faber and Lin 1983, Aaronson 1983). For these systems TG argument requires $m_X \simeq 500$ eV. However it must be stressed that the TG argument is a necessary condition for the particle mass in order to have collapse on a given scale. For dwarf galaxies is

$$M_{Dw} \simeq 10^8 - 10^5 \, M_{\odot} \quad , \text{ three orders of magnitude below } M_{X_c} \quad .$$

X density perturbations over dwarf galaxies scales have been previoulsy erased by Landau damping, and in this case it is unclear how dwarf galaxies have gained their dark haloes.

A particles decouple when they are nonrelativistic and their velocity dispersion is so low that damping processes are not of cosmological interest. In this case all the A density perturbations which enter the horizon at $z > z_{eq}$ will be flattened by a factor $M^{2/3}$ and their final spectrum will be

$$\begin{cases} \delta_A \propto M^{-\frac{1}{2} - \frac{n}{6}} & M \geqslant M_{eq} \\ \\ \delta_A \propto M^{-(n-1)/6} & M \leqslant M_{eq} \end{cases} \qquad (1.11)$$

A minimum mass scale is set be the post recombination baryonic

Jeans mass $M_{Jb} \simeq 10^{6} M_{\odot}$, if $M < M_{Jb}$ it follows that pressure

effects prevent the baryonic density contrast δ_b from reaching δ_A .

In this scenario the available power is widely distributed below

M_{eq} . A-dominated Universe have received the attention of some authors

(Peebles 1984; Blumenthal et al. 1984), and the theoretical situation is not

fully clarified. Peebles (1984) has suggested that a strong point in

favour of A-dominated Universe would be a positive detection of dark

matter around globular clusters, since these systems would be the first

to gain their dark haloes. On this point the experimental situation is

controversial. In any case preliminary numerical simulations (Mellott

et al.1983) have shown that large scale structures are equally formed

both in an X or an A dominated Universe.

With respect to γ -dominated models the collapse of large scale

structures is non-dissipative and the flattening of the formed pancakes

will be smaller than in the γ case.

Dekel (1983) has shown how a non-dissipative scenario for the

supercluster formations is compatible with the observed flattening of

the local Super Cluster. The dissipative scenario, in which galaxies

form after SC collapse, yields a galaxy distribution which is too flat

compared with observations. For these models, where the Universe is

gravitationally dominated by X or A particles, the theoretical situation

is still far from being fully clarified.

In the following chapters we shall mainly concentrate either on

X-dominated Universe, or on the possibility that the Universe is

gravitationally dominated both by X and γ particles.

II. EVOLUTION OF ADIABATIC PERTURBATIONS IN A UNIVERSE DOMINATED BY MASSIVE WEAKLY INTERACTING QUANTA

Fluctuation evolution in a photino dominated Universe

As we have already seen in § I.2 a γ-dominated Universe seems to suffer from several difficulties both on large scales $(M > 10^{15} M_{\odot})$ and on small scales ($M \simeq 10^{5} M_{\odot}$). These arguments will not be revised here, however none of them excludes the possibility of a neutrino dominated Universe. An alternative possibility is that dark matter is made of X particles, which are collisionless like neutrinos but much more massive ($m_X \simeq K_e V$).

In the following paragraphs the results are presented for a numerical integration for adiabatic perturbations involving a generic X particle in a $\Omega = 1$ Friedmann Universe. The integration is from an initial redshift $z_i = 10^{5}$, down to $z_g \simeq 2.10^{3}$. The X perturbations are coupled to the matter radiation fluid through the gravitational field equations. For the X particles a fully Bolzmannian kinetic treatment is used, while matter and radiation are treated in the ideal fluid approximation. Our notation follows that of Peebles (1982), but the numerical scheme of integration is different. A comparison of the

observed clustering with the computed mass variances shows that a

photino dominated Universe with $m_x \simeq 2 \, keV$ and $h = 0$ or $h = 1$

as a spectral index for the initial X perturbation, might be favoured

over a neutrino dominated Universe where only spectra with $h > 2$ would

be allowed (Valdarnini 1984).

II.1 Assumptions and notations

For small perturbations the line element in a flat Friedmann Universe

is

$$ds^2 = dt^2 - a^2(t) \left[\delta_{\alpha\beta} - h_{\alpha\beta} \right] dx^\alpha dx^\beta \qquad \alpha, \beta = 1, 2, 3 \quad (2.1)$$

where t is the cosmic time in time-orthogonal coordinates, $a(t)$ is the

scale factor for the expanding Universe and $h_{\alpha\beta}$ are the metric

perturbations. We choose units so that the speed of the light and the

Bolzmann constant are $c = k_B = 1$. Neglecting the baryon contribution,

we take the total density to be $\rho = \rho_r + \rho_x$, where ρ_r is the

radiation density and ρ_x is that of the collisionless particles.

The cosmological density parameter is defined as

$$\Omega = \rho / \rho_c , \qquad (2.2)$$

where $\rho_c = \dfrac{3 H_o^2}{8 \pi G}$ and $H_o = 100\, h\, Km\, sec^{-1} M_{pc}^{-1}$. The

present value of the radiation temperature is

$$T_r (t_o) = 2.7 \theta \,^\circ K \ . \tag{2.3}$$

In the computation $\Omega = h = \theta = 1$. For the generic X particle the

suppression factor α_X is defined as

$$\alpha_X = T_X \big/ T_{rad} \ . \tag{2.4}$$

We assume for the X particles a Fermi-Dirac distribution with zero

chemical potential.

According to Peebles (1982) the radiation energy density is

$$\rho_r = \frac{8 \pi^5}{15 h_P^3} \ T_r^{\ 4} \ . \ ) \tag{2.5}$$

Here , h_P is the Planck constant.

The X energy density ρ_X is given by

$$\rho_X = \frac{g_X}{h_P^3} \int_0^\infty d^3 p_1 \ p^0 \ \frac{1}{e^{p'/T_X} + 1} \ ) \tag{2.6}$$

here g_x is the sum of spin degree of freedom for the X particle,

p_o is the X particle energy , $p_o^2 = p_1^2 + m_x^2$. With

the definition $q = p_o / T_x$ and $p = p_1 / T_x$ the integral

(2.6) becomes ($q^2 = p^2 + m_x^2 / T_x^2(t)$)

$$\rho_x = \frac{4\pi\, g_x}{h_p^3}\, T_x^4 \int_0^\infty p^2\, q\, dp\, \frac{1}{e^p + 1} \equiv \frac{4\pi\, g_x}{h_p^3}\, T_x^4\, \rho_{1x} . \quad (2.7)$$

From eq.s (2.4), (2.5) and (2.7) the ρ_x / ρ_r ratio is found

$$\frac{\rho_x}{\rho_r} = C_x\, \rho_{1x} \quad , \quad C_x = \frac{15\, g_x\, \alpha_x^4}{2\pi^4} \quad . \quad (2.8)$$

We can assume that X particles are today nonrelativistic, for $T_x \ll m_x$

the ρ_{1x} integral takes the value $\rho_{1x}(\eta \gg 1) \simeq \frac{3}{2}\, \zeta(3)\, \eta$

and the present value of the cosmological density parameter is ($\Omega \simeq \Omega_x$)

$$\Omega = \frac{\rho_{ox}}{\rho_c} = \frac{8\pi G}{3 H_o^2}\, \rho_{ro}\, \frac{15}{2\pi^4}\, g_x\, \alpha_x^4\, \frac{m_x}{T_{x_o}}\, 1.803 \quad , $$

then the mass of the X particle is

$$m_x = 70.5\, \frac{\Omega_x h^2}{\alpha_x^3\, g_x}\, eV \quad . \quad (2.9)$$

The present value of the cosmic scale factor $a(t)$ is given by (choosing $a(t) = m_x / T_x(t)$)

$$a_0 = 3.02 \cdot 10^5 \ \Omega_x h^2 / \beta_x \alpha_x^4 \ . \tag{2.10}$$

For the time unit τ we make the choice $\tau^{-2} = \frac{8\pi G}{3} \rho_r \alpha^4$, which will be particularly useful afterwards, then

$$\tau = 6.88 \cdot 10^8 \ \alpha_x^8 \beta_x^2 / (\Omega_x h^2)^2 \ \text{sec} \ , \tag{2.11}$$

and the length unit ℓ is

$$\ell = a_0 c \tau = 2.03 \ \alpha_x^4 \beta_x / (\Omega_x h^2) \ \text{Mpc} \ . \tag{2.12}$$

In these units the equation for $a(t)$ is

$$\frac{da}{dt} = \left[\frac{8\pi G}{3} \rho_r \alpha^2 \tau^2 \right]^{1/2} \left[1 + \frac{\rho_x}{\rho_r} \right]^{1/2} = \left(1 + c_x c_{,x}(a) \right)^{1/2} a^{-1} \ . \tag{2.13}$$

Finally the X density contrast δ_x is written as

$$\delta_x = \int \delta_x(k) \, e^{i \vec{k} \cdot \vec{x}} \, d^3 k \ , \tag{2.14}$$

where $\lambda = 2\pi a(t) k^{-1}$ is the comoving wavelength. In the comoving coordinates mass associated with the density perturbation with wavelength λ is

$$M_x = \frac{\pi}{6} \rho x_0 \lambda_0^3 \quad , \tag{2.15}$$

the index o refers to the present epoch. From eqs. (2.10), (2.12) (2.14) is

$$M_x = 3 \cdot 10^{14} k^{-3} \alpha_x^{12} \beta_x^3 \theta^6 / (\Omega_x h^2)^2 M_\odot \quad . \tag{2.16}$$

II.2. Fundamental equations

The set of fundamental equations for the time evolution of X density perturbation, coupled to matter and radiation through the gravitational field, is described in appendix A. Here we report only the required e equation in convenient units.

In what follows all the variables of interest will be developed in Fourier series, i.e. we consider only plane wave. In the linear approximation the gravitational interaction between perturbations with different wavelength can be neglected and each perturbation evolves in

time independently from the other (see Press and Schechter(1974) and
§ II.4. for a discussion on the validity of the approximation).

However we shall apply the linear theory understanding, hereafter,
the Fourier transforms for all the variables of interest.

The wave propagation is chosen along the x^3 axis. The angle
between the direction of x^3 and $\vec{p}$ will be called Θ and will
only appear in the treatment through $\cos \Theta = \mu$. Unless necessary
the index of x^3 will be dropped hereafter.

The perturbed Boltzmann equation

For X particles we write the distribution function f as

$$f = f_0 + f_1 , \qquad (2.17)$$

here f_0 is the imperturbed Fermi-Dirac distribution. Choosing a wave
propagation along the x^3 axis the Liouville eq. (A2.9) becomes (to $A2.9$
the first order in f_1)

$$\frac{\partial f}{\partial t} + i \frac{k}{a} \frac{p}{q} f = \frac{\gamma}{4} \equiv \left[(1-\mu^2) \dot{h} + (3\mu^2 - 1) \dot{h}_{33} \right] , \qquad (2.18)$$

where $h = h_\alpha^\alpha$ and γ is defined by

$$g_1 = g \, p \, \frac{e^p}{(e^p + 1)^2} \qquad . \qquad\qquad (2.19)$$

We expand g into Legendre polynomials, distinguishing between its real part, composed of even harmonics, and its imaginary part, composed of odd harmonics,

$$g = \sum_{\ell=0}^{\infty} \left\{ \sigma_{2\ell} \, \frac{4\ell + 1}{2} \, P_{2\ell} \; + \; i \, \sigma_{2\ell+1} \, \frac{4\ell + 3}{2} \, P_{2\ell+1} \right\} \quad . \qquad (2.20)$$

Then according to (2.18)

$$\left\{ \begin{array}{l} \dot{\sigma}_0 = \dfrac{k}{a} \, \dfrac{p}{q} \, \sigma_1 \; + \; \dfrac{\dot{h}}{3} \\[3ex] \dot{\sigma}_\ell = (-)^\ell \dfrac{k}{a} \, \dfrac{p}{q} \left[\sigma_{\ell+1} \, \dfrac{\ell+1}{2\ell+1} \; + \; \sigma_{\ell-1} \, \dfrac{\ell}{2\ell+1} \right] + \left(\dot{h}_{33} - \dfrac{\dot{h}}{3} \right) \dfrac{\delta_{\ell 2}}{5} \quad , \quad \ell \geqslant 1 \; . \end{array} \right. \qquad (2.21)$$

are the propagation equations at fixed 1.

The matter-radiation fluid and the field equations

We treat matter and radiation as a single ideal fluid; this approximation is certainly valid before recombination. The equations for the density contrast δ_r and the matter velocity v are

$$\dot{\delta}_{\mathsf{r}} = \frac{4 \, k \, \sigma}{3 \, \alpha} \; + \; \frac{2}{3} \, \dot{h} \quad , \quad \dot{\sigma} = - \frac{k}{4} \, \frac{\delta_{\mathsf{r}}}{\alpha} \qquad , \tag{2.22}$$

here the matter velocity is the real part of $i \, \sigma$.

In the weak field approximation the equations for $\dot{h}$ and $\dot{h}_{33}$ are (see eq.s (A1.8)):

$$\ddot{h} + 2 \, \frac{\dot{\alpha}}{\alpha} \, \dot{h} = 8 \pi \, G \, \tau^2 \, \Delta \left[T_{oo} - T/2 \right]$$

$$\tag{2.23}$$

$$\dot{h}_{33} - \dot{h} = i \, k \, 16 \pi \, G \, \tau \, T_{o3} \qquad .$$

the eq.s (A2.5),(A2.6), and(A2.7) give us

$$\Delta \left[T_{oo} \right]_x = \frac{g_x}{h_p^3} \, T_x^4 \int_0^\infty p^2 \, dp \, d\Omega \, f_1$$

$$\Delta \left[T \right]_x = \frac{g_x}{h_p^3} \, m_x^2 \, T_x^2 \int_0^\infty \frac{p^2}{q} \, dp \, d\Omega \, f_1 \tag{2.24}$$

$$\left[T_{o3} \right]_{;x} = - \, \alpha(t) \, \frac{g_x}{h_p^3} \, T_x^4 \int_0^\infty p^3 \, \mu \, f_1 \, dp \, d\Omega \qquad .$$

In what follows it is useful to define the following integrals

$$\left\{ \begin{array}{l} g_I^{(+)} = \frac{1}{2} \int_{-1}^{+1} g \, d\mu = \frac{\sigma_0}{2} \\[3em] g_I^{(-)} = -\frac{i}{2} \int_{-1}^{+1} g \, \mu \, d\mu = \frac{\sigma_1}{2} \end{array} \right. \qquad (2.25)$$

thus eqs. (2.24) become

$$\frac{\Delta[T_{00}]_x}{\rho_x} = c_{1x}^{-1} \int_0^\infty p^3 q \, g_I^{(+)} \frac{e^p}{(e^p + 1)^2} \, dp$$

$$\frac{\Delta[T]_x}{\rho_x} = c_{1x}^{-1} \cdot a^2 \int_0^\infty \frac{p^3}{q} \, g_I^{(+)} \frac{e^p}{(e^p + 1)^2} \, dp$$

$$\hspace{10cm} (2.26)$$

$$\frac{[T_{03}]_x}{\rho_x} = -i \, a \, c_{1x}^{-1} \int_0^\infty g_I^{(-)} \, p^4 \frac{e^p}{(e^p + 1)^2} \, dp \quad .$$

Finally we can write eqs. (2.23) as

$$\left\{ \begin{array}{l} \ddot{h} + 2 \frac{\dot{a}}{a} \dot{h} = 16 \pi G \, \tau^2 \rho_F \left\{ \frac{\Delta[T_{00} - T/2]_F}{\rho_F} + \frac{\rho_x}{\rho_F} \frac{\Delta[T_{00} - T/2]_x}{\rho_x} \right\} \\[3em] \dot{h}_{33} - \dot{h} = -i K 16 \pi G \, \tau \left\{ T_{03_F} + T_{03_x} \right\} \end{array} \right.$$

$$\hspace{10cm} (2.27)$$

for the radiation is $\quad \Delta\left[T_\vdash\right] = 0 \qquad , \quad T_{03_\vdash} = -\frac{4}{3} i \alpha \sigma \rho_\vdash \qquad ;$

then we have

$$
\begin{cases}
\ddot{h} + 2 \frac{\dot{\alpha}}{\alpha} \dot{h} = 6\left[\delta_\vdash + c_x e_{1x} \delta_{x,y}\right] \alpha^{-4} \\[4mm]
\dot{h}_{33} - \dot{h} = \frac{6}{\alpha^3 K}\left[\frac{4}{3}\sigma + c_x e_{1x} \hat{f}_x\right] ,
\end{cases}
\tag{2.28}
$$

where $\delta_{x,y}$ and $\hat{f}_x$ are defined as

$$
\begin{cases}
\delta_{x,y} = e_{1x}^{-1} \int_0^\infty \mathcal{g}_I^{(+)} \frac{p^3}{q}\left[p^2 + \frac{1}{2}\alpha^2\right] \frac{e^p}{(e^p+1)^2} dp , \\[4mm]
\hat{f}_x = e_{1x}^{-1} \int_0^\infty \mathcal{g}_I^{(-)} p^4 \frac{e^p}{(e^p+1)^2} dp .
\end{cases}
\tag{2.29}
$$

With the previous definitions the density contrast δ_x is then

$$
\delta_x = e_{1x}^{-1} \int_0^\infty \mathcal{g}_I^{(+)} q p^3 \frac{e^p}{(e^p+1)^2} dp
\tag{2.30}
$$

to be distinguished from $\delta_{x,y}$ given by (2.29), which enters

as a source term in the equations for the gravitational field.

The set of eqs. (2.21), (2.22) and (2.28) constitute our system of fundamental equations.

In eq. (2.28) the X density perturbations act as source terms for the gravitational field which enters itself as a source term in eq. (2.21), the matter-radiation fluid interacts with the collisionless particles only in eq. (2.28), i.e. through the gravitational field.

The system of preceding equations requires to be numerically integrated; to do this we need an approximate solution which will give us the starting values for the numerical integration; this is done in the next paragraph.

II.3 Solution of the initial system

For $a \ll 1$ it is $\varrho_{1x} \simeq \frac{7}{120} \pi^4$ and eq. (2.13) can be solved analytically, yielding

$$ t = \frac{a^2}{2 \sqrt{1 + \sigma}} \quad , \quad \sigma = c_x \varrho_{1x} \quad . \tag{2.31} $$

The integration starts at a redshift z_{in} such that

$$ \lambda / t_{in} = \frac{4\pi}{K} a_{in}^{-1} \gg 1 \qquad \text{and all the wavelengths of} $$

interest are larger than the horizon scale. For our purpose it is convenient to split g , defined in eq. (2.19), into a sum of even and odd functions

$$g = g^+ + i\, g^- \quad ,$$

then eq. (2.18) becomes

$$\begin{cases} \dfrac{\partial g^+}{\partial t} = \dfrac{P_0}{6}\,\dot{h} + P_2(\mu)\left(\dot{h}_{33} - \dfrac{\dot{h}}{3}\right) + \dfrac{k\mu}{a}\,\dfrac{p}{q}\,g^- \\[4mm] \\[4mm] \dfrac{\partial g^-}{\partial t} = -\dfrac{k\mu}{a}\,\dfrac{p}{q}\,\dot{g}^+ \quad . \end{cases} \qquad (2.32)$$

With the approximation $\lambda/t_{ih} \gg 1$ we can neglect the g^- term in the first of eqs. (2.32), the integration over μ yields

$$\begin{cases} \dfrac{d \cdot g_I^{(+)}}{dt} = \dfrac{\dot{h}}{6} \\[4mm] \\[4mm] \dfrac{d}{dt}\,a\,\dfrac{d g_I^{(-)}}{dt} = -k \displaystyle\int_{-1}^{+1} \mu\,\dfrac{dg^+}{dt}\,d\mu = -\dfrac{k}{30}\left[\dot{h} + 2\dot{h}_{33}\right] \quad , \end{cases} \qquad (2.33)$$

the integration of $\dfrac{d\,g_I^{(+)}}{dt}$, $\dfrac{d\,g_I^{(-)}}{dt}$ over momenta gives

$$\dot{\delta}_x = c_{1x}^{-1} \int_0^\infty p^3 \frac{d\,g_I^{(+)}}{dt} \frac{e^p}{(e^p+1)^2}\, dp \simeq \frac{2}{3}\dot{h}$$

$$\left\{ \rule{0pt}{60pt}\right.$$

(2.34)

$$\frac{d}{dt} \propto \frac{d\dot{\delta}_x}{dt} = -\frac{k}{30}\left[\dot{h}+2\dot{h}_{33}\right]\int_0^\infty p^4 \frac{e^p}{(e^p+1)^2}\, dp \simeq -\frac{2}{15} k\left[\dot{h}+2\dot{h}_{33}\right] .$$

Since at ultrarelativistic epochs $\delta_{x,y} \simeq \delta_x$ we can now try to solve the eq. (2.28) for the gravitational field $\dot{h}$, making the fundamental assumption

$$\delta_x = \delta_{\uparrow} = D(t) ,$$ (2.35)

i.e. we are dealing with adiabatic perturbations.

The first of eqs. (2.28) becomes $\left(\dot{\delta}_{\uparrow} \simeq \frac{2}{3}\dot{h}\right)$

$$a^2 \frac{d}{dt}\, a^2\, \dot{D} = 4(1+\sigma) D ,$$ (2.36)

giving the growing solution

$$D(t) \propto t \propto a^2 \propto h(t) \quad . \tag{2.37}$$

The last expression allows us to find the $\sigma's$ values at ultrarelativistic epochs. The integration of eq.(2.32) gives (we make the hypothesis $h_{33} \propto t$, this will be confirmed later)

$$
\left\{
\begin{aligned}
\sigma^+ &= \left\{ \frac{\dot{h}}{6} + P_2(\mu)\left(\dot{h}_{33} - \frac{\dot{h}}{3}\right) \right\} t = \frac{\gamma}{4} t \\
\\
\\
\sigma^- &= -\frac{2k}{3a} \sigma^+ t = -\frac{2kt^2}{3a} \left\{ \frac{P_1(\mu)}{10}\left(\dot{h} + 2\dot{h}_{33}\right) + \frac{3}{5} P_2(\mu)\left(\dot{h}_{33} - \frac{\dot{h}}{3}\right) \right\} ,
\end{aligned}
\right.
\tag{2.38}
$$

and with the aid of eq. (2.20) for the initial values of the $\sigma's$ it is found

$$
\left\{
\begin{aligned}
\sigma_0 &= \frac{\dot{h}}{3} t_{ih} \\
\sigma_1 &= -\frac{2}{45} k \frac{t_{ih}^2}{a_{ih}} \left(2\dot{h}_{33} + \dot{h} \right) \\
\sigma_2 &= \left(\dot{h}_{33} - \frac{\dot{h}}{3} \right) \frac{t_{ih}}{5} \\
\sigma_3 &= -\frac{2}{35} k \frac{t_{ih}^2}{a_{ih}} \left(\dot{h}_{33} - \frac{\dot{h}}{3} \right) \\
\sigma_\ell &= 0 \quad , \quad \ell \geqslant 4 \quad .
\end{aligned}
\right.
\tag{2.39}
$$

We need now the initial values for σ and $\dot{h}_{33}$. From eq. (2.22) the integration of σ is straightforward and yields

$$\sigma = - \frac{k\,D\,t_{ih}}{6\,a} \qquad . \qquad (2.40)$$

For $\dot{h}_{33}$ we have to solve the second of eqs. (2.28). With the aid of eqs. (2.34), (2.40) we can write

$$\dot{h}_{33} = \dot{h} + \frac{6}{a^3 k}\left[-\frac{2}{5}\frac{kDt}{a} + \sigma\,f_x \right] , \qquad (2.41)$$

then

$$\frac{d}{dt}\,a\,\frac{df_x}{dt} + \frac{2k}{15}\left[3\dot{h} + \frac{12}{a^3 K}\left[-\frac{2}{5}\frac{kDt}{a} + \sigma\,f \right]\right] = 0 \qquad . \qquad (2.42)$$

Since it is $a(t) = (2t)^{1/2}(1+\sigma)^{1/4}$ and $\dot{h} = \dfrac{3}{2}\dfrac{D}{t}$

the last equation can be rewritten as

$$t^{3/2}\frac{d}{dt}\;t^{1/2}\frac{d\mathbf{\mathcal{f}}}{dt}\;+\;\frac{2\sigma\mathbf{\mathcal{f}}}{5(1+\sigma)}\;+\;\frac{kDt}{a}\;\frac{23+27\sigma}{45(1+\sigma)}=0\,,\qquad(2.43)$$

for which the growing solution is

$$\mathbf{\mathcal{f}}(t)=-\frac{2}{9}\;\frac{23+27\sigma}{15+19\sigma}\;\frac{kDt}{a}\qquad.\qquad(2.44)$$

We neglect the homogeneous solution of eq. (2.43) since it gives a less rapidly growing mode with respect to eq. (2.44). Finally it is found that for $\dot{h}_{33}$, through eq. (2.41).

$$\dot{h}_{33}=\frac{39\sigma+35}{38\sigma+30}\;\frac{D}{t}\qquad.\qquad(2.45)$$

For the sake of clarity let us summarize all the initial values

for the variables of our system

$$\dot{h} = \frac{3}{2} \frac{D}{t_{ih}}$$

$$\dot{h}_{33} = \frac{39\sigma + 35}{38\sigma + 30} \frac{D}{t_{ih}}$$

$$\sigma = - \frac{k D t_{ih}}{6 \alpha}$$

$$\bar{\sigma}_0 = \frac{\dot{h}}{3} t_{ih} .$$

$$\bar{\sigma}_1 = - \frac{2}{45} k \frac{t_{ih}^2}{\alpha} \left(2\dot{h}_{33} + \dot{h} \right)$$

$$\bar{\sigma}_2 = \left(\dot{h}_{33} - \frac{\dot{h}}{3} \right) \frac{t_{ih}}{5}$$

$$\bar{\sigma}_3 = - \frac{2}{35} k \frac{t_{ih}^2}{\alpha} \left(\dot{h}_{33} - \frac{\dot{h}}{3} \right)$$

$$\bar{\sigma}_\ell^{\cdot} = 0 \quad , \quad \ell \geqslant 4 \quad .$$

$$(2.46)$$

II.4   Numerical integration

The relation between z and a(t) is

$$1 + z = a(t)^{-1} 3.02 \cdot 10^{5} \, \Omega_x h^2 / \alpha_x^4 \, \beta_x \, \Theta^4 . \qquad (2.47)$$

We choose the initial and final values for z to be $z_{ih} = 10^9$,

$z_{Fih} = 2 \cdot 10^3$. The integration is made with 60 points

$a_1 = a_{ih}$, $a_2, \ldots,$ $a_h = a_{Fih}$: uniformly placed

in the logarithmic interval between a_{ih} and a_{Fih} . The t_h

are pre-calculated and a cubic spline is used to calculate a(t) in

the interval t_h, t_{h+1} .

The time interval Δt is chosen as the smaller of a/100à and

2π a/100 k at each step of integration. The routine which integrates

the set of differential equations is the Merson code of the CERN

library. The required accurancy is fixed to be 10^{-5} , at each time

step.

The integration over p is made for a set of N_p points

chosen in order to perform a Gauss-Laguerre quadrature. We tested

different values of N_p , but taking $N_p = 10$ seems not to increase

the accuracy of the final results, owing to other causes of errors.

The system 2.21 is truncated at a suitable l_{max} (chosen to be even) at the last equation for σ_l is therefore

$$\dot{\sigma}_l = \frac{k}{\sigma} \frac{p}{g} \sigma_{l-1} \frac{l}{2l+1} \quad , \quad l = l_{MAX} \quad . \quad (2.48)$$

As a convergence criterion for the set of variables we take at z_F

$$\left| \sigma_{l_{MAX}} / \sigma_3 \right| \leq 10^{-2} \quad , \quad (2.49)$$

at least for the first six points of the Gauss-Laguerre integration.

The initial amplitude for the δ's are $\delta_r(z_{in}) = \delta_x(z_{in}) = 10^{-4}$.

The following cases have been considered: $\alpha^3_x = \alpha^3_y = 4/11$, $\beta_x = \beta_r = 6$ (neutrino species); $\alpha^3_x = \frac{1}{25}$, $\beta_x = 2$; $\alpha^1_x = \frac{1}{90}$, $\beta_x = 2$.

The values of k have been chosen in order to cover the mass range $M_x = (10^9 - 10^{20}) M_\odot$, with 5 values of k for

each order of magnitude in M_X .

II.5   The concept of mass variance

In the discussion of our results we shall see later that a useful

concept is the mass variance one. We dedicate a paragraph to the mass

variance concept, since many of the results that we have got make use

of it.

The mass variance $\delta M/M$ is defined as the r.m.s. mass fluctuations

in the mass found within a randomly chosen sphere of radius R.   With

this definition $(\delta M/M)^2$ is given by (LSS, § 26)

$$\left(\frac{\delta M}{M}\right)^2 = \frac{1}{V^2} \iint \frac{[\rho(\vec{x}_1) - \bar{\rho}][\rho(\vec{x}_2) - \bar{\rho}]}{\bar{\rho}^2} d^3x_1 \, d^3x_2 , \quad (2.50)$$

where V is the sphere volume.

In the linear theory two simplifying assumptions are that the Fourier

transform δ_k of the primeval density contrast has a power law form

$|\delta_k|^2 = A \, k^h$, A being an arbitrary constant, and each of

the δ_k components has a randomly assigned phase. There is no

'a priori' justification for these assumptions, but they seem reasonable

and are not in contradiction with observations. With the random phase

assumption the integral (2.50) can be calculated, yielding

$$\left(\frac{\delta M}{M}\right)^2 = \frac{V}{(2\pi)^3} \int d^3k \; |\delta_k|^2 \; W(k R) \quad , \tag{2.51}$$

here is

$$W(y) = \frac{9}{y^6} \left[\sin y - y \cos y \right]^2 \quad , \tag{2.52}$$

so that $W(y \ll 1) \simeq 1$ and $W(y \gg 1) \simeq y^{-4}$.

For $-3 < h < 1$ the integral (2.51) gives ($M \propto k^{-3}$)

$$\left(\frac{\delta M}{M}\right)^2 \simeq \text{const} \times \int_0^{k(M)} |\delta_k|^2 k^2 \, dk \; \propto \; M^{-1-\frac{h}{3}} \quad . \tag{2.53}$$

For $h = 1$ at large k the argument of the integral behaves as $k^{h+2} k^{-4} \propto k^{-1}$ and the integral diverges.

The reason is that increasing h we increase the amplitude of the spectrum at small scales $(\ |\delta_k|^2 \propto M^{-h/3}\ )$ and $\delta M/M$ becomes sensible to the fluctuations at the edge of the sphere, which has a sharp boundary. The difficulty can be avoided introducing a gaussian window e^{-r^2/R^2} in the integral (2.50) (we are simply smearing the boundaries of the sphere). In such a case the integral (2.51) is still a good approximation to calculate $\delta M/M$, unless $h > 4$ (Peebles and Groth 1976). For $h > 4$, when the small scale matter distribution enters in the non-linear regime, the coupling between perturbations with different wavelengths becomes important and the linear theory cannot be applied (Press and Schechter 1974).

However in this discussion we shall always consider $h \leq 4$.

For small fluctuations $(\ \frac{\delta M}{M} \ll 1\ )$ in an Einstein-De Sitter Universe $\frac{\delta M}{M}$ will grow as $\frac{\delta M}{M} \propto (1+z)^{-1}$ after recombination.

An important property of $\frac{\delta M}{M}$ is that the growth of $\frac{\delta M}{M}$ on mass scale M, which is still in the linear regime $(\ \frac{\delta M}{M} \ll 1\ )$ is unaffected by non linear clustering $(\ \frac{\delta M}{M} \gg 1\ )$ below the mass scale M. The proof of this is complicated and it involves an appropriate solution of the $BBGKY$ equation (Davis and Peebles 1977, LSS § 70). Let us try to give here a rough justification of it: if we model the matter as a particle distribution

with mean number density N , then $\delta M/M$ is a measure of the number

excess $\delta N/N$ of galaxies from a uniform distribution within distance

R of a randomly chosen galaxy; clearly the value of $\delta N/N$ will not

change if several points inside the sphere are strongly clustered on

scales $r \ll R$.

II.6   Results and discussion

In Fig.s 2.1 − 2.3 we show the time evolution of the $\delta's$,

for several values of the mass and $\alpha^3_\chi = \dfrac{1}{25}$. In the case

$\alpha^3_\chi = \dfrac{1}{50}$ the shape of the curves is similar.

The final amplitudes

$$\left| \delta_k \left(z = z_{Fin} \right) \right|$$
(2.54)

are plotted in Fig.s 2.4 − 2.6. In the figures the values of n refer

to·the initial amplitudes at a fixed redshift which are supposed to be

$| \delta_k |^2 = A \, k^n$. The final amplitude for $n = 0$

yields a sort of transmission factor for any kind of initial $\delta's$.

The physical meaning of this factor has already been discussed in the literature (Bond et al 1982; Blumenthal et al 1982). The main difference between the photino case and the neutrino one is that photinos become nonrelativistic earlier than the Universe becomes dominated (at a redshift z_{eq}). The X perturbation which enter the horizon at a redshift $z_H > z_{eq}$ show a characteristic plateau between z_H and z_{eq}, while the matter-radiation density is still sufficiently great to inhibit the growth of δ_X. Fluctuations will survive only if they involve a mass $M > M_{X_c} \simeq m_{p\ell}^3 \, m_X^{-2} \simeq 10^{12} \left[m_X / keV \right]^{-2} M_\odot$ (free-streaming scale), here $m_{p\ell}$ is the Planck mass. The mass variance $\frac{\delta M}{M}$ is obtainable from the approximate relation

$$\left(\frac{\delta M}{M}\right)^2 \simeq \frac{V}{2\pi^2} \int_0^{k(M)} k^2 \, |\delta_k|^2 \, dk \quad , \qquad (2.55)$$

which has a transparent physical meaning. However, in our results, a more detailed expression of the window function is used (LSS § 26), as it does not imply technical difficulties. However the quality of the results is not likely to be much improved by this more accurate approach, owing to the large number of other uncertain elements involved.

The final mass variances are shown in Fig.s 2.7 — 2.9, where $\frac{\delta M}{M}$ is set to 1 at the low mass end. An interesting difference between photinos and neutrinos is the large mass-range in $\frac{\delta M}{M}$ for different spectral indices n.

This occurs since, in the photino case, for $M \gg M_{\chi_c}$ the final spectrum δ_k depends strongly on n. Assuming that the distribution of visible matter is a good trace of the dark, Fig.s 2.7—2.9 give an indication of the mass scale which first reaches the non-linear regime.

Observationally $\frac{\delta M}{M}$ may be determined through $\xi(r)$, the two-point correlation function (LSS). According to Peebles (1981):

$$\left(\frac{\delta M}{M}\right)^2 = \frac{3 J_3}{x^3} \qquad , \qquad J_3(x,t) = \int_0^X x^2 \, \xi(x,t) \, dx . \quad (2.50)$$

$\frac{\delta M}{M}$ is now $\simeq 1$ over scales $R \simeq 8 h^{-1} M_{pc}$ meaning that a mass scale, in baryons and collisionless matter, $M \simeq \left(10^{15} - 10^{16}\right) M_\odot$ is now reaching a non-linear collapse. Assuming that galaxies formed at $1 + z_G = 5 \pm 2$, according to the QSO distribution in z, we have $\frac{\delta M}{M}\left(R \simeq 8 h^{-1} M_{pc}\right) = \frac{1}{1 + z_G}$ at the redshift z_G.

The considered ranges are shown as boxes in Fig.s 2.7—2.9. The

position of these boxes seems to indicate that an $n = 0$ spectrum is strongly favoured in a photino dominated Universe. The conclusion which is drawn from Fig.s $2.7 - 2.9$ is that the case $\Omega_x = 1$, $m_x = 2 \, keV$, $n = 0$ (white noise) is in good agreement with the observed clustering over scales $R < 10 \, h^{-1} \, Mpc$. Also the $n = 1$ case is marginally consistent, owing to observational errors. This is in contrast to a neutrino dominated Universe, where only spectra with $n > 2$ would be allowed.

We should finally like to make some comparisons with the results obtained in previous papers by other authors dealing with related problems. In the neutrino case ($\alpha^\lambda_\nu = 4/11$, $g_\nu = 6$) the final amplitude δ_k can be compared with that obtained by Peebles (1982). From Fig. 2.4 the amplitude δ_k at $M = 10^{14} \, M_\odot$ and $n = 0$ is down from the $k = 0$ limit by a factor $10^{3.8}$. For this mass it is found that $\frac{k}{\ell} = 0.7$ and from curve 5 in Fig. 2 ($\alpha^\lambda_\nu = \frac{4}{11}$, $g_\nu = 4$) of Peebles (1982) δ_k is down by factor $10^{3.1}$. The difference is then limited to a factor 5 which can be entirely ascribed to the different values of g_ν considered in the two cases: if Ω is fixed, increasing g_ν , the neutrino mass is reduced. The damping at small masses is then less severe.

For the photino case a further comparison for the final δ_k can be made with the paper of Bond et al. (1982).

After rescaling the results to those in Fig. 2 of Bond et al. (1982)

$\delta(z)$

$M_x = 6.1 \cdot 10^{15} M_\odot$

$1+z$
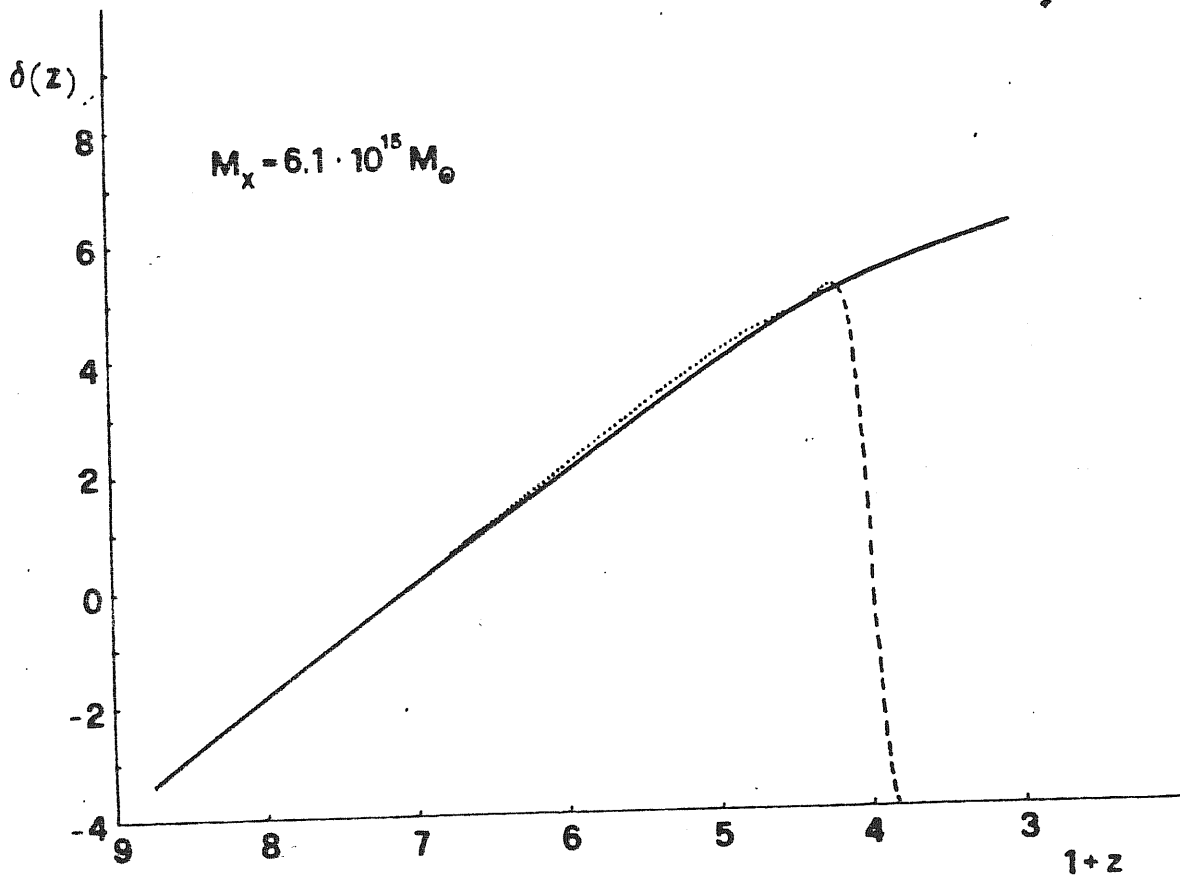
Fig. 2.1 Time evolution for δ_x and δ_{rad}, in the case $\alpha_x^3 = \frac{1}{25}$, $\beta_x = 2$, $\Omega_x = 1$, $h = 1$, $k \doteq 0.01$. The solid line is δ_x, the dashed one is δ_{rad}. The dashed line is terminate at the first zero of δ_{rad}.
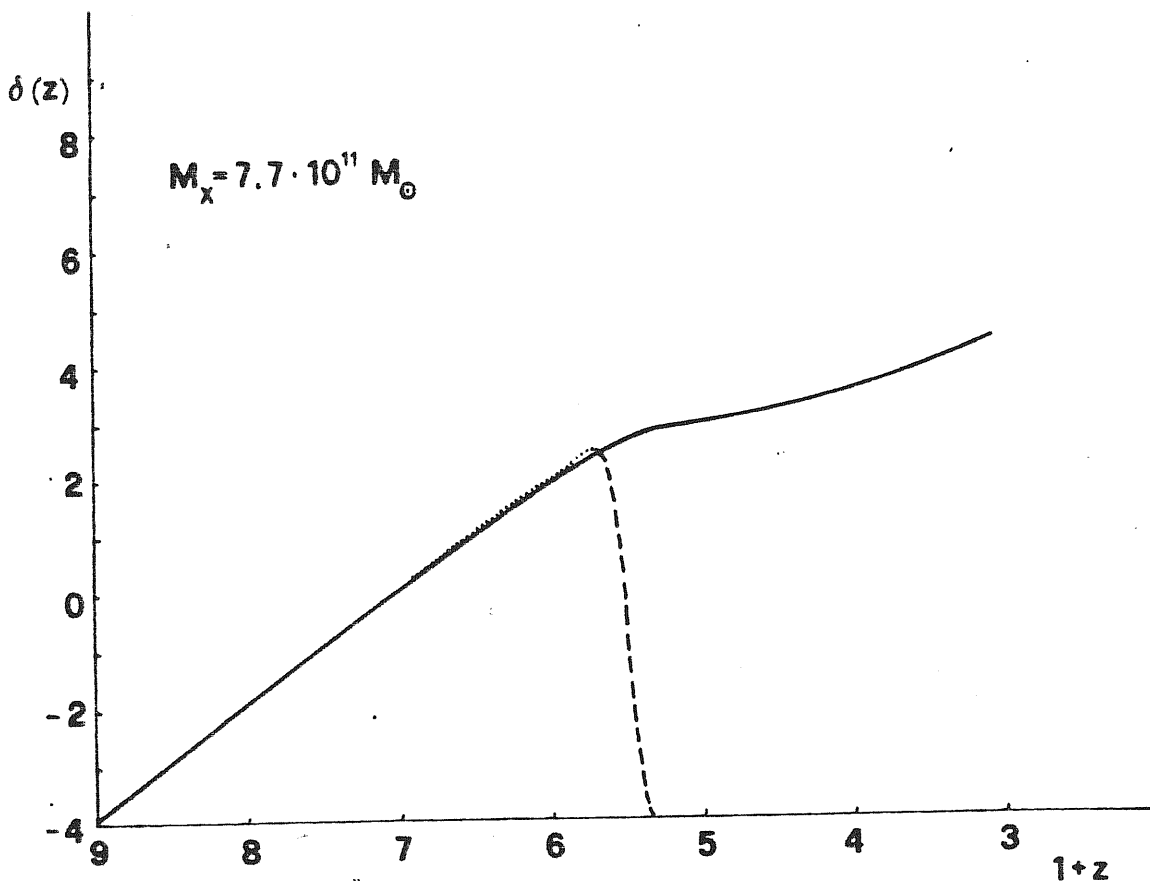
Fig. 2.2   The same as for Fig. 2.1, except for k = 0.2.
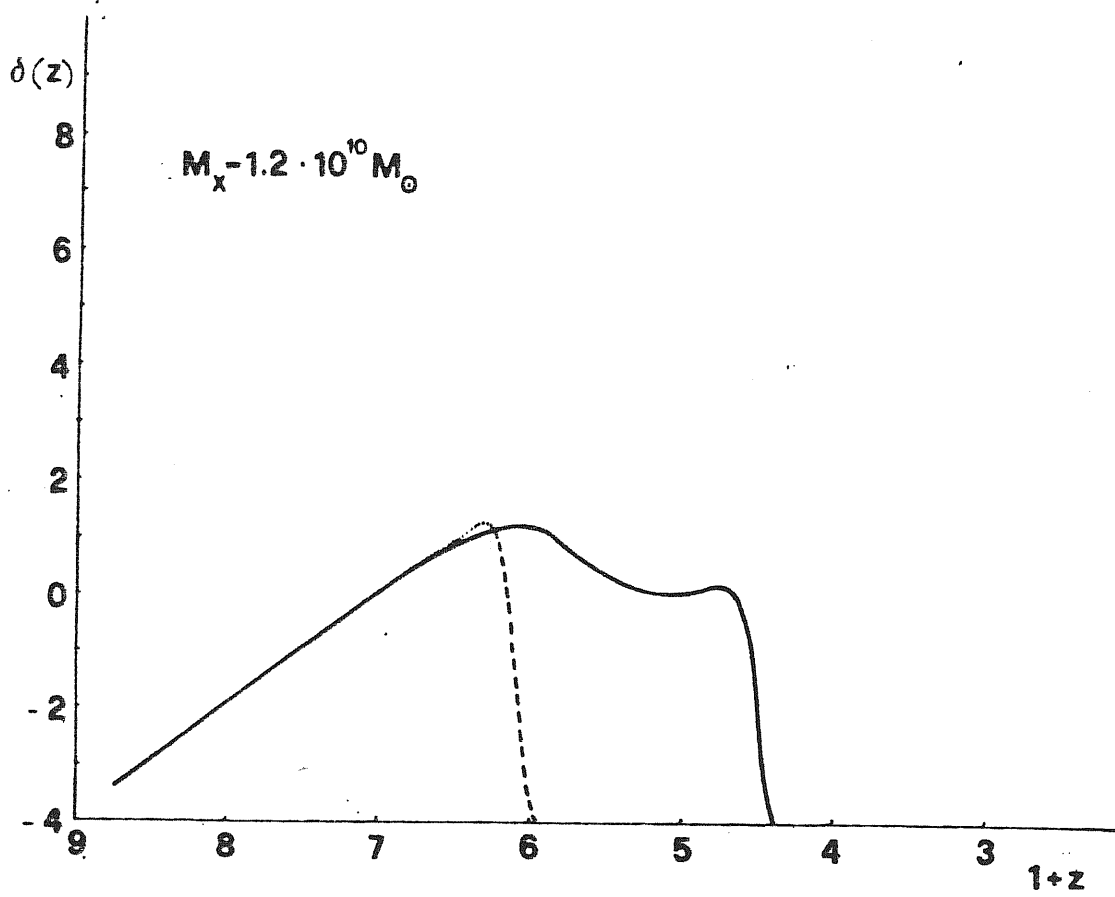
Fig. 2.3   The same as for Fig. 2.1, except for k = 0.8.
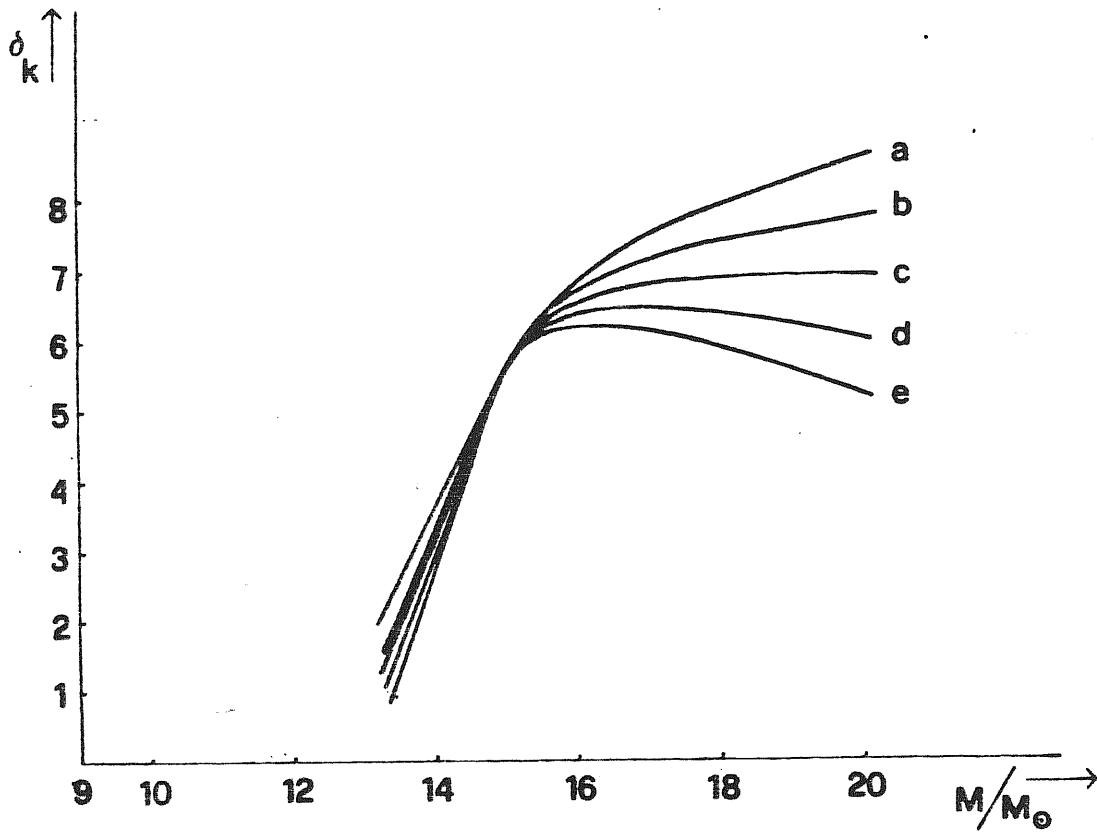
Fig. 2.4   Final amplitudes δ_k, as a function of k, for different spectral indices n

(a: n = -2; b: n = -1; c: n = 0; d: n = 1; e: n = 2) in a neutrino domin-

ated Universe.   Here $\alpha_x^3 \equiv \alpha_\nu^3 = \frac{4}{11}$, $\beta_x = \beta_\nu = 6$, $\Omega = 1$, h = 1.
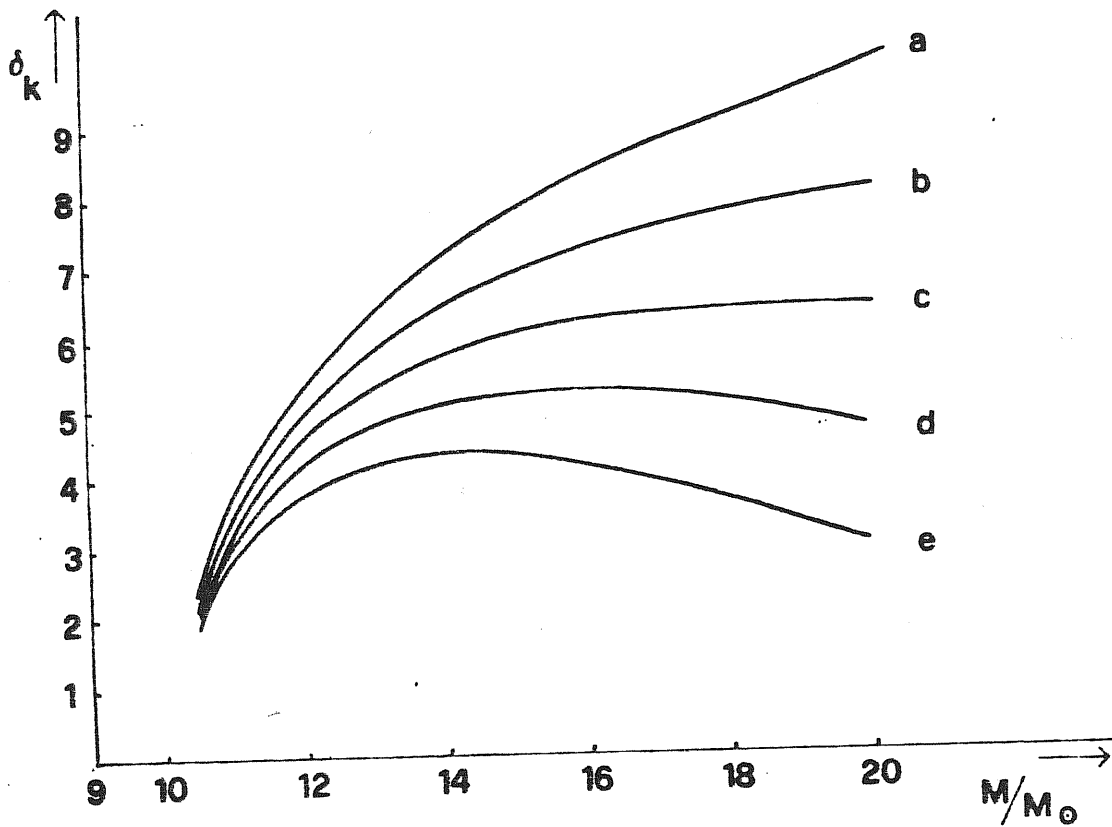
Fig. 2.5   As in Fig. 2.4 in the photino case $\alpha_x^3 = \frac{1}{25}$, $\beta_x = 2$, $\Omega_x = 1$, $h = 1$.
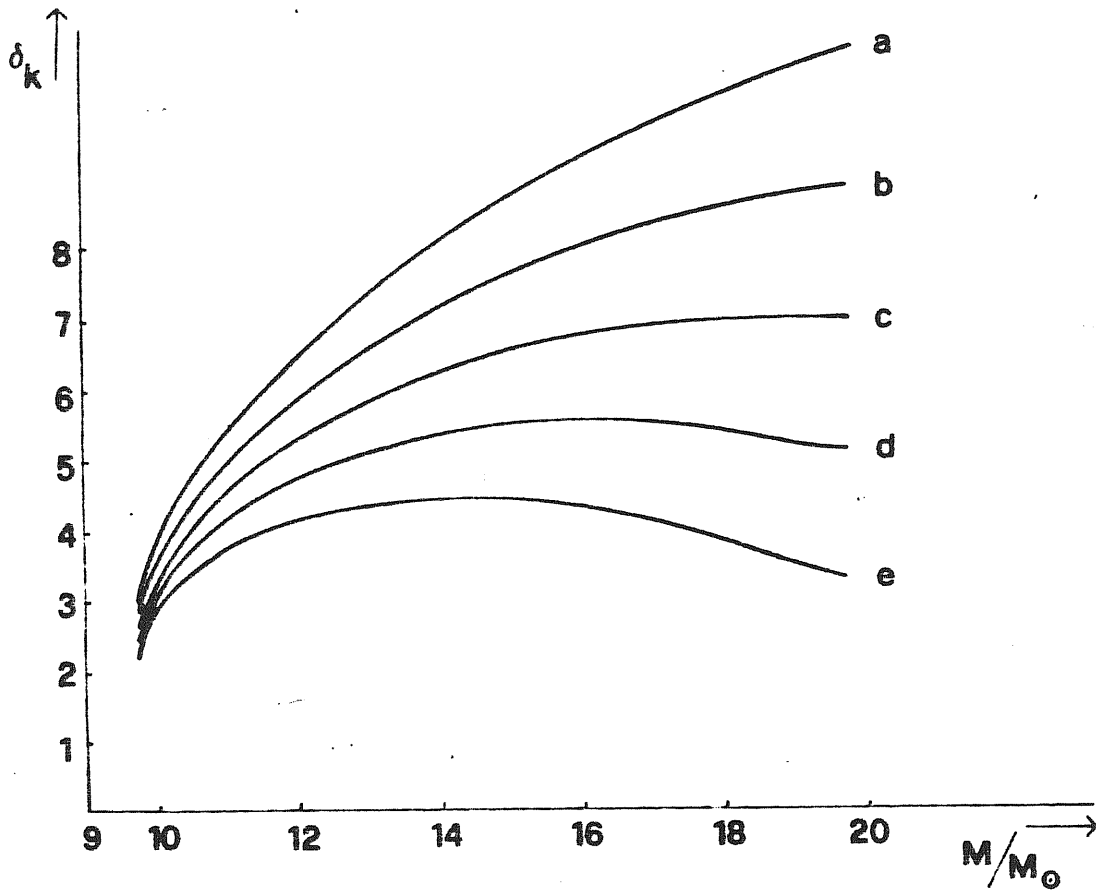
Fig: 2.6   The same as for Fig. 2.4 for $\alpha_x^3 = \frac{1}{50}$, $\beta_x = 2$, $\Omega_x = 1$, $h = 1$.
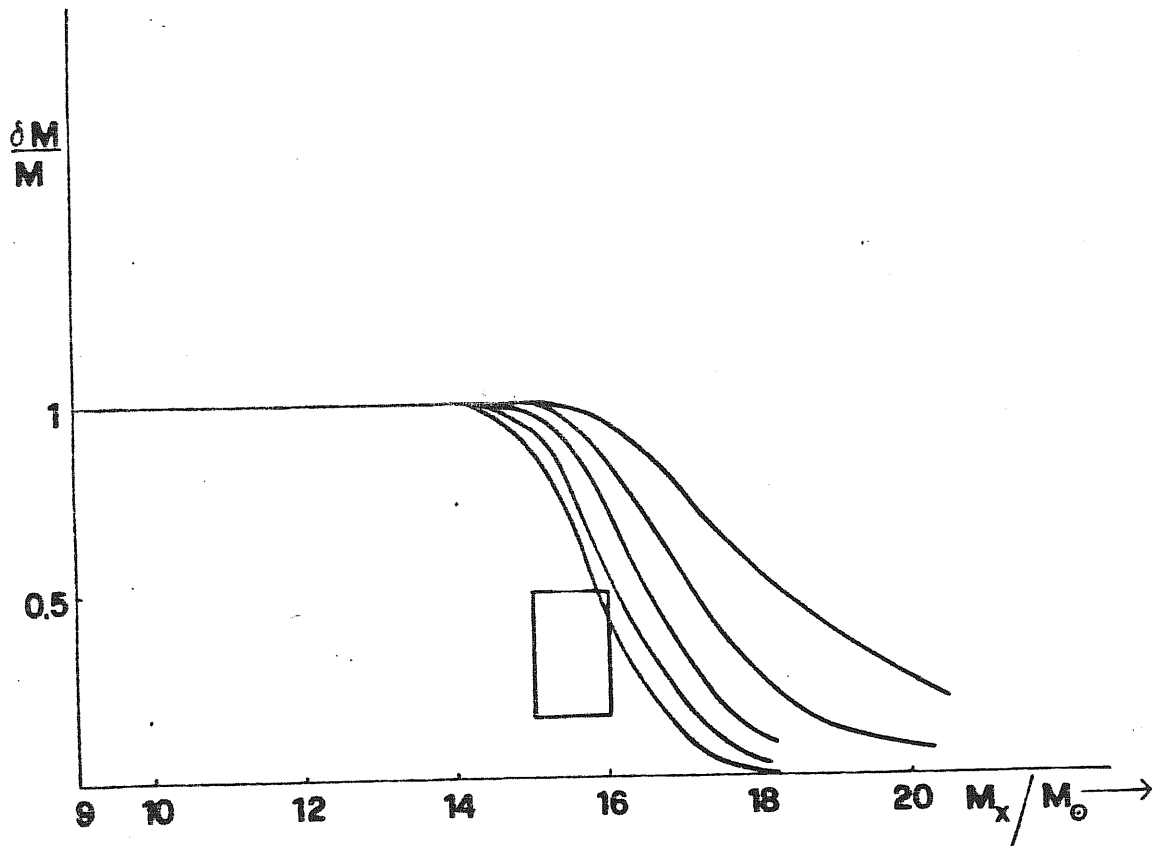
Fig. 2.7   Final mass variance, plotted as function of M, in a neutrino dominated

.. Universe $\alpha_x^3 = \alpha_\nu^3 = \dfrac{4}{11}$, $\beta_x = \beta_\nu = 6$.   The meaning of a,b,c,d,e is the same

as in Fig.s 2.4,2.5,2.6.
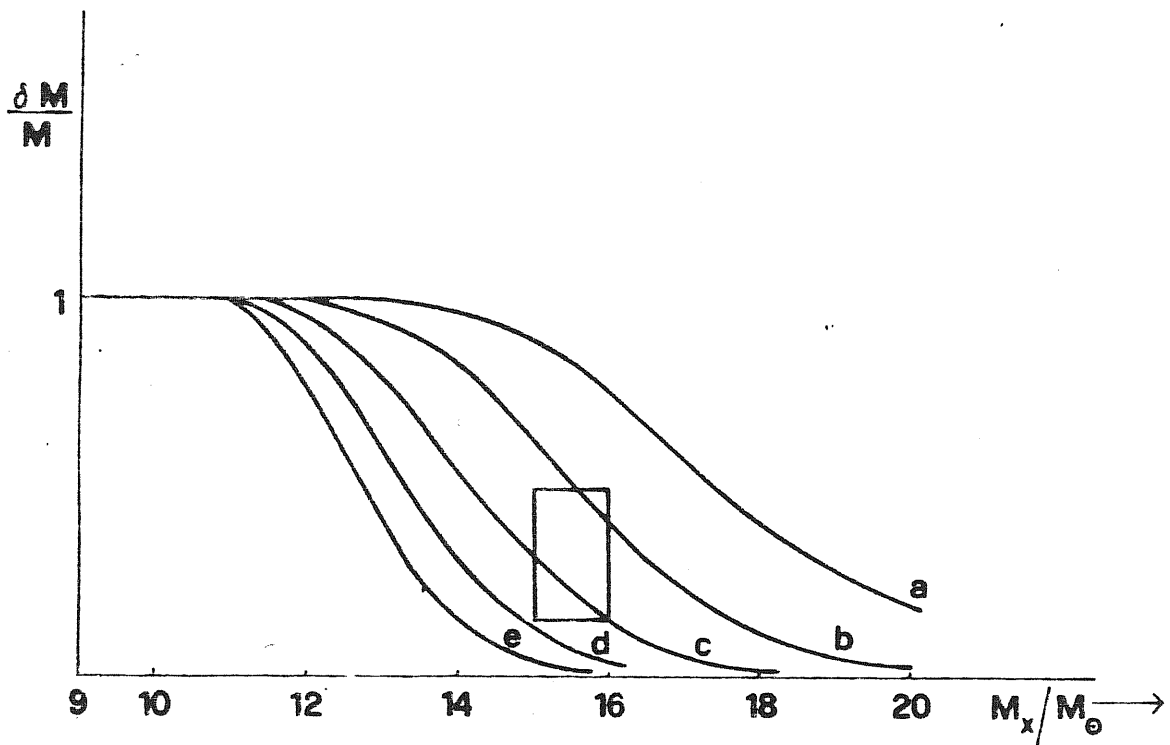
Fig. 2.8   As in Fig. 2.7, but in a photino dominated Universe, with $\alpha_x^3 = \frac{1}{25}$, $\beta_x = 2$,

$\Omega_x = 1$, $h = 1$.
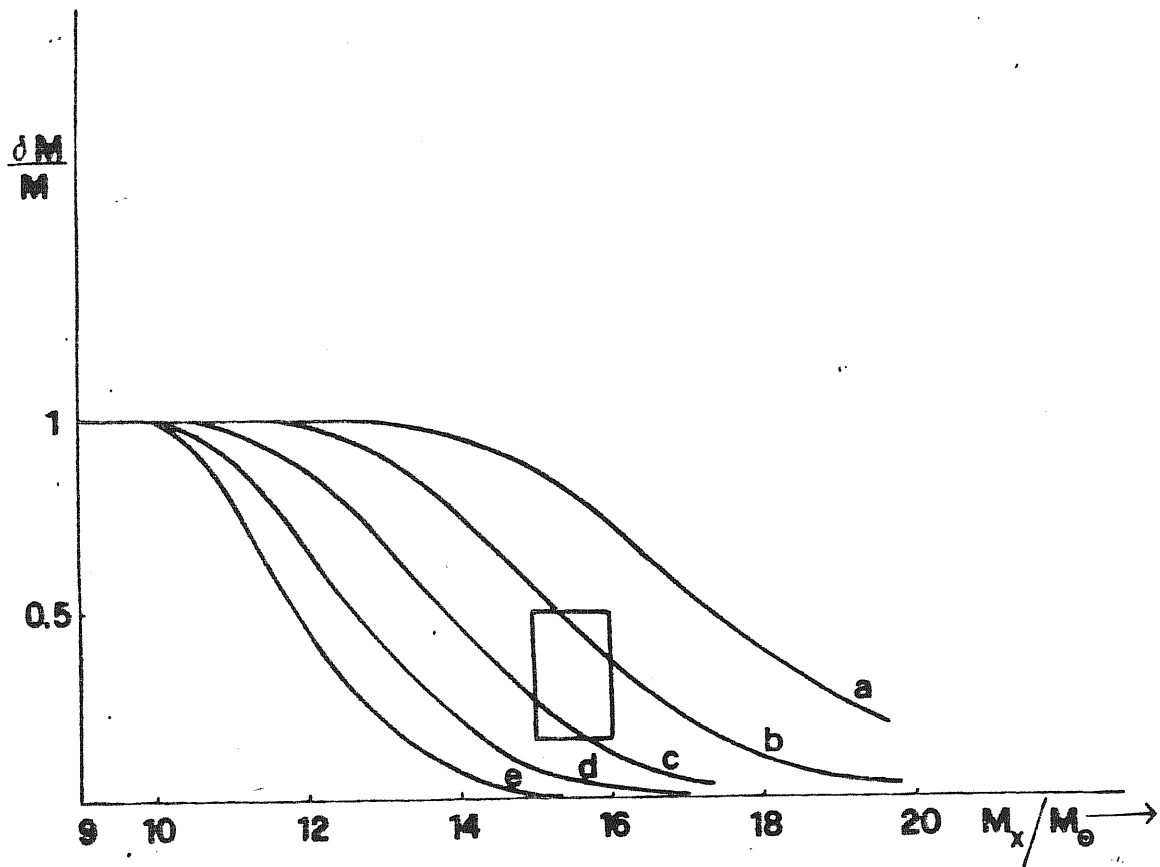
Fig. 2.9   The same as for Fig. 2.8, in the case $\alpha_x^3 = \frac{1}{50}$, $\beta_x = 2$.

it is found that $\frac{\delta\rho}{\rho} = k^{3/2} |\delta_k|$ (for $\alpha^3{}_X = \frac{1}{25}$, $\beta^3{}_X = \nu$

and $n = 0$) is in good agreement with their X case except for the

bending of the spectrum at low masses (M $< 10^{12} M_{\odot}$),

which is slightly steeper in our case. The difference can be entirely

attributed to the different X masses which in the two cases have

been considered. For $\alpha^3{}_X = \frac{1}{25}$, $\beta_X = \nu$ $\Omega_X = 1$ this is

m_X = 880 eV, while in Bond et al. (1982) m_X = 1 keV. However

using the full mass variance instead of $K^{3/2} |\delta_k|$ is likely to

be more significant.

Fluctuation evolution in a two component dark mass model

In the following paragraphs we investigate the evolution of

adiabatic perturbations in a scenario dominated by dark matter made of

two kinds of collisionless quanta of different masses. These masses

are taken around 10 eV (massive γ) and in the keV

range (X-particles, tentatively photinos). We considered γ-dominated

and X-dominated cases. While the γ component moderately alters the

dynamics of X-dominated models, we find that the presence of X-particles

even as a minor component of dark mass, can lead to a drastic

modification of the density fluctuation spectra, at the beginning of

non-linear stages (Valdarnini and Bonometto 1984).

II.7   Notations

Our fundamental assumptions are the same which have been used to investigate the evolution of adiabatic perturbations in a X-dominated Universe. The total background density

$$\rho = \rho_h + \rho_\gamma + \rho_x \qquad (2.57)$$

is assumed to be critical. Both γ and X are assumed to decouple from radiation before the beginning of our computation.   The suppression factors

$$\alpha_\gamma = T_\gamma / T_{rad} \quad , \quad \alpha_x = T_x / T_{rad} \qquad (2.58)$$

are therefore constants over all the period of our computation (T_γ and T_x are background temperatures).

The ratio of the energy densities ρ_r, ρ_x to the radiation energy density ρ_r are given by

$$\frac{\rho_r}{\rho_r} = c_r \, e_{1r} \qquad , \qquad \frac{\rho_x}{\rho_r} = c_x \, e_{1x} \qquad , \qquad (2.59)$$

here is $c_{r,x} = \dfrac{15 \, \beta_{r,x} \, \alpha_{r,x}^4}{2 \pi^4}$, β_x (β_r) is the sum of spin degree of freedom for $X(\gamma)$ particles, and

$$e_{1 \, x,r} = \int_0^\infty p^2 \, q_{x,r} \, \frac{dp}{e^p + 1} \qquad (2.60)$$

$$q_x = \left(p^2 + m_x^2 / T_x^2 (t) \right)^{1/2} , \quad q_r = \left(p^2 + m_r^2 / T_r^2 (t) \right)^{1/2} .$$

In what follows our scale factor will be normalized so that

$$a(t) = m_x / T_x(t) \qquad (2.61)$$

then

$$q_x = \left(p^2 + a^2\right)^{1/2} \quad , \quad q_r = \left(p^2 + (a/a_r)^2\right)^{1/2} \quad , \tag{2.62}$$

with

$$a_r^{-1} = \frac{m_r}{m_x} \frac{\alpha_x}{\alpha_r} \quad .$$

The masses $m_{x,r}$ are given by

$$m_{x,r} = 70.5 \ \Omega_{x,r} \ h^2 / d^3_{x,r} \ g_{x,r} \ eV \tag{2.63}$$

as usual Ω_x (Ω_r) is the density parameter for $X(r)$.

With the choice of (2.61) for the scale factor $a(t)$ its present value a_0 , and our time and length units are the same as that given by eq.s (2.10), (2.11) and (2.12).

The equation for $a(t)$ is then

$$\frac{da}{dt} = \left(1 + c_x \ e_{1x} + c_r \ e_{1r}\right)^{1/2} a^{-1} \quad . \tag{2.64}$$

The mass associated with a perturbation of wavelength $\lambda = 2\pi a(t) k^{-1}$ is given by

$$M = 3.10^{14} k^{-3} \alpha_x^{12} \beta_x^3 / (\Omega_x h^2) \ M_0 \ , \qquad (2.65)$$

which is the same as eq. (2.16) for an X-dominated Universe $(\Omega_x = 1, \Omega_y = 0)$

This is not surprising since we have chosen $\Omega = \Omega_x + \Omega_y = 1$ and the choice of the X parameters Ω_x, β_x and α_x fully determines our length scale.

The analysis made in § II.2, II.3 can be repeated here for the two component case. Here we give only the system of equations and the solution of the initial system. The equations for $\dot{h}$ and $\dot{h}_{33}$ are

$$\ddot{h} + 2 \frac{\dot{a}}{a} \dot{h} = 6 \left[\delta_r + c_x e_{1x} \dot{\delta}_{x,y} + c_y e_{1y} \delta_{y,y} \right] a^{-4}$$

$$(2.66)$$

$$\dot{h}_{33} - \dot{h} = \frac{6}{a^3 k} \left[\frac{4}{3} \sigma + c_x e_{1x} \delta_x + c_y e_{1y} \delta_y \right] ,$$

with $\delta_{x,y}$, $\delta_{r,y}$, ϱ_x and ϱ_r given by

$$\delta_{x,y} = \frac{1}{2} \, e_{1x}^{-1} \int_0^\infty dp \, \frac{p^3}{q} \, \sigma_{0x} \left[p^2 + \frac{1}{2} \, a^2 \right] \frac{e^p}{(e^p + 1)^2}$$

$$\delta_{r,y} = \frac{1}{2} \, e_{1r}^{-1} \int_0^\infty dp \, \frac{p^3}{q_r} \, \sigma_{0r} \left[p^2 + \frac{1}{2} \left(\frac{a}{a_r} \right)^2 \right] \frac{e^p}{(e^p + 1)^2}$$

$$\varrho_x = \frac{1}{2} \, e_{1x}^{-1} \int_0^\infty dp \, p^4 \, \sigma_{1x} \frac{e^p}{(e^p + 1)^2}$$

$$\varrho_r = \frac{1}{2} \, e_{1r}^{-1} \int_0^\infty dp \, p^4 \, \sigma_{1r} \frac{e^p}{(e^p + 1)^2} \qquad . \tag{2.67}$$

The $\sigma_{x,r}$'s satisfy the set of equations

$$\left\{ \begin{array}{l}
\dot{\sigma}_{0\,x,r} = \dfrac{k}{\alpha} \, \dfrac{p}{q_{x,r}} \, \sigma_{1\,x,r} + \dfrac{\dot{h}}{3} \\[3em]
\dot{\sigma}_{\ell\,x,r} = \left(\dfrac{\ell}{.} \right) \dfrac{k}{\alpha} \, \dfrac{p}{q_{x,r}} \left[\sigma_{\ell+1\,x,r} \, \dfrac{\ell+1}{2\ell+1} + \sigma_{\ell-1\,x,r} \, \dfrac{\ell}{2\ell+1} \right] + \\[2em]
\qquad \left(\dot{h}_{33} - \dfrac{\dot{h}}{3} \right) \dfrac{\delta_{\ell 2}}{5} \quad , \quad \ell \geq 1 \quad .
\end{array} \right.$$

Finally the x and r density contrast read

$$\delta_{x,r} = \frac{1}{2} \, e_{1\,x,r}^{-1} \int_0^\infty dp \, p^3 \, q_{x,r} \, \sigma_{0\,x,r} \frac{dp}{(e^p + 1)^2} \qquad . \tag{2.69}$$

Initial condition can be conveniently set at $T \gg m_\chi$ when all components are relativistic and the system made of the above equations can be analytically integrated. Then dynamical variables relate to as follows:

$$\sigma = - \frac{k}{a} \frac{t}{6} \delta_r$$

$$\dot{h} = \frac{3}{2} \frac{\delta_r}{t}$$

$$\dot{h}_{33} = \frac{3\omega + 3S}{38\omega + 30} \frac{\delta_r}{t}$$

$$\sigma_0 = \frac{\dot{h}}{3} t$$

$$\sigma_1 = - \frac{2t^2}{45} \frac{k}{a} \left(2\dot{h}_{33} + \dot{h} \right)$$

$$\sigma_2 = \frac{t}{5} \left(\dot{h}_{33} - \frac{\dot{h}}{3} \right)$$

$$\sigma_3 = - \frac{2t^2}{35} \frac{k}{a} \left(\dot{h}_{33} - \frac{\dot{h}}{3} \right)$$

$$\sigma_\ell = 0 \qquad , \quad \ell \geq 4 \ .$$

$$(2.70)$$

Here $\omega = (\rho_r + \rho_\chi) / \rho_r$ at the time t. Provided that the temperature $T \gg m_\chi$ at t, (2.70) however hold.

II.8   Numerical integration

We integrated numerically our system from a redshift $z_{in} = 10^9$

down to $z_{fin} = 2 \cdot 10^3$. At z_{in} particles with $m \leq 10^3$ eV are still

ultrarelativistic. At z_{fin} particles with $m \geq 5$eV are already nonrelativistic.

The independent variable was t and the integration steps were taken

to be

$$\Delta t = 10^{-2} MIN \left(a / \dot{a} , \lambda \right) \qquad (2.71)$$

This step length was then reduced up to 100 times more by the MERSON

integration routine of the Cern library. A finite number of ℓ and p

were chosen. The p points were fixed in order to allow Gauss-Laguerre

integration over such a variable when performing the integrals in 2.60

and 2.67. We limited the number of p points to 10, after checking

a number of cases also with 7 and 14 points and finding a difference in

the final values of physical variables never exceeding 5% (and mostly

below it) when passing from 10 to 14 points.

To fix the value ℓ_{max} of (ℓ_{max} + 1 variables   ), we set

the constraints that

$$\left| \bar{\sigma}_{\ell_{MAX}} / \bar{\sigma}_3 \right| \leqslant 10^{-3} \quad , \qquad (2.72)$$

even at z_{fin}. This requirement would lead to different ℓ_{max} according to M. We can make a zero-th order evaluation of ℓ_{max} by considering the system 2.68, where the term which drives stimulus from small to great ℓ is $(k/a)(p/q)$. This term is large for large K (small M) while $\frac{p}{q}$ never exceeds the unit.

However it is then clear that for large p (if the regime is not ultrarelativistic) it may be needed to consider more harmonics. For this reason our ℓ_{max} was variable with p; this allowed to reduce considerably the integration time.

The precision requested to the integration routine was 10^{-5} . It is however known that this precision applies to each step. Then we checked how the final results varied changing the required precision. In the cases we considered we found that results varied by less than 3% if the precision varied from 3.10^{-4} to 10^{-6} . Therefore we believe that our results may be affected by a numerical error which should not exceed such a percentage.

II.9   Results and discussion

(a) $z \geqslant 2000$

We shall report here results concerning the numerical integration

of the following cases:

A) $\Omega_x = 0.2$, $\Omega_y = 0.8$, $\alpha^3_x = 0.04$

B) $\Omega_x = 0.2$, $\Omega_y = 0.8$, $\alpha^3_x = 0.02$

C) $\Omega_x = 0.8$, $\Omega_y = 0.2$, $\alpha^3_x = 0.04$

D) $\Omega_x = 0.8$, $\Omega_y = 0.2$, $\alpha^3_x = 0.02$

In all above cases we took $\alpha^3_y = 4/11$; $\Omega_x + \Omega_y = 1$, $\beta_x = 2$, and $\beta_y = 6$.

The integration was started at z_{in} with an equal $\delta_x = \delta_y = \delta_r$

over all mass scales. This corresponds to assuming an initial spectrum

with n = 0. Of course, in the linear approximation, other initial spectra

are obtained just multiplying the final δ_k by $k^{n/2}$. We took the

values of k in such a way that at least 5 values of mass were considered

for each decade in M.

For collisionless systems a critical mass scale M_c exists under

which density fluctuations are gradually erased. Here M_c is defined as

the mass-scale for which the mass-variance $\delta M/M$ holds 0.95

(at z = 2000) assuming an initial spectrum with n = 0 (see equation 2.55

and the discussion thereafter). The value of M_c would be even more different

if other values of n were taken. Such n dependence becomes increasingly

relevant as greater masses of the collisionless component quanta are

considered. In the following table the values of the relevant parameters

for the different cases are shown.

TABLE

case	$M_{C(X)}/M_\odot$	$M_{C(\nu)}/M_\odot$	$m_X(eV)$	$m_\nu(eV)$
A	2.10^{13}	10^{15}	176	25.8
B	3.10^{12}	9.10^{14}	352	25.8
C	5.10^{11}	10^{14}	705	6.5
D	10^{11}	10^{14}	1410	6.5

The value of m_X for the case A hardly fits the photino mass range.

There are however a number of , possibilities for inserting such

a particle in different schemes of fundamental interactions.

In fig. 2.10 - 2.13 the evolution of the density contrasts is shown

(for a number of cases). The principal results can be summarized as follows.

While, for $M > M_{c(\nu)}$, δ_X and δ_Y show a continuous growing (fig. 2.13), for

$M < M_{c(\nu)}$, the ν density fluctuation, initially erased at the entry

in the horizon essentially because of Landau damping, has a later restart.
This effect is to be entirely attributed to the presence of gravitational
potential wells due to X density fluctuations; they are able to re-capture
γ 's as soon as the critical mass for γ gravitational instability
has become sufficiently low. As a more severe damping of initial γ
fluctuations corresponds to a longer permanence of γ -fluctuations below
such critical mass, this secondary growing of γ -perturbations has a
later start for mass scales which were more drastically affected by
free-streaming. For mass scales $M < M_{c(X)}$ both γ and X are erased
and no possibility of later growing modes is to be expected. This can
be seen clearly in fig. 2.10 where the slight γ -oscillations are
likely to be ascribed to a response to the gravitational field due to
oscillating δ_{γ} .

As a consequence of these effects a γ component of density
fluctuations in the mass range $10^{11}.M_\Theta < M < 10^{15} M_\Theta$ is
present at recombination. How and how much this component depends on
different parameters can be understood from Fig. 2.14 – 2.17, where the
density contrasts are plotted as z_{fin} = 2000. For a given α_X the
growing of δ_{γ} below $M_{c(\gamma)}$ is obviously more relevant for X-dominated
models (cases C and D) rather than for γ -dominated ones (cases A
and B). For a given Ω_X , considering smaller α_X leads to greater

m_X and hence lower $M_{c(X)}$ values. Therefore the growing of δ_γ below $M_{c(\gamma)}$ is greater in the cases B and D in respect to A and C.

The X-dominated cases (C and D) are quite similar to a pure X case. The most interesting effects take place in γ-dominated cases (A and B). Here δ_γ keeps the γ-dominance behaviour at $M > M_{c(\gamma)}$), while, for $M < M_{c(\gamma)}$ the bending of δ_γ is much softer than in a pure γ case, thanks to the action of residual X fluctuations, as previously stressed. It should be stressed that in X-dominated cases $M_{c(\gamma)}$ is smaller than in the cases A and B in spite of the fact that the smaller m_γ value would seem to lead to a greater free-streaming mass scale. This is again entirely due to the presence of δ_X , whose gravitational action keeps δ_γ to higher values, in respect to the $\Omega_X = 0$ case, partially inhibiting γ free streaming.

b)   z < 2000.

The evolution of δ 's at $z < 2000$ and until onset of non-linear stages was calculated analytically, considering the two modes in the solution of dynamical equations for a set of two media subject to gravitational coupling in Newtonian approximation (Wasserman, 1981).

As is known it turns out to be

$$\left|\begin{matrix} \delta_X(t) \\ \\ \delta_\gamma(t) \end{matrix}\right| = C_+ \left(t/t_{in}\right)^{2/3} + C_- \left(t/t_{in}\right)^{-1} + \left|\begin{matrix} -\dfrac{\Omega_\gamma}{\Omega_X} \\ \\ 1 \end{matrix}\right| \left[C_0 + C_\gamma \left(t/t_{in}\right)^{-1/3}\right] \qquad (2.73)$$

where

$$c_+ = \frac{3}{5} \left[\Omega_x \left(\delta_x^{ih} + t_{ih} \, \dot{\delta}_x^{ih} \right) + \Omega_y \left(\delta_y^{ih} + t_{ih} \, \dot{\delta}_y^{ih} \right) \right]$$

$$c_- = \frac{2}{5} \left[\Omega_x \left(\delta_x^{ih} - \frac{3}{2} t_{ih} \, \dot{\delta}_x^{ih} \right) + \Omega_y \left(\delta_y^{ih} - \frac{3}{2} t_{ih} \, \dot{\delta}_y^{ih} \right) \right]$$

$$c_0 = \Omega_x \left[\left(\delta_y^{ih} + 3 t_{ih} \, \dot{\delta}_y^{ih} \right) - \left(\delta_x^{ih} + 3 t_{ih} \, \dot{\delta}_x^{ih} \right) \right]$$

$$c_\psi = 3 t_{ih} \, \Omega_x \left(\dot{\delta}_x^{ih} - \dot{\delta}_y^{ih} \right)$$

$$(2.74)$$

with t_{in} corresponding to $z = 2000$. The baryon action was neglected. The time evolution of $\delta_{x,y}$ was followed down to $z = 5$. In fig. 2.16 and fig. 2.19 the amplitudes $\Omega_x \delta_x$, $\Omega_y \delta_y$ and $\delta = \Omega_x \delta_x + \Omega_y \delta_y$ are shown, in a number of cases.

In the X-dominated cases the final spectra are mostly like a pure X case. In the y-dominated case we notice a time evolution which gradually leads to δ_x and δ_y to reach a similar behaviour. This common shape is attained for $z \simeq 100$. From fig. 2.19 we can also see that the final

spectrum is taken up by δ_X , below $M_{c(\gamma)}$, down to $M_c(X)$. This leads

to a much softer decrease of δ_γ in the above mass interval than

below $M_c(X)$.

The total mass variance

$$\left(\frac{\delta M}{M}\right)^2 = const \times \int_0^{K(M)} k^2 |\delta_k|^2 \, dK \qquad (2.75)$$

is plotted at $z = 5$, for C and B cases, in fig. 2.20 and fig. 2.21.

In the case of X-dominance, $\delta M/M$ is essentially equal to the one

shown in fig.s 2.8, 2.9. In the γ -dominated case, the mass scale at

which $\delta M/M$ (obtained from 2.75 , making use of the whole δ) holds

0.95 is shifted towards lower masses. This is clearly due to the power

present below 10^{15} - $10^{16} M_\odot$ which is now clearly greater than

in the pure γ -case. This displacement depends quite strongly on the

spectral index n. In fact, although $\delta (k)$, for n = 0, exhibits a

bending at $M_{c(\gamma)}$, the change of slope is not very drastic and can be

compensated by the $K^{n/2}$ factor even for quite reasonable n values.

In conclusion, while in the X-dominated cases the presence of a γ

component is scarcely noticeable, in the γ -dominated case final spectra
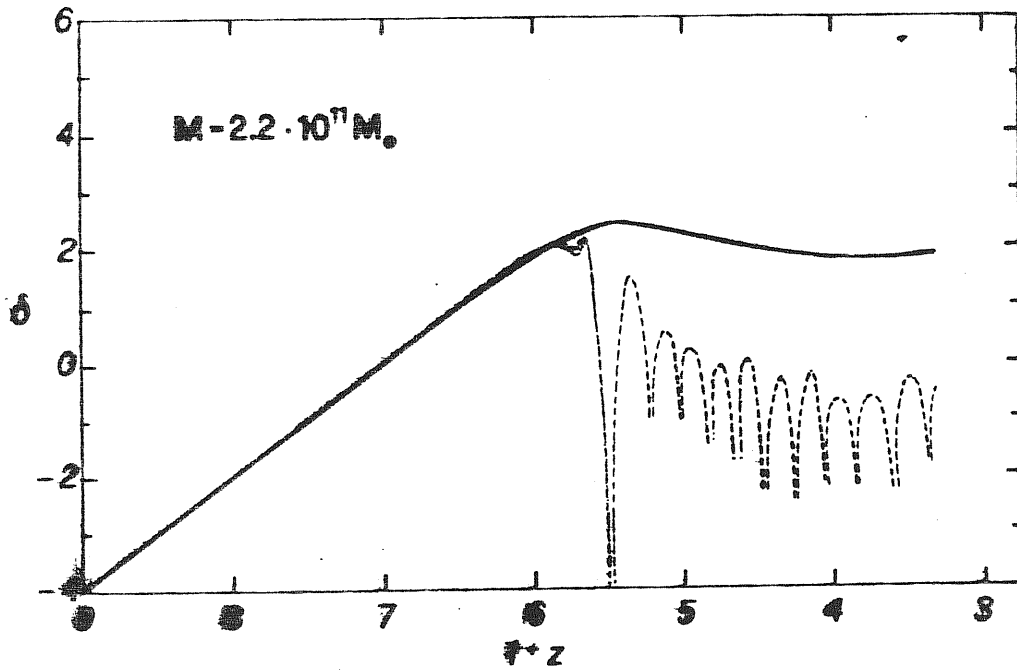
$$M = 2.2 \cdot 10^{11} M_\odot$$

Fig. 2.10   Density constrasts are plotted vs. redshift z. The dashed line gives δ_r, the continuous and dotted lines refer to X and ν respectively; δ_r is plotted only until its first zero. This figure refers to the case B, M = 2,2 . $10^{11} M_\odot$. These mass include both X and ν contributions.
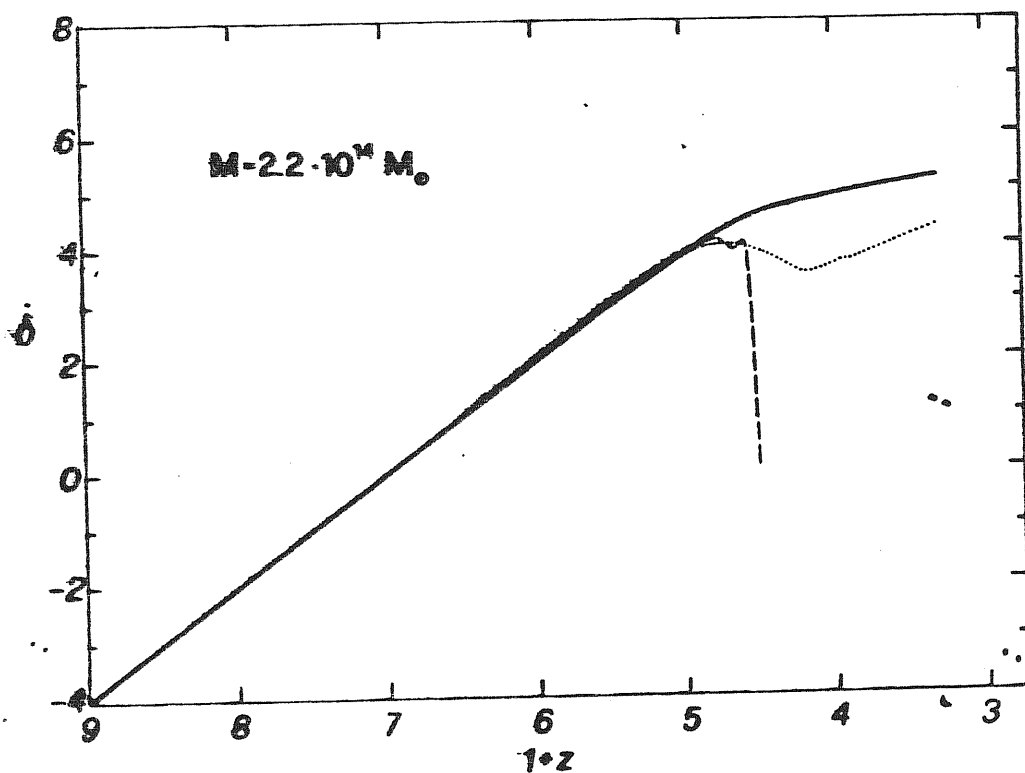
$$M = 2.2 \cdot 10^{14} M_\odot$$

Fig. 2.11   The same as Fig. 2.10 in the B case, M = 2.2 . 10^{11} . $M_\odot$.
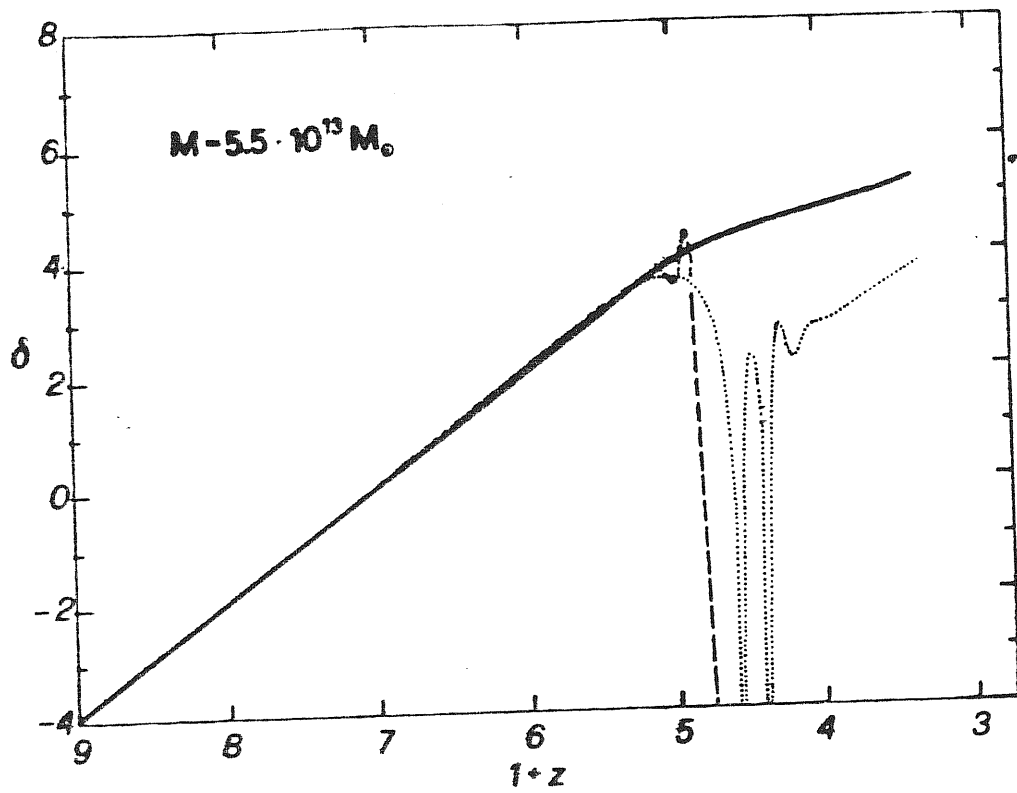
Fig. 2.12   The same as Fig. 2.10 in the C case, $M = 5.5 \cdot 10^{13} \ M_\odot$.
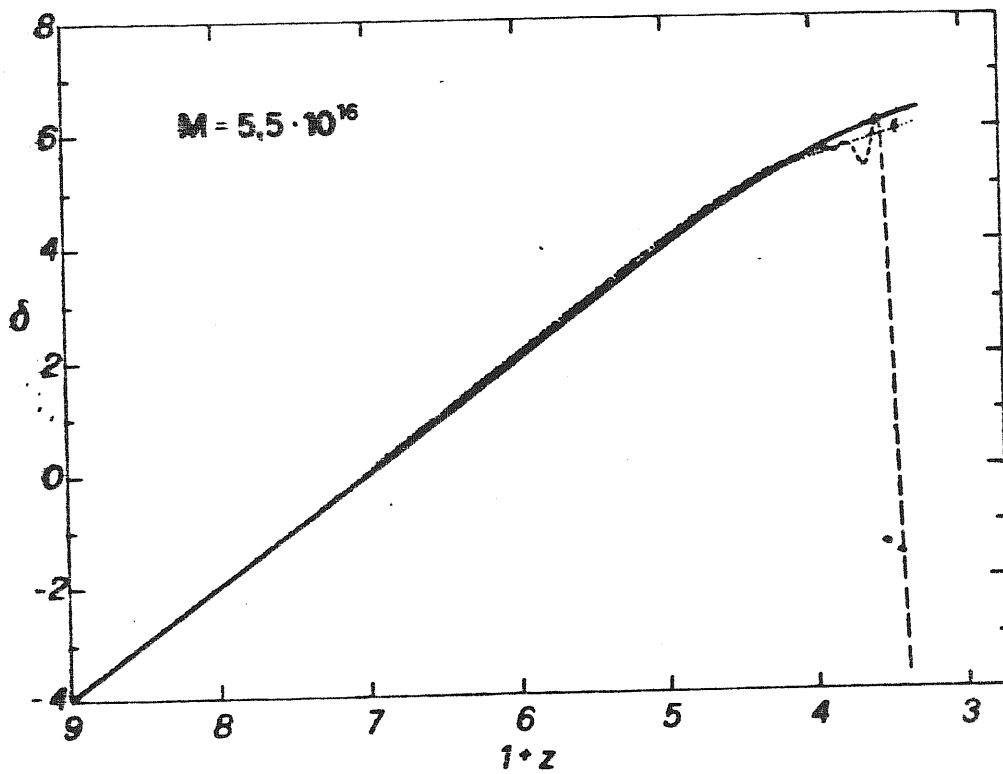
Fig. 2.13   The same as Fig. 2.10 for the D case, $M = 5.5 \cdot 10^{16} \ M_\odot$.
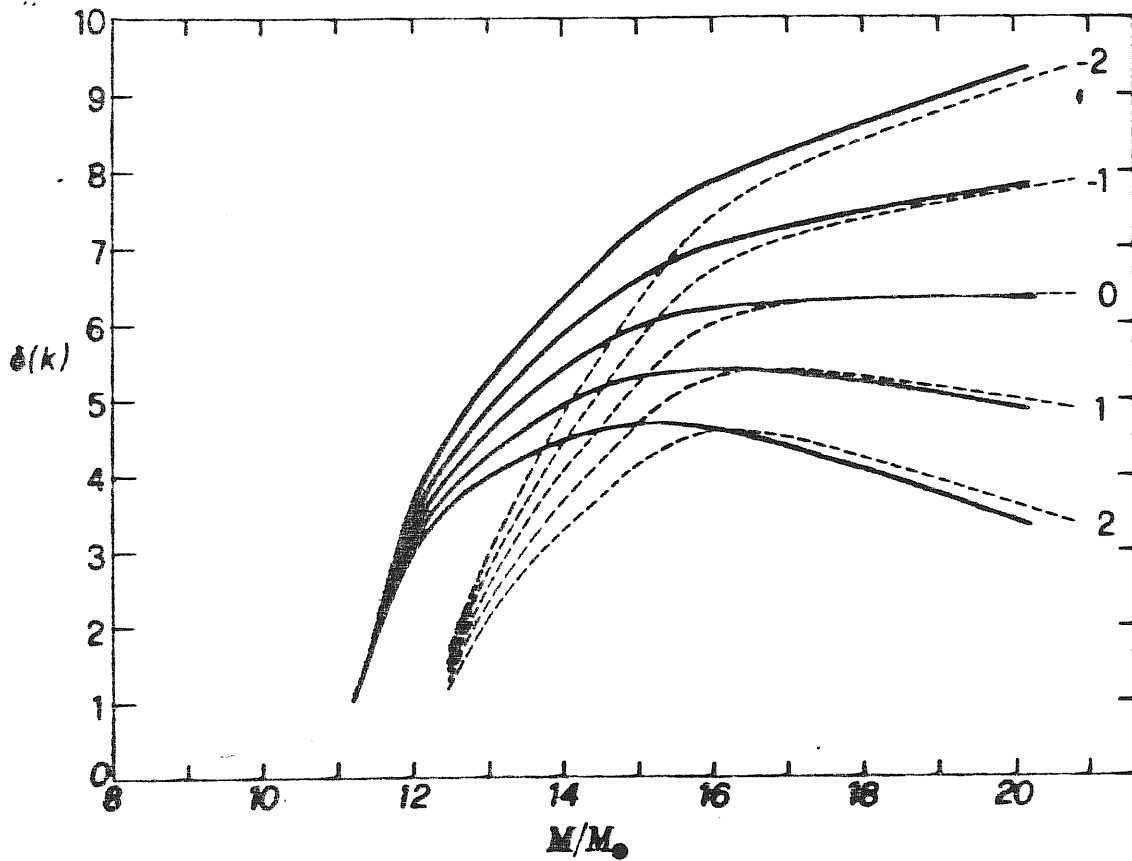
Fig. 2.14 The final amplitudes δ_X, δ_ν are plotted vs. the mass scale of the pertur-
bation at z = 2000. The continuous line refers to δ_X and the dashed line
to δ_ν. Different curves are labelled by the value of the primordial spectral
index n, here Ω_X = 0.2, Ω_ν = 0.8, α_X^3 = 0.04.
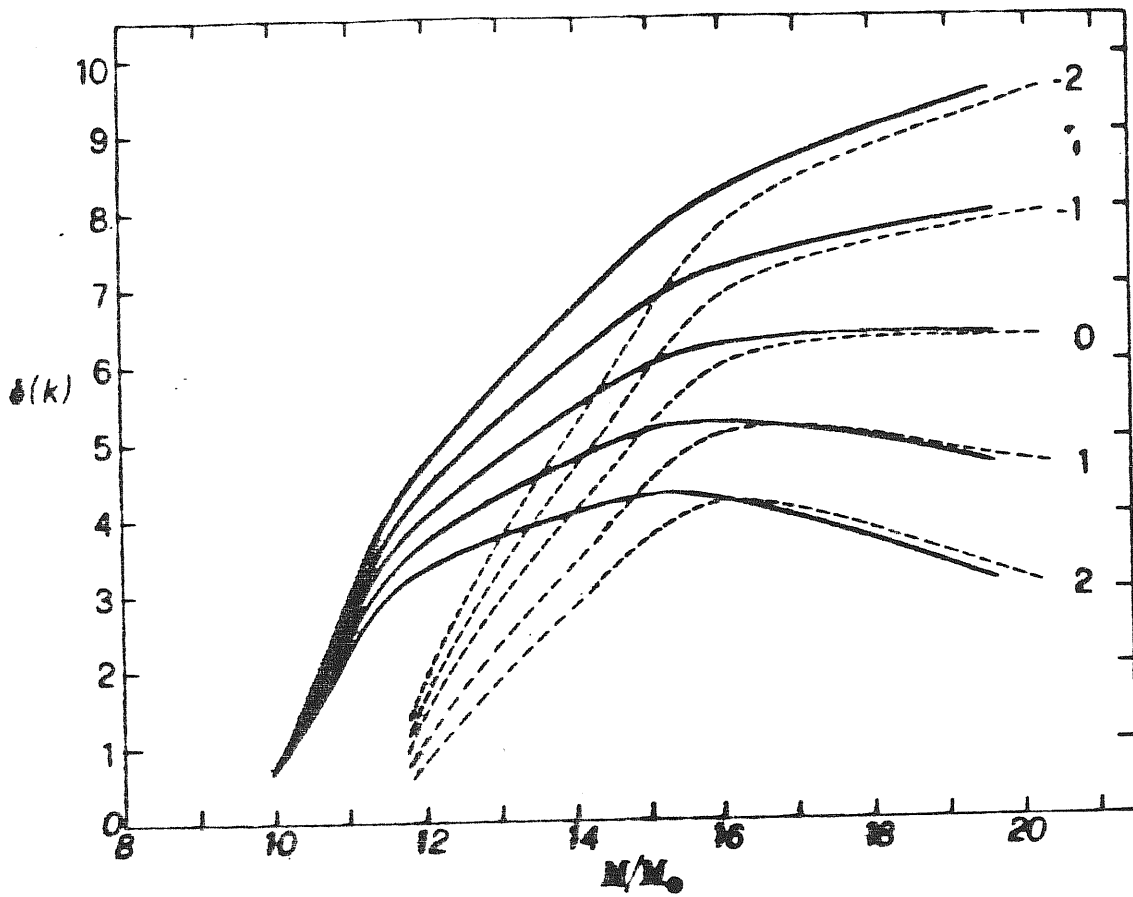
Fig. 2.15   The same as Fig. 2.14 for $\Omega_X = 0.2$, $\Omega_\nu = 0.8$, $\alpha_X^3 = 0.02$ (case B).
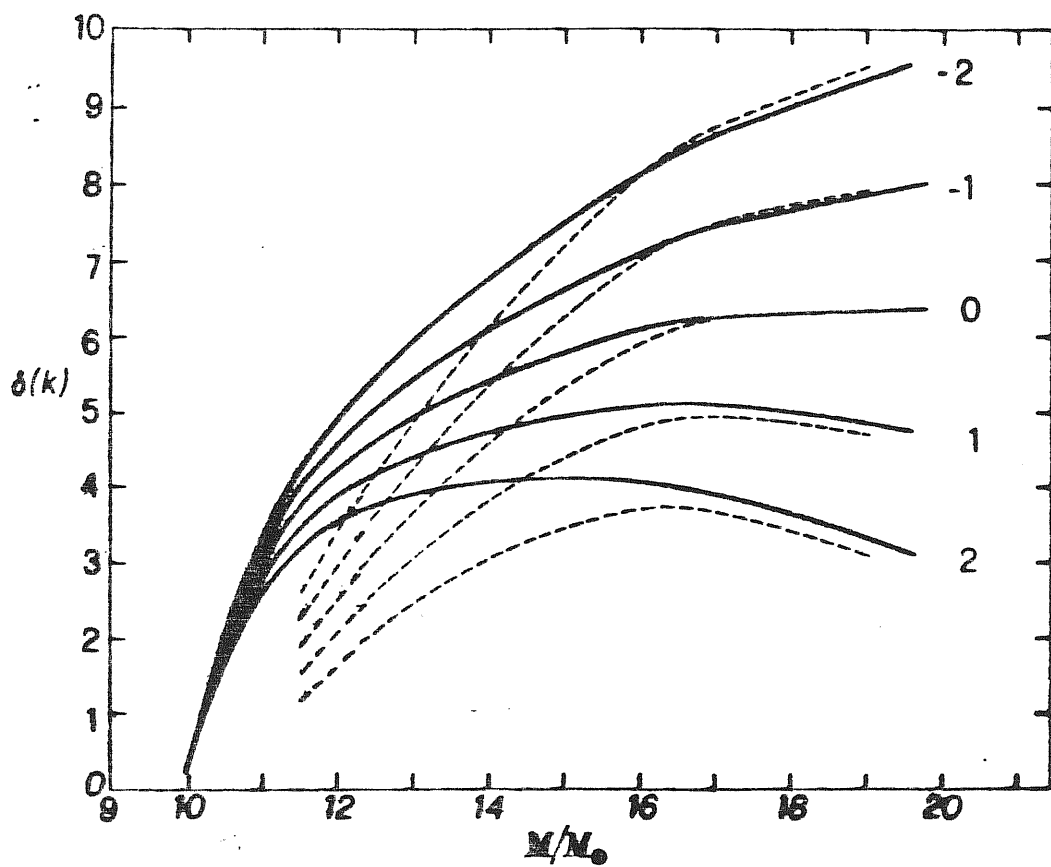
Fig. 2.16   The same as in Fig. 2.14 for $\Omega_x = 0.8$, $\Omega_\nu = 0.2$, $\dfrac{\alpha^3}{x} = 0.04$ (case C).
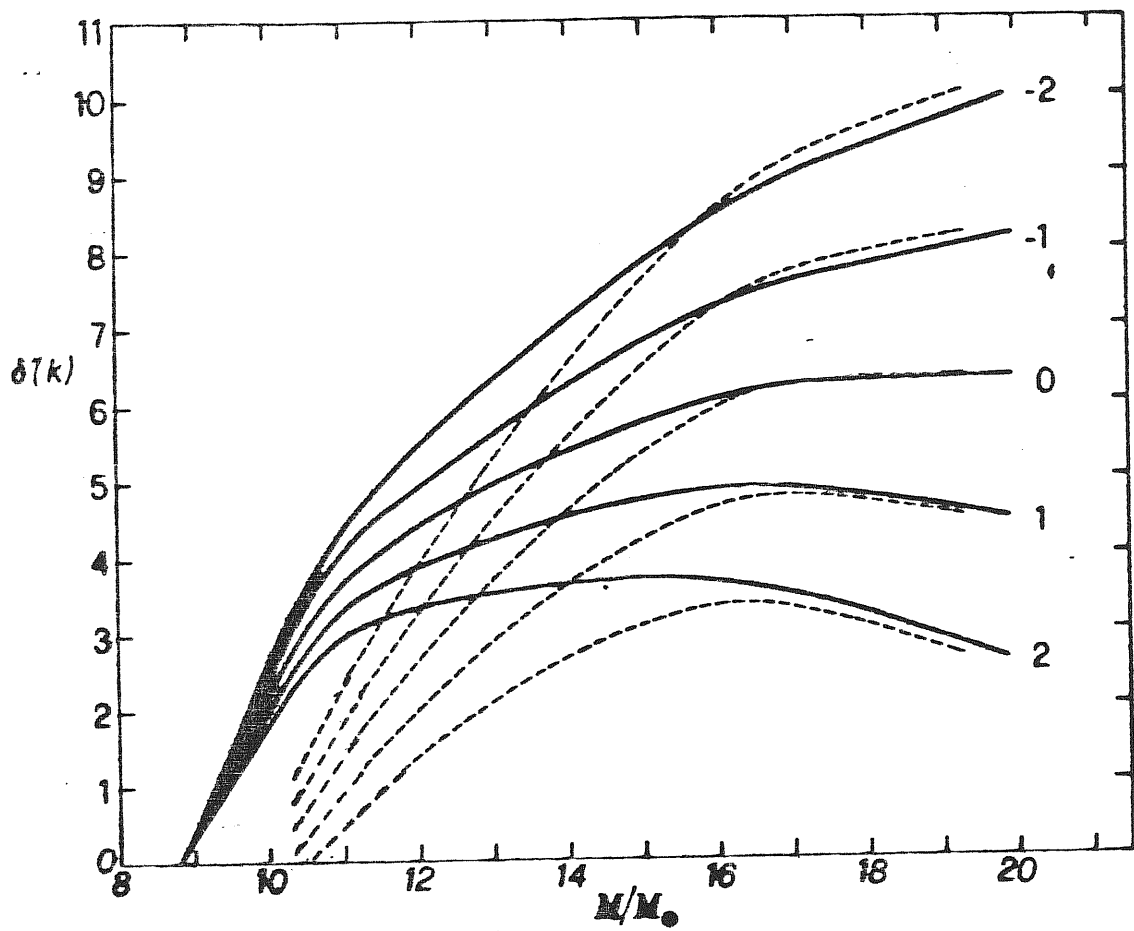
Fig. 2.17   The same as in Fig. 2.14 for $\Omega_x = 0.8$, $\Omega_\nu = 0.2$, $\alpha_x^3 = 0.02$ (case D).
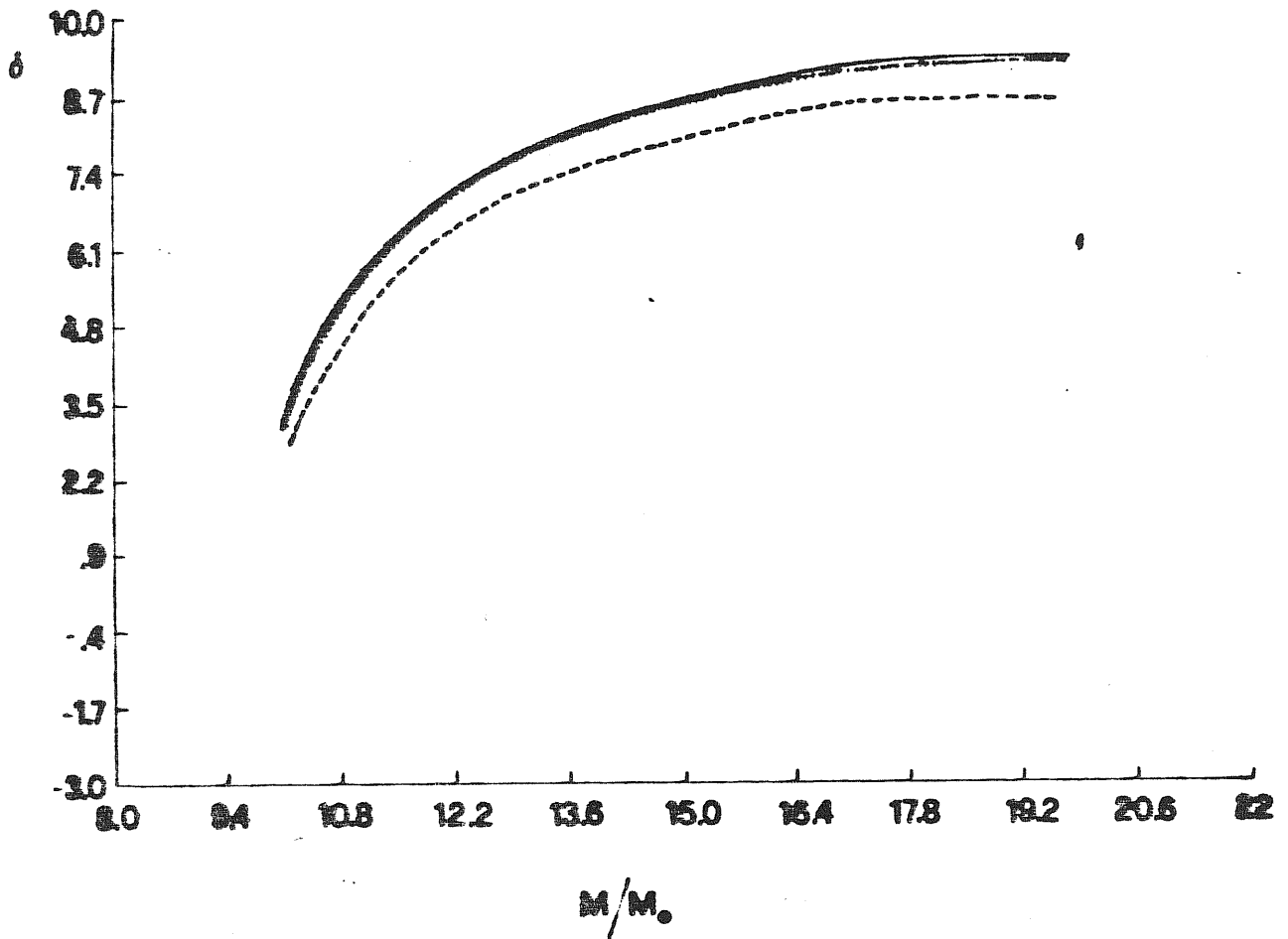
Fig. 2.18   The total density contrast $\delta(k)$ (continuous line), the density contrast

$\delta_\nu(k)$ (dashed line) and $\delta_x(k)$ (point line), for a primordial spectral

index n = 0 are shown at z = 5 for Ω_x = 0.8, Ω_ν = 0.2, α_x^3 = 0.04.
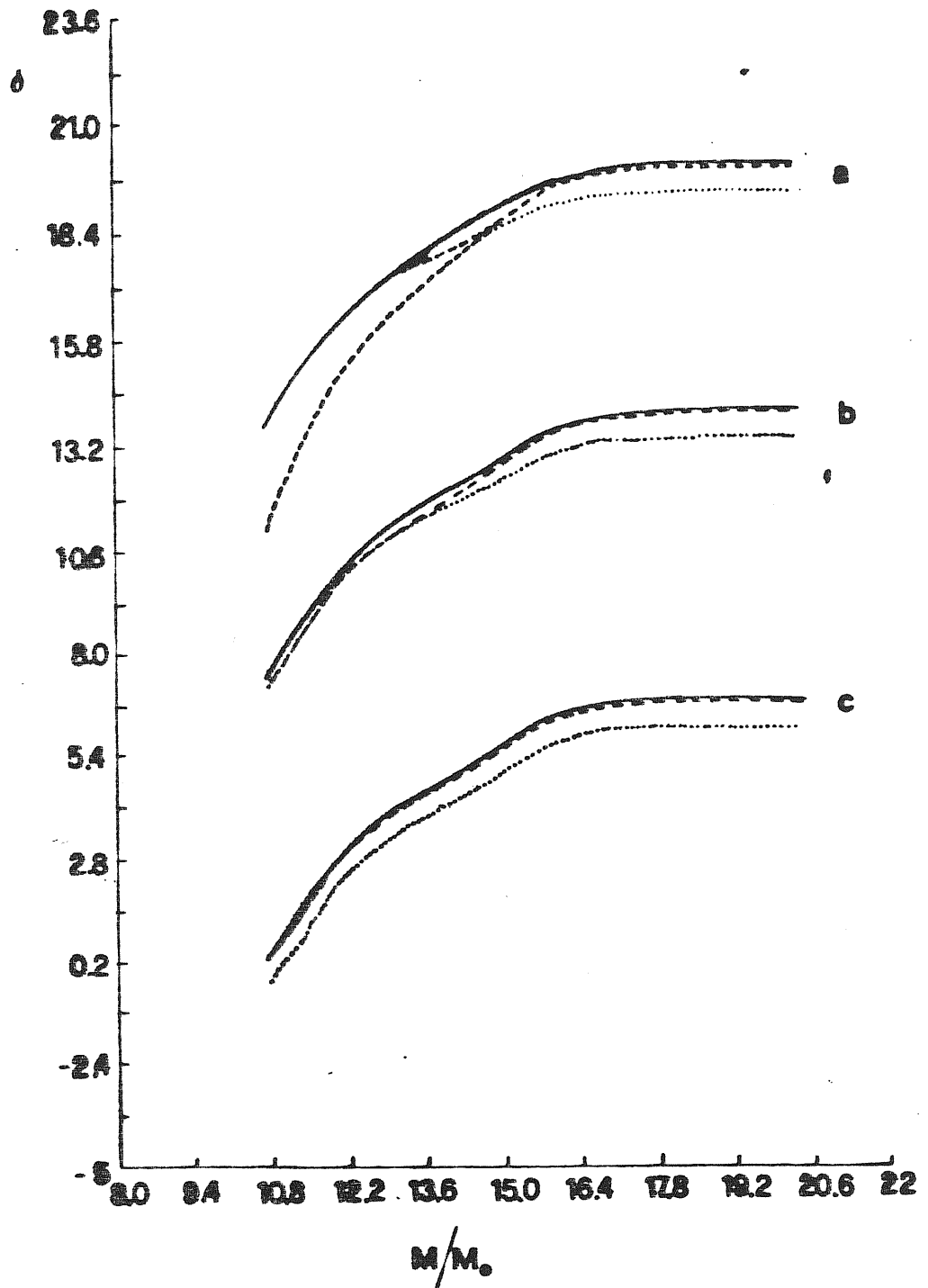
Fig. 2.19   The time evolution of the total density contrast $\delta(k)$ and of $\delta_\nu(k)$ and

$\delta_x(k)$ is shown from $z = 2000$ (curves a) through $z = 500$ (b) down to $z = 5(c)$.

Here $\Omega_x = 0.2$, $\Omega_\nu = 0.8$, $\alpha_x^3 = 0.02$.   The units of δ's are arbitrary.
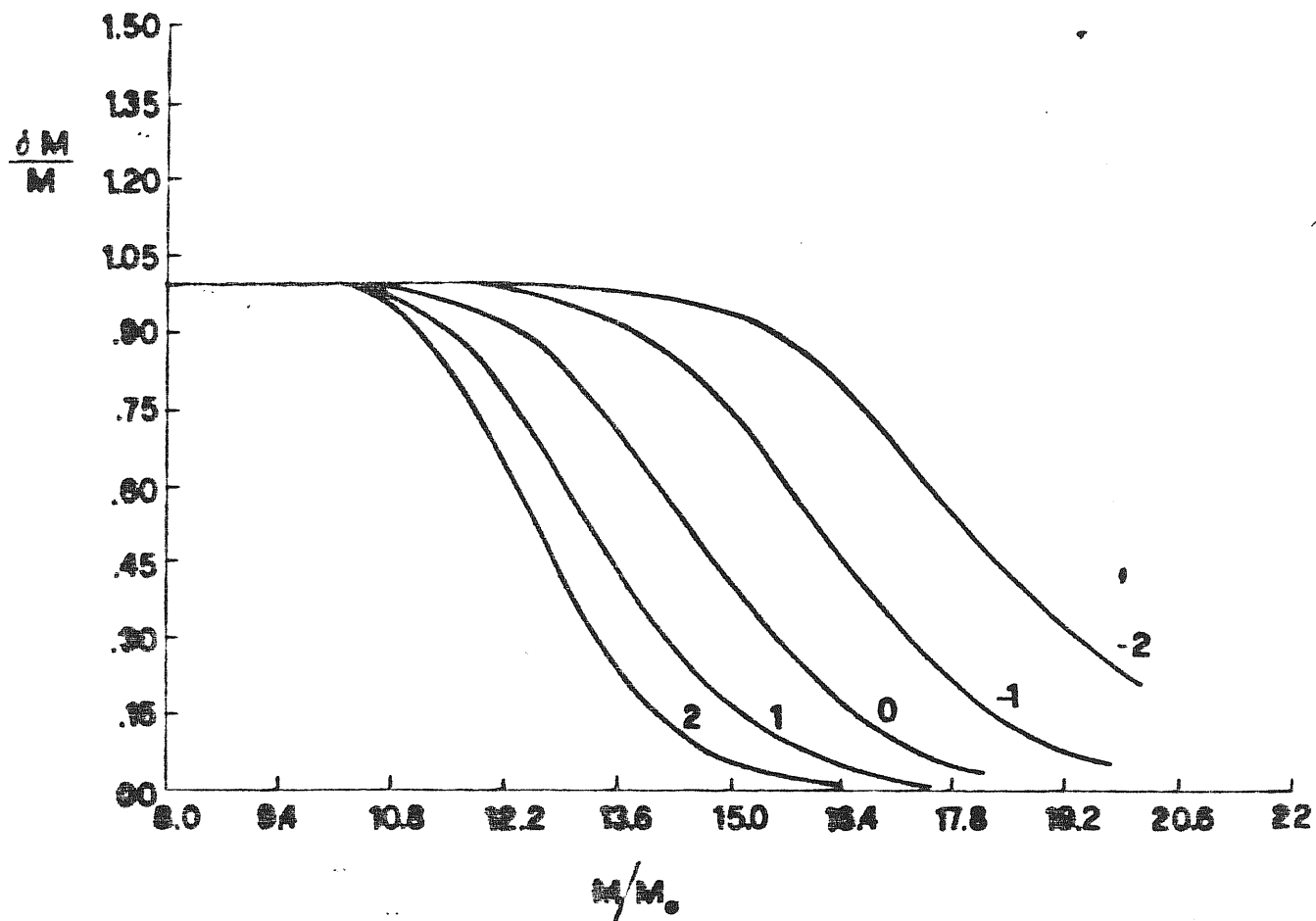
Fig. 2.20   Mass variance at z = 5 for $\Omega_x = 0.8$, $\Omega_\nu = 0.2$, $\alpha_x^3 = 0.04$.   Different curves

are labelled with the value of the primordial spectral index n.
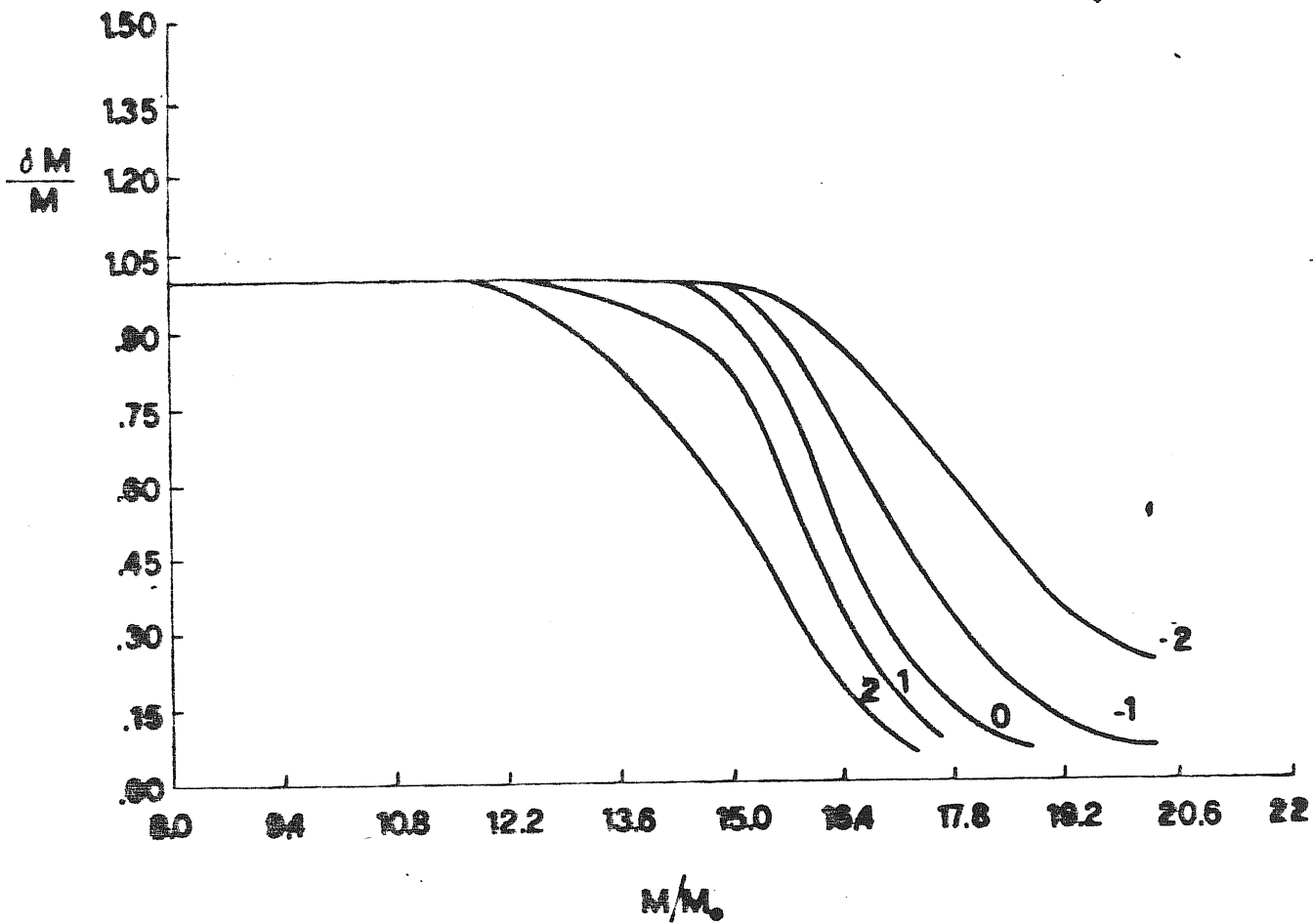
Fig. 2.21   Final mass variance at $z = 5$ for $\Omega_x = 0.2$, $\Omega_\nu = 0.8$, $\alpha_x^3 = 0.02$.

are strongly sensible to the presence of a small initial X component

and the minimal mass scale over which perturbations are to be studied

is fixed, in several cases, by $M_{c(X)}$. Therefore, if the presence of

X particles as a component of dark matter is confirmed, their influence

on the shape of the density fluctuation spectrum, at the beginning of

the non-linear stage, could be sensible, even if their contribution

to dark mass were modest.

II. 10   The pancake   mass in a two component dark matter model

In the preceding paragraphs we have seen that the typical mass

scale over which nonlinear collapse will first begin ("pancake" mass)

can be worked out by computing the   mass variance $\frac{\delta M}{M}$ as a function

of the mass scale M. this has been done in : § II.6 in the single

component case.

A relevant dependence of the "pancake" mass M_{NL} was also found.

The dependence is increased when greater values of m⁻ are assumed.

However, there exists a definite connection between M_{NL} and m. While

for neutrinos $(m_\nu \simeq 30 eV)$ $M_{NL} \simeq 10^{14} - 10^{15} M_\odot$, for massive photinos

$(m \simeq KeV)$ $M_{NL} \simeq 10^{10} - 10^{13} M_\odot$. In the former case M_{NL} lies

in the super-cluster mass range; in the latter case M_{NL} could fit

individual galaxy mass scales.

If dark matter is made of quanta of different masses, some simple relations which connect m and M_{NL} may break down. We shall consider, as an example, the case of two particles of masses $\simeq$ 30eV and $\simeq$ 1 KeV respectively, leading altogether to a density parameter $\Omega = 1$ but contributing to Ω in different percentages. The result is that M_{NL} can lie in different points of the interval between the values related to 30eV and 1keV, according to the value of n and to the fraction Ω_ν and Ω_χ whose sum yields $\Omega = 1$ (Bonometto and Valdarnini 1984). Here $\alpha_\nu = (4/11)^{1/3}$ as usual, while we shall take $\alpha_\chi = 0.21$ in order to have $\Omega_\chi = 0.25$ and $m_\chi = 1keV$ when the numbers of independent spin states g_ν and g_χ are taken to be 6 and 2 respectively.

Our fundamental assumptions and the numerical integration are the same as those which have been used in § II.7 and II.9 and will not be reported. We give here only the main results.

In fig. 2.22 we report the time evolution of $\Omega_\chi \delta_\chi$, $\Omega_\nu \delta_\nu$ and $\delta = \Omega_\chi \delta_\chi + \Omega_\nu \delta_\nu$ from $z = 2000$ down to $z = 5$ for $h = 0$. In these figures δ_χ and δ_ν have been calculated according to eqs. (2.73), (2.74).

In fig. 2.23 we plot the n-dependence on M_{NL} , defined as the
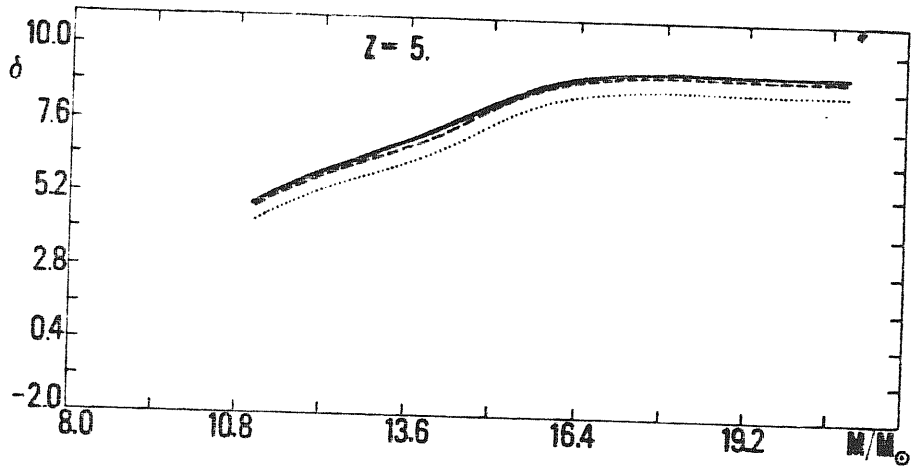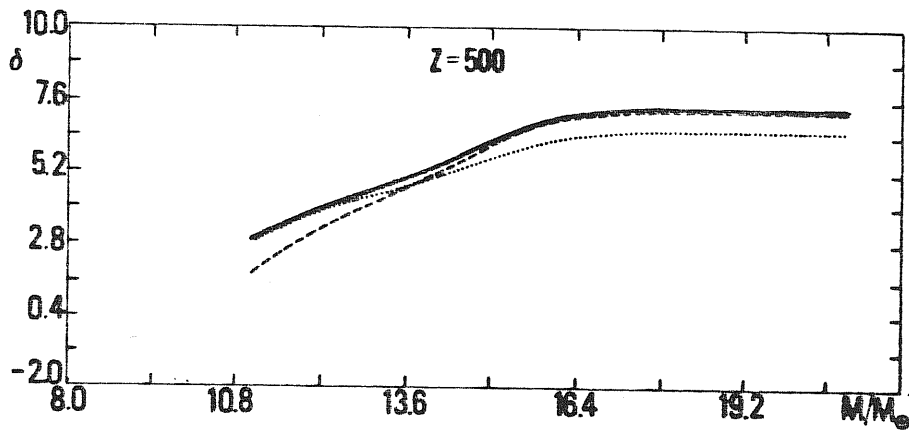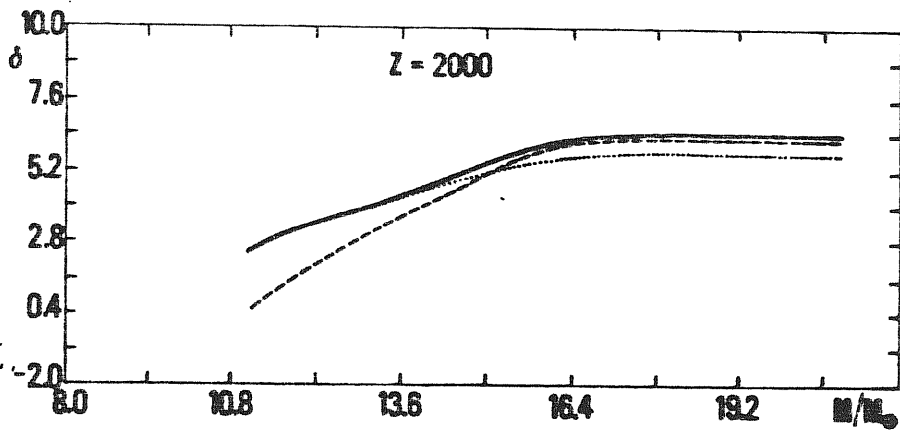
Fig. 2.22 The time evolution of the total density contrast $\delta(k)$ (continuous line) and of the density contrasts $\delta_\nu(k)$ (dashed line) and $\delta_x(k)$ (point line), for a primordial spectral index n = 0, is shown from z = 2000 (plot a), through z = 500 (plot b), until z = 5 (plot c). Here Ω_x = 0.75, Ω_ν = 0.25 and m_x = 1 keV.
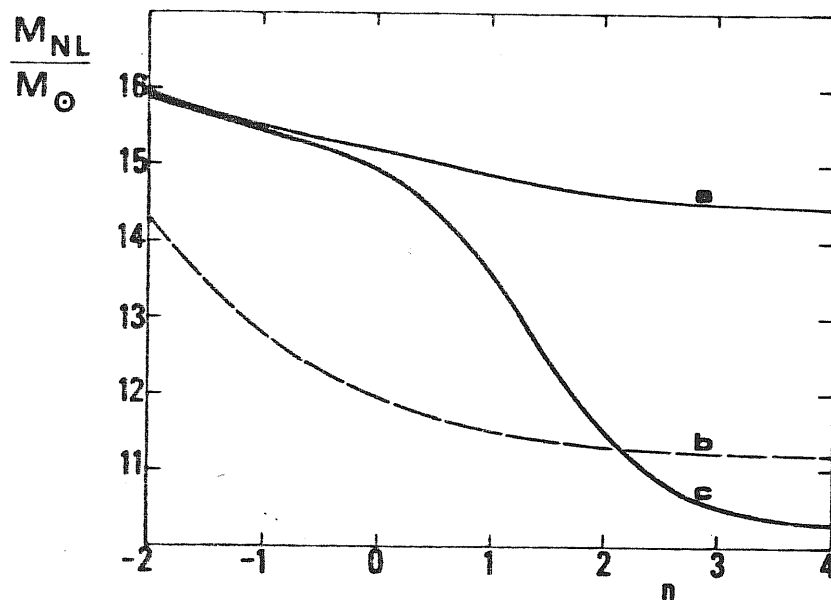
Fig. 2.23   The n dependence of the 'pancake' mass is plotted when dark matter is made

of ν($m = 30$ eV, 6 helicity states; curve a), of X ($m = 880$ eV, 2 helicity

states; curve b), and both ν and X($m = 20$ eV, with 6 states; $m_x = 10^3$ eV,

with 2 states; curve c). The dependence on n is becoming more and more rele-

vant when going from a to c.

mass scale where $\frac{\delta M}{M} = 0.95$, for the 'classical' pure ν and X cases and for the present, intermediate case. The results for pure X were obtained in § II.6 with $m_x = 880$ eV. This is to be taken into account when explaining why the two-particles result appear to give a lower value of M_{NL} than a pure X case (for large n).

An indication of the typical value of M_{NL} related to a given value of m, in a world model with $\Omega = 1$, can be obtained from the relation

$$M_{NL} \simeq 10^{15} M_0 \left(30 \, eV/m\right)^3 ,$$
(2.75)

which yields the mass involved in a fluctuation essentially entering its own horizon when $T = m$. Of course (2.75) does not take into account the way in which different mass-scales contribute to the 'pancake' mass when n is varied. Fig. 2.23 shows the effects of n in fixing M_{NL}, which is relevant for low values of m. However, once n is obtained, either from clustering data or from background data, a direct relation exists between M_{NL} and $\dot{m}$. the point is that both m and M_{NL} are quantities whose determination is not impossible

in the near future.

If a precise fit of M_{NL} and m will turn out to be possible, a limit on the abundance of 'supersymmetric' particles can be set by using the method presented here. On the contrary, if this fit will turn out to be impossible, the present results could lead to the prediction of the mass and abundance of further weakly interacting quanta. In our opinion the possibility that large-scale data can lead to detailed information on masses of weakly interacting particles is appealing and may even deserve more detailed inspection.

III. SMALL SCALE MW BACKGROUND FLUCTUATIONS IN A PHOTINO DOMINATED
UNIVERSE

III.1 Origin of MW small scale fluctuations

An adiabatic perturbation will include fluctuations in dark matter,

baryonic matter, and radiation. In order to build the present inhomo-

geneous picture of the Universe, the size of fluctuations in dark and|or

baryonic matter must have become non-linear by a redshift $z_{h\ell} \simeq 1 - 5$

After decoupling the (baryonic and/or dark) matter fluctuation spectrum

is expected to have the following shape:

$$ |\delta(k)|^2 = A k^h , \tag{3.1} $$

for $k < k_D$ (k_D fixes the critical damping scale for the fluctuation

spectrum, see below), which it is expected to drop exponentially at greater

K. This yields a mass variance

$$ \frac{\delta M}{M} \propto M^{-\alpha} , \tag{3.2} $$

with $\alpha = \frac{1}{2} + \frac{h}{6}$ for

$$M \gtrsim M(K_D) = \frac{\pi}{6} \bar{\rho}_o \left(\frac{2\pi}{K_D} \right)^3 \quad , \qquad (3.3)$$

and flat for $M \lesssim M(K_D)$. The value of K_D depends on the

underlying physical theory.

If dark matter does not exist or is so scarse as to bear no dynamical

weigth, K_D is caused by the so-called Silk damping (Silk 1968), acting

before and during recombination on matter density fluctuations.

If, instead, dark matter dominates the collapse of the material component

of the Universe, is connected with the size of the horizon when dark

matter quanta become nonrelativistic (see Szalay and Marx 1976).

The normalization of the initial fluctuation spectrum is therefore to be

such as to allow $\delta M / M$ to become 1 by $t_{h\ell}$ over the mass scale

$M_D = M(K_D)$ .This sets also the normalization of the MW background

fluctuations.

Before recombination, over each scale, $\delta_r = \delta\rho_r / \rho_r$ is related to

$\delta_m = \delta\rho_m / \rho_m$ through the approximate relation

$$\delta_r = \frac{4}{3} \delta_m \quad . \qquad (3.4)$$

A naive extension of such a relation down to after recombination would give

$$\frac{\delta T}{T} \simeq \frac{1}{3} \delta_m \qquad (3.5)$$

If we assume this relation to be qualitatively true at $z_o \simeq 800$,

where we require

$$\delta_m \simeq \frac{z_{h\ell}}{z_o} \qquad , \qquad (3.6)$$

it turns out that

$$\frac{\delta T}{T} \simeq z_{h\ell} / z_o \simeq 10^{-3}. \qquad (3.7)$$

This rough argument is however to be corrected owing to a number of

different considerations:

i) The normalization of δ_m is operated over a scale corresponding to k_D

   Clearly $\Delta T / T$ can be originated by different scales k.

ii) The normalization of δ_m might refer to dark matter rather than to

   baryonic matter. Then we have to consider the growing of dark matter

   perturbations since dark matter becomes the dominant form energy in

   the Universe until z_o .

iii) Of course (3.5) is only a very rough approximation, we ought to

   determine which was the value of δ_r in the last scattering band.

In what follows we shall debate these points in detail. It may be however

worth mentionig soon that:

i) The smallest angular scales over which $\delta T/T$ are potentially obser-

vable, are connected with mass scales $\simeq 10^{15} - 10^{16}\ M_\odot$.

ii) In the case of baryonic matter dominance M_D ranges, instead,

around $10^{13}\ M_\odot$.

iii) In the case of dark matter made of γ ($m_\gamma \simeq 30\,eV$), free streaming

causes $M_D \simeq 10^{15}\ M_\odot$.

iv) If the mass m_χ of the dark matter quanta is grater, we expect M_D

to be smaller.

Therefore: in the canonical massive γ case, there is indeed a direct con-

nection between δ_m and δ_γ , for both concern a similar scale.

In the other cases, instead, a relevant importance is assumed by the steep-

nesss of $S(k)$. Very steep spectra can allow δ_m to be large at M_D ,

while δ_γ is small over $10^{15}\ M_\odot$. Moreover, when larger values of

h are considered, the value of M_D itself becomes strongly dependent

on n.

Besides these general points much care has to be taken to work out the

expression of $\delta T/T$ taking into account different wavelength contributions.

In this chapter we report the results of a numerical calculation for small

scale fluctuations in the cosmic background radiation in an Universe dominated

by weakly massive interacting quanta (Bonometto,Lucchin and Valdarnini 1984; Valdarnini and Bonometto 1984; see also Vittorio and Silk 1984, Bond and Eftstathiou 1984). For the mass of these particles two possibilities have been considered: either massive neutrinos or low mass photinos ($m_\chi \simeq 1 \ KeV$).

The integration start at the redshift z_{ih} ($z_{ih} = 8 \cdot 10^5$ in the photino case and $z_{ih} = 8 \cdot 10^6$ in the ν case) and is halted at the final redshift $z_{out} = 800$.

In the following section we debate the relation between the observed small scale MW background anisotropies and the results of our integration.

In §III.3 and III.4 the fundamental assumptions and the numerical integration of the model are presented. Finally results and discussions are debated in §III.5 .

III.2 Connection with the observed small scale temperature fluctuations

The main output of our integration are the transmission factors for 'matter' and radiation, defined as

$$ \tau_m (k) = \frac{\delta_m (k, z = z_{out})}{\delta_m (k, z = z_{ih})} \quad , \quad \tau_r (k, \mu) = \frac{\delta_r (k, \mu, z = z_{out})}{\delta_r (k, \mu, z = z_{ih})} \tag{3.8} $$

here 'matter' refers to both ordinary and dark matter; for radiation the

the transmission factor depends also on $\mu = \cos \Theta$, Θ being the angle between the observer and the wave propagation direction.

Our integration has been done with a spectral index n=0 for the primeval fluctuations, in the linear approximation other spectra can be sipmly obtained multiplying the final δ 's by $k^{h/2}$.

The observed small scale radiation fluctuations are the r.m.s. fluctuations for a beam switched between the two directions $\mu_1 = \dfrac{\vec{K} \cdot \hat{h}_1}{|\vec{K}|}$, $\mu_2 = \dfrac{\vec{K} \cdot \hat{h}_2}{|\vec{K}|}$, here $\hat{h}_1$ and $\hat{h}_2$ are unit vectors specifying the directions of obser- vations.

One must further take into account that what is observed in a given direction is a temperature which receives its contribution from the various frequencies of the spectrum, then $\delta T / T$ will be given by

$$\left(\frac{\delta T}{T}\right)^2 (\Theta) = \frac{1}{16} \left\langle \delta_r (\vec{x}, \mu_1) , \delta_r (\vec{x}, \mu_2) \right\rangle , \qquad (3.9)$$

where the mean is all over the spatial points $\vec{x}$; here $\delta_r (\vec{x}, \mu)$ is the Fourier spectrum of $\delta_r (\vec{k}, \mu)$ and $\cos \Theta = \hat{h}_1 \cdot \hat{h}_2$.

In order to compare with observations, the radiation fluctuations must be convolved with the antenna response beam, for which a Gaussian form is assumed

$$\mathcal{g}\left(|\hat{h}_1 - \hat{h}_2|\,;\sigma\right) = \frac{1}{2\pi\sigma^2}\,exp\left\{-\frac{1}{2\sigma^2}\,|\hat{h}_1 - \hat{h}_2|^2\right\}\,, \qquad (3.10)$$

here σ is the half-width antenna beam; then $\delta_{\vdash}(K,\mu)$ must be replaced by

$$\delta_{\vdash}(k,\mu) \longrightarrow \delta_{\vdash}(k,\mu,\sigma) = \int \delta_{\vdash}(k,\mu')\,\mathcal{g}\left(|\hat{h}'-\hat{h}|\,;\sigma\right)\,d\Omega'\,. \qquad (3.11)$$

In the small angle approximation ($\theta \ll 1$) the final expression for eq.(3.9) is (Doroshkevich,Zel'dovich and Sunyaev 1978)

$$\left(\frac{\delta T}{T}\right)^2(\theta,\sigma) = \frac{1}{2\pi^2}\,\frac{1}{16}\,\int_0^\infty dk\,k^2 \int_{-1}^{+1} d\mu\,|\delta_{\vdash}(k,\mu)|^2\,e^{-k^2\sigma^2 t_0^2(1-\mu^2)}\,.$$

$$\cdot\left\{1 + \frac{1}{3}\,J_0\left[2k\,\theta t_0\,(1-\mu^2)^{1/2}\right] - \frac{4}{3}\,J_0\left[k\,\theta t_0\,(1-\mu^2)^{1/2}\right]\right\}\,, \qquad (3.12)$$

here J_0 is a Bessel function, $t_0 \simeq 2c/\Omega H_0$ and

$$|\delta_{\vdash}(k,\mu)|^2 = A\,k^h\,\tau_{\vdash}^2\,(k,\mu,t=t_{out})\,, \qquad (3.13)$$

$A^{1/2}$ is the initial perturbation amplitude in the n=0 case. In eq.(3.12) an useful approximation can be done as follows: the mass variance $\delta M/M$ is (in the $K \rightarrow \infty$ limit)

$$\left(\frac{\delta M}{M}\right)^{2}_{M \to 0} = \frac{A}{2\pi^{2}} \int_{0}^{\infty} k^{n+2} \tau^{2}_{m}(k) \, dK \qquad ; \qquad (3.14)$$

then eq.(3.12) can be rewritten as

$$\left(\frac{\delta T}{T}\right)^{2}(\theta,\sigma) = \frac{1}{16} \left(\frac{\delta M}{M}\right)^{2} \frac{\int_{0}^{\infty} dk \, k^{n+2} \, T^{2}_{k}(k,\theta,\sigma)}{\int_{0}^{\infty} dK \, k^{n+2} \, \tau^{2}_{x}(k)} \qquad , \qquad (3.15)$$

where

$$T^{2}_{k}(k,\theta,\sigma) = \int_{-1}^{+1} d\mu \, \tau^{2}_{k}(k,\mu) \, e^{-k^{2}\sigma^{-2} t^{2}_{0}(1-\mu^{2})^{1/2}} .$$

$$\cdot \left\{ 1 + \frac{1}{3} J_{0}\left[2k\theta t_{0}(1-\mu^{2})^{1/2}\right] - \frac{4}{3} J_{0}\left[k\theta t_{0}(1-\mu^{2})^{1/2}\right] \right\} . \qquad (3.16)$$

If $z_{h\ell}$ is the redshift at which $\frac{\delta M}{M}$ becomes one, thus eq.(3.15) can be put in the following form

$$\left(\frac{\delta T}{T}\right)^{2}(\theta,\sigma) = \frac{1}{16} \left(\frac{1+z_{h\ell}}{1+z_{out}}\right)^{2} \frac{\int_{0}^{\infty} dk \, k^{n+2} \, T^{2}_{k}(k,\theta,\sigma)}{\int_{0}^{\infty} dk \, k^{n+2} \, \tau^{2}_{m}(k)} . \qquad (3.17)$$

III.3 Assumptions and fundamental equations

Here we shall continue the discussion within the framework of the model

presented in chapter II: we take Ω =h=1 and the metric element in the

standard synchronous gauge (see eq. (2.1)). The total background density

reads

$$\rho = \rho_b + \rho_r + \rho_X \tag{3.18}$$

the X label referring either to photinos or to neutrinos, ρ_r is the radia-

tion energy density and ρ_b that of baryons. For baryons we take a den-

sity parameter Ω_b =0.03.

For X particles the notations and fundamental equations are the same of

§II.1,II.2 and will not be reported here. An important difference arises

here in the numeric treatment of radiation and matter. In chapter II we were

interested in dark matter dynamics and a single fluid approximation has

been done for matter and radiation. This treatment is clearly inadequate

here since we wish to calculate the small fluctuations in the cosmic back-

ground radiation. To follow the evolution of radiation density fluctuations

through decoupling stages, a numerical solution of the Boltzmann equation

for the radiation brightnessis needed.

Then let us return to the linearized Boltzmann equation (A3.3) for the

radiation brightness $i_\vdash$. In our reference frame (see §II.1) this equation reads

$$\frac{\partial i_\vdash}{\partial t} + \frac{ik\mu}{a(t)} i_\vdash - \left[\frac{2}{3} P_0 \dot{h} + 2 P_2(\mu)\left(\dot{h}_{33} - \frac{\dot{h}}{3} \right) \right] =$$

$$= t_c^{-1} \left[\delta_\vdash + 4\mu v_m^- - i_\vdash \right] \qquad\qquad (3.19)$$

here v_m is the matter velocity , t_c is the collision time $t_c^{-1} =$ $n_e \sigma_T c x(z)$ in the time units defined by eq.(2.11); for the ionization degree x(z) one has to take into account the presence of massive weakly interacting particles which clearly affect the expansion rate and then x(z) (Bonometto et al. 1983).In eq.(3.19) the radiation density contrast $\delta_\vdash$ is defined as

$$\delta_\vdash = \int i_\vdash \frac{d\Omega}{4\pi} \qquad . \qquad\qquad (3.20)$$

Eq.(3.19) must be completed with the continuity and motion equation for matter. From eq.s (A3.8) we have

$$\begin{cases} \dot{\delta}_m = \frac{\dot{h}}{2} - \frac{iK}{a} v_m \\ \\ \frac{dv_m}{dt} + \frac{\dot{a}}{a} v_m = \frac{1}{\eta}\left[\frac{3}{4} \delta - v_m \right] \end{cases} \qquad (3.21)$$

here δ_m is the matter density contrast, $\eta = \dfrac{3}{4} \dfrac{\rho_m}{\rho_r}$ and $\mathcal{F}$ is

the radiation momentum

$$\mathcal{F} = \int i_r \, \mu \, \frac{d\Omega}{4\pi} \ . \tag{3.22}$$

To follow the evolution of radiation density fluctuations through decoupling

stages an useful approach is to develop the radiation brightness i_r

into spherical harmonics (Wilson and Silk 1981, Bonometto et al. 1983b)

$$i_r (k, \mu, t) = \sum_{\ell=0}^{\infty} \delta_\ell \, P_\ell (\mu) \, (-i)^{\ell} \ . \tag{3.23}$$

Then eq. (3.19) can be rewritten as

$$\begin{cases} \dot{\delta}_0 = \dfrac{2}{3} \dot{h} - \dfrac{k}{a} \dfrac{\delta_1}{3} \\[2ex] \dot{\delta}_1 = t_c^{-1} \left[4 i v_m - \delta_r \right] - \dfrac{k}{a} \left[\dfrac{2}{5} \delta_2 - \delta_0 \right] \\[2ex] \dot{\delta}_2 = - t_c^{-1} \delta_2 - 2 \left(\dot{h}_{33} - \dfrac{\dot{h}}{3} \right) - \dfrac{k}{a} \left[\dfrac{3}{7} \delta_3 - \dfrac{2}{3} \delta_1 \right] \\[2ex] \dot{\delta}_\ell = - t_c^{-1} \delta_\ell - \dfrac{k}{a} \left[\delta_{\ell+1} \dfrac{\ell+1}{2\ell+3} - \delta_{\ell-1} \dfrac{\ell}{2\ell-1} \right] , \ \ell \geq 3 \end{cases} \tag{3.24}$$

With the defintion (3.23) one has

$$\delta_r = \delta_o \qquad \qquad \mathcal{Y} = - i \frac{\delta_1}{3} \qquad , \qquad (3.25)$$

and eq.s(3.21) become

$$\left\{ \begin{array}{l} \dot{\delta}_m = \dfrac{\dot{h}}{2} \; - i \dfrac{k}{a} \, \sigma_m \\[4mm] \dfrac{d\sigma_m}{dt} \; + \; \dfrac{\dot{a}}{a} \, \sigma_m \; = \; \dfrac{1}{\eta} \left[-i \dfrac{\delta_1}{4} \; - \; \sigma_m \right] . \end{array} \right. \qquad (3.26)$$

Finally the gravitational field equations read

$$\ddot{h} - 2 \frac{\dot{a}}{a} \dot{h} = 6 \, a^{-4} \left[\delta_r \; + \; \frac{\rho_m}{2 \rho_r} \, \delta_m \; + \; c_x \, e_{1x} \, \delta_{x, \mathcal{Y}} \right]$$

$$\dot{h}_{33} - \dot{h} = \frac{6}{a^3 K} \left[- \frac{\delta_1}{3} \; - i \, \frac{\rho_m}{\rho_r} \, \sigma_m \; + \; c_x \, e_{1x} \, \mathcal{Y}_x \right] \qquad (3.27)$$

here $c_x, \, e_{1x}, \, \delta_{x, \mathcal{Y}}, \, \mathcal{Y}_x$ have the usual meaning.

The eq.s (3.24),(3.26), and (3.27) are completed by the set of eq.s (2.21)

(2.29) for X particles. The integration starts at an initial redshift

such that the single fluid approximation can be made for matter and radiation, then the initial conditions for the system of equations are the same as have been found in §II.3, with $\delta_m = D = \delta_r = \delta_o$, $\delta_1 = 4i\sigma_m$, $\delta_{\ell > 1} = 0$.

III.4 Numerical integration

For the X particles the set of eq.s(2.21) has been truncated at a ℓ_{max} (ℓ_{max} =120) such that the same stability criterion used in §II.4 is satisfied (see eq.2.49) . The integration over p has been made with a set of points p_i , in order to compute a Gauss-Laguerre quadrature for the X harmonics σ_o , σ_1 . The number of values p_i used to perform the integrals is 10; we have checked in a number of cases the effects of taking a different number of values p_i (7 or 14).This allows the conclusion that the accuracy reached taking 10 p_i ranges about a few percent. The maximum number of radiation harmonics has been 30, together with $\dot{h}$, δ_m and σ_m out system of 33+10(ℓ_{max} +1) equations has been integrated by means of a MERSON code of the CERN library, this code has been modified in order to treat more than 100 equations.

The following cases have been considered: γ - dominated Universe, with α^3_γ =4/11 β_γ =6 m_γ =32eV and photino-dominated Universe with α^3_X =1/25 β_X =2 m_X =880eV.

III.5 Results and discussion

In Fig.3.1 we show the expected values of $\Delta T/T$ for two possible antenna beams (σ =1'.8 and σ =3') for the γ and the X case. We illustrate five values of n, between -2 and +2. The curves directly yield $\Delta T/T$ (on a logarithmic scale) if $z_{h\ell}$ =1. For the sake of comparison, we indicate the observational limit of Uson and Wilkinson(1984), although it refers to an antenna beam of 1'.5 .

The difference between the calculated $\dfrac{\Delta T}{T}$ for the X and γ cases is due to the different transmission factors, which determine the normalization of $\Delta T/T$ in eq.(3.17) .

Let us stress that the Uson and Wilkinson (1984) observations refer to temperature fluctuations in the cosmic background radiation over an angular scale $\theta \simeq$ 4'.5, i.e. the corresponding mass scale is of the same order of the critical damping mass for neutrinos.

In the neutrino case the main contribution to the integrals in eq.(3.17) arises from the same mass range. For X particles the transmission factor τ_X is cut-off at much lower mass scales than for neutrinos (see also Fig.s 2.4-2.6), then the main contribution to the integral $\int_{o}^{\infty} dk\, k^{n+2}\, \tau_X^2 (k)$ comes from mass scales much below those giving the main contribution at $\Delta T/T$.

Then, in the X case, a decrease of n implies an increase of $\Delta T/T$,
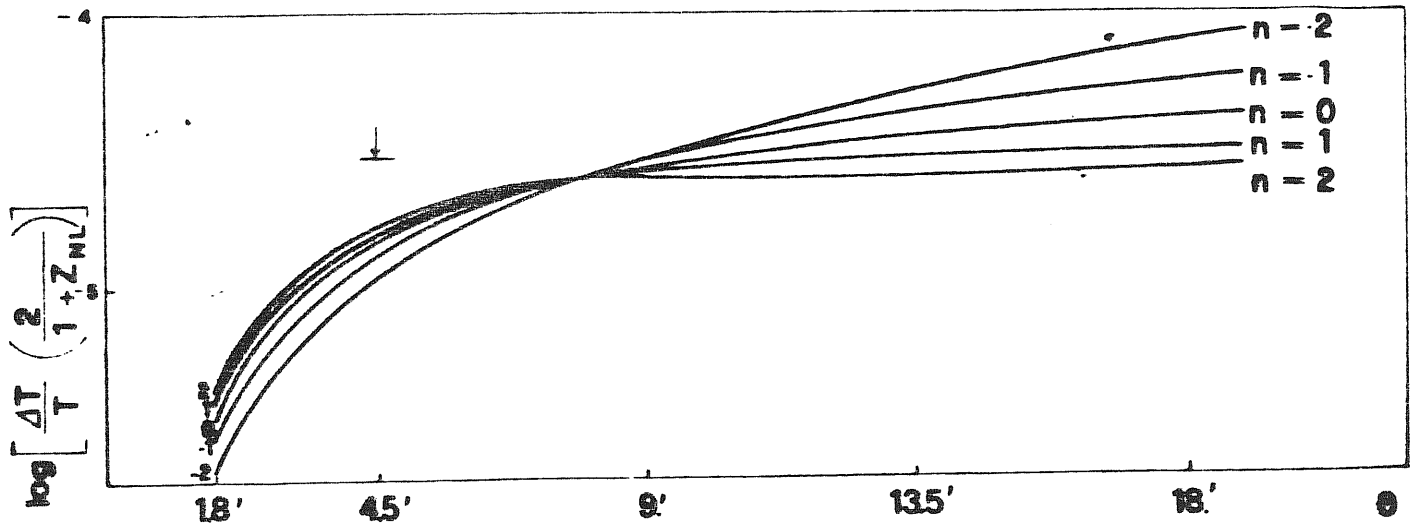
Fig. 3.1a
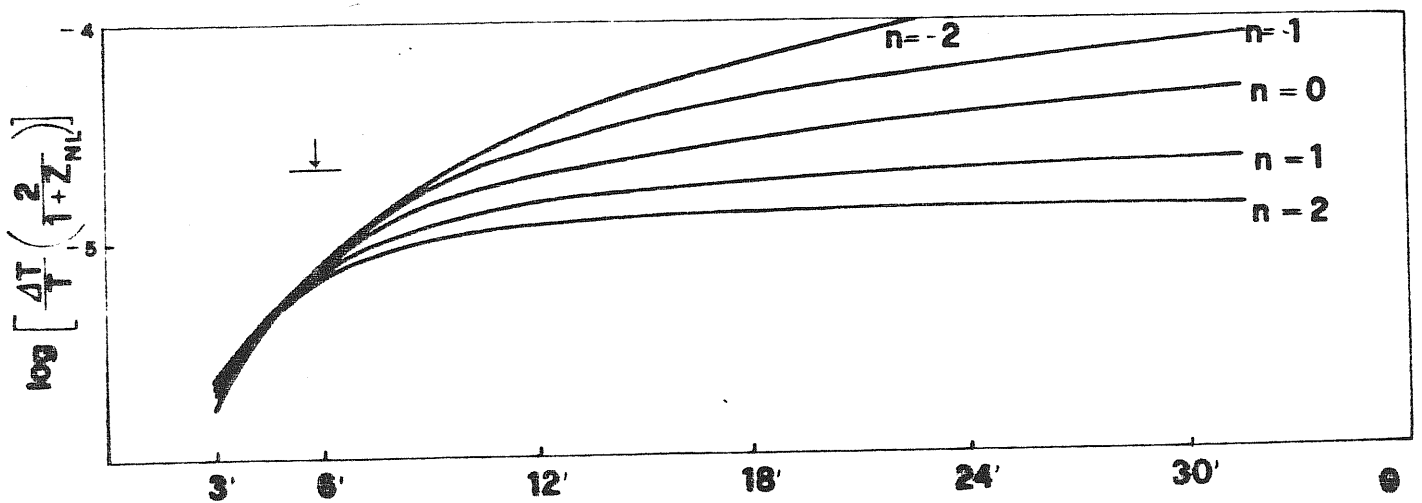
Fig. 3.1b

Fig. 3.1   The expected small scale anisotropies of MW background temperature are plotted

for the cases: a) ν,   σ = 1'.8; b) ν,   σ = 3'; c) X, σ = 1'.8; d) X, σ = 3'.
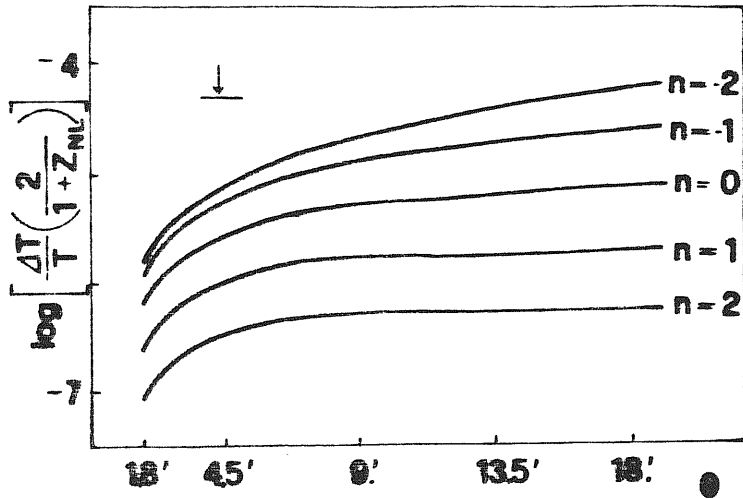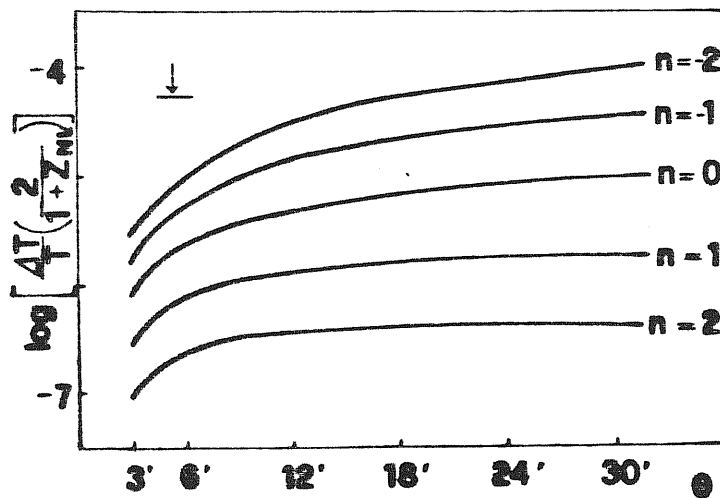
Fig. 3.1 c

Fig. 3.1 d

owing to the k^{h+2} factor in the integral over τ_x .

The present results can be compared, in the case of γ's, with those of

Szymanski and Jaroszynski (1983) which were however normalized to the

observed covariance function and calculated assuming an istantaneous hydro-

gen recombination and for the limit $\sigma =0$. Our results seem to indicate a

smaller $\Delta T/T$, which is not unexpected due to our more accurate treat-

ment of recombination. The present results can be also compared with those

obtained by Vittorio and Silk (1984) for the γ case, with which they

agree within 20%.

After completion of our calculation we received the results of calculations

by Bond and Efstathiou (1984) where $\Delta T/T$ are also computed both for the

neutrino case for the case in which the Universe is dominated by 'cold'

dark matter (axions, for example). Although their detailed results refer

to cases different from ours, the values of $\Delta T/T$ they calculate seem

to be smaller than ours by a factor $\simeq 2$. The critical aspect of this com-

parison is the different system of normalization they adopted. Here we

have preferred to normalize to $\delta M/M$ instead of making reference to any

observational data on clustering, for severe dobts exist on whether ligth

is really a good tracer of mass.

Our conclusions are therefore that a massive neutrino picture is consistent

with present limits on small-scale anisotropy of MW background radiation

if $z_{h\ell} \leq 2.5$, for the case n=1. It is possible to push $z_{h\ell}$ up to 4.5 if the fluctuation spectrum has n=-2. In the case of 'photino' of 880 eV, instead, the limiting values of $z_{h\ell}$ are 5.3,8.2,16,49,140 for n= -2,-1,0,+1,+2 , respectively. In this latter case and if primeval fluctuations have an n=1 (Zel'dovich) spectrum their trace in the MW background will be potentially observable only if $\Delta T / T \simeq 10^{-6}$ can be experimentally detected.

IV. FORMATION OF GALAXIES IN THE GRAVITATIONAL INSTABILITY THEORY

IV.1 The adiabatic and isothermal picture

It is now widely accepted that the present structures (galaxies, clusters) have been formed through the gravitational instability of primeval density perturbations which needed to be present in the early phase of the expanding Universe.

These primeval density fluctuations can be classified as adiabatic, where both the radiation and matter density are perturbed but the specific entropy is kept constant, or isothermal modes, where only the matter density is perturbed. At present the existence of isothermal density perturbations at early epochs is not favoured by grand unified theories, GUT.

In the GUT's scheme an excess of baryons over antibaryons is generated by non-conserving baryonic processes which violate CP at the baryosynthesis epoch ($T \simeq 10^{28}\,{}^{o}K$, see Weinberg 1982). In these theories the specific entropy is a constant which depends only on microphysical parameters and any preexisting isothermal perturbation would have been erased at the baryosynthesis epoch.

Adiabatic perturbations with a mass smaller than the Silk one (Silk 1968,

Peebles and Yu 1970, Wilson and Silk 1981, Bonometto et al. 1983b)

$$M_D \simeq 1.3 \cdot 10^{12} \, (\Omega h^2)^{-3/2} \, M_\odot \quad , \tag{4.1}$$

are erased at the matter-radiation decoupling by radiation diffusion.

At $z \gg z_{eq}$ the Jeans mass of the matter-radiation fluid is of the same

order as the horizon one $M_J \simeq M_H \simeq 10^{16} \left(\dfrac{1 + z_{eq}}{1 + z} \right)^3 \, M_\odot$;

between the equivalence and the recomination the Jeans mass takes a costant

value $M_J \simeq 10^{16} \, (\Omega h^2)^{-2} \, M_\odot$ and after the recombination (owing to

the drastic drop in the radiation pressure) M_J falls to $M_J \simeq$
$10^6 \, (\Omega h^2)^{-1/2} \left(\dfrac{1 + z}{1 + z_r} \right)^{3/2} M_\odot$, where $z_r \simeq 2 \cdot 10^3$.

Adiabatic perturbations which have $M > M_J$ when they cross the horizon

will grow in amplitude until the condition $M > M_J$ is satisfied.

Those adiabatic perurbations with $M_J (z = z_r) > M > M_D$ will start

to oscillate with nearly constant amplitude as $M < M_J$ until the recom-

bination; thereafter they will restart to grow as $\delta \propto (1 + z)^{-1}$ since

for them it is now $M > M_J$.

Adiabatic perturbations with $M < M_D$ will be erased during the recombina-

tion .

The growth of isothermal modes with $M > M_{Jm} \simeq 10^6 \, (\Omega h^2)^{-1/2} \, M_\odot$

is inhibited before the recombination by Thomson scattering (Peebles 1965).

However a small radiation density perturbation $\delta_{r\ IS}$ is initially present in the isothermal mode (LSS, §94). This $\delta_{r\ IS}$ is small as long as $\rho_b \ll \rho_r$ but becomes comparable to the matter density fluctuations in the matter dominated era.

For adiabatic perturbations with $M > M_D$ the mass of the perturbation after the recombination is many orders of magnitude greater than the Jeans mass, so pressure effects are not important: each small deviation from spherical symmetry (owing to the tidal forces by neighbouring perturbations) will be amplified in the non-linear collapse stages (Barrow and Silk 1981), in this case it is likely that the collapse of the perturbations is one-dimensional and that a thin pancake is formed in the final collapse phase. Zel'dovich (1970) has been the first to point out this feature for adiabatic perturbations.

In one-dimensional approximation the trajectory of a particle in the direction normal to the pancake plane is given by (Zel'dovich 1970)

$$z(q,t) = a(t)\,q + b(t)\,S(q) , \tag{4.2}$$

where $a(t)$ is the cosmic scale factor, q is the particle lagrangian coordinate, b(t) is a growing function of time which describes the perturbation evolution and S(q) represents the displacement of a particle from

its equilibrium position. The b(t) and S(q) functions are supposed to be determined by the initial amplitude and velocity of the perturbation.

For a sinusoidal plane wave perturbation it can be shown, in a Ω =1 Universe (Zel'dovich 1970, Zel'dovich and Sunyaev 1972)

$$z(q,t) = \alpha(t) \left[q - \alpha(t) B \sin kq \right] \quad , \tag{4.3}$$

where B is a generic constant and k is the comoving wavenumber of the perturbation. Mass conservation yields

$$\rho(z,t) = \bar{\rho} \; \frac{1}{1 + \frac{\partial S}{\partial q} \frac{b(t)}{\alpha(t)}} = \bar{\rho} \; \frac{1}{1 - B\alpha(t)k\cos kq} \quad . \tag{4.4}$$

From eq. (4.4) it can be seen that an infinite density is achieved at $t=t_c$ in the z=0 plane, with t_c determined by the relation

$$k B \alpha(t_c) = 1 \quad . \tag{4.5}$$

The reaching of an infinite density in the pancake plane at $t=t_c$ is prevented by pressure effects, when densities and velocities become large a shock wave is created at z=0 which will propagate outward.

As a first approximation the motion of the shock wave will be one-dimensional,

normal to the pancake plane. The velocity at which the material strikes

on the shock wave is $\dot{z} \simeq - \frac{3}{2} q / t_c^{1/3}$ and the baryon post-shock

temperature will be of the order of

$$T \simeq 10^6 (1 + z_c) q \,^\circ K \quad , \qquad\qquad (4.6)$$

where z_c is the redshift corresponding to t_c, q is determined from the

mass fraction of the perturbation which is shocked.

The post- shocked temperature and density are sufficiently great that a

fraction of the shocked gas cools radiatively at T $10^4 {}^\circ$K. In this scenario

a two-phase medium is expected (Doroshkevich and Shandarin 1974, Doroshkevich

et al. 1978): a thin layer of cooled gas surrounded by a hot gas at

T $\simeq 10^6 {}^\circ$K, and the pancake boundaries are determined by the shock wave

front which propagates outwards.

In the central region the physical conditions become favourable to galaxy

formation and owing to gravitational instability the cooled gas will fragment

into protogalactic clouds of mass $\simeq 10^7 - 10^9 M_\odot$, while in the

outer regions of the pancake the gas will be hotter ($T \simeq 10^6 {}^\circ K$) and

thermal instability might be important in forming protogalactic clouds

(Doroshkevich et al. 1978).

In the inner regions of the pancake the motion is one-dimensional and the

specific angular momentum of the gas will be rather low compared with

the boundary regions, where the gas motion is likely to be turbolent (the

velocity field of the gas which flows through an oblique shock wave can

gain a whirl component since the gas itself has gained entropy and the

Thomson theorem is violated, clearly the motion of the shock wave cannot

be approximate as one-dimensional, see e.g. Doroshkevich 1973).

A simple suggestion of the theory is that elliptical galaxies are expected

to be preferentially found in the inner and denser regions of clusters.

whereas spiral galaxies must be found mainly in the outer regions of clusters.

In the case of a neutrino dominated Universe a shock wave cannot arise for

collisionless particles but a neutrino pancake can be formed as well owing

to the high-frequency cut-off in neutrino density perturbations below M_{γ_c} .

After recombination baryons will be caught inside neutrino perturbation

potential wells and they will dissipate their energy through radiative

processes, while neutrinos do not.

A thin baryonic pancake is expected inside a three times thicker neutrino

pancake (Shukurov 1980), with neutrinos which are non-dissipative and

oscillate back and forth along trjectories normal to the pancake plane.

The fraction of gas which cools radiatively at $T \simeq 10^4 \,°K$ is found to be a

small fraction of the one which has undergone the heating from the shock

wave, about 10% (Shapiro et al. 1983, Bond et al. 1984). Numerical expe-

riments in a neutrino dominated Universe with Ω_γ =0.9, Ω_b =0.1

(Shapiro et al. 1983) have shown that at $z \simeq 1$ only 10% of baryons

(i.e. 1% of the closure density) will partecipate in the galaxy formation

inside the neutrino pancake, which has formed at $z_{r_c} = 6$, the remainder

of the baryonic gas will remain under the form of hot intergalactic gas.

The baryons which cool at $T \simeq 10^4 \, {}^\circ K$ are only a small fraction of the total

baryonic content of the pancake; this is essentially due to the Hubble flow

in the pancake plane, which led to a rapid decrease of the gas density and

temperature, thus reducing the ability of baryons to cool by means of ra-

diative processes. A crucial problem in the pancake theory with massive

neutrinos is the persistency of large scale structures. 3-D numerical simu-

lations (Mellott et al. 1983, Frenk et al. 1983, Klypin and Shandarin

1983 , but see Mellott et al. for a detailed discussion) have shown that

large scale structures cannot survive in a $\Omega = 1$ Universe owing to the

interactions with neighbouring trajectories.

This difficulty can be overcome with $\Omega \simeq 0.1$ or if pancake formation occurs

very recently, at $z \simeq 1$. As we have already seen both of these constraints

are unlikely to be satisfied in a neutrino dominated Universe.

Isothermal density perturbations with $M > M_{J_h} \simeq 10^6 M_\odot$ will begin to

grow in an Einstein-De Sitter Universe after recombination as $\delta_b \propto (1+z)^{-1}$

until they reach the non linear stage $\delta_b \simeq 1$, thereafter

they will separate from the Hubble flow to form bound systems.

At each epoch t_c there is a characteristic mass scale $M_c(z_c)$

which reaches the non-linear regime.

The characteristic mass scale with a density contrast of nearly unity

amplitude is today $M_{c_o} \simeq M_c(z=0) \simeq 10^{15} \Omega h^2 \quad M_\odot$,

for a primordial mass spectrum $\left\langle \left(\frac{\delta \rho}{\rho} \right)^2 \right\rangle \propto \left(\frac{M}{M_c} \right)^{-\alpha}$ this

yields (Rees 1978, White 1982)

$$M_c(z) \simeq 10^{15} (1+z)^{-1/\alpha} (\Omega h^2)^{1-\frac{1}{2\alpha}} M_\odot$$

$$t_c \simeq t_o \left(M_c / M_{c_o} \right)^{3\alpha/2}$$

$$(4.7)$$

where $\alpha = \frac{1}{2} + \frac{h}{6}$ and t_o is the Universe age. At each epoch between

the recombination and today perturbations on mass scales $M \gg M_c(z)$

will still be in the linear regime, while the ones with $M \ll M_c(z)$

will have already collapsed and formed virialized systems.

The growth of density perturbations over mass scales $M \gg M_c(z)$ will

proceed in a dissipationless way through the gravitational clustering of

perturbations which have already reached the non linear stage.

Since this picture lacks a preferred scale it is often referred to as the

' hierarchical clustering ' picture .

N-body numerical experiments (Aarseth, Gott and Turner 1979; Efstathiou

and Eastwood 1981) have shown that in a hierarchical clustering scenario

with Ω =1 and n=0 the slope of the computed two-point correlation

function $\xi(r)$ does not agree with the observed one at large radii

(R > $1h^{-1}$Mpc) and it is in fact much steeper.

An important extension of the h.c. scenario has been proposed by White

and Rees (1978). These authors note that the h.c. picture lacks a preferred

scale and that there is no natural explanation for the existence of galactic

size object. There is another point which weakens a pure non-dissipative

clustering : as a perturbation of mass M_c reaches the non-linear stages,

perurbations with masses $M \ll M_c$, which have already collapsed and

formed virialized systems, will be destroyed within few crossing times

$t_{cr} \simeq t_c (M_c)$ from the collapse of the perturbation which is just entering in

the non-linear stage.

This effect is mainly due to tidal disruption, coalescence and dynamical

friction and it has been confirmed by means of N-body numerical simulations

(White 1976) .Since many groups and clusters of galaxies have crossing

times much less than the Hubble age, $t_{cr} \ll H_o^{-1}$, a pure non

dissipative scenario does not explain the existence of galaxies in clusters.

The role of dissipation in galaxy formation processes has been remarked

by Rees and Ostiker (1977).

Let us consider a uniform spherical cloud with density ρ and temperature $T > 10^{4}\,°K$. The gravitational free-fall time scale of the cloud is

$$t_{grav} \simeq (24\pi G\rho)^{-1/2} \simeq 2.10^{7} h^{-1/2} \; yr \quad , \tag{4.8}$$

where n is the cloud number density in units of 1 particle cm^{-3}; the cooling time scale is given by

$$t_{cool} \simeq \frac{3}{2} \frac{k_{B} T}{h \Lambda(T)} \quad , \tag{4.9}$$

where $\Lambda(T)$ is the cooling function (Cox and Tucker 1969), $t_{cool} \simeq T^{3/2} h^{-1}$ for $T < 10^{6}\,°K$. The ratio of the cooling time scale to the free-fall one is (for $T < 10^{6}\,°K$)

$$\frac{t_{cool}}{t_{grav}} \sim \left(\frac{M_{J}}{10^{12} M_{\odot}}\right) \quad , \tag{4.10}$$

where $M_{J} \simeq \left(\frac{\pi k_{B}}{G m_{p} \mu}\right)^{3/2} T^{3/2} \rho^{-1/2}$ is the cloud Jeans mass. For $t_{cool} > t_{grav}$ a cloud of mass M and radius R will contract quasi-statically at a temperature $T \simeq \frac{G M m_{p}}{k_{B} R}$, the cloud will be pressure supported and its temperature will follow a $M \simeq M_{J} \simeq const$ ($T \propto \rho^{1/3}$) track in in a logT-log n plane.

As soon as $t_{cool} < t_{grav}$ the cloud will be able to cool radiatively within

a collapse time; the gas temperature will fall at $T \simeq 10^4 \, °K$ and the

cloud Jeans mass will drop to $M_J \simeq 10^8 (T/10^4 \, °k)^{3/2} h^{-1} M_\odot$, this

will lead the gas to fragment into small clouds with masses much less than

the total mass and galaxy size objects will form through the clustering

of these clouds.

From eq. (4.10) only clouds with masses $M < 10^{12} M_\odot$ will be able to fragment.

(Rees and Ostriker 1977).

White and Rees (1978) have proposed that baryons which fall inside dark

matter potential wells must dissipate their energy through radiative proces-

ses within a cooling time shorter than the crossing time of the perturba-

tion itself, i.e.

$$t_{cool} \simeq \frac{3}{2} \frac{k_B T_H}{h \, \Lambda(T_H)} \qquad (4.11)$$

where $T_H \simeq \frac{m_p}{k_a} \frac{G M_H}{R_H}$ is the halo virial temperature (M_H and

R_H are the mass and radius of the halo) must be shorter than the collapse

time of the perturbation. t_{grav} is of the same order of the Hubble age

at the epoch of the halo formation (which happens at a redshift z_H), then

$$t_{cool} (T_H) \leqslant 10^{10} (1 + z_H)^{-3/2} (\Omega h^2)^{-1/2} \, yr \, . \qquad (4.12)$$

The latter constraint yields a characteristic baryonic mass of the same order of the Rees and Ostriker one.

Owing to baryon dissipation galaxies will be strongly concentrated objects and will survive to the disruption of their dark haloes in clusters of galaxies. In the White and Rees (1978) scenario the bulk of the mass contribution is given by dark matter, while galaxies have formed through the cooling and collapse of the baryonic component.

IV.2 The angular momentum of a protogalaxy

One of the most important parameters in the galaxy formation theory is the amount of angular momentum which is possessed by a protogalaxy.

Following an old idea of Hoyle(1949) Peebles (1969) has suggested that protogalaxies can gain their angular momentum through tidal torques by neighbouring protogalaxies. Peebles (1969) calculation yields a dimension-less spin parameter

$$\lambda \simeq J \, |E_b|^{1/2} \, G^{-1} \, M^{5/2} \simeq 0.1 \qquad (4.13)$$

where J is the total angular momentum, E_b is the binding energy and M the protogalactic mass.

A more detailed calculation has been done by Efstathiou and Jones (1979)

with the aid of a N-body simulation. They found

$$\lambda_m \simeq 0.06 \pm 0.02 \quad , \tag{4.14}$$

roughly independent from the protgalaxy mass.

The mean value of λ in eq.(4.14) is in agreement with the low rotatio-

nal velocity observed in elliptical galaxies (Illingworth 1981, however

the flattening of elliptical galaxies cannot be explained in purely rotatio-

nal terms, see discussion in §IV.3).

The tidal torque theory is well developed only in the hierarchical clustering

picture. In the pancake scenario protogalaxies gain their angular momentum

through turbolent flow at the pancake boundaries, and in this case to esti-

mate the mean angular momentum of a protogalaxy is a much harder task.

Gott and Thuan (1976) have suggested that the key parameter in determing

if a protogalaxy will become an elliptical or a spiral galaxy is the amount

of energy which is dissipated during the protogalaxy collapse (see also

Sandage et al. 1970).

If the star formation rate per unit volume is approximately proportional

to the square of the gas density ρ (Schimdt 1959), then the rate of

the star formation time scale τ_s to the free-fall one τ_c of the

protogalaxy ($\tau_c \propto \varrho^{-1/2}$) behaves as $\tau_s / \tau_c \propto \varrho^{-1/2} \propto \tau_c$.

In the Gott and Thuan picture elliptical galaxies formed from perturbations

which have the largest density fluctuation $\delta\varrho/\varrho$ at the recombination.

These density perturbations are expected to complete the star formation

by the time of maximum collapse, then the protgalaxy will collapse in a

non dissipative way.

Spiral galaxies will form from denisty perturbations with smaller amplitude

at the recombination, τ_c is larger than for density fluctuations which

have created the elliptical galaxies and the star formation is not completed

by the time of maximum collapse.A substantial amount of gas is still pre-

sent in the protogalaxy at this epoch.The gas is dissipative and when hits the

plane dissipates its vertical velocity to form a disk.

The collapse time τ_c of a spherical inhomogeneity is related to the

amplitude $\delta\varrho/\varrho$ of the density perturbation at recombination by (Gunn

and Gott 1972)

$$\tau_c \simeq \frac{\pi}{H_o \, \Omega^{1/2} \, (1+z_r)^{3/2}} \left(\frac{\delta\varrho}{\varrho} \right)^{-3/2} . \tag{4.15}$$

For elliptical and spiral galaxies Gott and Thuan (1976) take

$\tau_c \simeq 10^8$ yrs and $\tau_c \simeq 10^9$ yrs, respectively.Then they found

$$\left\{ \begin{array}{l} \left(\frac{\delta \rho}{\rho} \right)_{\text{Ellipticals}} \simeq 0.25 \\ \\ \left(\frac{\delta \rho}{\rho} \right)_{\text{Spirals}} \simeq 0.06 \end{array} \right. \qquad\qquad (4.16)$$

at $z=z_r$, for $H_o=50$ Kmsec^{-1}Mpc^{-1} and $\Omega_b=0.1$.

A point which weakens the model is the assumption $\tau_s \propto \rho^{-1}$ even

at high redshift ($z \simeq z_r$) for Pop. II stars.

In the Gott and Thuan (1976) theory both elliptical and spiral galaxies

have formed from protogalaxies with, roughly, the same angular momentum.

For elliptical galaxies the mean value of λ is in agreement with the

observed rotation, but for spiral galaxies there are problems in explaining

the observed rotation.

To become centrifugally supported the disk material must have $\lambda \simeq 1$.

In a dissipative collapse it is $\lambda \propto R^{-1/2}$, then the gas in the disk

must be collapsed by a large factor, since initially it was $\lambda_i \simeq 0.06$.

For $M \simeq 10^{11} M_\odot$ and a typical disk length scale $\alpha^{-1} \simeq$ 3Kpc it is

found that the initial radius of the protogalaxy needs to be $R_I \simeq 1$ Mpc,

with a collapse time $\tau_c \simeq 3 \cdot 10^{10}$ yrs, larger than the Universe age.

A possible way to avoid this difficulty has been suggested by Fall and

Efstathiou (1980): since spiral galaxies are observed to be embedded in

dark haloes, the collapse of the dissipative gas has been amplified by the

dark halo potential well. If the initial gas radius was R_I and R_F the

final one,it is found

$$\frac{R_I}{R_F} \simeq \frac{9\pi}{125 \lambda^2_H} F \quad , \quad (4.17)$$

where λ_H is the dark halo spin parameter and F is the gaseous mass/

dark mass ratio at the galaxy formation epoch.

For $\lambda_H \simeq 0.07$ and $F \simeq 1/10$ one has $R_I/R_F \simeq 10$, a results which

is in agreement with dynamical arguments of Eggen,Lynden-Bell and Sandage

(1962).

Then, if one takes into account the presence of dark haloes, the observed

angular momentum of spiral galaxies can be well explained within the frame-

work of the tidal torque theory.

However now there are problems with the low rotation observed for elliptical

galaxies. The mass-to-light ratio for giant elliptical galaxies at the

De Vaucoulers radius is $(M/L) \simeq$ 10h, of the same order as the observed

one for spiral galaxies at the Holmberg radius.

In the White and Rees (1978) theory in order to explain the mass-to-light

ratio the visible material must have been collapsed by a factor 10 in radius

radius. Then it is difficult to understand why elliptical galaxies are

observed to rotate so slowly, with values of the spin parameter $\lambda \simeq 0.07$

of the same order as the pre-collapse one.

Kashlinsky (1982) has suggested the possibility that elliptical galaxies are formed in dark haloes with low values of λ_H , but the tidal torque theory is mass invariant to the first order.

The argument is still open and object of investigation in the literature.

IV.3 Numerical experiments

The luminosity profile of elliptical galaxies is well represented by the De Vaucoulers law $r^{1/4}$ (De Vaucoulers 1959; Kormendy 1977)

$$\log I(r) = \log I_0 - 3.33 \, (r/r_e)^{1/4} \tag{4.18}$$

where r_e is the radius which encloses half the light. King (1966) has shown that in elliptical galaxies the observed light distribution is fitted with a Maxwellian velocity distribution with a tidal cut-off.

The two-body relaxation time t_r for a self gravitating system of N stars is of the order of (i.e. t_r is defined as the time scale such that the individual star energies change by a fractional amount $\Delta \epsilon/\epsilon \simeq 1$)

$$t_r \simeq \frac{N}{8 \ln N} \, t_{cr} \tag{4.19}$$

where $t_{cr} \simeq R/V$, R and V are the characteristic radius and velocity

of the system. For elliptical galaxies it is $N \simeq 10^{11}$, $R \simeq 10 kpc$,

and $V \simeq 200 \, km \, sec^{-1}$ and then $t_R \simeq 10^{10} yr$, larger than the

Universe age.

Then two-body relaxation cannot be responsible for the relaxed stellar

distribution observed in elliptical galaxies.

Lynden-Bell (1967) has suggested that in a collapsing system the gravita-

tional potential ϕ undergoes strong fluctuations, so the individual

star energies will undergo strong changes owing to the rapid fluctuations

in the gravitational potential; this process is called violent relaxation.

Since $t_{cr} \ll t_R$ the system can be effectively regarded as collisionless

and the stellar distribution function $f(\vec{x}, \vec{v}, t)$ will obey the

Vlasov equation

$$\frac{\partial f}{\partial t} + \vec{v} \cdot \frac{\partial f}{\partial \vec{r}} - \vec{\nabla} \phi \cdot \frac{\partial f}{\partial \vec{v}} = 0 \quad , \tag{4.20}$$

In eq. (4.20) the stellar mass does not appears, so the final coarse grained

distribution $\bar{f}$ will not depend upon stellar masses, i.e. we do not

expect to see mass segregation in the final equilibrium configuration.

It has been shown by Lynden-Bell (1967) that the most probable final

coarse grained distribution for a collisionless system which undergoes

gravitational collapse is of the type (in the non degenerate limit)

$$\overline{f} = A e^{-E} \; , \tag{4.21}$$

where $E = \frac{1}{2} \sigma^2 + \phi$ is the individual star energy per unit mass. This

distribution function corresponds to the isothermal sphere and yields an

infinite total mass for the system.

However during the violent relaxation process several stars will be thrown

into high energy orbits, these stars will not undergo the strong fluctuations

of the gravitational potential in the inner regions and will not reach a

fully relaxed distribution. This incomplete violent relaxation produces

a truncated distribution; such as the King one (1966).

Many of the numerical simulations which have been done on the gravitational

collapse of a protogalaxy regard non dissipative systems.

Although the evidence for metallicity gradients (Faber 1977) seems to

suggest that dissipation might have played an important role in the formation

of elliptical galaxies, at least in the inner regions, in what follows we

shall mainly concentrate on non dissipative models.

In the numerical simulation for the gravitational collapse of a protogalaxy

a set of N points in a physical tridimensional space is left free to evolve in

time under the action of its own gravitational forces.

The time evolution of the system is followed for several colapse times, until the system seems to achieve an equilibrium state. Different final conditions will be achieved according to the different initial conditions which have been imposed on the system at the onset of the collapse. Numerical schemes differ mainly in the way of evaluating the gravitational potential ϕ of the system during its evolution. The summation method (Aarseth 1972.) is based on the direct solution $\phi \propto \Sigma\, m_i m_j / r_{ij}$ for the N particles. At small radii a cut-off is introduced in the potential ($\phi \simeq$ const as $r \to 0$) to avoid strong fluctuations in the forces between particles which would introduce an unphysical two-body relaxation, which is not observed in real galaxies. The maximum number of particles which can be handled with this technique is of the order of $N \simeq$ 2000-4000 . In the other numerical scheme the potential is calculated over a mesh solving the Poisson equation (particle-mesh algorithm) with the aid of Fourier transform (Hohl and Hockney 1969; Hohl 1971) .

The advantage of this method is that a much larger particle number can be trated ($N \simeq$ 20.000 - 50.000) , but the potential spatial resolution is limited by the minimum grid spacing.

In our numerical experiments (see chapter V) we have preferred to use a large number of particle and to solve the potential the latter technique has been used.

Numerical experiments for the gravitational collapse of non dissipative

rotating systems have shown that (Gott 1973; Ostriker and Peebles 1973;

Hohl and Zang 1979; Miller and Smith 1979):

i) In these numerical experiments the radial density profiles are steeper

than in reality, i.e. $\rho \sim r^{-4}$ while for elliptical galaxies is

$\rho \sim r^{-3}$

iv) System for which the rotation kinetic energy-potential energy ratio

is larger than $t = \overline{T_{rot}} / |W| > 0.14$ develop a bar instability and

the final system is a bar rotating end-over-end. Then rapidly rotating

elliptical galaxies would be expected to be prolate objects.

The problem of the density profile $\rho(r)$ which is steeper than

in reality can be solved with the accretion of background material onto

the protogalaxy (Gott 1975). In this way it is possible to show that the

final $\rho(r)$ behaves as $\rho(r) \propto r^{-2.7}$ (Gott 1975, but for

a different opinion see Prior and Lecar 1983).

It has been suggested (Miller 1978) that elliptical galaxies can be pro-

late objects rotating around the minor axis. This hypothesis has been

criticized by Bynney (1980) ; a comparison between different models can

be done with a diagram of the peak rotational velocity v_p over the central

velocity dispersion σ , v_p/σ , versus the ellipticity ε of the

system. Binney (1980) finds that the prolate model for elliptical galaxies

does not agree with the observed distribution of points in the $v_p / \sigma - \varepsilon$

diagram (see also Davis et al. 1983).

After the discovery that rotation is dynamically unimportant for elliptical

galaxies (see Ilingworth 1981 for a review on the subject) a central point is

the explanation of the observed flattening for these systems.

Binney (1976) has suggested that the flattening of elliptical galaxies,

rather than to rotation, is due to an anisotropic stellar velocity distri-

bution. Aarseth and Binney (1978) have investigated in detail this hypo-

thesis: in their numerical simulation the protogalaxy begins to collapse

with a disk shaped spatial stellar distribution (as suggested in the pan-

cake theory of galaxy formation) .

In the inner regions the violent relaxation is effective in producing an

isotropic velocity distribution , while in the outer regions, owing to

the geometry of the initial configuration, the azimuthal velocity dispersion

is much smaller than the radial one.

In the Aarseth and Binney (1978) experiment the density profiles are in

good agremeent with the Hubble ones, but unfortunately the imprint of the

initial conditions is too strong, their minimum flattening corresponds to

an E5 elliptical type, while the large majority of elliptical galaxies is

of $\simeq$ E3 type. the model of Aarseth and Binney (1978) is triaxial

(a > b > c) and this seems a natural way to explain the observed isophote

twisting (Carter 1978; Leach 1981) seen in several elliptical galaxies.

The growth of the bar instability for rotating system can be suppressed

with the introduction of a non rotating halo of stars, which reduces the

$$t = \overline{T}_{rot} \, / \, |W| \qquad \text{ratio.}$$

This has been checked in various numerical simulations, with the halo re-

presented by a fixed external potential (Hockney and Brownrigg 1974;

Berman et al. 1978; Combers and Sanders 1981) or the halo itself was

allowed to follow a dynamical evolution (Hohl 1978). In the latter case

the halo was bulge-like, concentrated at the center of the system.

In these cases it is found that the introduction of a dark halo is effecti-

ve in suppressing the growth of the bar instability.

In the next chapter we shall show a numerical experiment where both the

halo (extended) and the spheroidal system collapse and undergo dynamical

evolution.

These conditions ought to be appropriate to mimic in the numerical experiment

the dynamical evolution of an elliptical galaxy embedded in a dark halo.

V. NUMERICAL INTEGRATIONS ON THE COLLAPSE OF NON-DISSIPATIVE ROTATING

STELLAR SYSTEMS IN THE PRESENCE OF A DARK HALO

V.1 Introduction

In this chapter the results obtained are presented in a series of numerical

experiments to simulate the gravitational collapse of a protogalaxy in the

presence of a dark halo. This research program has yet to be fully investiga-

ted and the discussion of the results is only qualitative, so this chapter

is intended to be an exposition of the work done at the moment of writing

the thesis. In these numerical experiments we assume for simplicity that

both dark matter and baryons behave in a collisionless way.

the numerical treatment of a mixed scheme, where both a gaseous and a

stellar component is present for baryons (Miller and Smith 1981) ,

is much more complicated and will not be tackled here.

The model used here to simulate the gravitational collapse of a galaxy

consists on N representative particles which moves inside a tridimensional

32^3 active array of cells. Each particle shares its mass density

contribution among the eight nearest grid points, according to the cloud-

in-cell CIC method (Birsdall and Fuss 1969).

The gravitational potential ϕ is obtained from the density by solving

the Poisson equation over a 64x64x32 mesh with the aid of Fast-Fourier-Transforms (Hohl and Hockney 1969).

The potential calculation requires a mesh larger than the 32^3 active array, in order to avoid periodicity effects associated with the Fourier transforms (Hockney 1970; Eastwood and Brownrigg 1979).

The force acting on each particle is calculated by differencing the potential at the nearest grid points; forces are weighted with the same CIC procedures used in the density computation.

The velocity and position of a particle are advanced by a timestep DT, using the time-centered leapfrog method (Buneman 1967).

Then the new density is calculated and the full procedure is repeated until a steady-state is achieved.

The details of the integration are described in §V.2 .

Let us now consider which conditions the protogalactic baryonic gas must satisfy in order to undergo a collisionless gravitational collapse (Kashlinsky 1982)

From eq.(4.12) the gas in the halo should cool and fragment for a halo mass $M_H \leqslant 5 \cdot 10^{12} M_\odot$. However this condition is not suuficient to allow gas fragmentation because of halo tidal forces. These forces will disrupt gas gragments unless the local gas density exceeds the halo one, i.e.

$$\rho_\gamma (r_\gamma) \geqslant \rho_H (r_\gamma)$$

then gas fragments will successfully form at a gas radius r_g (making

the rough assumption that both the halo and the gas have nearly uniform

density)

$$r_g \leqslant F^{1/3} R_H \simeq \frac{R_H}{2} \qquad (5.1)$$

where $F = M_g / M_H \simeq 1/10$, M_g is the gas mass and R_H is

the halo radius.

Collisions between fragments will be negligible if the fragment mean

free path ℓ_F is larger than the gas radius r_g when it fragments.

If the condition $\ell_F > r_g$ is satisfied coalescence between fragments

is not important and their collapse is non-dissipative; the criterion $\ell_F \gtrless r_g$

turns out to depend on the gas angular momentum at the onset of fragmentation.

Let us suppose that at the beginning of non-linear phases the total angular

momentum J per unit mass was the same for the two matter components (Fall

and Efstathiou 1980), i.e.

$$\frac{\overline{J}_g}{M_g} = \frac{\overline{J}_H}{M_H} \qquad . \qquad (5.2)$$

since the halo+gas systems have undergone the same external torques.

From eq.(4.1) the gas and halo spin parameters λ_g and λ_H ,respectively,

are related by

$$\lambda_{\gamma} (r_{\gamma}) \simeq \lambda_{H} (R_{H}) \; F^{-1/2} \; (r_{\gamma} / R_{H})^{-1/2} \; . \tag{5.3}$$

The initial fragment radius r_{γ} is of the order of the gas Jeans length at r_{γ} , so

$$r_{F} \simeq r_{J} \simeq \left(\frac{\pi k_{B} T_{\gamma}}{m_{p} G} \right)^{1/2} \; \ell_{\gamma}^{-1/2} \; , \tag{5.4}$$

we take the fragment mass $M_{F} \simeq M_{J} (T_{\gamma})$, and the gas temperature $T_{\gamma} \simeq 10^{4} \, °K.$

At the onset of gas fragmentation the fragment spin parameter λ_{γ} is of the same order of λ_{γ} . We assume that $\ell_{F} \simeq \dfrac{1}{n_{F} \, \sigma_{F}}$, where n_{F} is the fragment number density and σ_{F} their final geometrical cross-section. Then the condition

$$\ell_{F} \simeq \frac{1}{n_{F} \sigma_{F}^{2}} \simeq \frac{1}{n_{F} \lambda_{\gamma}^{4} r_{J}^{2}} > r_{\gamma} \; , \tag{5.5}$$

where $n_{F} \simeq \dfrac{M_{\gamma}}{M_{F}} \dfrac{1}{r_{\gamma}^{3}}$ and $\sigma_{F} \simeq \lambda_{F}^{4} \, r_{F}^{2}$, yields

$$\lambda_{H} \lesssim F^{3/8} \; (r_{\gamma} / R_{H})^{5/8} \; \left(T_{\gamma} / T_{H} \right)^{1/8} \; , \tag{5.6}$$

here $\overline{T}_H \simeq \dfrac{G M_H}{R_H} \dfrac{m_p}{k_B}$ is the halo virial temperature.

Taking $M_H \simeq 10^{12} M_\odot$, $R_H \simeq 50 \, Kpc$, and $M_g \simeq 10^{11} M_\odot$,

eq.(5.6) gives $\lambda_H \leqslant 0.1$, then eq.s(5.1),(5.3) imply that for

$$\lambda_g \leqslant 0.5 \qquad\qquad (5.7)$$

collisions between gas fragments are not important and their collapse will

proceed in a collisionless way.

It must be stressed that the hypothesis of a halo of finite extension

is arbitrary, for example in spiral galaxies the rotational curve is

is flat up to the limits of detectability and the total halo extension

is unknown, however we are forced to make this approximation since we

must put the dark halo inside a computational box of finite extension.

As long as we are interested in the dynamics of the visible part of the

galaxies (i.e. at radii much less than R_H) the assumption of a halo of

finite extension is still reliable.

V.2 Numerical integration

Many of the numerical techniques used here are describeed in the

Hockney and Eastwood bock (1981), here we describe only the essential features.

a) Initial particle position

In the literature the initial particle positions are usually assigned by distributing the particle coordinates at random inside a given geometrical configuration (spherical or ellipsoidal) in order to produce a uniform mass density. This procedure generates Poissonian noise on length scales below the grid spacing L . To avoid these statistical fluctuations the initial particle coordinates have been determined in such a way that the initial mass density of our system is fully uniform. This has been done in the following way: for a given initial geometrical configuration of el-lipsoidal type , with semi-axes a > b > c, the N particles are distributed inside the ellipsoid with an interparticle separation D. A separate code is used to determine D such that the N particles fill the ellipsoid volume

$$V = \frac{4\pi}{3} a \, b \, c \quad .$$

b) Initial particle velocities

Each particle has an initial velocity which is the sum of a solid-body rotation with angular velocity $\Omega = \alpha_r \, \Omega_o$ ($\Omega_o = (GM / R_I^3)^{1/2}$, M and R_I are the mass and the initial radius of the system) plus a peculiar thermal velocity.

The initial peculiar particle velocities have been determined from a

given velocity distribution specified by a cut-off velocity $V_c = \alpha_V \sqrt{\dfrac{GM}{R_I}}$

Two possible kinds of velocity distribution have been considered. In

the uniform case (U) the cartesian components for the peculiar velocity

of each particle have been randomly chosen, with equal probability, in the

interval between 0 and V_c , and the maximum allowed velocity modulus was

V_c . In the other case the velocity distribution was gaussian (G) with

velocity dispersion $\sigma = V_c$, and a $3-\sigma$ cut-off has been introduced

to avoid very high particle velocities.

Then the initial particle velocity distribution is fully determined by the

two parameters α_r and α_V .

c) Charge assignments and forces

The mass density $\rho\,(\vec{x}_P)$ at the grid point $\vec{x}_P$ ($\vec{x}_P =$

(iL,jL,kL); i,j,k integers with $1 \leqslant$ i,j,k $\leqslant$ 32; L : grid length)is

given by

$$\rho\,(\vec{x}_P) = \frac{m}{L^3} \sum_{i=1}^{N} W\,(\vec{x}_i - \vec{x}_P) \quad , \qquad (5.8)$$

here $\vec{x}_i$ are the coordinates of the N particles of mass m and

$$W\,(\vec{x}) = \begin{cases} \left(1 - \dfrac{|\vec{x}|}{L}\right)\left(1 - \dfrac{|\vec{y}|}{L}\right)\left(1 - \dfrac{|\vec{z}|}{L}\right) & \text{for } -\vec{x} \leq L \leq \vec{x} \\[2em] & \qquad\qquad (5.9) \\[1em] 0 & \text{otherwise} \end{cases}$$

is the CIC charge assignment function.

The potential ϕ at the grid point $\vec{X}_p$ is given by

$$\phi(\vec{X}_p) = L^3 \sum_{p'} G_{p-p'} \; \rho(\vec{X}_{p'}) \; , \qquad (5.10)$$

where

$$\begin{cases} G_{i,j,k} = (i^2 + j^2 + k^2)^{-1/2} & (0 \leq i,j,k \leq 32 \; ; \; i^2 + k^2 + j^2 \neq 0) \\[2em] G_{0,0,0} = 1 \end{cases} \qquad (5.11)$$

is the Green function for our isolated system.

The choice $G_{0,0,0}=1$ is equivalent to setting the self-potential of a star equal to unity, we have introduced this cut-off in the potential to avoid two-body relaxation effects in our integration.

The summation in eq.(5.10) can be avoided with convolution methods, eq.(5.10) can be rewritten as

$$\hat{\phi}_{i,j,k} = \hat{G}_{i,j,k} \; \hat{\rho}_{i,j,k} \qquad (5.12)$$

where the symbol $\hat{f}$ denotes the discrete Fourier transform

$$\hat{f}_{j,k,\ell} = \frac{1}{(2N_g)^3} \sum_{m,n,p=0}^{2N_g} f_{m,n,p} \; e^{i \frac{2\pi}{2N_g} [jm + nk + p\ell]} \qquad (5.13)$$

here $N_g=32$ is the number of active grid points and j,k,l are harmonics wave number. In eq.(5.13) the mass density ρ is taken to be 0 outside the active array.

After $\hat{\phi}$ has been found the potential $\hat{\phi}$ can be obtained with the inverse transform.

The field $E_x(\vec{x}_p)$ is defined by ($\vec{x}_p$ = (pL,mL,nL))

$$E_x(\vec{x}_p) = \frac{\phi_{p+1,m,n} - \phi_{p-1,m,n}}{2L} \quad , \qquad (5.14)$$

and similarly for $E_y(\vec{x}_p)$, $E_z(\vec{x}_p)$.

The force acting on a particle of coordinate $\vec{x}_i$ is

$$\vec{F}(\vec{x}_i) = m\sum_{p}' W(\vec{x}_i - \vec{x}_p)\, \vec{E}(\vec{x}_p) \, . \qquad (5.15)$$

d) Equation of motions

The velocities and coordinates of a particle are advanced at the time t, according to the standard leapfrog scheme

$$\begin{cases} \vec{v}_i^{(n+1/2)} = \vec{v}_i^{(n-1/2)} + DT_V^{(n)}\, \vec{F}(\vec{x}_i) \\[3em] \vec{x}_i^{(n)} = \vec{x}_i^{(n-1)} + DT_x^{(n)}\, \vec{v}_i^{(n+1/2)} \end{cases} \qquad (5.16)$$

here n is the timestep number and $DT_V^{(n)}$, $DT_X^{(n)}$ are determined by

$$
\begin{cases}
DT_V^{(n)} = \frac{1}{2} \left(DT_X^{(n)} + DT_X^{(n-1)} \right) \\
\\
DT_X^{(n)} = MIN \left(\frac{L_l}{V_{MAX}} , \frac{1}{\sqrt{4\pi G \rho_{MAX}}} \right)
\end{cases}
\tag{5.17}
$$

where V_{max} and ρ_{max} are the maximum velocity and density of the

system at the time t. Two different timesteps have been used for velocities

and coordinates in order to keep as close as possible to second order

accuracy in the integration. Initially $DT_V^{(o)} = DT_X^{(o)}$.

Particles which escape the grid boundaries undergo a Keplerian force, with

all the mass inside the cube concentrated at the center.

When these particles cross the grid boundaries a linear interpolation pro-

cedure between the Keplerian forces and the grid forces is used to determi-

ne the forces acting on them, in order to avoid jumps in the velocities.

In all our integrations the number of escaped particles from the cube

has never exceeded 15% of the total particle number.

The calculations have been performed in dimensionless units x'=x/L,

$t'=t/t_u$, with $t_u = \sqrt{\dfrac{L^3}{G\,m}}$.

All the integration have been stopped at the final time $t=3t_c$, with

$t_c = 2\pi \sqrt{\dfrac{R_I^3}{GM}}$.

e) Diagnostics

The rotational kinetic energy of the system is defined as

$$T_c = \frac{1}{2} m \sum_{i=1}^{N} \overline{V_{\varphi,i}}^2 \quad ,$$

(5.18)

here $\overline{V_{\varphi,i}}$ is the average rotational velocity at $\vec{x}_i$. For the random

kinetic energy of the system the following definition is used

$$T_r = \frac{1}{2} m \sum_{i=1}^{N} \left(\sigma^2_{r_i} + \sigma^2_{\theta_i} + \sigma^2_{\varphi_i} \right) \quad ,$$

(5.19)

with

$$\sigma^2_r = \overline{v_r^2} - \overline{v}_r^2 \ , \quad \sigma^2_\theta = \overline{v_\theta^2} - \overline{v}_\theta^2 \ , \quad \sigma^2_\varphi = \overline{v_\varphi^2} - \overline{v}_\varphi^2 \quad .$$

(5.20)

In eq.s(5.18),(5.20) the mean velocities are determined averaging the

particle velocities over a spatial grid of radius 32L and spacing L/2 .

When T_r and T_c are calculated the particle velocities are shifted by a

timestep

$$\vec{v}_i^{(h)} \longrightarrow \vec{v}_i^{(h)} + \frac{DT_V^{(h)}}{2} \vec{F}_i^{(h)} \quad ,$$

(5.21)

in order to compare the kinetic energies and the potential energy at the

at the same time t.

The potential energy W is defined by

$$W = -\frac{1}{2} \sum_{i,j,k=1}^{32} \rho_{i,j,k} \, \phi_{i,j,k} \quad . \qquad (5.22)$$

The accuracy of the integration has been checked using the ratios

$$e(t) = \frac{E(t)}{E(t=0)} \quad , \quad E = T_c + T_r + W$$

$$\ell(t) = \frac{L_z(t)}{L_z(t=0)} \quad , \quad L_z = \sum_{i=1}^{N} x_i V_{y_i} - y_i V_{x_i} \qquad (5.23)$$

here $E(t)$ and $L_z(t)$ are the energy and angular momentum of the system

at the time t.

The variable e has never been found to change by more than 5% in our

integrations, while l(t) has achieved no more than a fractional change of

10% in several cases.

For this kind of problem and the computer resource we have available,

these numbers indicate a quite good accuracy.

V.3 Results and discussion

In the first series of numerical experiments we have investigated the

collapse of non-dissipative rotating systems with uniform density.

a) N-body simulations for the collapse of collisionless systems

This first series of numerical integrations will be entitled G since it considers

the non-dissipative collapse of a galaxy, without a dark halo.

The initial conditions of the models are shown in Table I.

Hereafter time is in units of $t_c = 2\pi \left(\dfrac{R_I^3}{GM} \right)^{1/2}$.

The time evolution of several systems under consideration is shown in

Fig.s5.1-5.3 . In these plots 2000 different particles have been randomly

chosen, at the beginnning of the integration, from the full set of N

particles; their spatial distribution is shown at various time in the x-y,

x-z planes.

The stellar energy distribution is shown in Fig.s5.4-5.7 at various epochs

for model G2-G5.

We do not show model G1 at all here since it starts to collapse in almost

virial equilibrium, without rotation, and has not shown particular characte-

ristics during its evolution.

Other quantities of interest are the behaviour of the mass density $\rho(r)$

versus radius, the radial and azimuthal velocity dispersions σ_r , σ_φ

and the average rotational velocity $\overline{v_\varphi}$.

TABLE I

	R_I^a	M^b	$R_I'^c$	N^d	q_r^e	q_v^f	Vel.^{g} Distr.	$T_r/|W|^h$	$T_c/|W|^i$
G1	14	1.10^{11}	14	3.10^4	0.1	1	U	0.5	4.10^{-3}
G2	14	1.10^{11}	14	3.10^4	0.1	0.7	U	0.25	4.10^{-3}
G3	14	1.10^{11}	14	3.10^4	0.1	0.33	G	0.25	4.10^{-3}
G4	10	1.10^{11}	10	3.10^4	1	0.33	G	0.25	0.33
G5	10	2.10^{11}	10	3.10^4	0.866	0.233	G	.125	.25

a) Initial radius in Kpc

b) Total mass in solar units

c) Initial radius in grid length units

d) Total number of particles used in the simulation

e) Initial angular velocity in units of $\Omega_o = (GM/R_I^3)^{1/2}$

f) Cut-off velocity for the peculiar velocity distribution in units of $(GM/R_I)^{1/2}$

g) Kind of velocity distribution (see §V.2)

h) Initial ratio of the random kinetic energy to the total gravitational energy

i) Initial ratio of the rotation kinetic energy to the total gravitational energy

The set of variables $\{ \rho(r), \sigma_r(r), \sigma_\varphi(r), \bar{v}_\varphi(r) \}$ is

calculated at the radius r and at the polar angle θ with the azimuthal

averages taken over a ring of thickness $\Delta r = 1 Kpc$ and angular width

$\Delta \theta = 10°$. The quantities $\{ \rho(r), \sigma_r(r), \sigma_\varphi(r), \bar{v}_\varphi(r) \}$

are shown at the final time t=3 in Fig.s5.8-5.11, for three different values

of the polar angle θ (θ = 90°,60°,45°). In order to reduce the di-

spersion between the quantities at different θ , the full set of N parti-

cles has been used in calculating the averages.

The evolution if the random and rotational kinetic energy to potential energy

ratios is shown in Fig.s12 for model G3-G5. The model G3 and G5 have the

same initial conditions as models I and IV of Hohl and Zang (1979, here-

after HZ) and our final $\{ \rho(r), \sigma_r(r), \sigma_\varphi(r), \bar{v}_\varphi(r) \}$ for these

models can be compared with the corresponding ones in HZ * .

These plots are in good agremeent with those of HZ, giving us a fiducial

test for our N-body code.

The collapse of non dissipative rotating systems has been already discus-

sed in the literature (Gott 1973; Miller and Smith 1979; HZ). Here we

report only the main features.

In models where the rotation is negligible (G2- G3) the collapse clearly

---

* Model G3 has the same $(T_r/W, T_c/W)_{t=0}$ as HZ but with $M=10^{11} M_\odot$ and $R_I=$ 14 Kpc, while in HZ is $M=2.10^{11} M_\odot$ and $R_I=10$ Kpc, so the variables shown in Fig. 5.9 must be rescaled to HZ units.

proceeds in almost a spherical way (Fig.5.1); the time evolution of the

$T_r / |W|$ ratio is shown in Fig. 5.12a for model G3, from this figure

it can been seen that $T_r / |W|$ becomes nearly constant for t≥1, indicating

that model G3 has already achieved a steady-state by t=1. This can also be

seen from Fig.s5.5 where the stellar energy distributions for model G3 are

similar at t=2 and t=3.

Fig. 5.5c shows a separation of the stellar energies into a two-component

core+halo structure. The halo component in the energy distribution arise

from fluctuations in the potential ϕ (see also $T_r / |W|$ in Fig.5.12a

at t < 1) which have thrown into high-energy orbits a fraction of the

stellar populations.

Model G2 has the same initial conditions as model G3 and it is equivalent

to it, expect for the different kinds of initial velocity distributions

in the two cases. The energy histograms for this model are shown

at different epochs in Fig.s 5.4 . The final separation into a core + halo

structure is much less pronounced than in model G3 (compare also Fig.s

5.8 with the correspondings 5.9 for model G3).

The different types of final stellar energy distributions for model G2 and

G3 support Henon's idea (Henon 1964; Gott 1973) that the halo population

is formed by those stars which initially have the highest $T_r / |W|$ ratios

with respect to the mean of the system, with outward directed radial velo-

cities. This fraction of stars will fall towards the center when the bulk

of the system has already passed the first collapse phase and is expanding

with $\dot{\phi}$ positive; in this way they will gain energy and a halo will

form. Owing to the different kinds of initial velocity distributions this

fraction of stars is smaller in model G2 than in G3 (see Fig. 5.4a and 5.5a).

Model G5 satisfies the Ostriker and Peebles criterion (1973), for this

model the initial $T_c / |W|$ ratio is grater than 0.14 and a bar develops

during the collapse stages.

A comparison between Fig.5.2 (model G4) and Fig.s 5.3 (model G5) shows

that at t=3 model G5 has already developed a bar , while G4 has not.

Model G4 has $T_c / |W|$ =0.33 at t=0 but it is rather hot ($T_r / |W|$ =0.25

at t=0) with respect to the initial conditions of Ostriker and Peebles

(1973), which were designed to prevent local Toomre (1964) instabi-

lities.

A comparison between Fig.s 5.6 and 5.7 (models G4 and G5) for the stellar

energy distribution clearly shows that model G5 has already achieved a

a steady-state by t=2.4 (see in particular Fig. 5.7c and 5.7d) while

model G4 is still far from equilibrium (compare Fig. 5.6c with 5.7d).

Fig. 5.7d shows that the occurence of a bar mode implies a more uniform

energy distribution,with respect to non- rotating systems.

In Fig. 5.12b,5.12c the time evolution of the $\left(T_r / |W|, T_c / |W| \right)$ ratios

is shown for model G4 and G5. Fig. 5.12C shows that rotational kinetic

energy is turned into random energy as the system develops a bar, this is

due to the flow of angular momentum towards outer regions (Hohl 1975),

which implies a reduction of rotational energy and by energy conservation

an increase in the energy of random motions.

This tendency is more pronounced for model G5 than for model G4.

The final $\rho(r)$ are shown in Fig.s 5.9a,5.10a,5.11a for model G3,G4,G5.

A comparison between Fig. 5.11a and 5.9a shows that the separation between

the core and the halo is less pronounced for model G5 than for the non-

rotating one G3, as already noted by HZ.

The change in the slope of $\rho(r)$ in models G3,G4,G5 can be identified

at a radius r_c= (8,4,4) Kpc, respectively. For $r > r_c$ models G3,G4,G5

have a density profile $\rho(r) \propto r^{-4}$, in agreement with those found

by Gott (1973).

The velocity dispersions σ_r , σ_φ are shown in Fig.s (5.9b,c),

(5.10b,c),(5.11b,c) for models G3,G4,G5. For these models $\sigma_r \simeq \sigma_\varphi$ at

$r < r_c$, while the radial fall off in σ_φ at $r > r_c$ is steeper

than for σ_r ,since the halo population has been formed from stars

with the highest radial velocities.

The rotation curves shown in Fig.s 5.10d,5.11d for models G4 and G5 are

characterized by an inner region of solid-body rotation and a radial fall
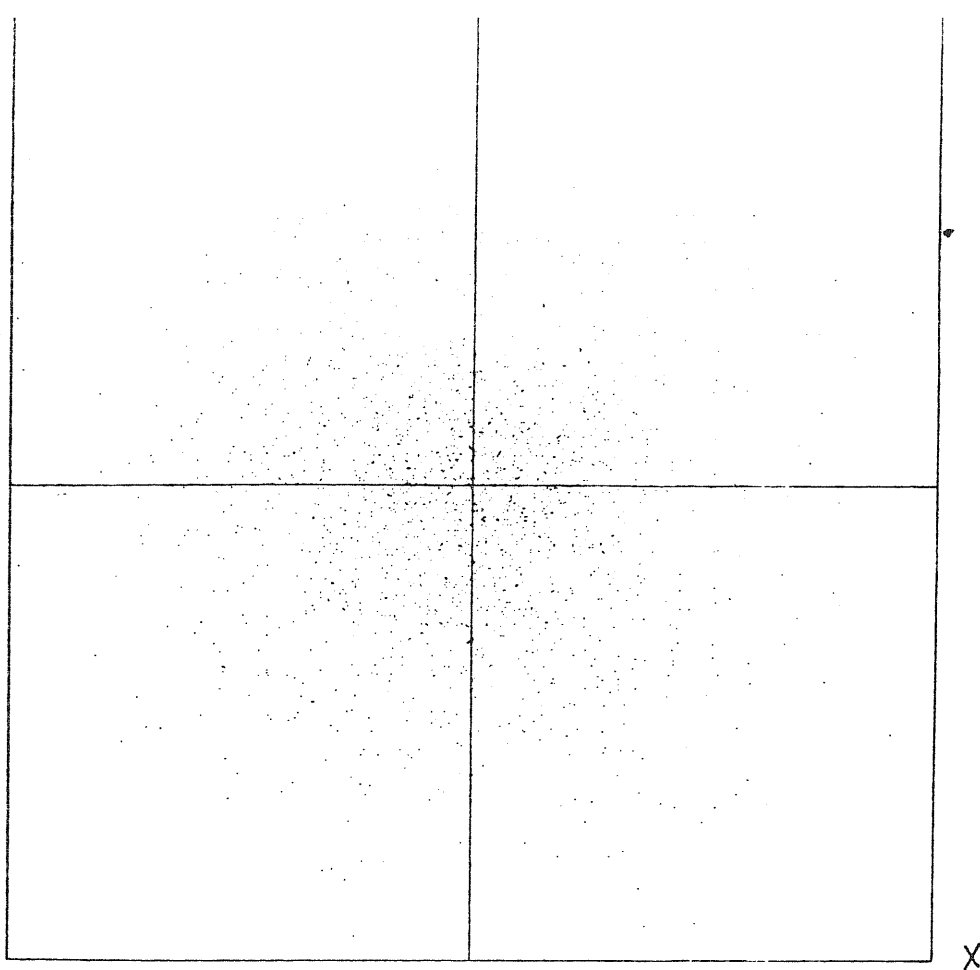
Fig. 5.1a   Particle plot of an initially nonrotating stellar system with $(T_r/|W|)_{t=0}$ =0.25 (model G3) in the x-y plane. Time is in units of $t_c = 2\pi(R_I^3/GM)^{-1/2}$, R_I is the initial radius of the system; here is t=0.175. Hereafter, in these plots, the box size is 32 Kpc.
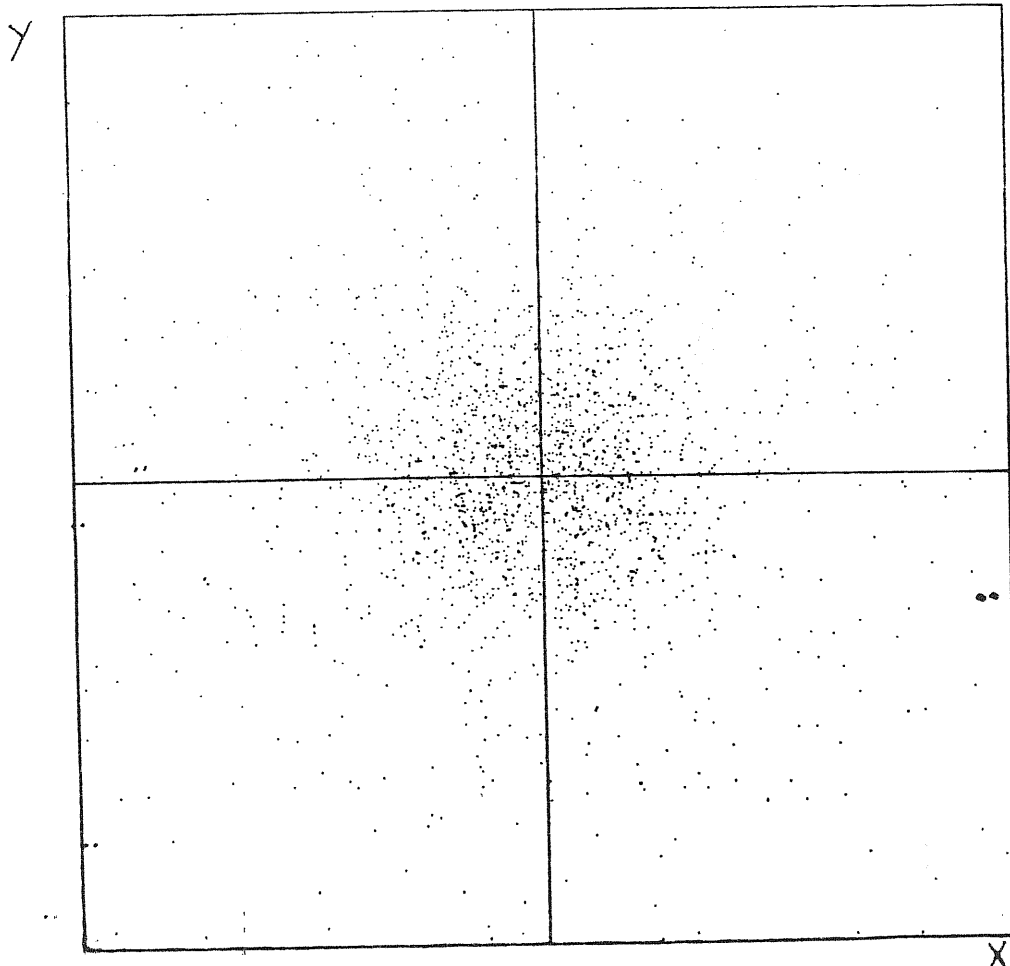
Fig. 5.1b   The same as for Fig.5.1a, expect for t=2.
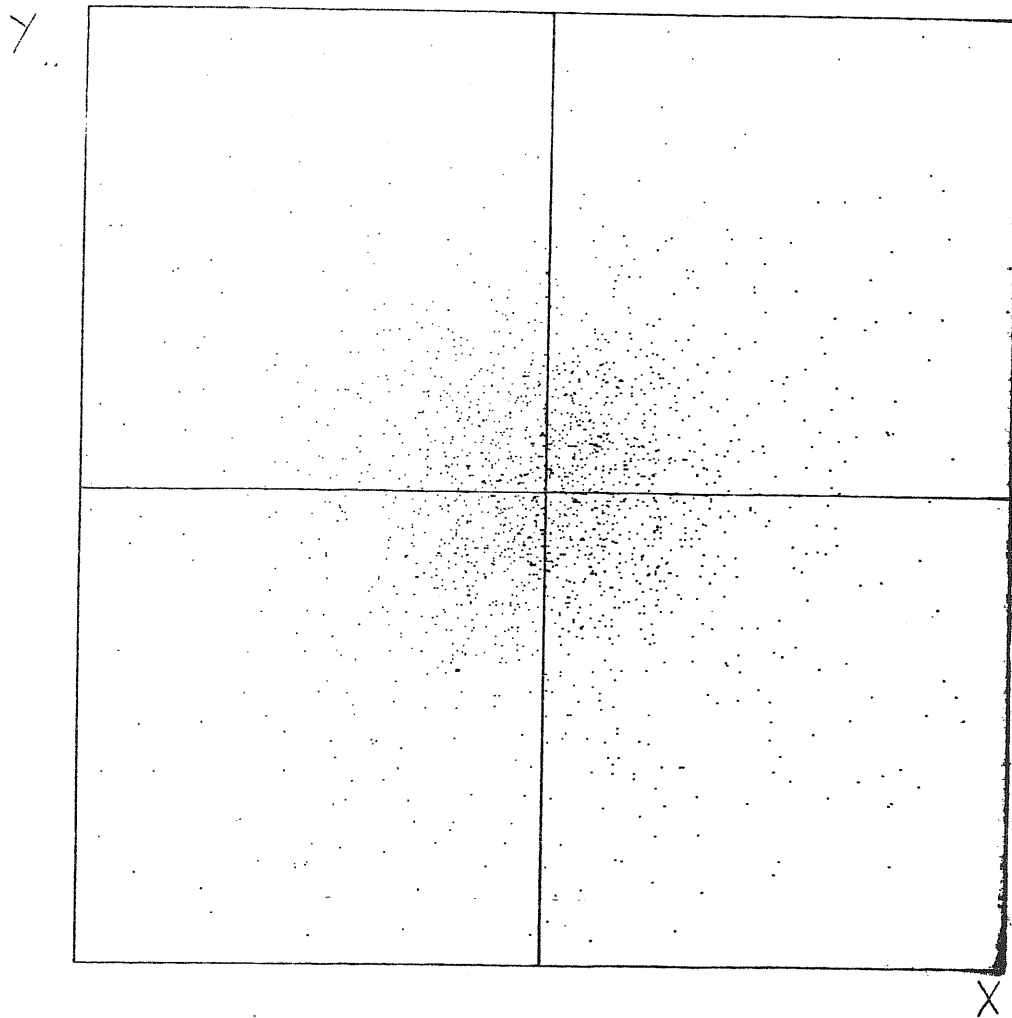
Fig. 5.1c   The same as for Fig.5.1a, expect for t=3.
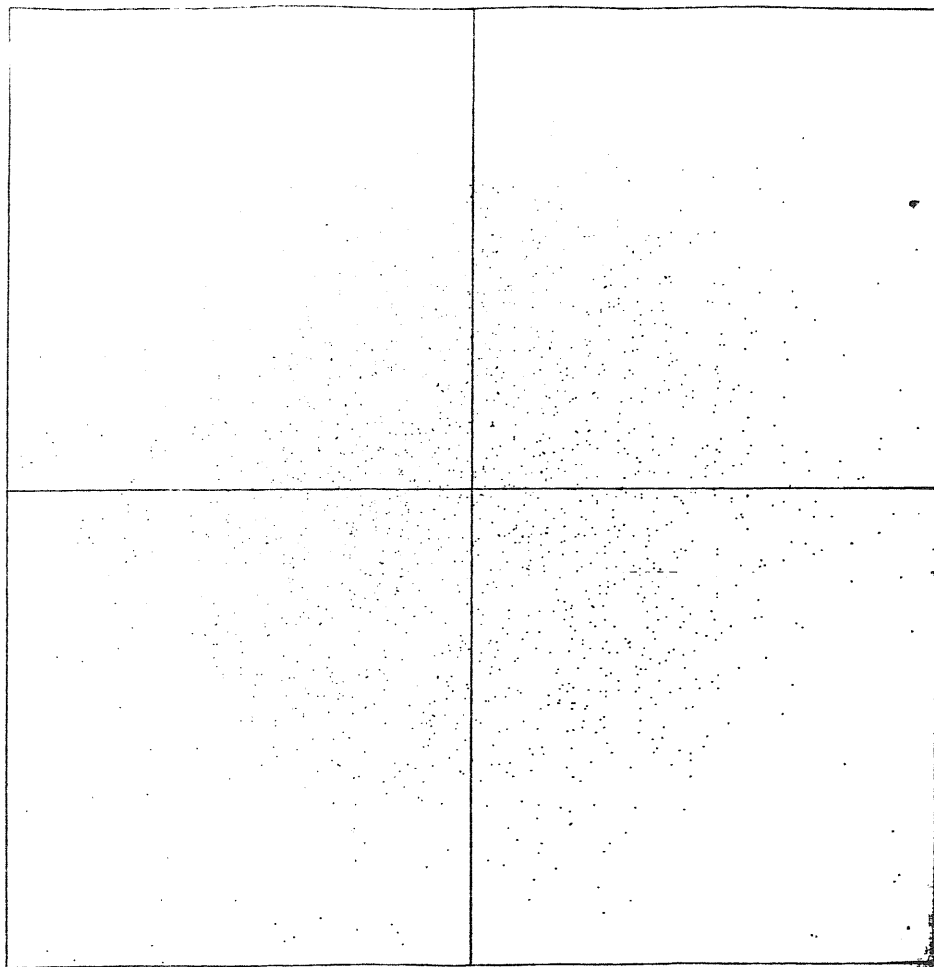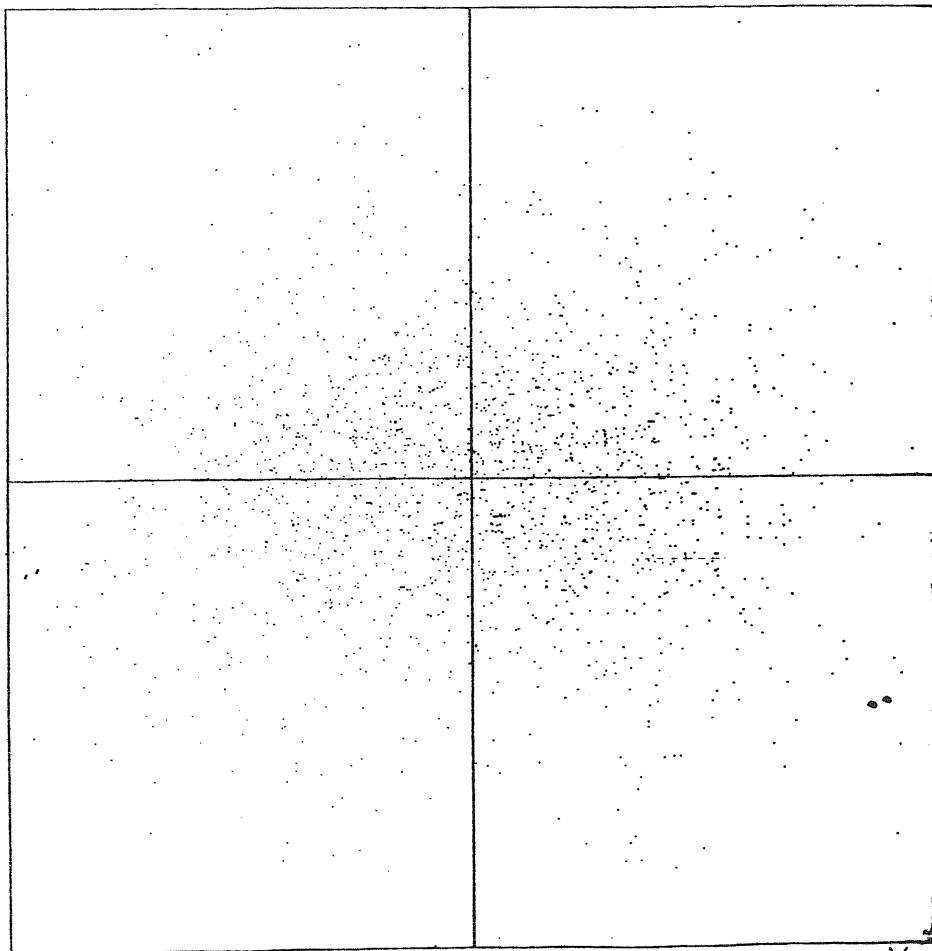
Fig. 5.2a Particle plot of an initially rotating spherical system (model G4) with

$(T_r/|W|, \ T_c/|W|)_{t=0}$ $= (0.25,0.33)$ in the x-y,x-z planes. Time units
are the same of Fig. 5.1a, here is t=0.8 .
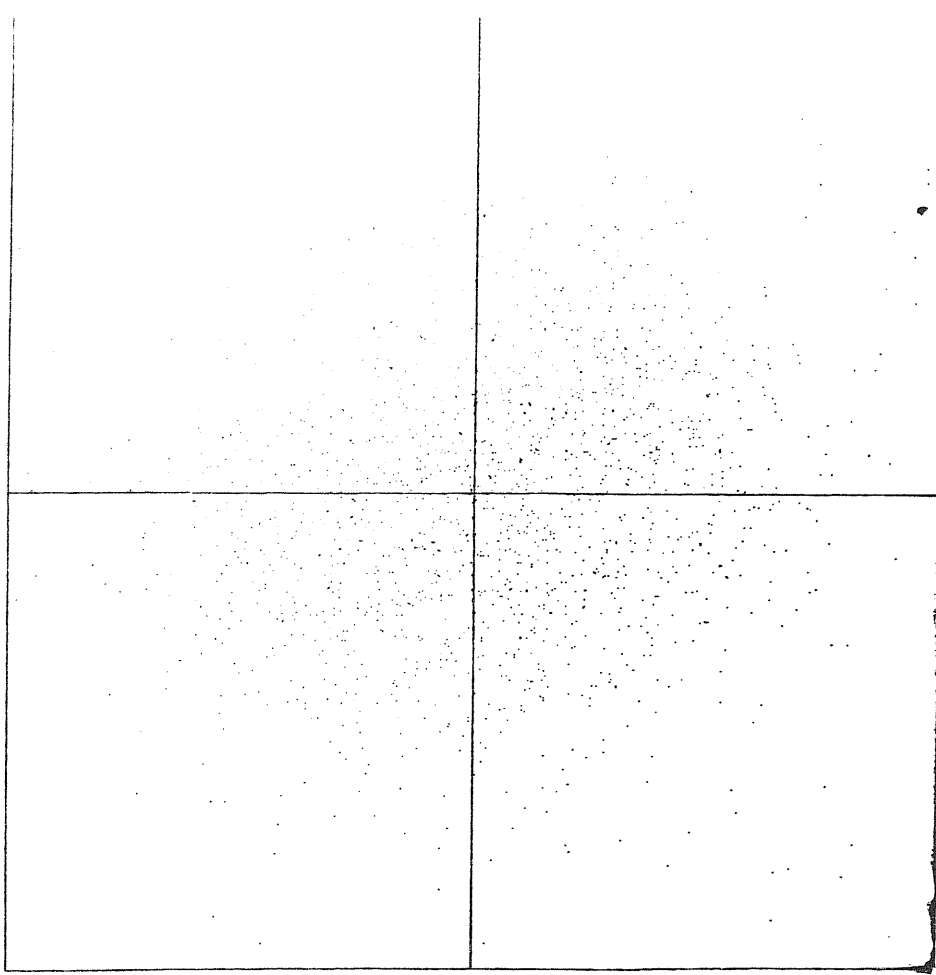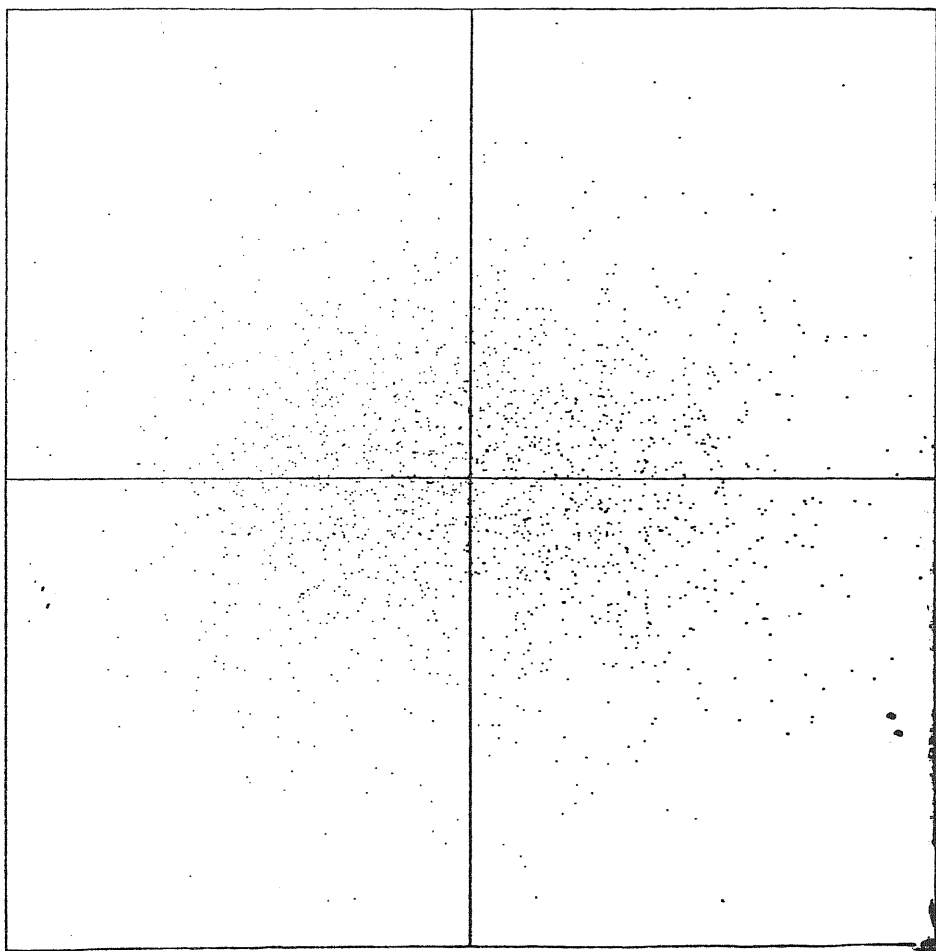
Fig. 5.2b   The same as for Fig.5.2a, expect for t=2.4 .
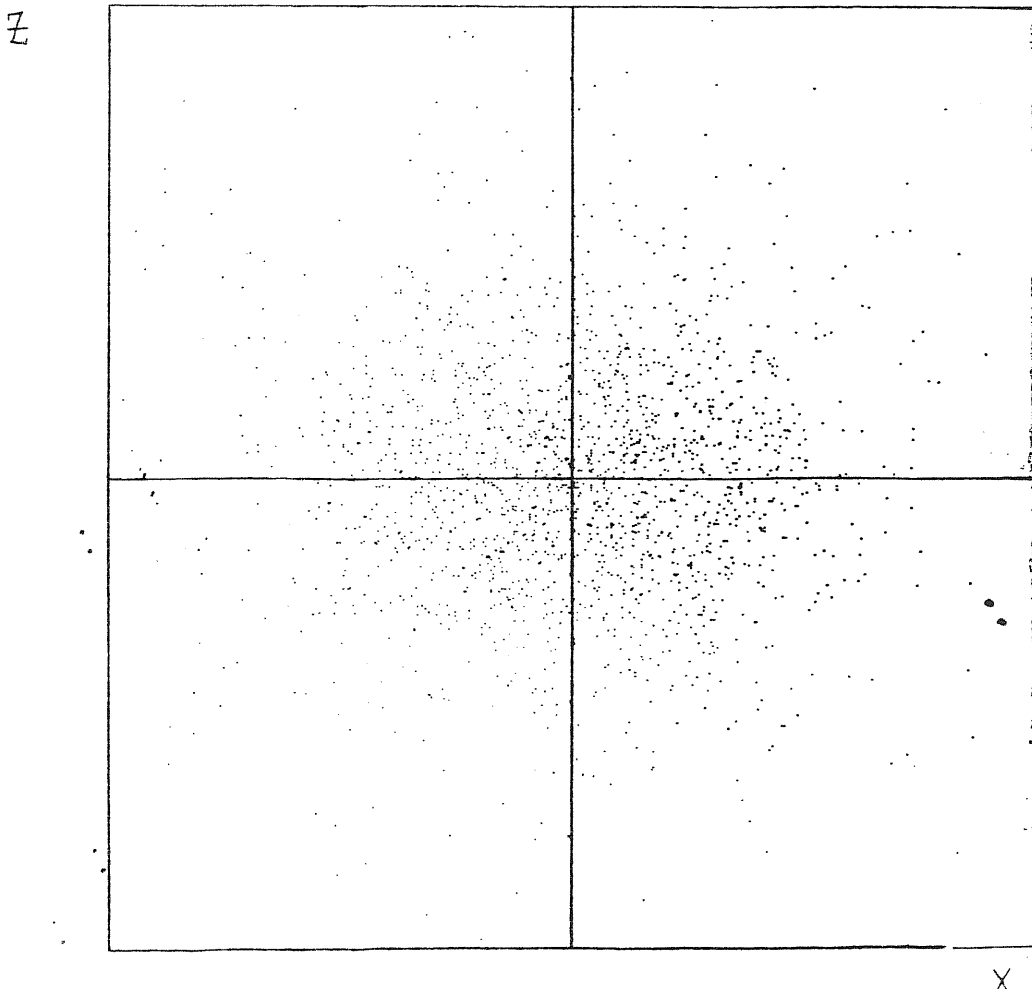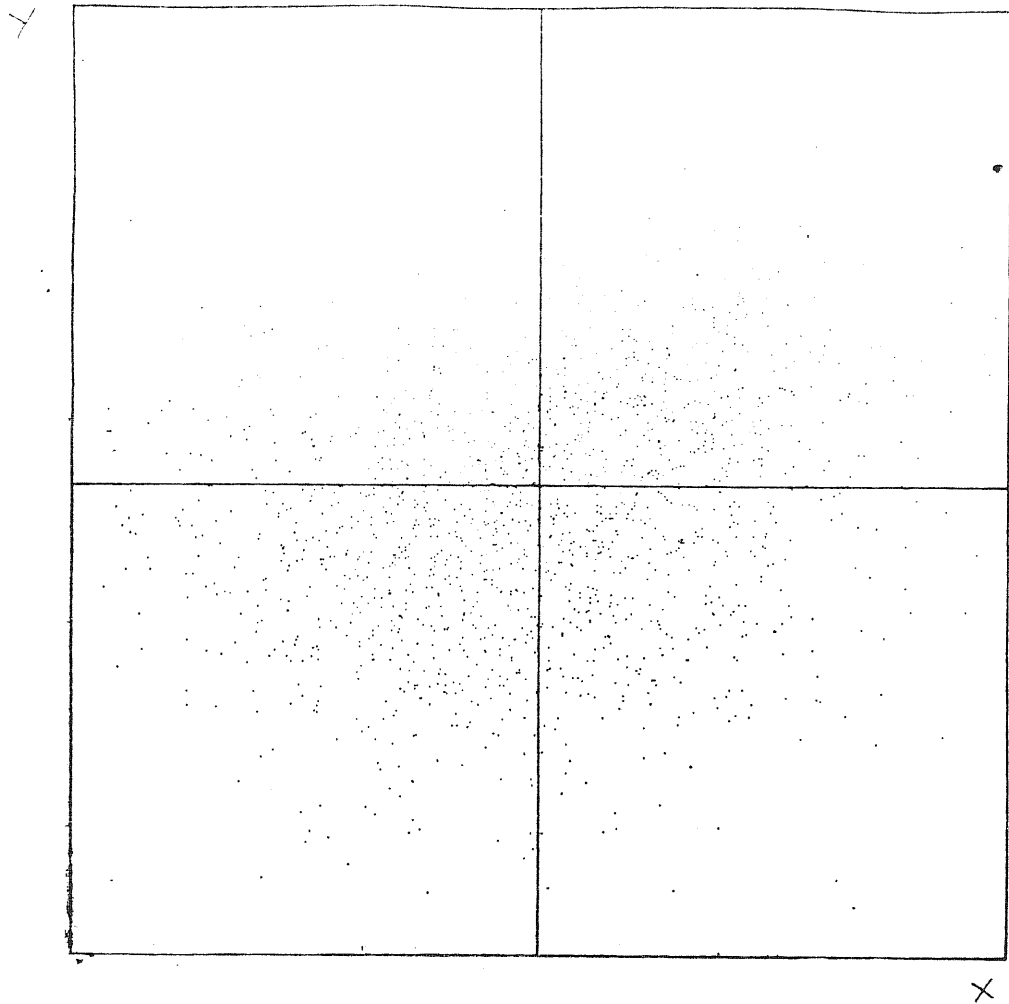
Fig.5.2c   The same as for Fig.5.2a, expect for t=3.
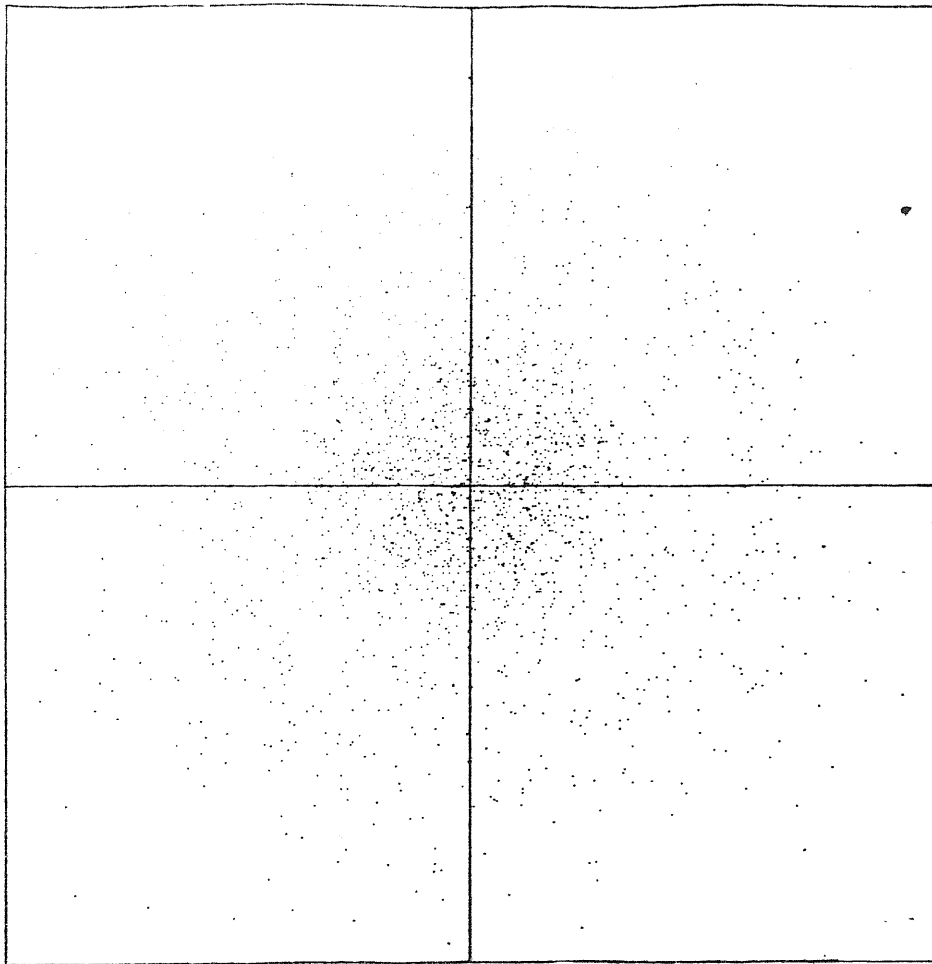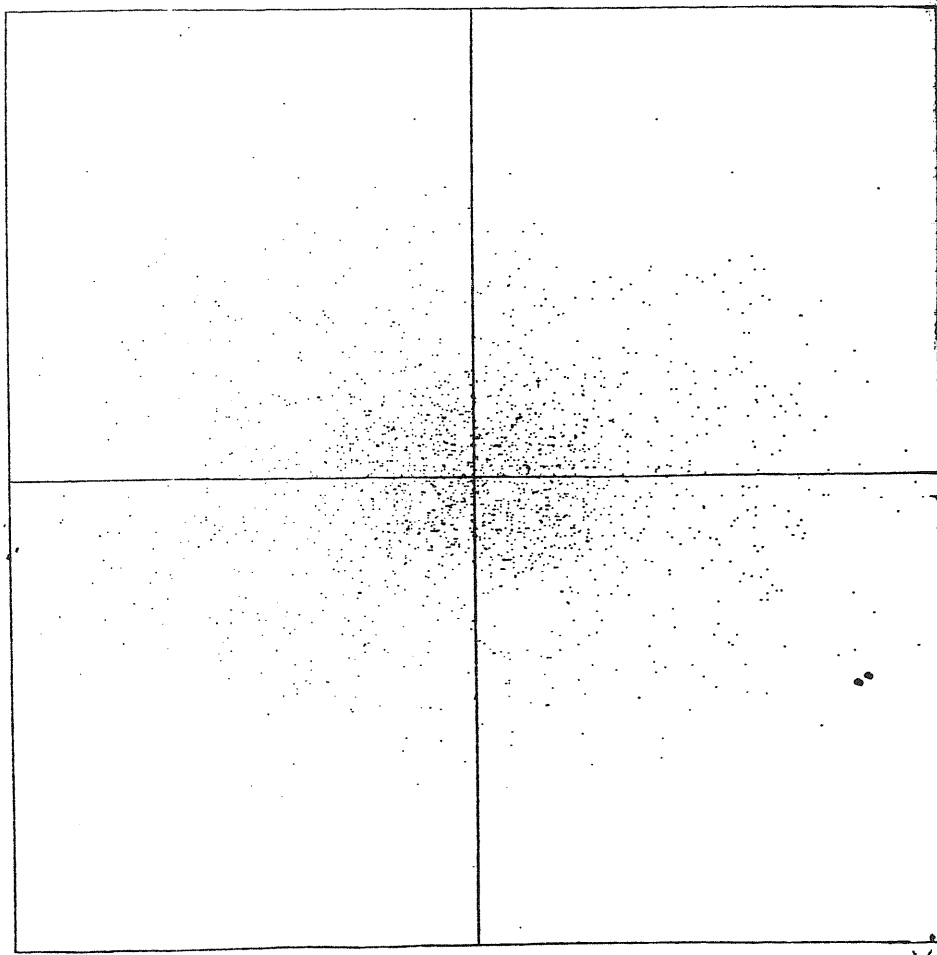
Fig. 5.3a   Particle plot of an initially rotating spherical system (model G5) with

$(T_r/|w|, T_c/|w|)_{t=0}$ =(0.125,0.25) in the x-y,x-z planes. Time
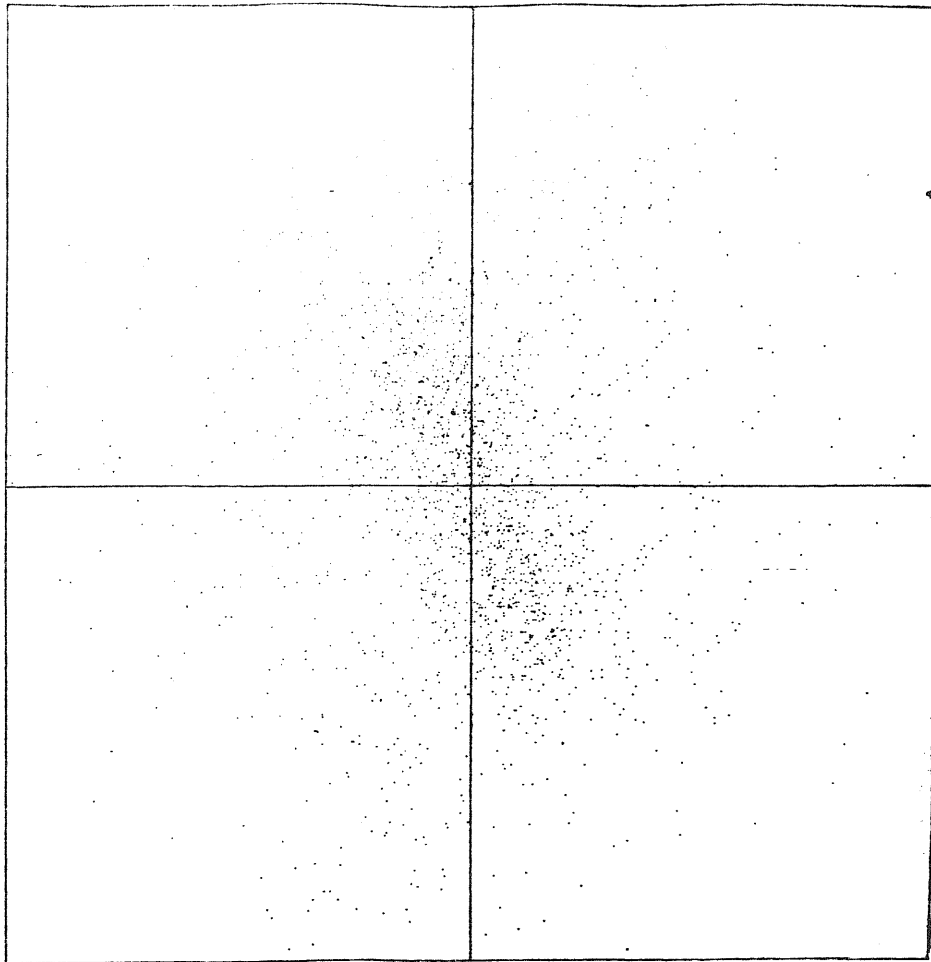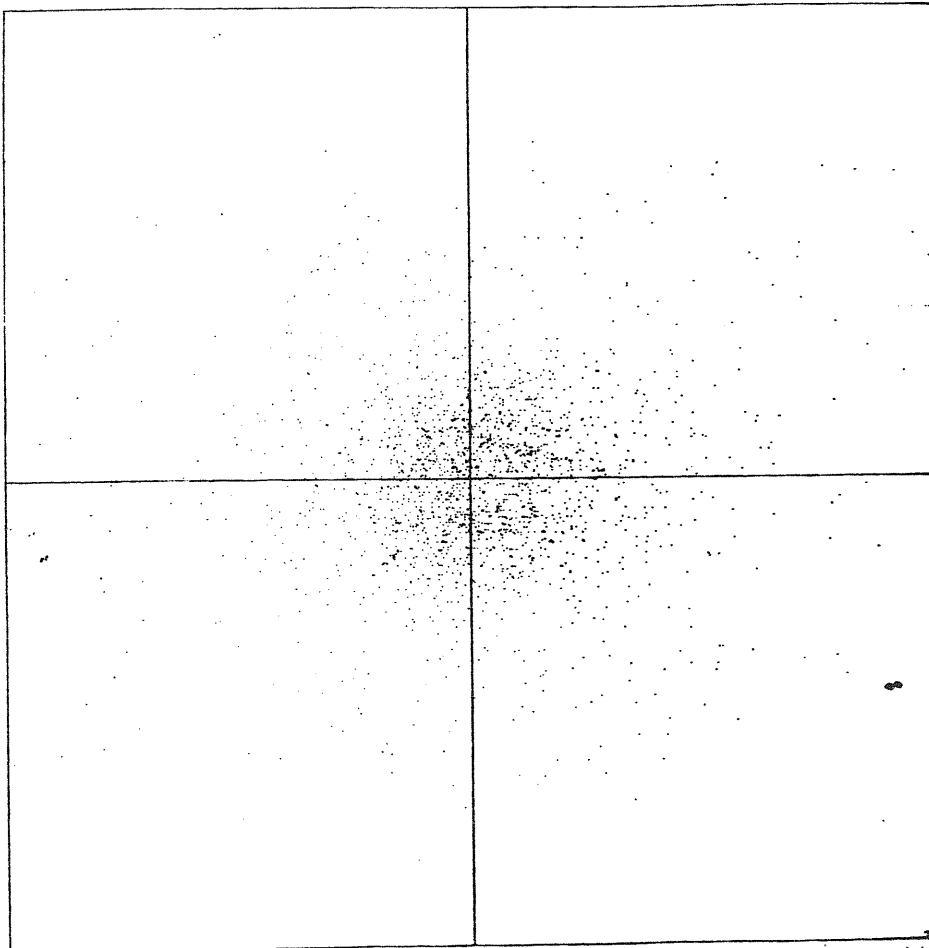
Fig. 5.3b   The same as for Fig.5.3a, expect for t=2.4 .
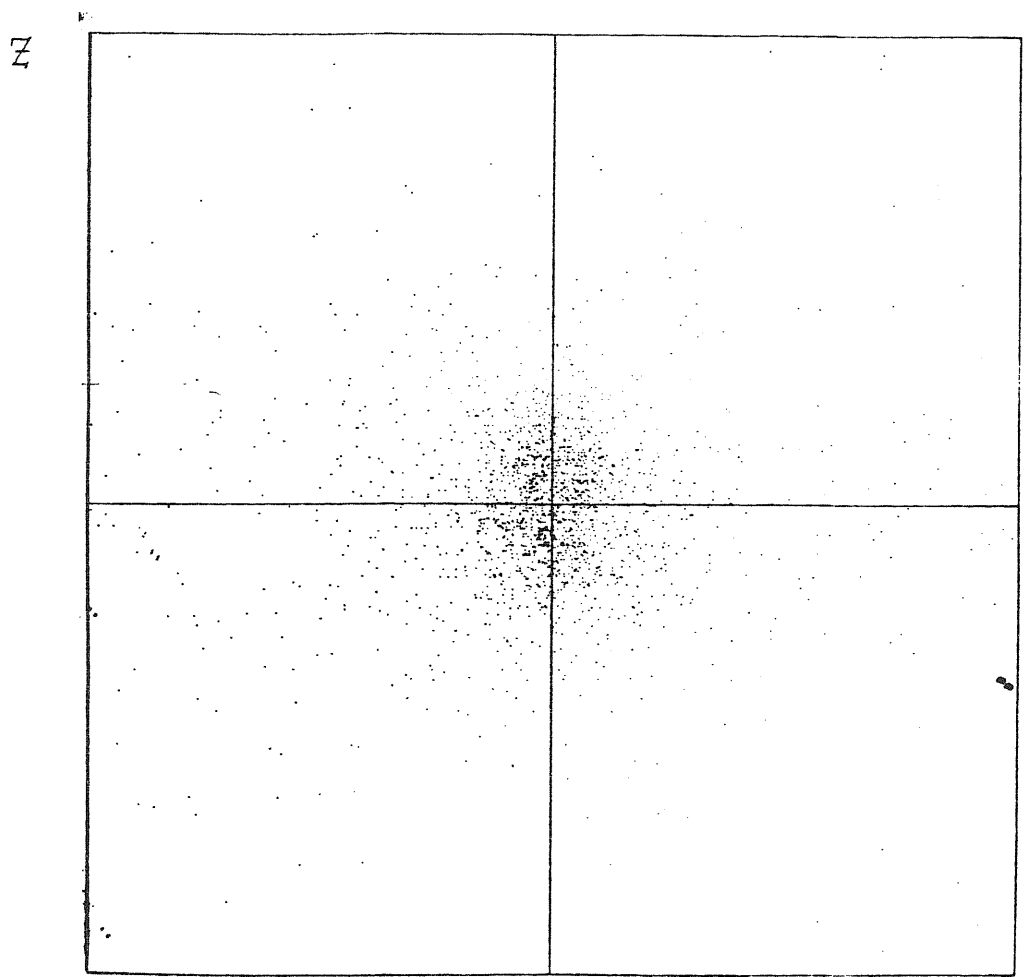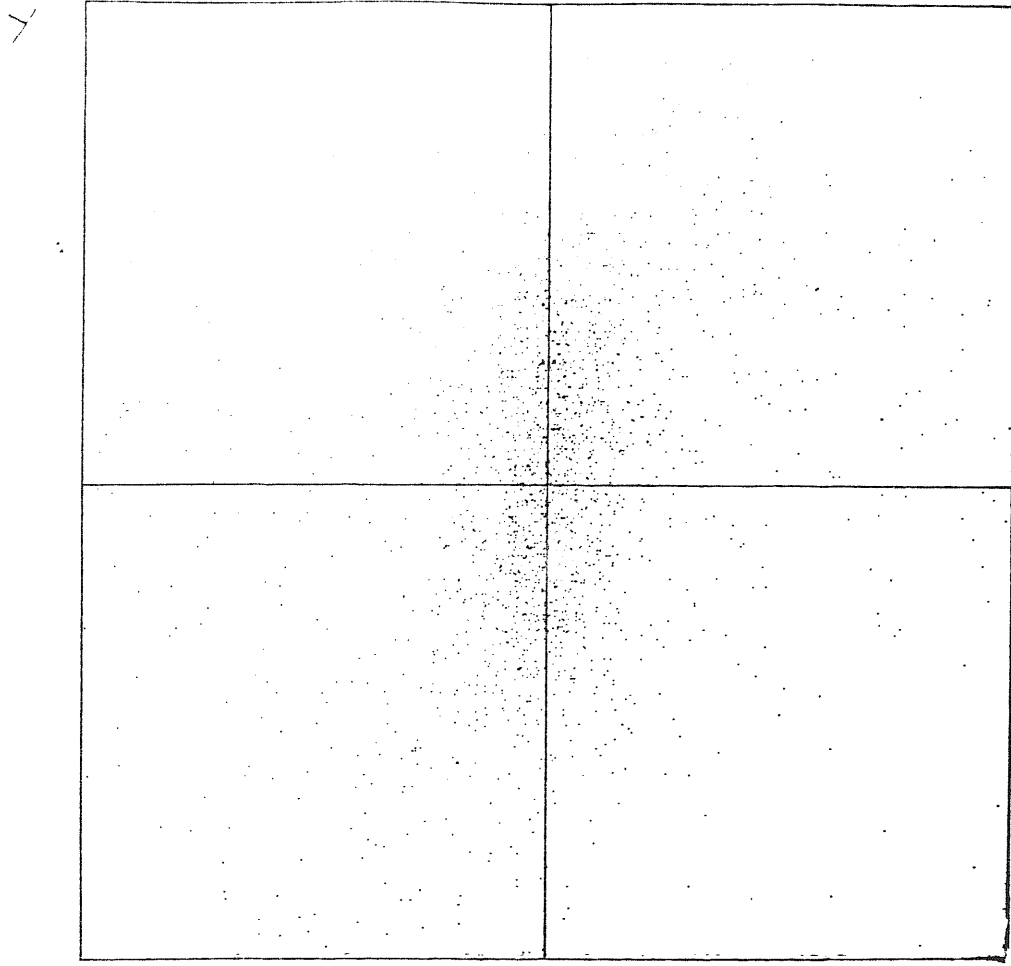
Fig. 5.3c   The same of Fig.5.3a; expect for t=3.
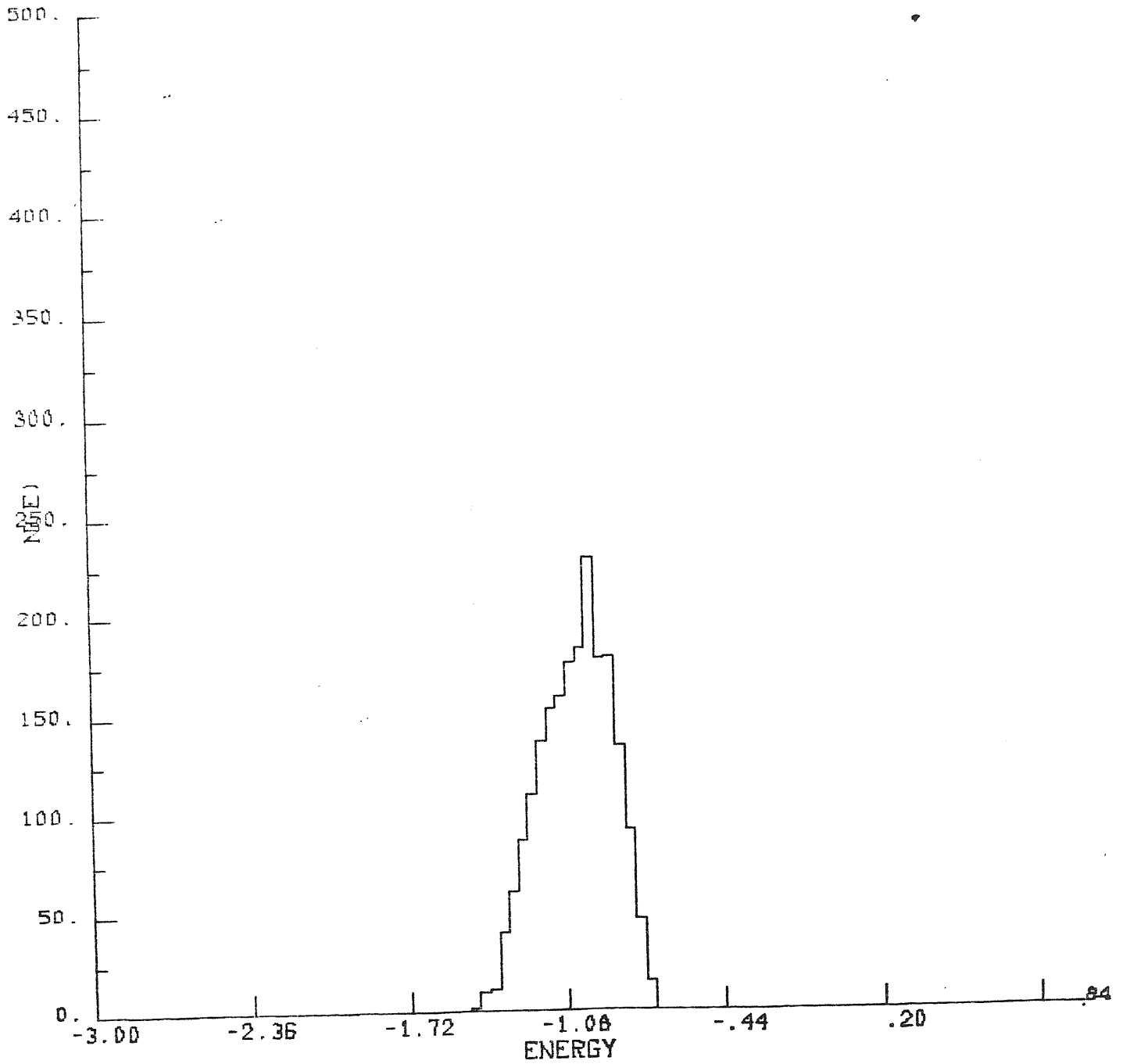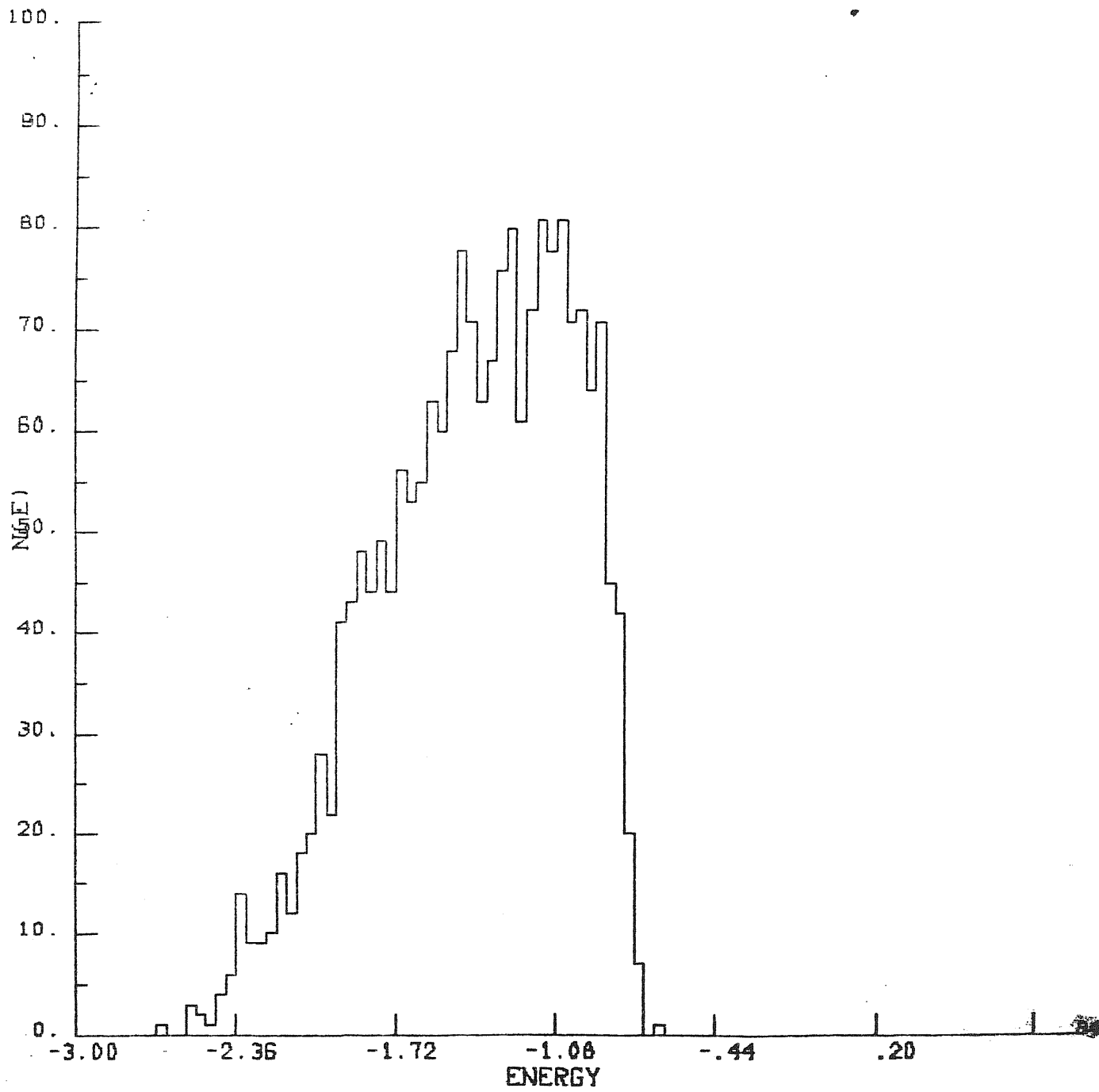
Fig. 5.4b   The same as for Fig.5.4a, expect for t=0.2.
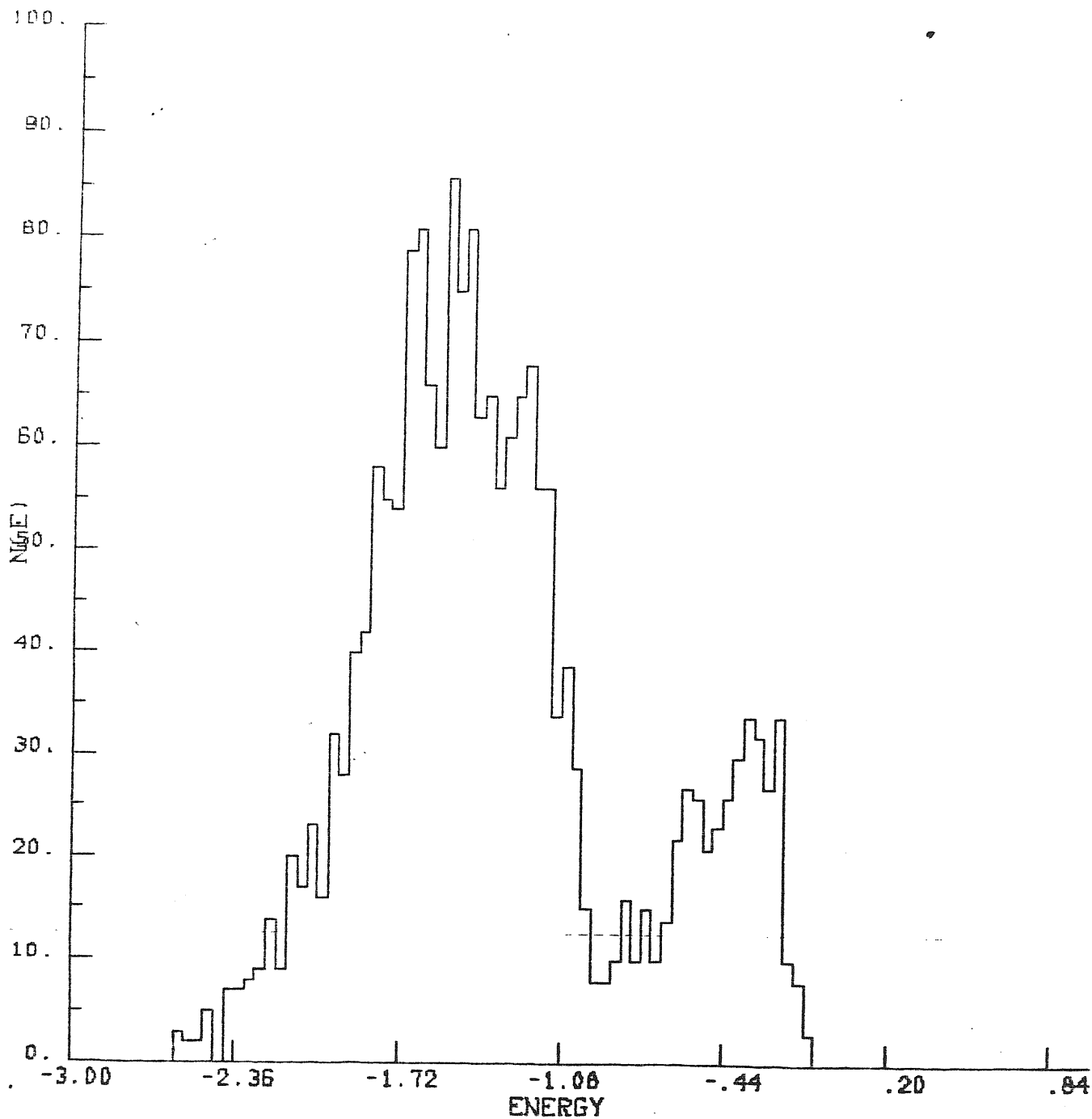
Fig. 5.4c   The same as for Fig.5.4a, expect for t=2.
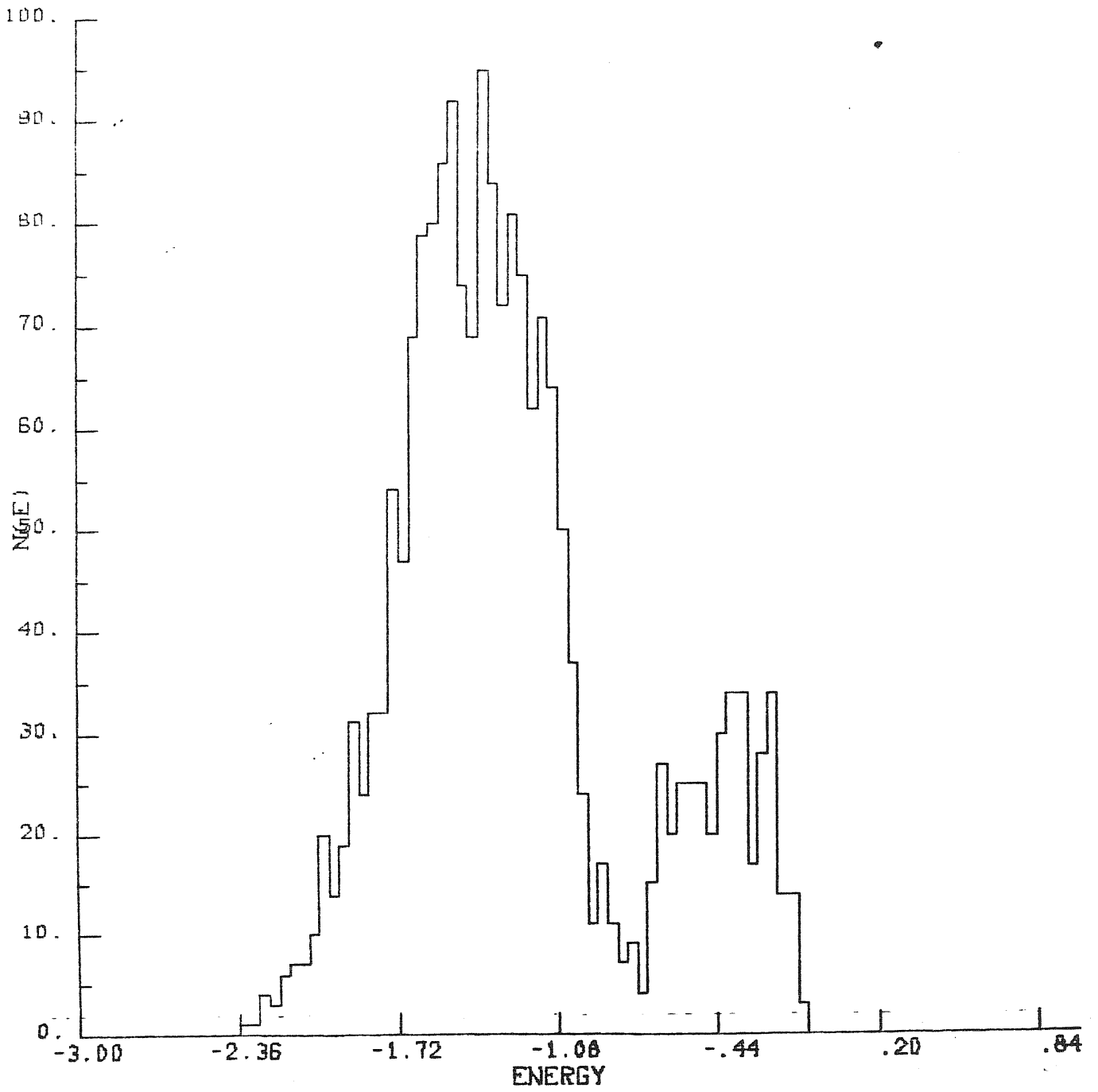
Fig. 5.4d   The same as for Fig. 5.4a, expect for t=3 .
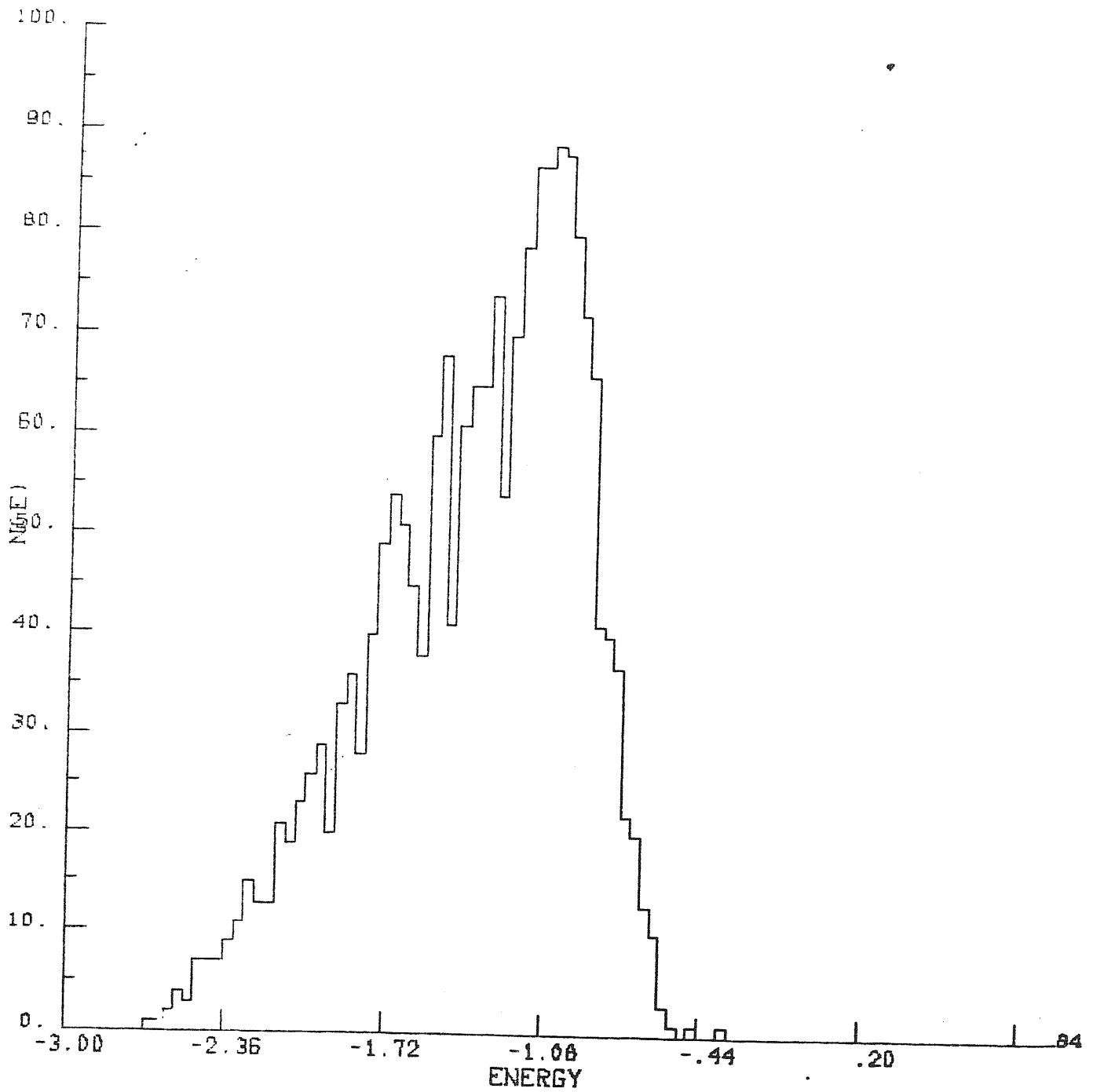
<u>Fig. 5.5a</u>   Stellar energy histogram for model G3. Units are the same of Fig.5.4a, here is t=0.2 .
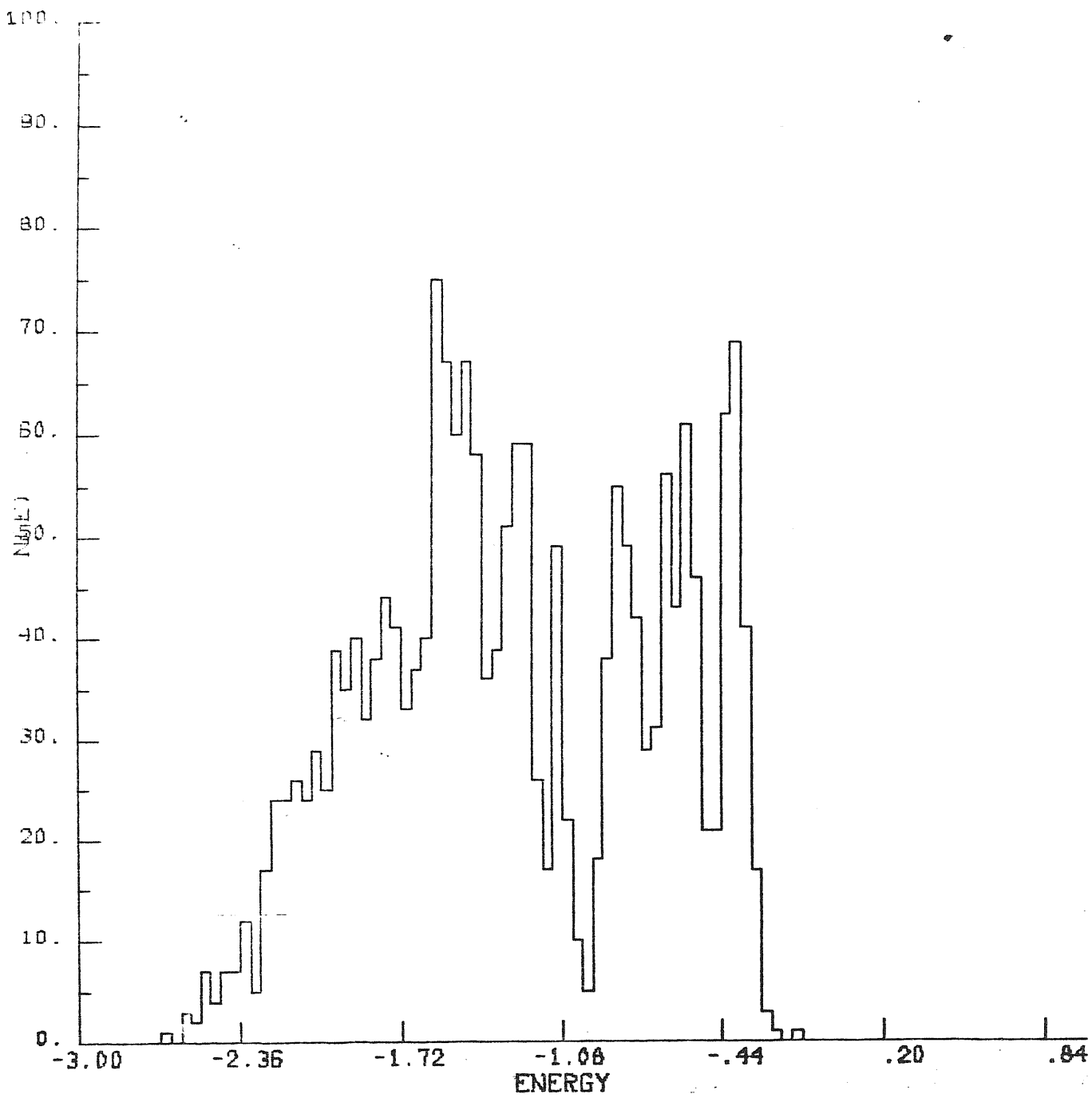
Fig 5.5b   The same as for Fig.5.5a, expect for t=2.
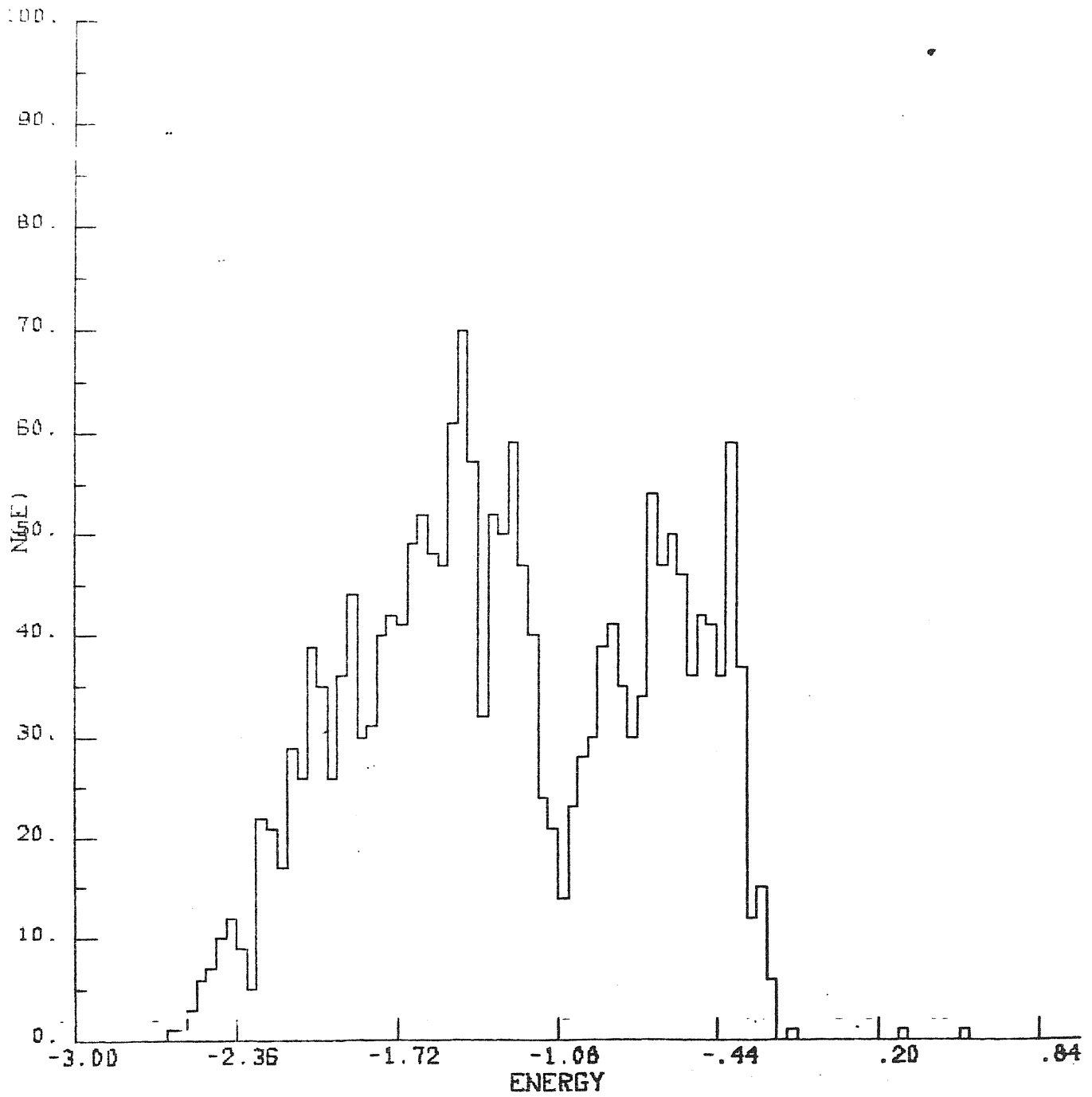
Fig. 5.5c   The same as for Fig.5.5a, expect for t=3.
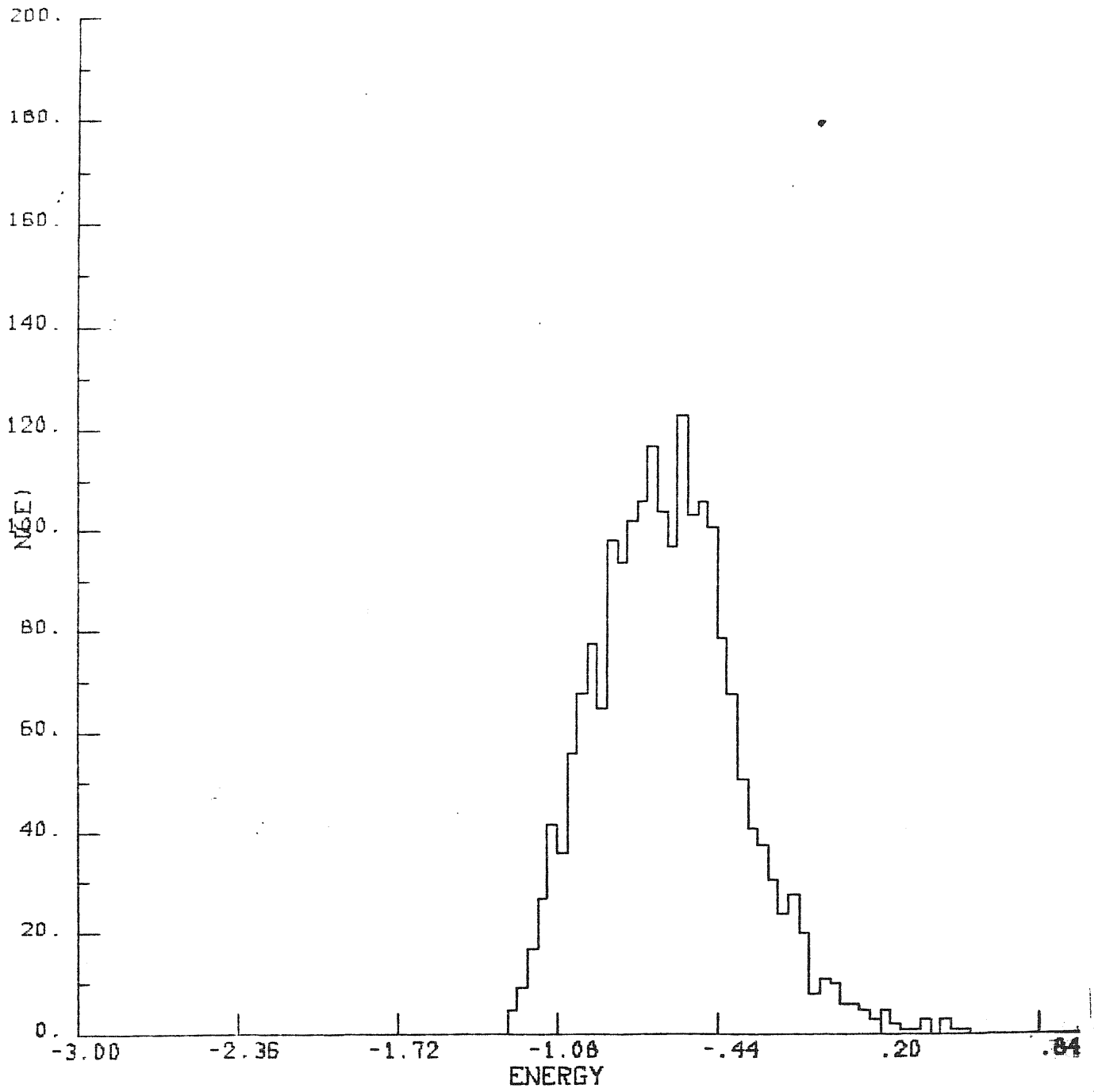
Fig. 5.6a   Stellar energy histogram for model G4. Units are the same of Fig.5.4a, here is t=0.8
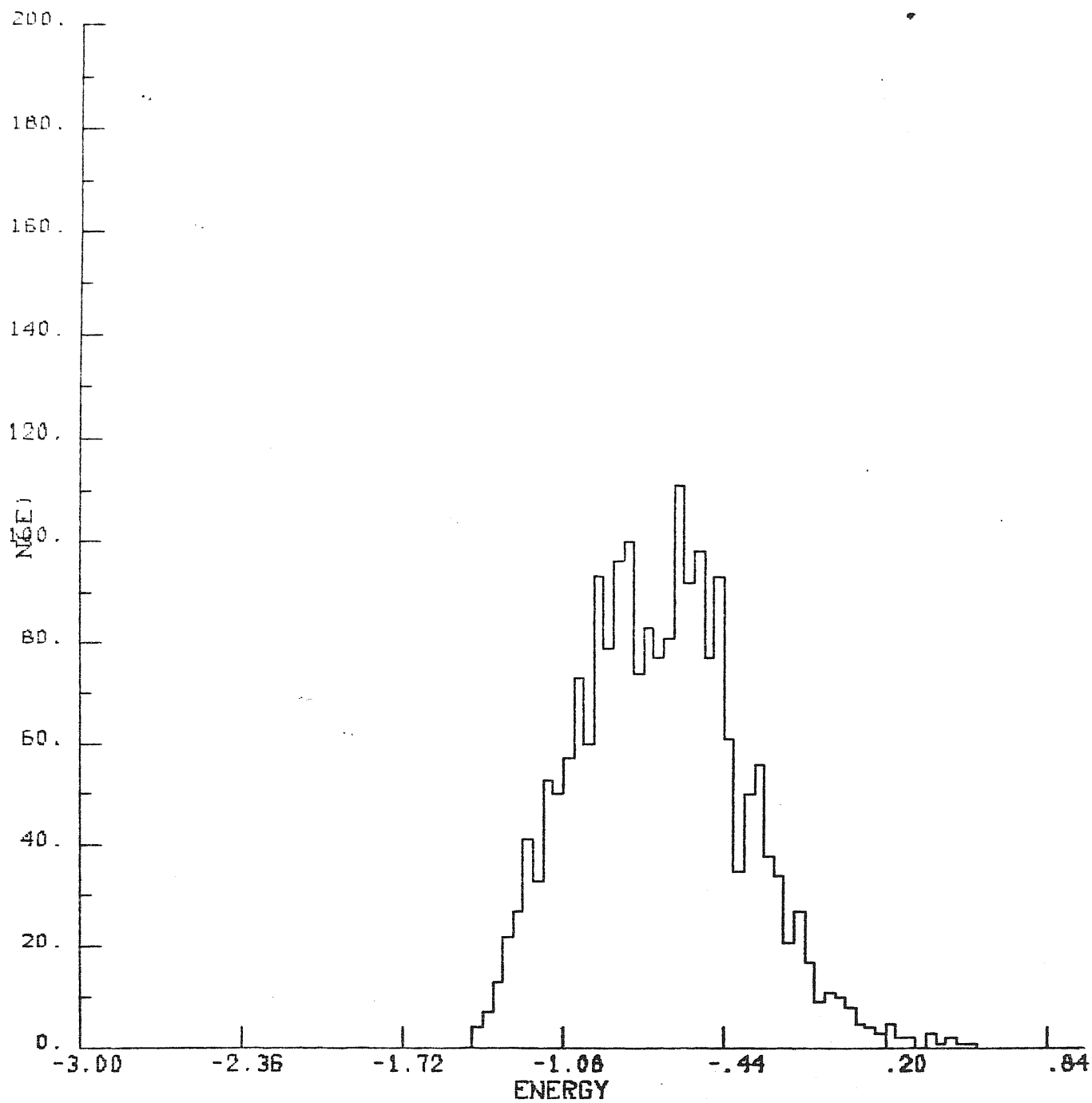
Fig. 5.6b   The same as for Fig. 5.6a, expect for t=2.4 .
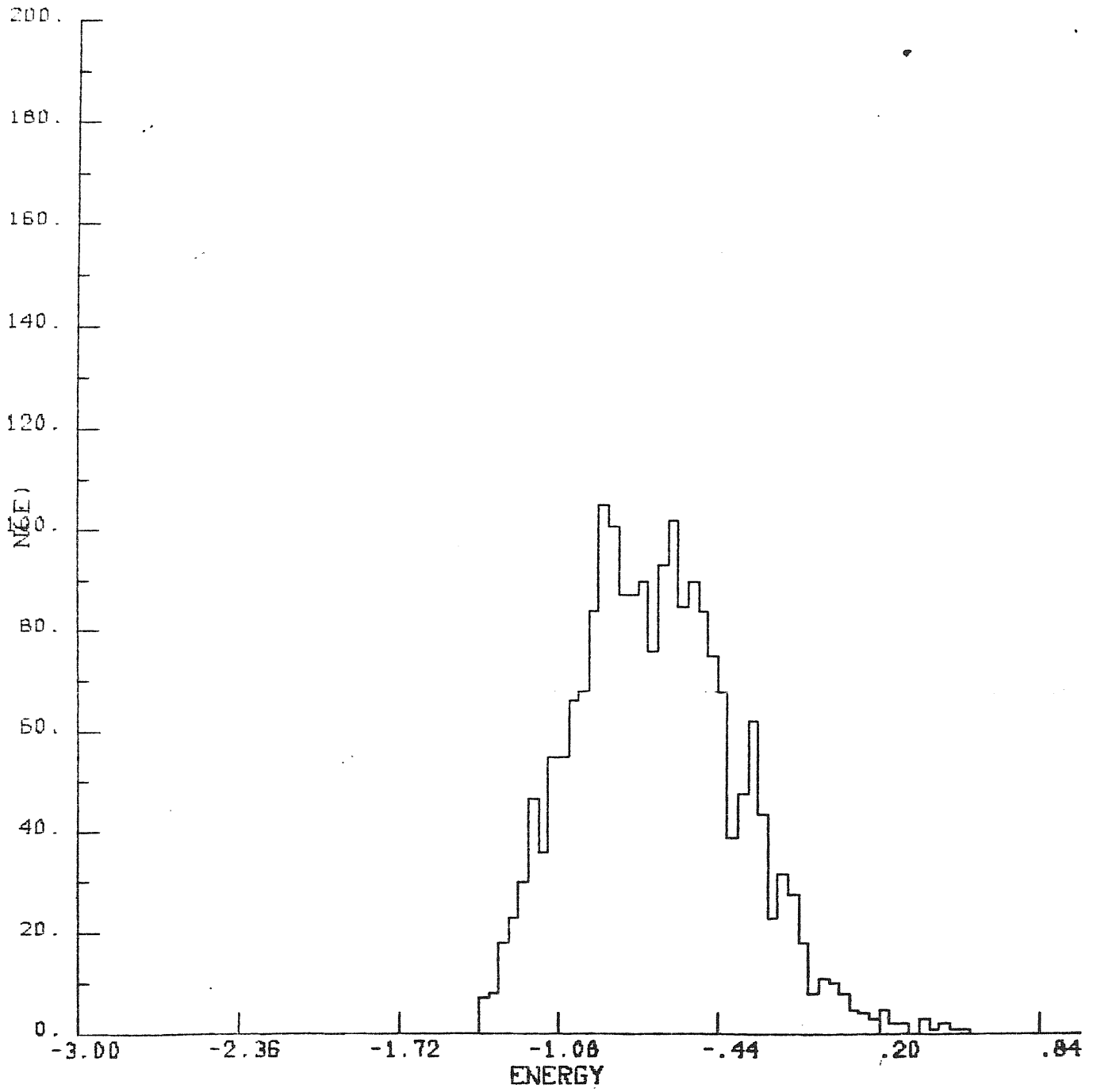
Fig. 5.6c   The same as for Fig.5.6a, expect for t=3.
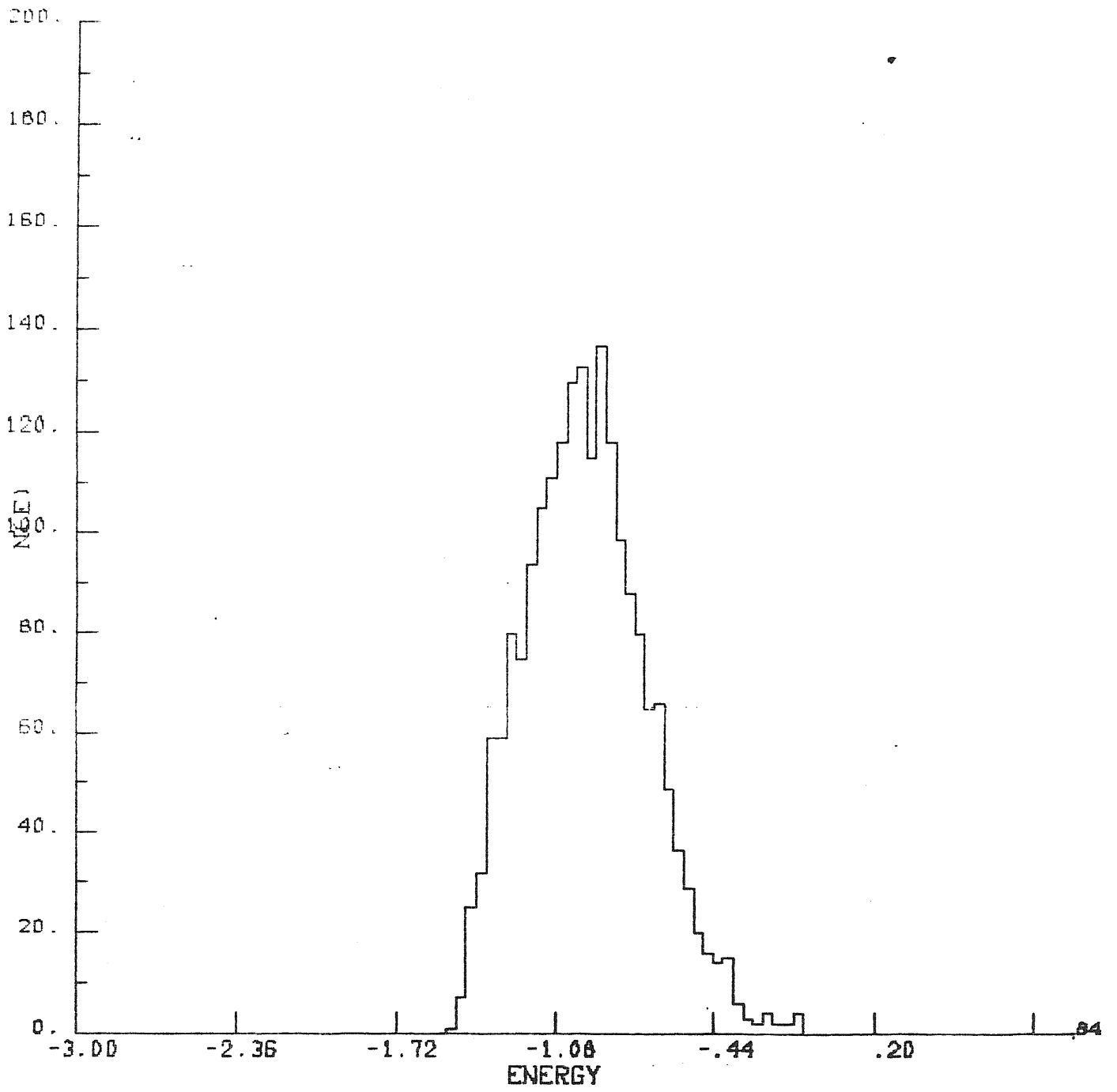
Fig.5.7a   Stellar energy histogram for model G5. Units are the same of Fig.5.4a, here is t=0.
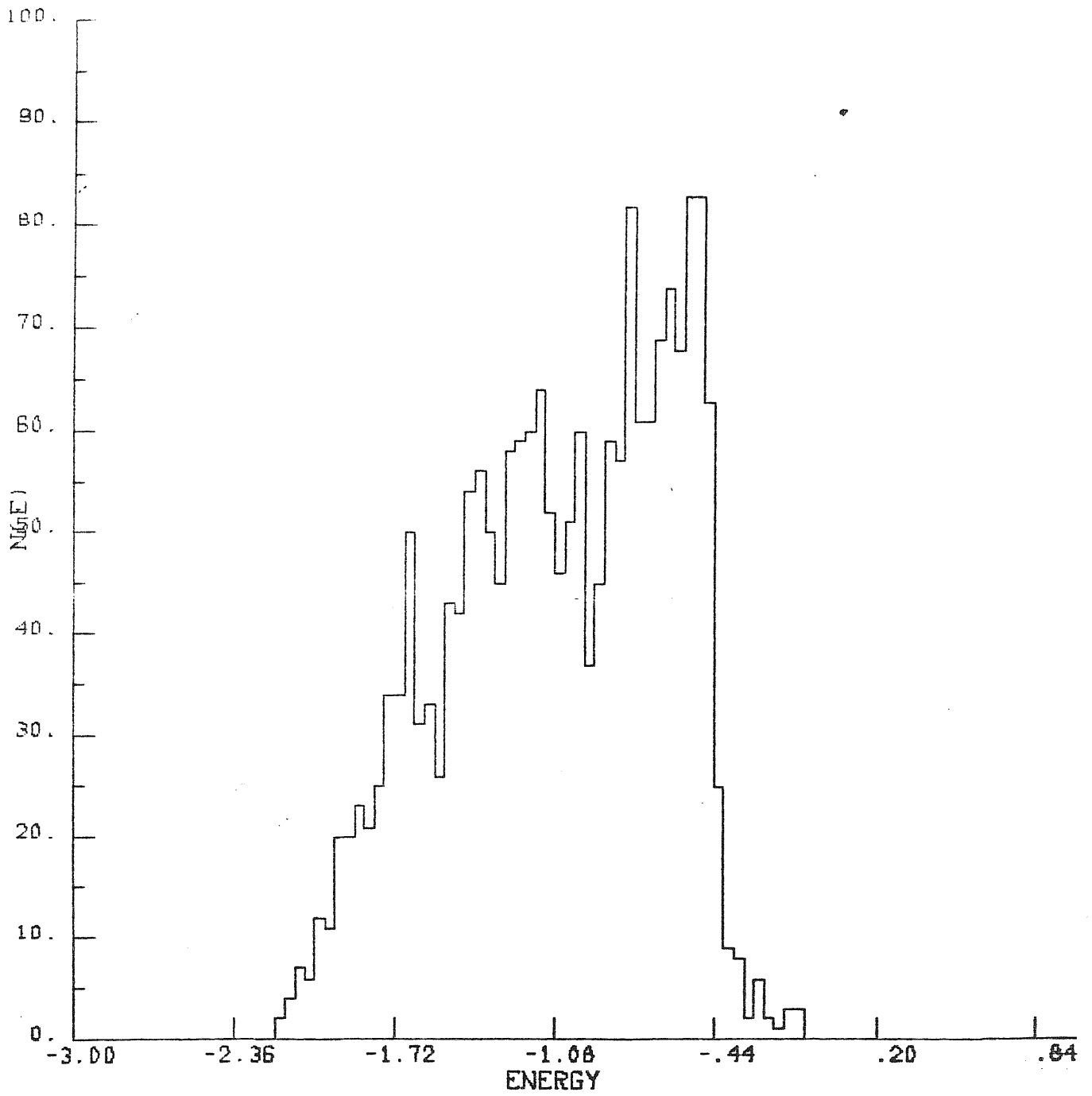
Fig. 5.7b   The same as for Fig.5.7a, expect for t=0.8 .
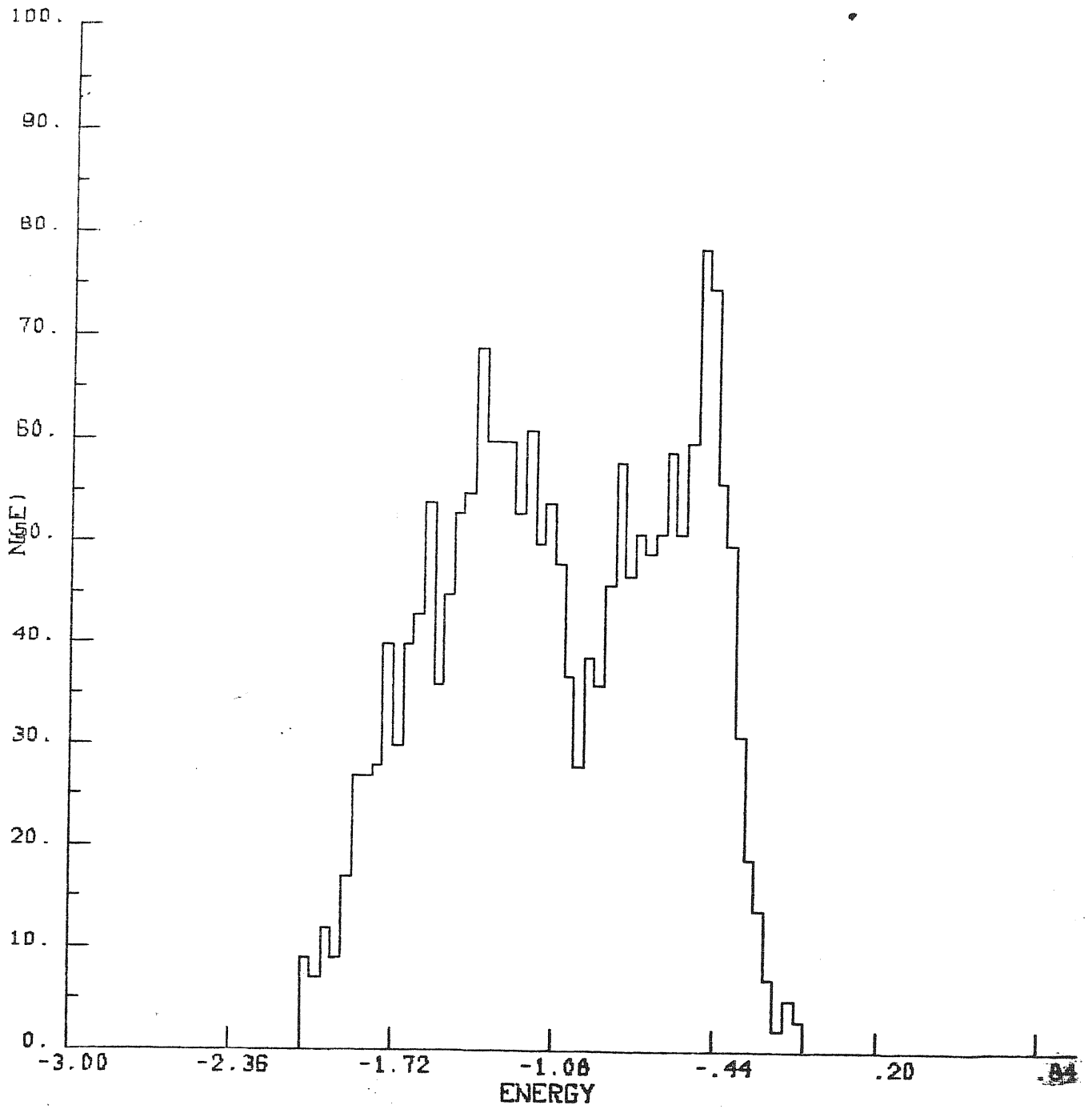
Fig. 5.7c   The same as for Fig.5.7a, expect for t=2.4 .
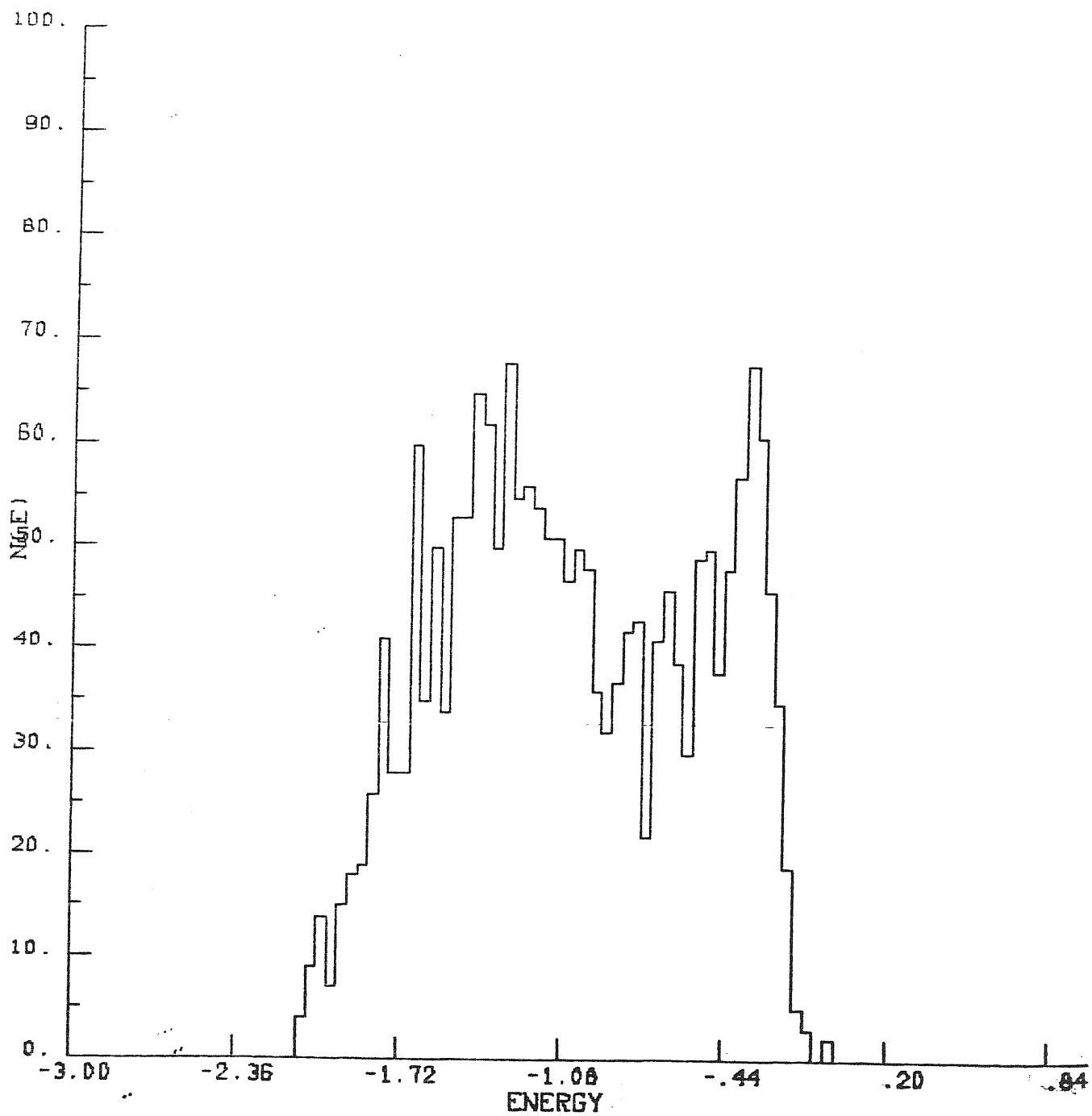
Fig.5.7d   The same as for Fig.5.7a, expect for t=3.
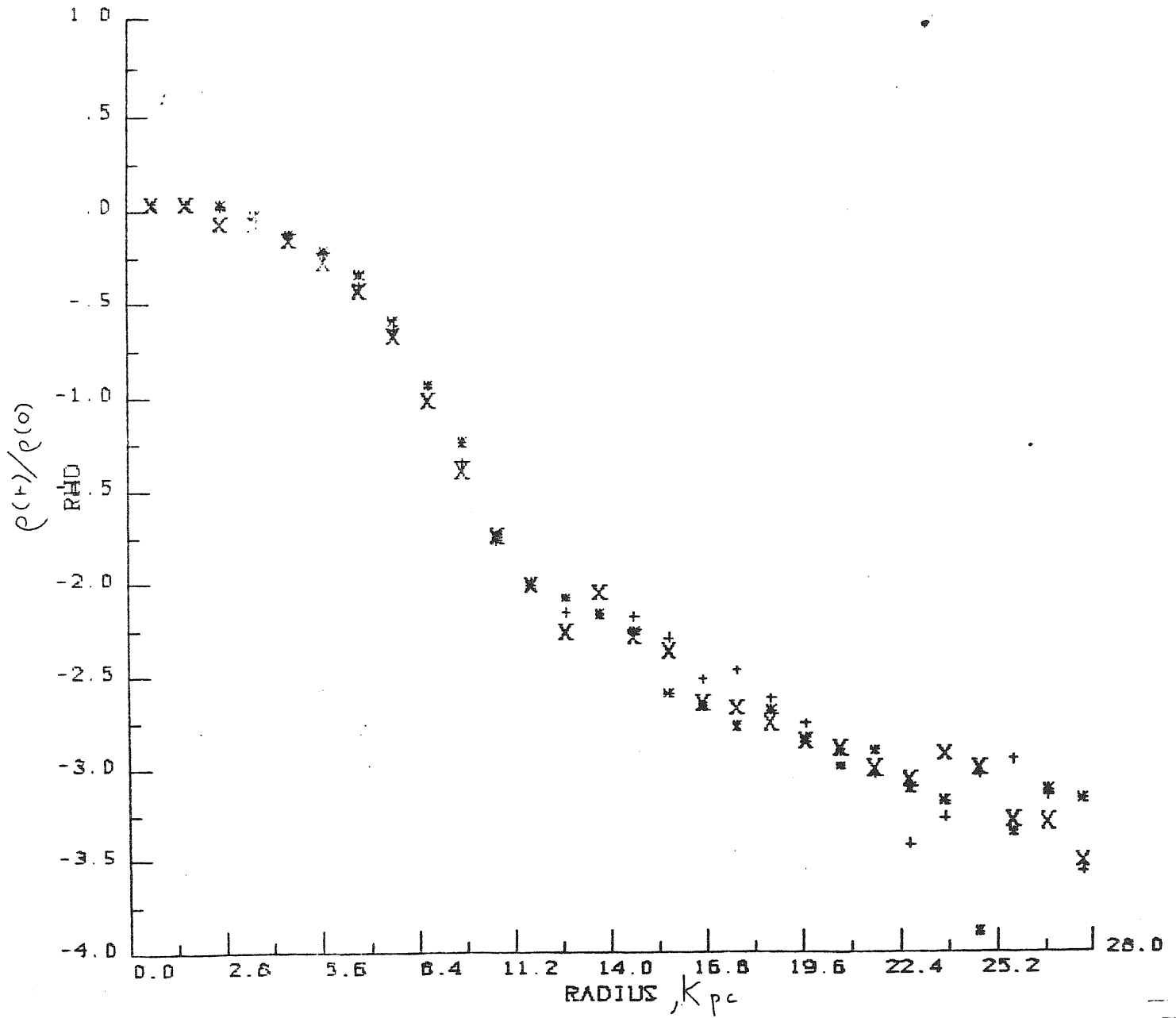
Fig. 5.8a Stellar density $\varrho(r)$ as function of the radius r and the polar angle ϑ at t=3.for model G2. The ordinate is $\log_{10}\left[\varrho(r)/\varrho(o)\right]^{\circ}$, the radius is in Kpc. Here is +: ϑ =90° , x: ϑ =60°, ✳: ϑ =45° .
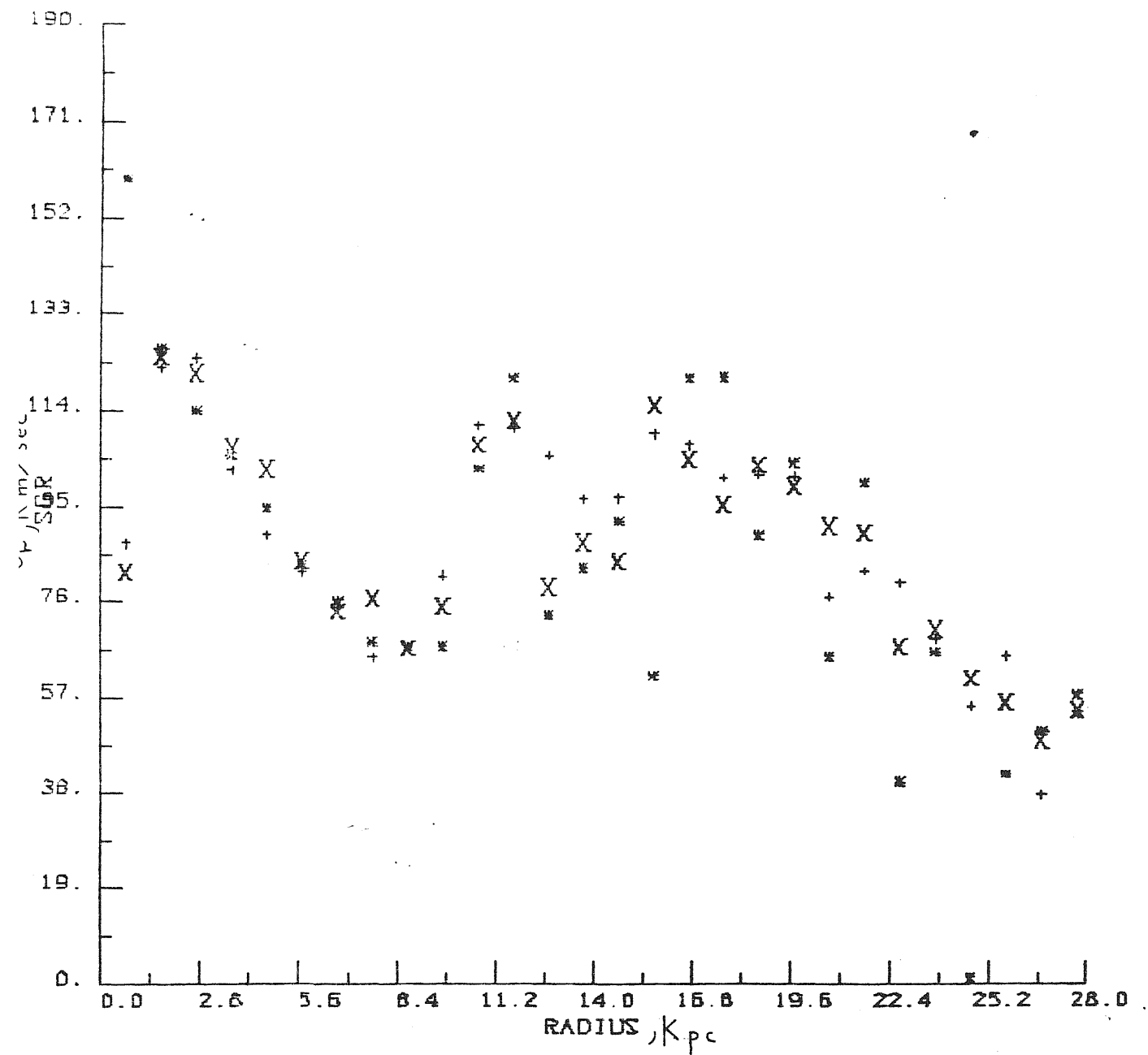
Fig.5.8b Radial velocity dispersion σ_r as function of the radius r and the polar angle ϑ at t=3 for model G2. The ordinate is σ_r in Kmsec^{-1}, the radius is in Kpc. Here is +: ϑ =90° , x: ϑ =60° , $*$: ϑ =45°.
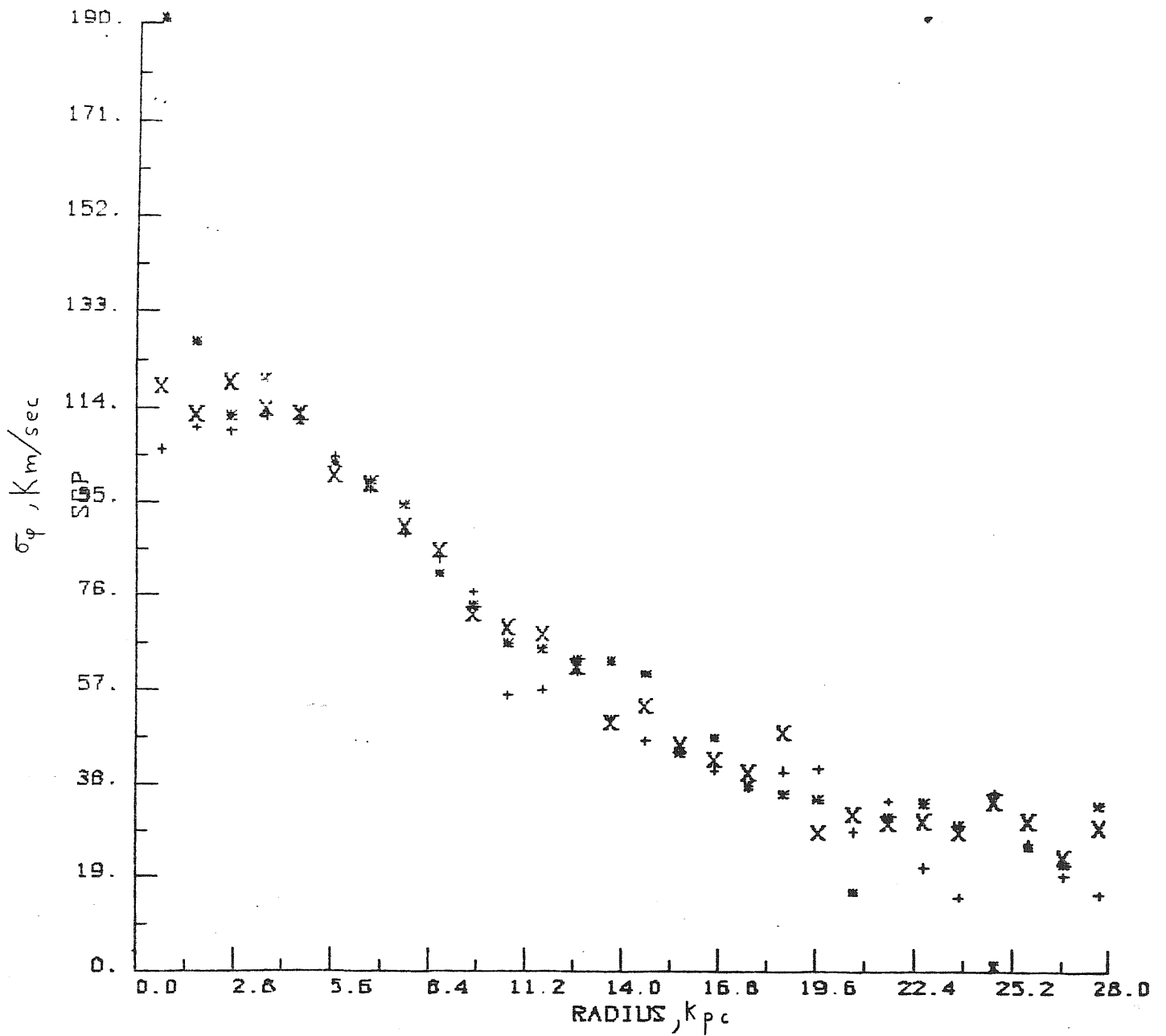
Fig.5.8c   Azimuthal velocity dipersion σ_φ as function of the radius r and the polar angle ϑ at t=3 for model G2. The ordinate is σ_φ in Kmsec^{-1}, the radius is in Kpc. Here is +: ϑ =90°, x: ϑ =60°, ∗ : ϑ =45° .
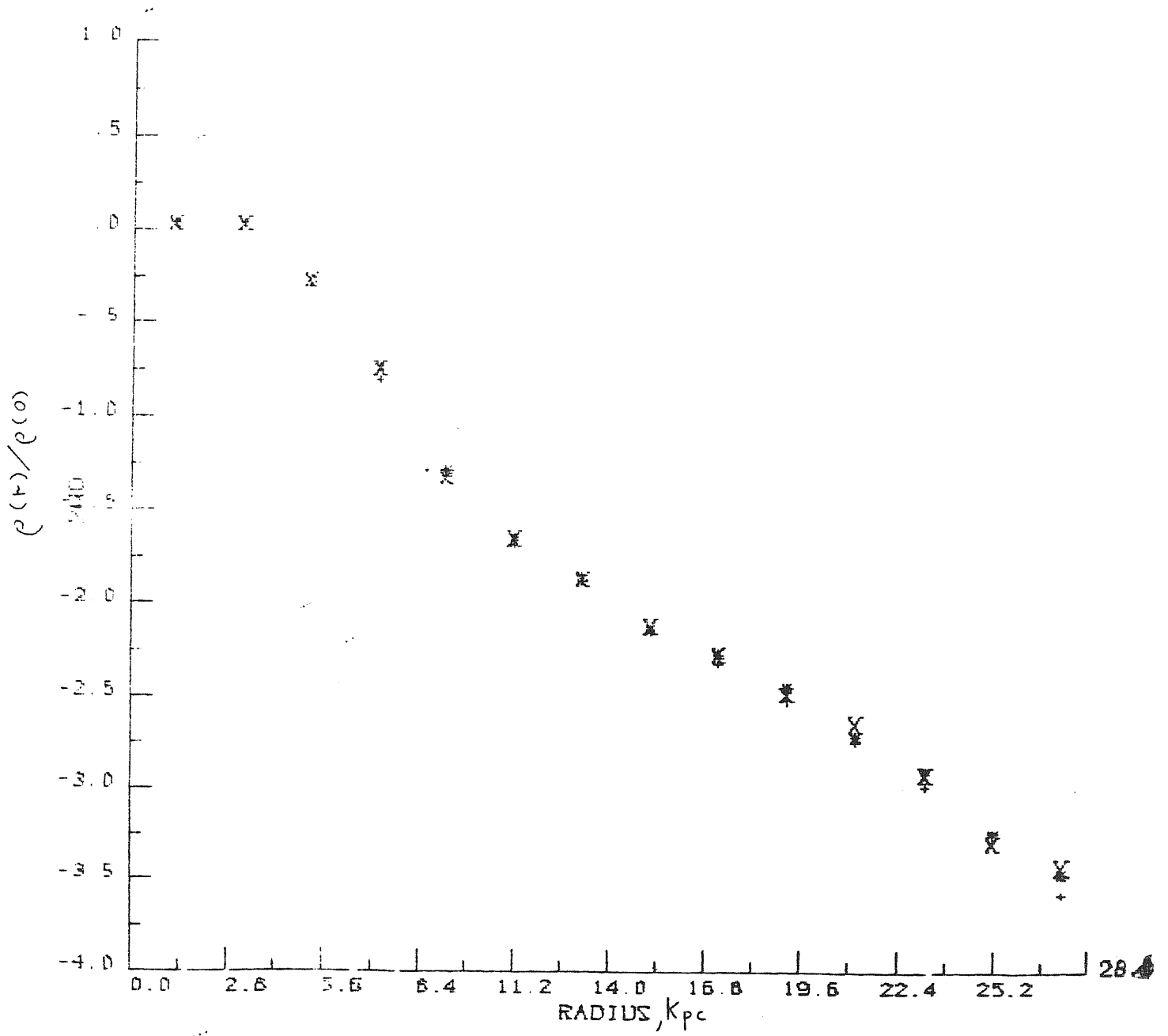
Fig.5.9a   The same as for Fig.5.8a, expect for model G3.
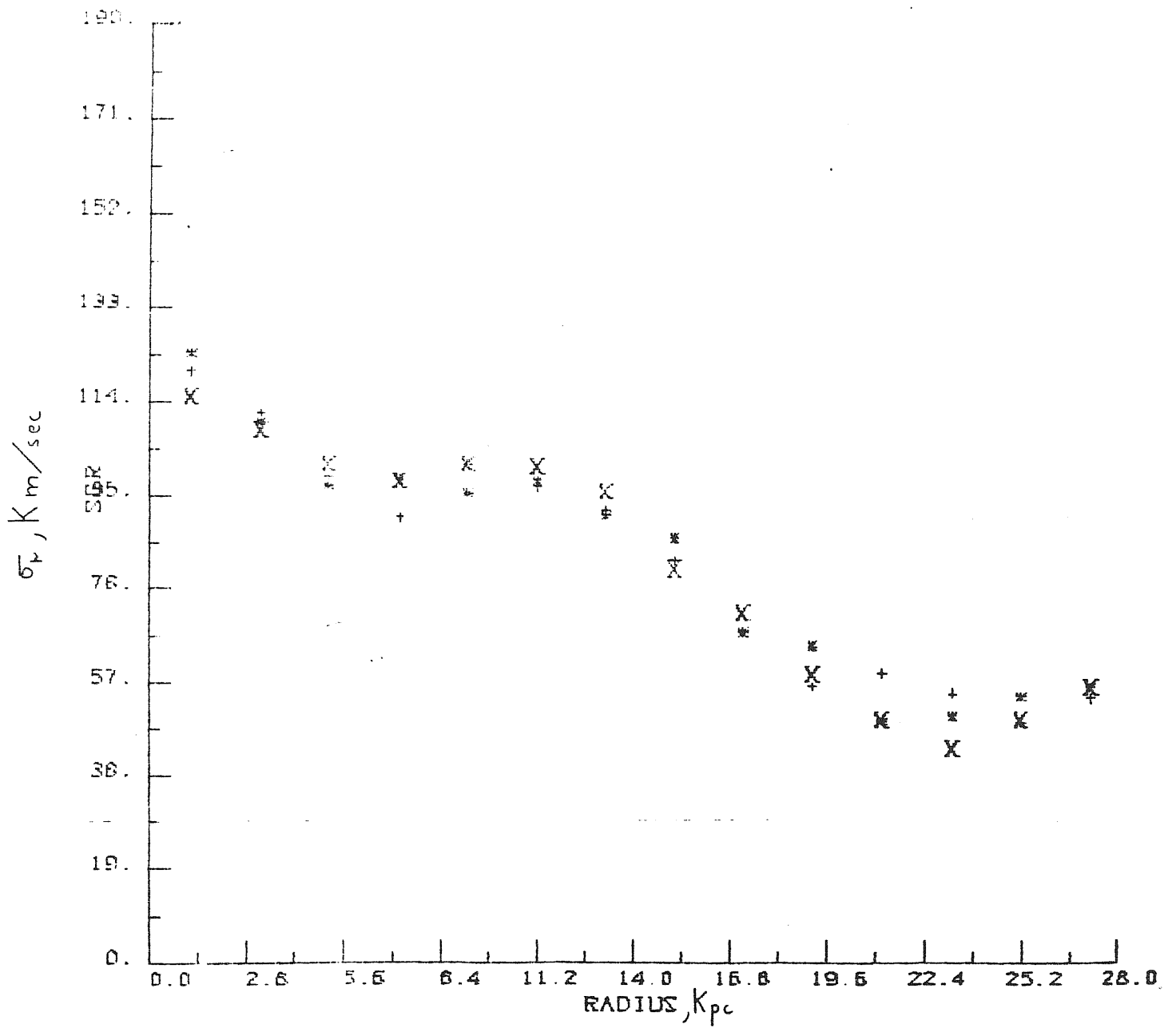
Fig.5.9b   The same as for Fig.5.8b, expect for model G3.
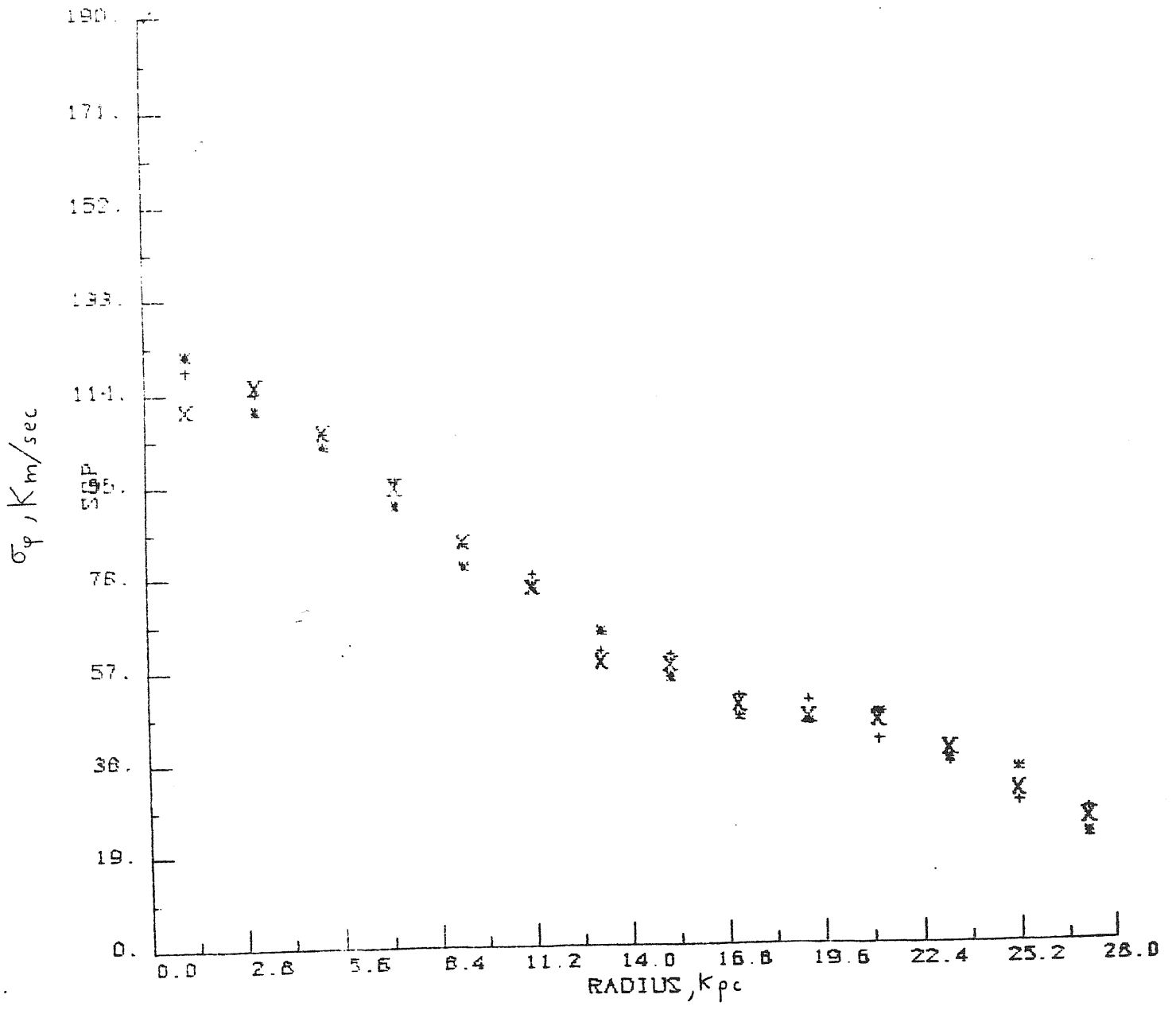
Fig.5.9c   The same as for Fig.5.8c, expect for model G3.
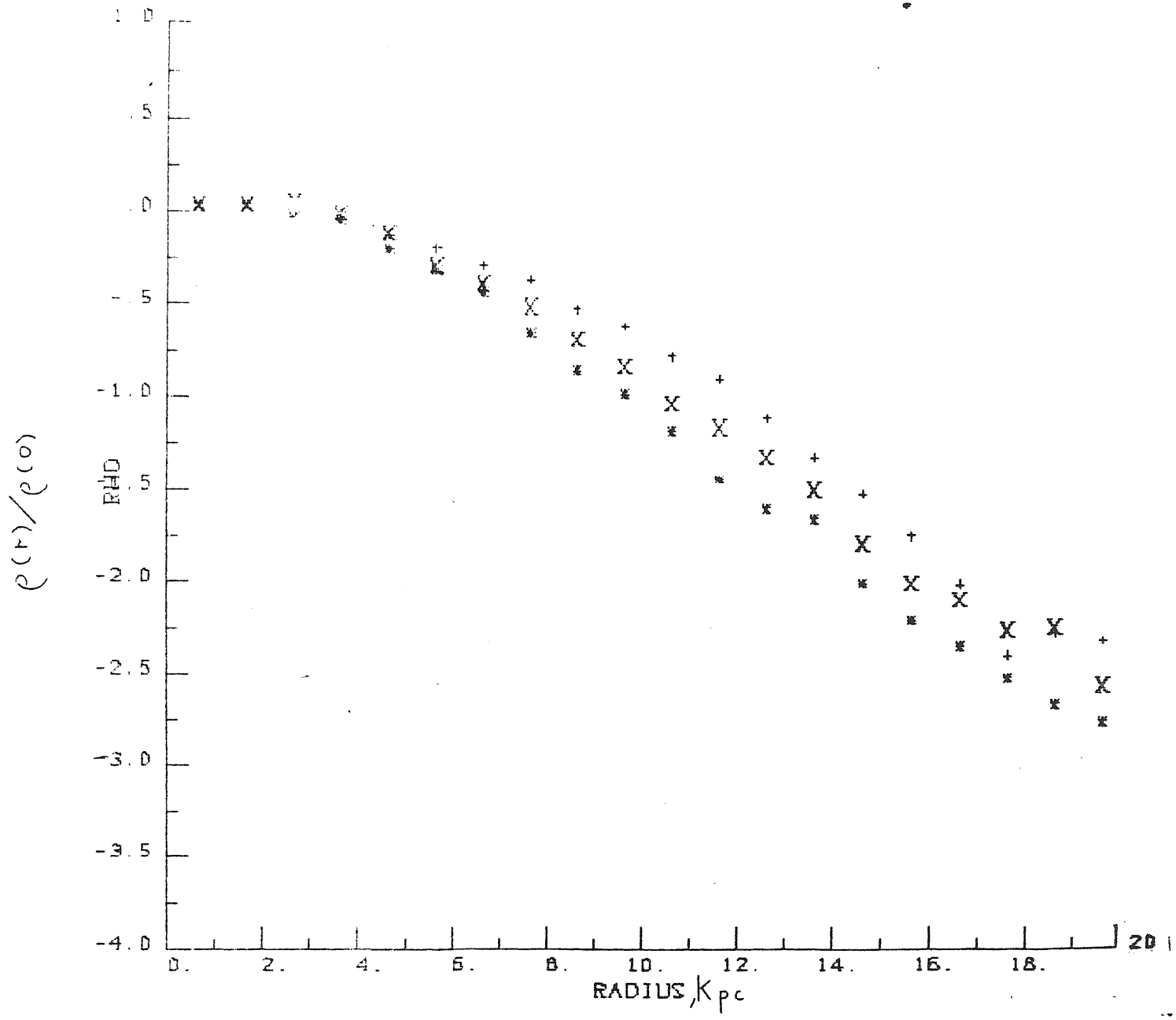
Fig.5.10a   The same as for Fig.5.8a, expect for model G4 .
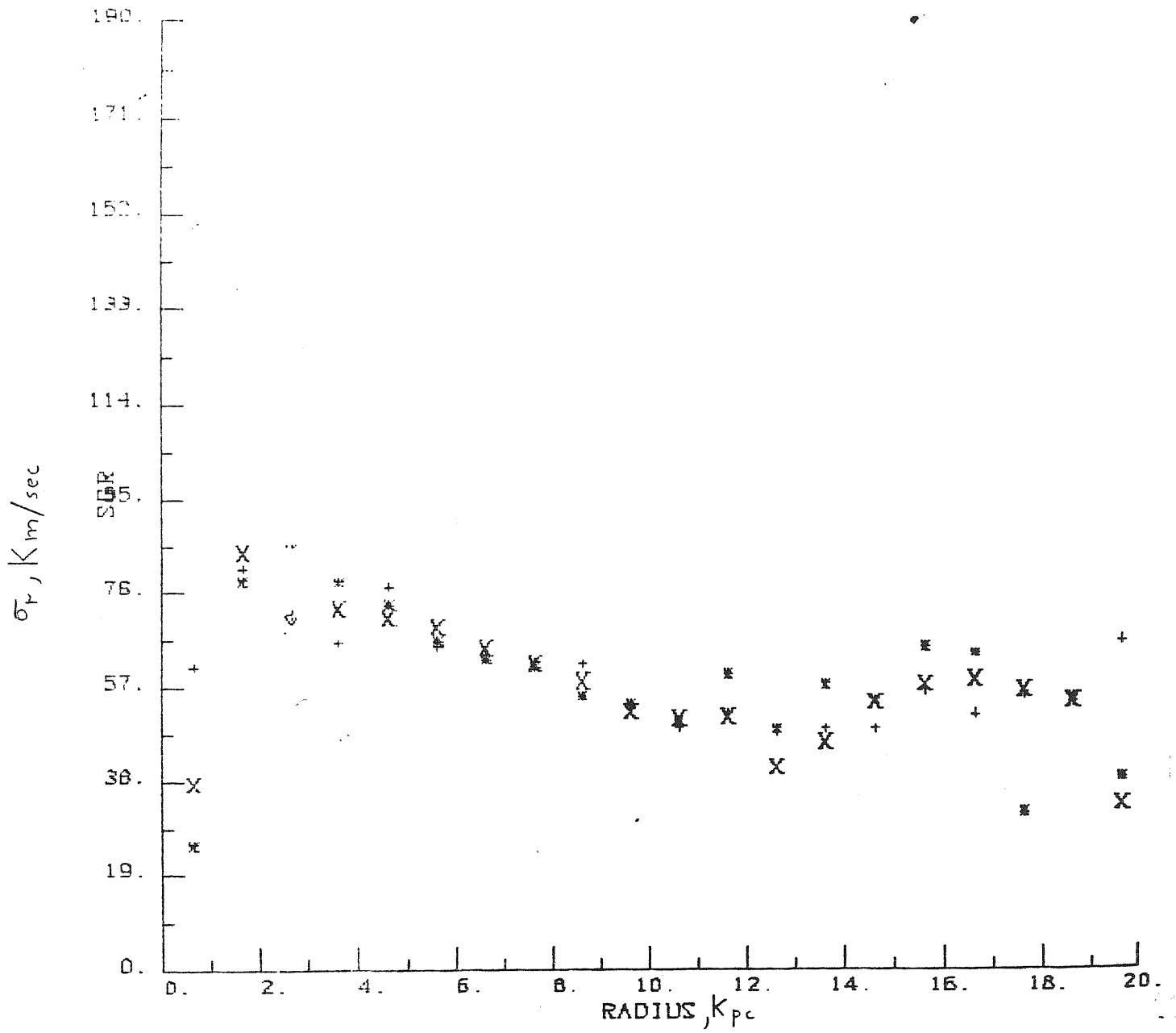
Fig.5.10b   The same as for Fig.5.8b, expect for model G4.
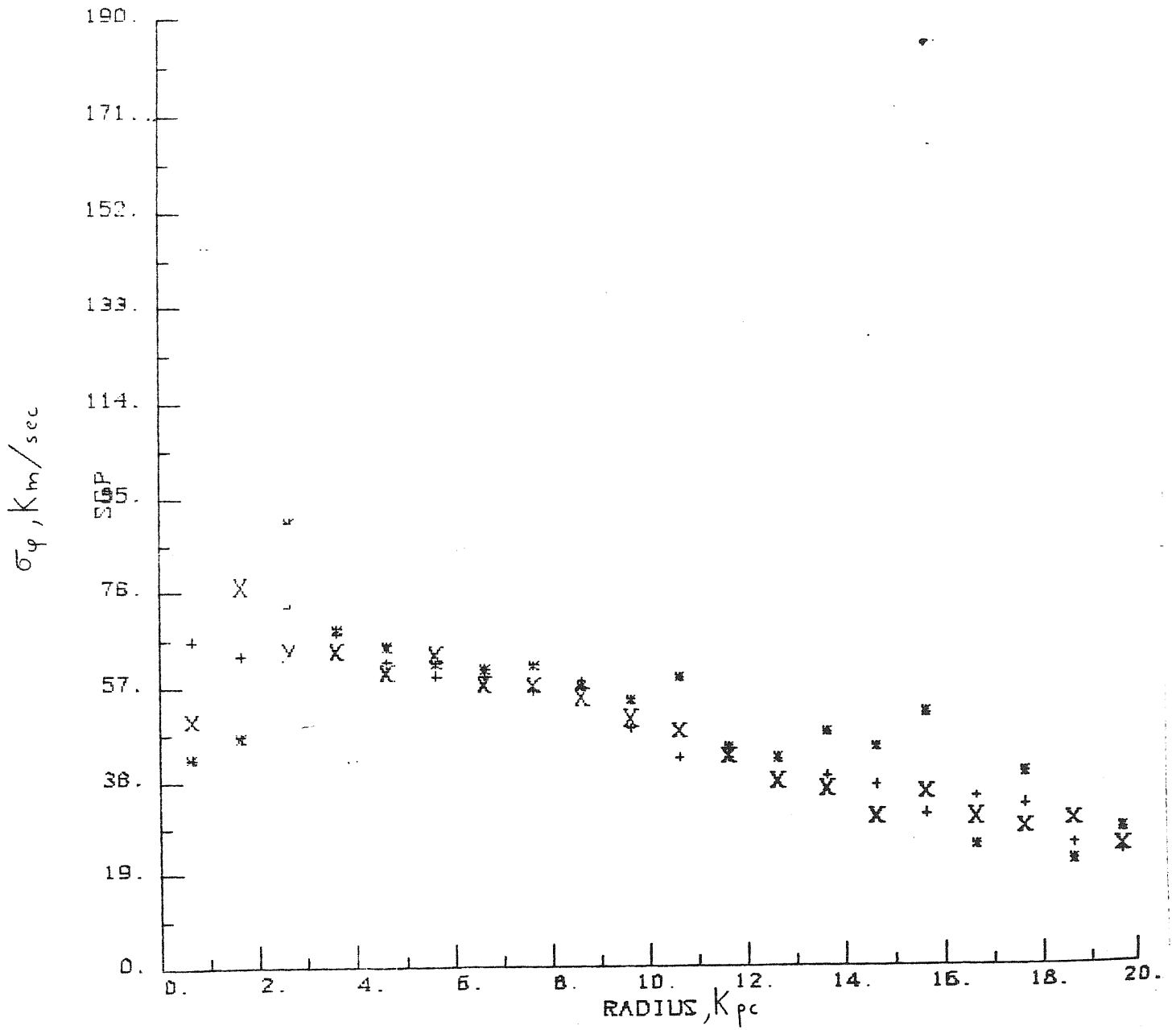
Fig.5.10ć'   The same as for fig.5.8c, expect for model G4.
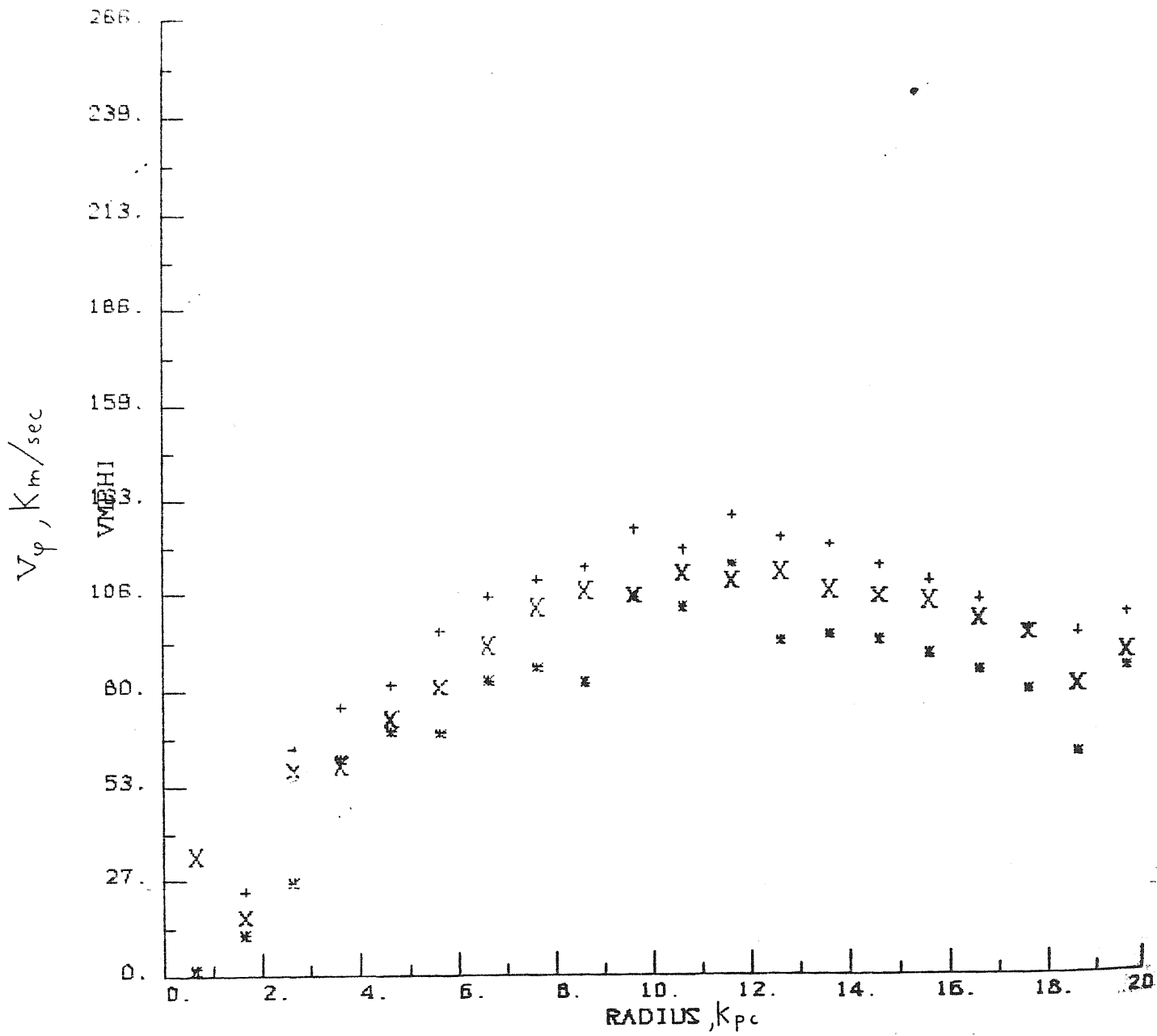
Fig. 5.10d Rotation curve $v_\varphi(r)$ as function of the radius and the polar angle at t=3 for model G4. the ordinate is $v_\varphi(r)$ in Kmsec^{-1}, the radius is in Kpc. Here is +: ϑ =90°,x: ϑ =60°, ⚹ : ϑ =45° .
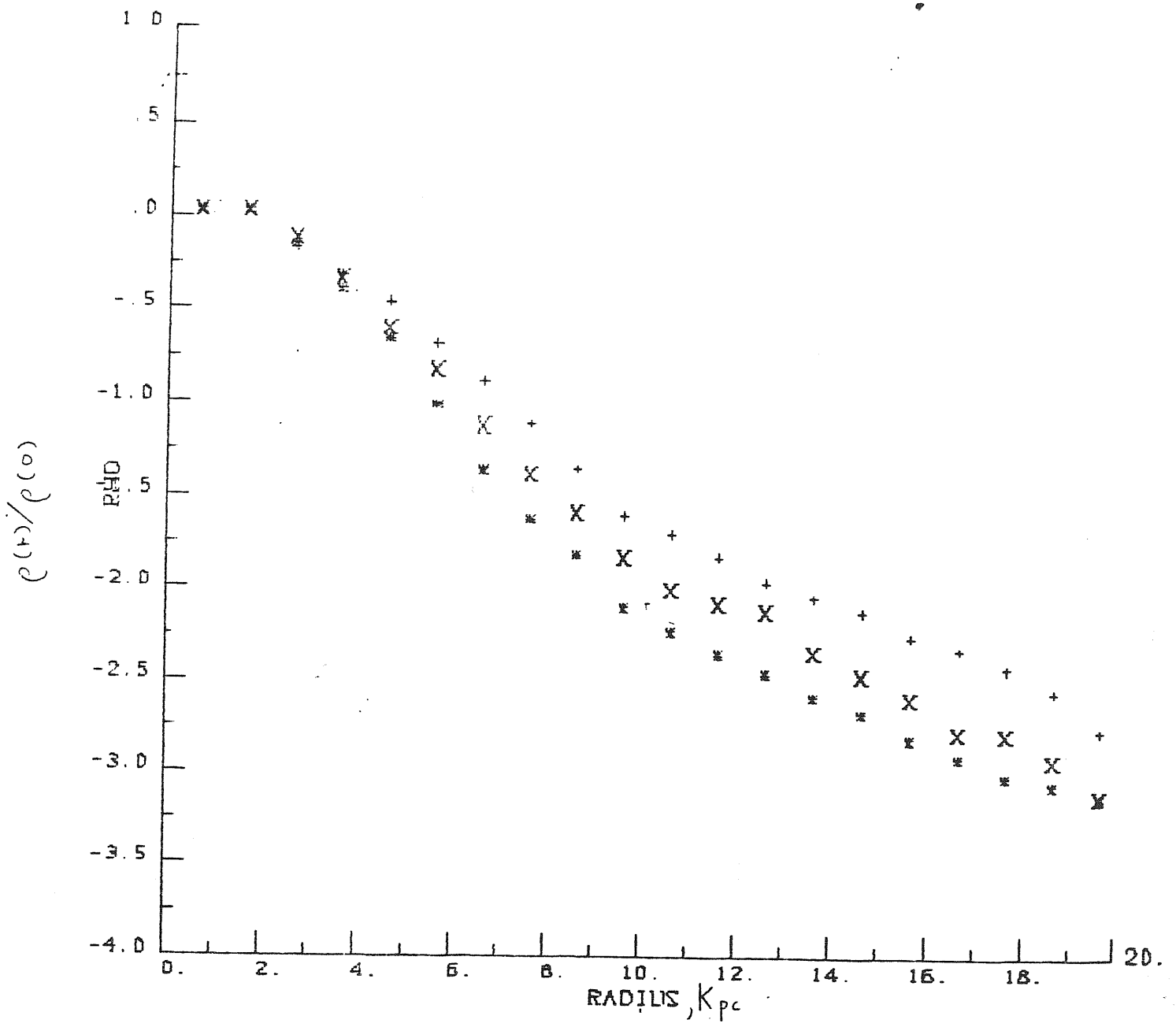
Fig.5.11a   The same as for Fig.5.8a, expect for model G5 .
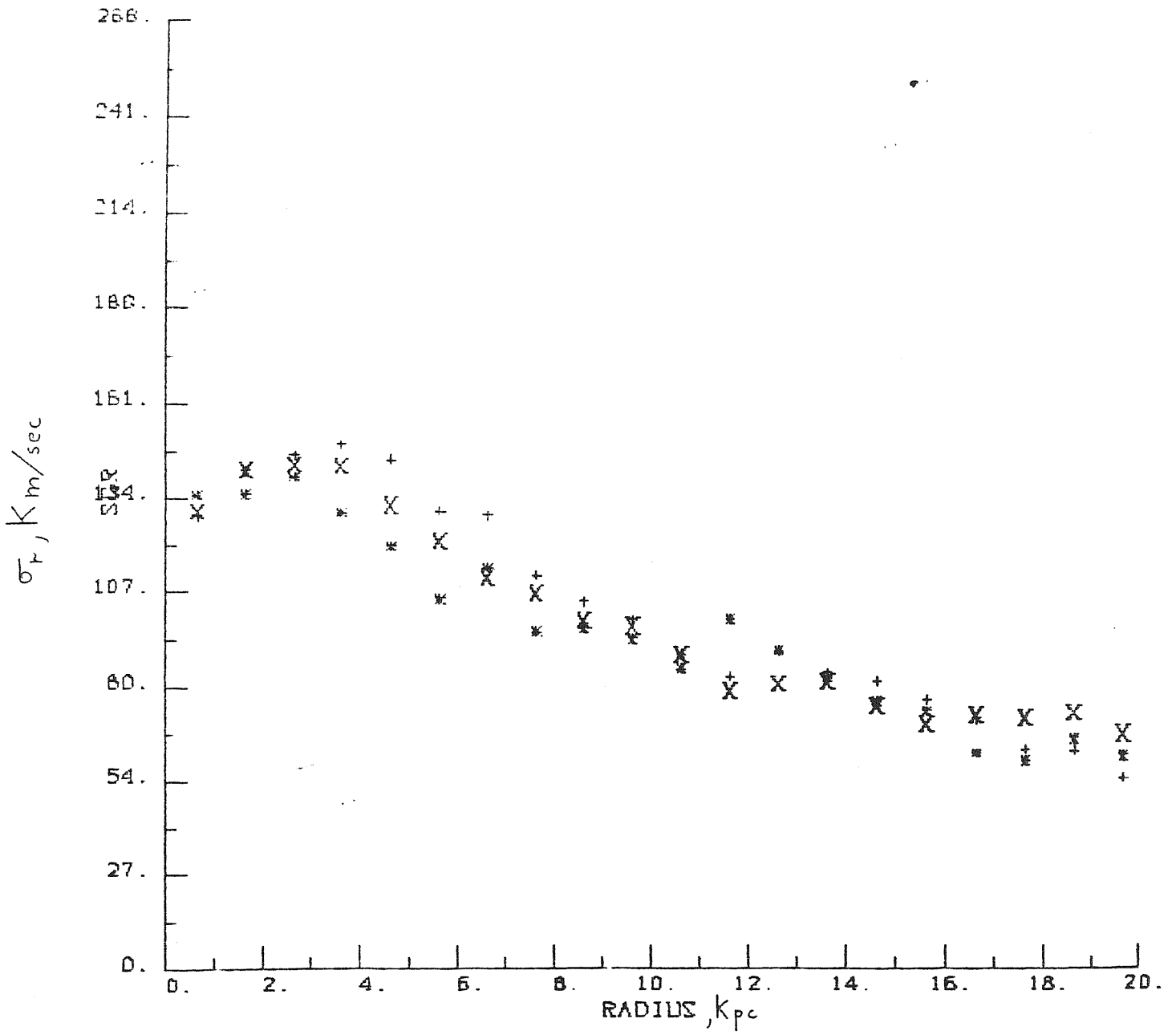
Fig.5.11b The same as for Fig.5.8b, expect for model G5.
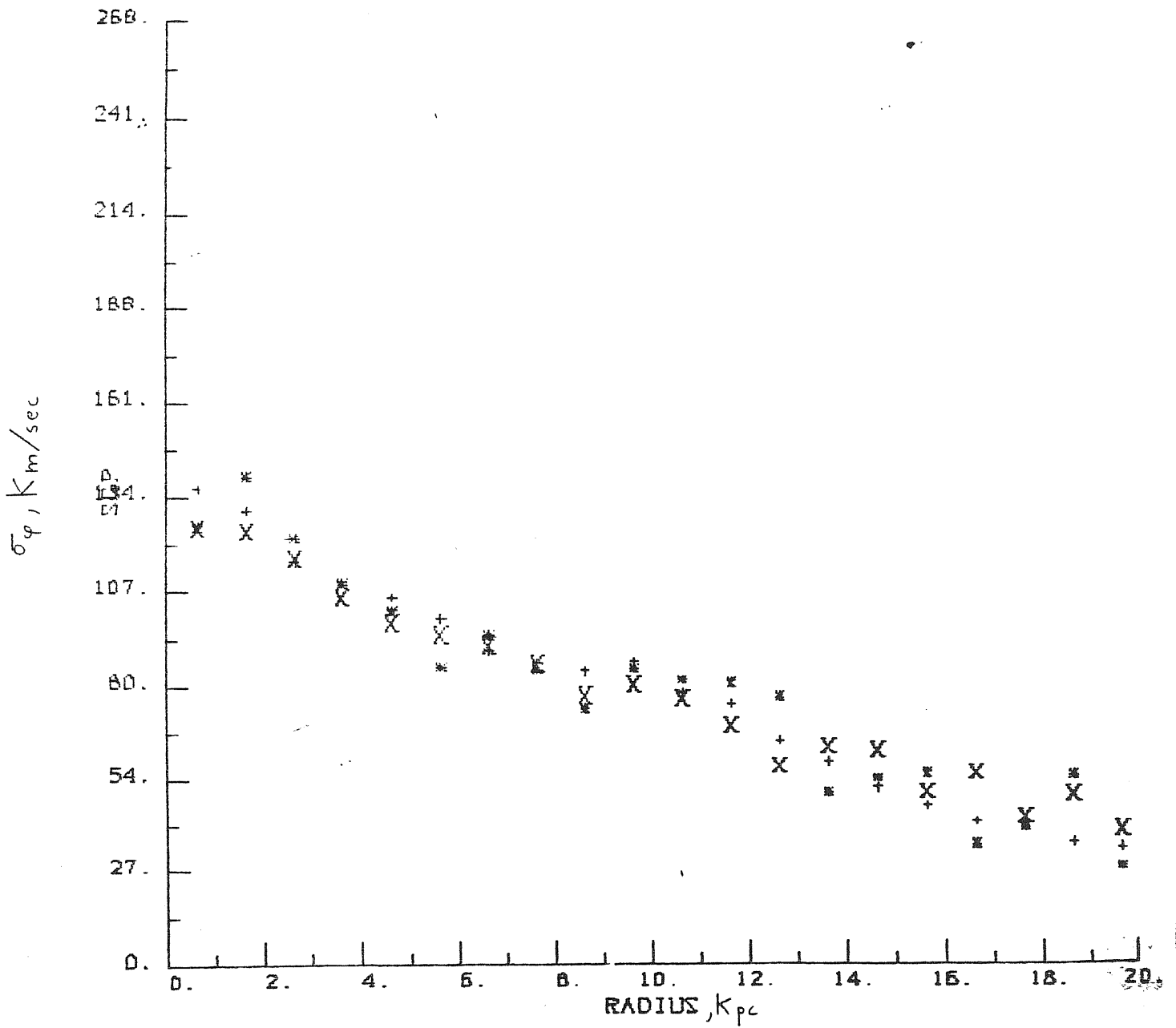
Fig.5.11c   The same as for Fig.5.8c, expect for model G5.
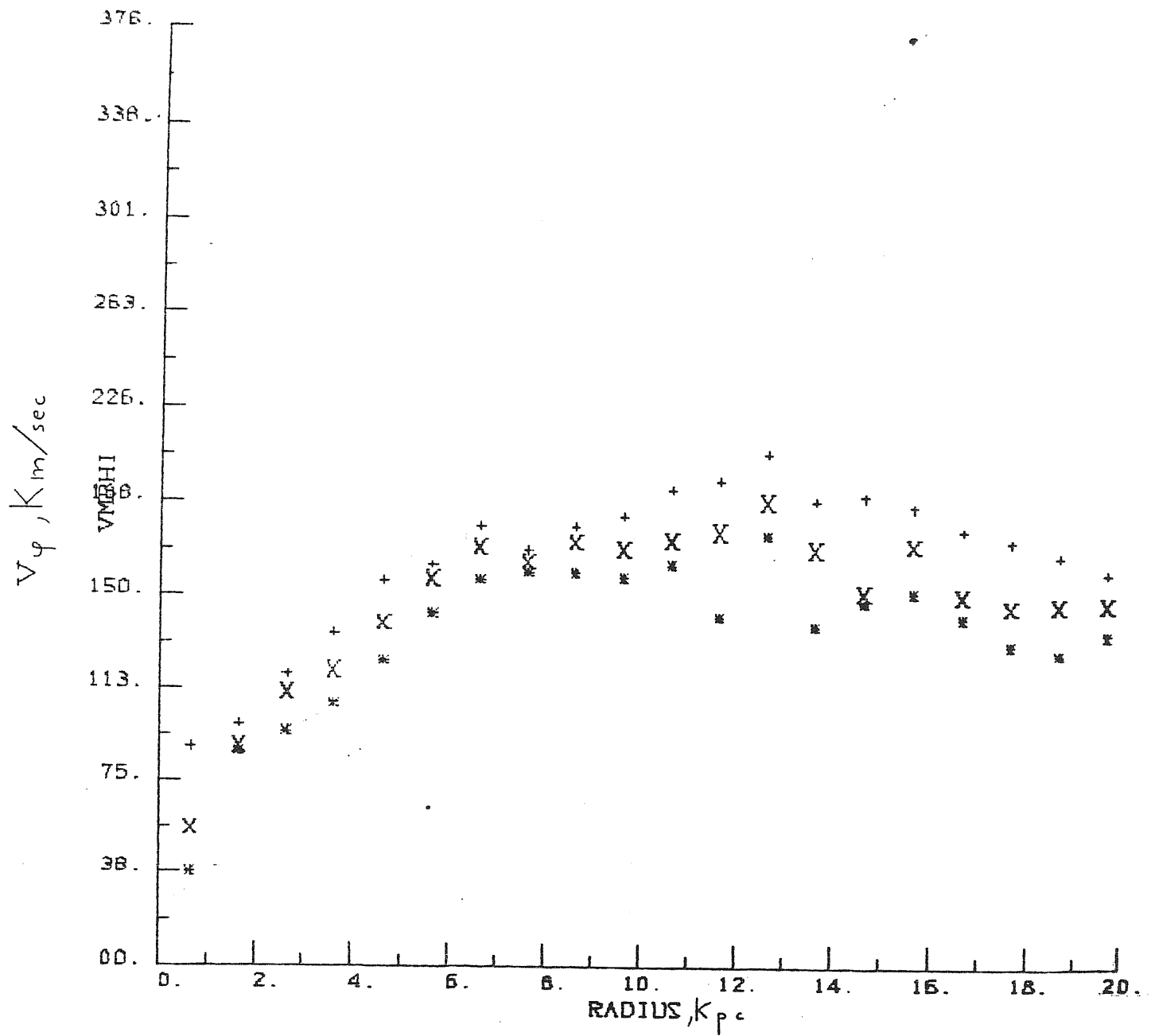
Fig.5.11d   The same as for Fig.5.10d, expect for model G5.
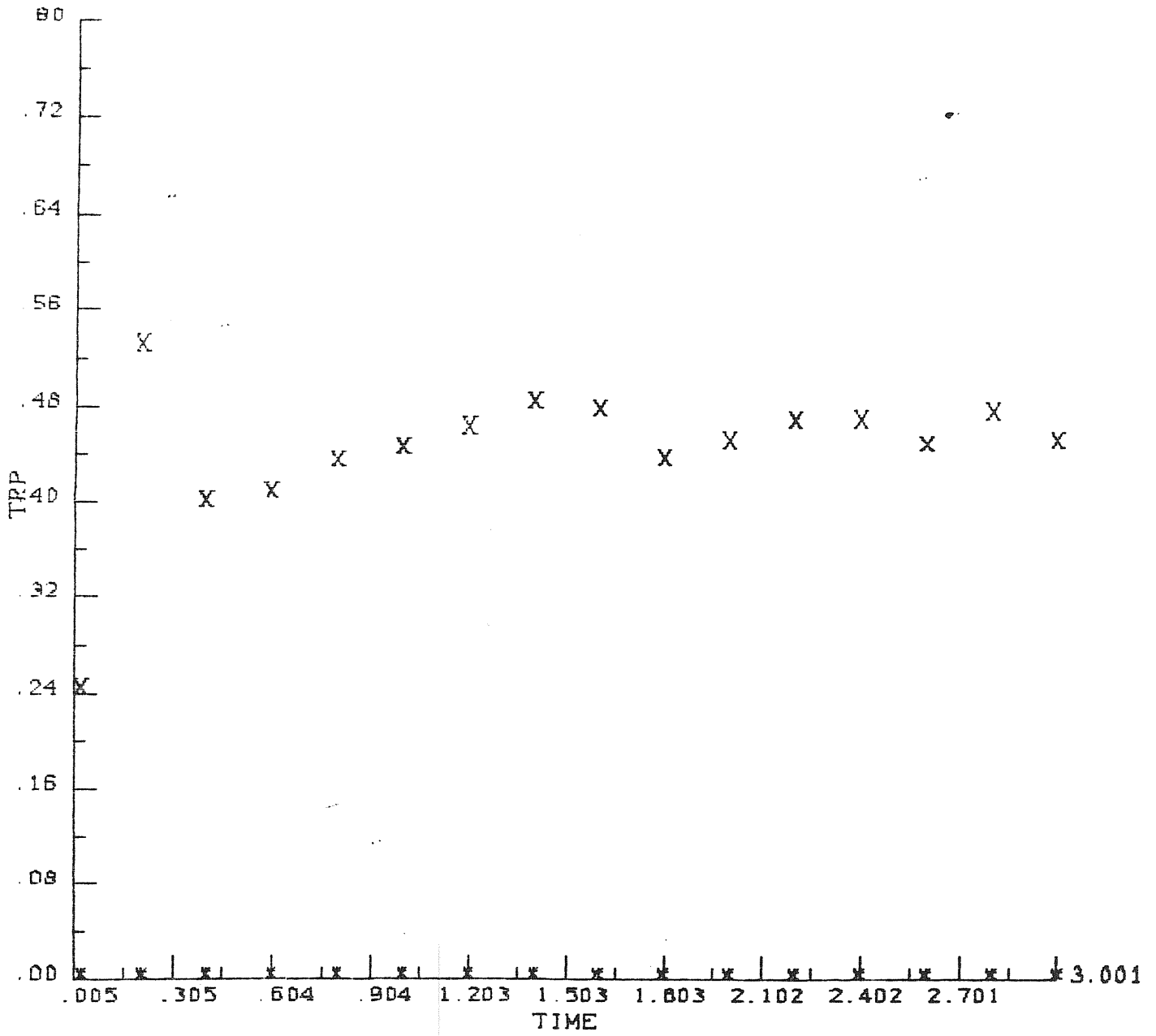
Fig.5.12a   Time evolution of the (T_r/W), (T_c/W) ratios for model G3. Time is in units of $t_c = 2\pi \left(R_I^3 / GM \right)^{-1/2}$. Here is $X: \frac{T_r}{|W|}$, $*: \frac{T_r}{|W|}$.
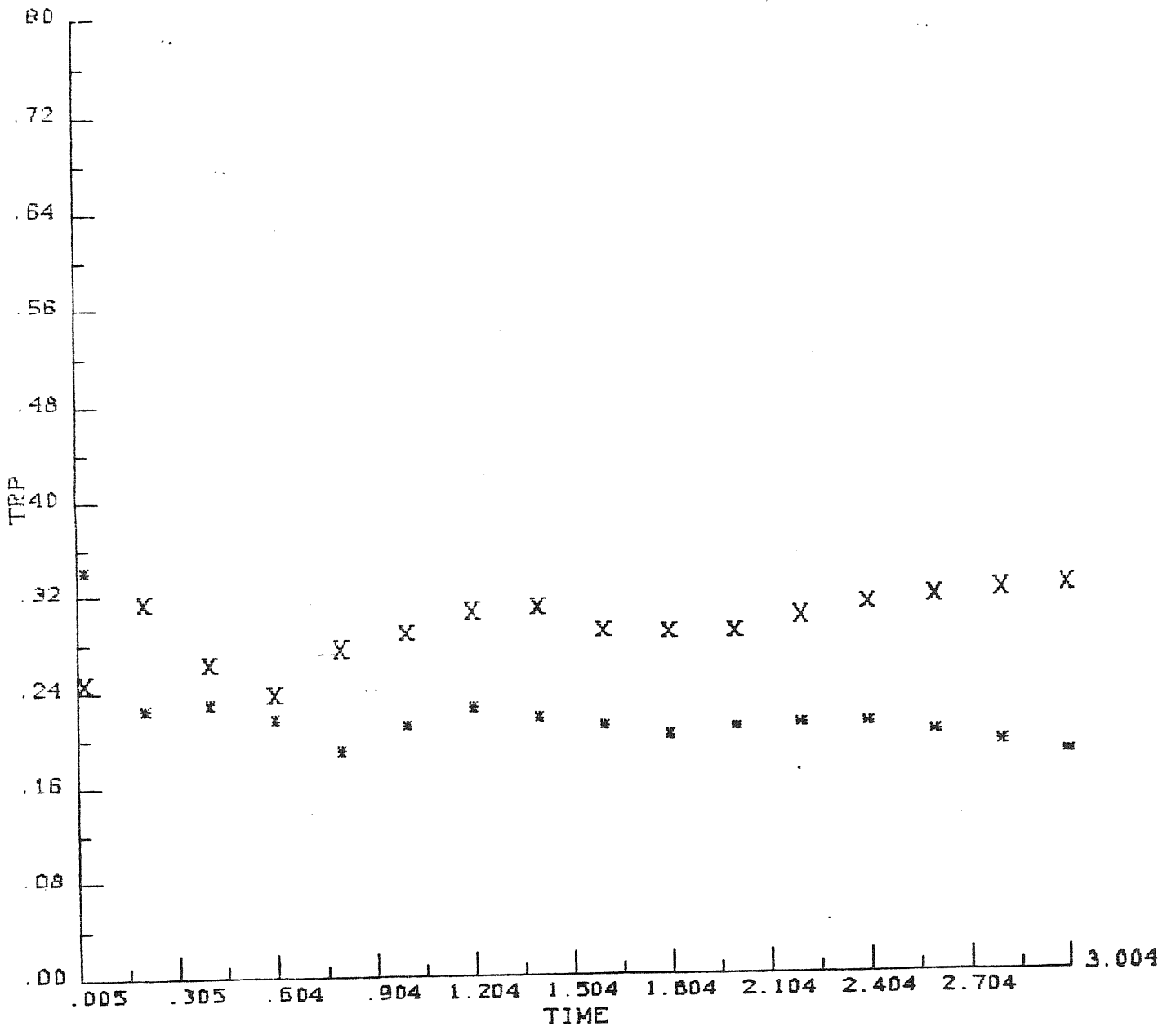
Fig.5.12b   The same as for Fig.5.12a, expect for model G4 .
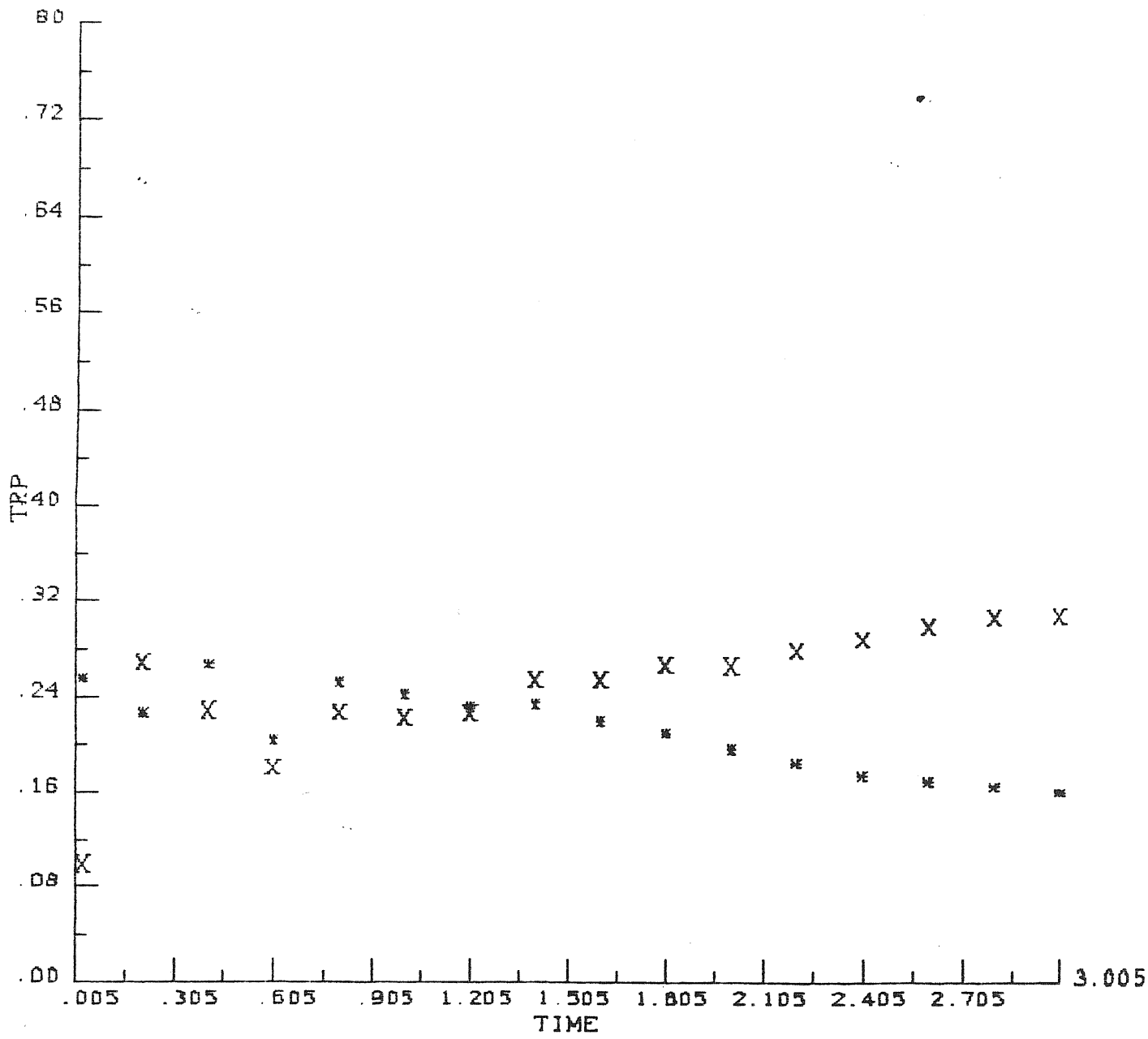
Fig.5.12c   The same as for Fig.5.12a, expect for model G5.

off $v_\varphi \propto r^{-1}$ at $r > 10$ Kpc.

In the inner regions of collapsed rotating systems the violent relaxation

is effective in producing a Maxwellian distribution with solid-body rotation

(Lynden-Bell 1967; Gott 1973), while the outer regions are composed of

halo stars with approximately the same angular momentum.

b) N-body simulations with limited resolution

Now we will try to numerically simulate the gravitational collapse of a

'dark' system together with a 'baryonic' component. In this simulation the

two matter components will be simulated by two sets of particles, with the

same mass, but with different initial conditions. The number of particles

and the initial radius for the two components are N_D, N_B and R_{I_D}, R_{I_B} ,

respectively.

From eq. (5.1) we have $R_{I_B} \simeq \dfrac{R_{I_D}}{2}$ .A further constraint on the baryonic

component arises from the observed mass-to-light ratios for elliptical

galaxies at the De Vaucoulers radius, we require $N_B \simeq N_D /(5-10)$, since

in the numerical integration we have set the mass of the particles equal

in order to minimize two-body relaxation effects between the two matter com-

ponents. Owing to storage limitations with the computer the maximum number

of particles which can be used in such a integration is about $N \simeq 7.10^4$,

for the same reason the maximum dimension of the active array is 32^3.

Then in such an integration the baryonic component is simulated with a poor resolution, spatial and in number of particles, with respect to the integrations made for models G.

To increase the accuracy of the integration for these low-resolution models the field calculation was changed from eq.(5.14) to $\left(\vec{x}_p = \left[(p + \frac{1}{2}) L_1, m L_1, n L_1 \right] \right)$

$$ E_x (\vec{x}_p) = \frac{\phi_{p+1,m,n} - \phi_{p,m,n}}{L_1} \qquad (5.24) $$

This localizes the field calculations so we could expect a better resolution.

To be sure that the results of the numerical integration for the baryonic component, in the presence of a dark halo, are not masked by the reduced numerical resolution, we have performed a series of numerical integrations (R) as in models G but with a reduced resolution, withouth the dark component. The final results for models R are then compared with the corresponding ones in models G.

The initial conditions for the integration of type R are given in Table II. Thereafter the peculiar particle velocity distribution is Gaussian with a 3-σ cut-off .

In table II the rotation period P of the bar in t_c units is also given.

The period P has been estimated by eye with an average over 5 estimates

TABLE II

	R_I [a]	M [b]	R_I' [c]	α_r [d]	α_V [e]	N [f]	P [g]
R1	10	2.10^{11}	5	0.866	0.233	3.10^3	3.2
R2	10	2.10^{11}	5	0.866	0.233	6.10^3	2.4
R3	10	2.10^{11}	7	0.866	0.233	6.10^3	1.6
R4	10	10^{11}	8	1	0.33	6.10^3	2.4
R5	14	10^{11}	8	0.1	0.33	6.10^3	---
R6	10	2.10^{11}	8	0.866	0.233	6.10^3	1.6

a) Initial radius in kpc

b) Total mass in solar units

c) Initial radius in grid length units

d) Initial angular velocity in units of $\Omega_o = (GM/R_I^3)^{1/2}$

e) Cut-off velocity for the peculiar velocity distribution in uints of $(GM/R_I)^{1/2}$

f) Total number of particles used in the simulation

g) bar period in uints of $2\pi/\Omega_o$

between t=1.5 and t=3. (in each measure the azimuthal poistions of the
bar in the x-y plane are spaced by 180°). Although this is a rough estimate
of P we do not think that the associated errors would be larger than 20% ,
since the error $\Delta \varphi$ in estimating the bar's azimuthal position in the
x-y plane cannot be greater than the angular width of the bar itself, i.e.
$\Delta \varphi \lesssim 20°$;for a discussion of the validity of this approximation see
also Carnevali (1983).

Let us discuss now several results of the R integrations.

Fig.s 5.13,5.14 show the particle distribution in the x-y,x-z,y-z planes
for models R1 and R2 at t=3.The plotted particles have been chosen with the
same criterion used for models G.

Model R1 differs from model R1 only in that it has twice the number of
particles. Model R1 has a bar period which is shorter than that in R1 by
a factor 3/4.

This reduction of P as the number of particles is increased is due to the
importance of the two-body relaxation effects in the two models.

This effect is more important in R1 than R2. This implies that model R1 has
a tendency for keeping more pronounced axial symmetry than in R2, as a
results the flow of angular momentum towards the outer regions is smaller
in R1 than in R2 and this implies a larger bar period for R1 with respect
to the one found in R2 (see also Carnevali 1983 for a discussion on two-

body relaxation effects in N-body integrations for rotating stellar bars).

This can also be seen from Fig.s 5.15 and 5.16 where the final stellar

energy distributions are shown at t=3 for the two models.

Model R1 shows a more uniform energy distribution, whereas for R2 a peak

structure is present in the stellar energy distribution.

In numerical integrations of this kind the two-body relaxation time

is connected to the number of particles used in the experiment by

(see § IV.3 and Hockney and Eastwood 1981, §II.3.4)

$$\frac{t_R}{t_c} \simeq \frac{N}{140} \quad / \qquad (5.25)$$

however eq.(5.25) refers to an average angular deflection of 90° for

the particle, since the averaged squared deflection is proportional to

t_R , in the R1 integration $\Delta\theta \simeq 30°$ at t=2; while for model R2

$\Delta\theta \simeq 30°$ at t=4.

Model R2 has the same number of particles as model R6 but with a reduced

spatial resolution.

The final particle distribution for model R6, together with the stellar

energy distribution, is shown in Fig.s5.18,5.19 .

Model R6 has a more extended final energy distribution than in R2, in fact it

is similar to the final one in its equivalent model G5.

Further the bar period in R6 is shorter than that in R2 and equals that

found in G5.

The explanation of the different behaviours of models R6 and R2 is the fol-

lowing: the numerical integration made in the R2 case is equivalent to the

one in R6 expect for the reduced spatial resolution, i.e. the integration

in R2 equals the one in R6 but with a reduced gravitational interaction,

owing to eq.(5.11).

This 'smoothing' of the gravitational interaction of model R2 implies a

smaller gravitational coupling between particles than in R6, the results

is a bar period which is larger in R2 than in R6.

For the same reason a comparison between the variables $\left\{ \rho, \sigma_r, \sigma_\varphi, \sigma_\varphi \right\}$

for model R2 (Fig.5.17) and model R6 (Fig.5.20,these quantities have been

calculated in the same manner as in models G)shows that the central values

of the velocity dispersions σ_r, σ_φ , are smaller in R2.

This is due to the reduced spatial resolution used in model R2, i.e. the

average forces dispersions are larger in R6 than in R2.

The agreement found between Fig.s 5.20 ($\rho, \sigma_r, \sigma_\varphi, \bar{\sigma}_\varphi$) for model R6 and

the corresponding ones for model G5 tell us that we can consider the inte-

gration made in R6 to be free of relaxation effects and of limitations

on spatial resolution.

Models R4 and R5 have shown a similar agremeent with the corresponding

models G and will not be discussed.

It must be noted that model R6 developed a bar with the same period as

the one in model G5, but the final bar position in the x-y plane at t=3

is different in the two cases.

This happens since in model R6 the bar is born at t $\simeq$ 2, while in model

G5 is already well developed at t $\simeq$ 1.5 . This results is not surprising

since the average number of particles per cell is smaller in R6 ($\bar{n} \simeq$ 12)

than in G5 ($\bar{n} \simeq$ 30); if the birth of the bar in these numerical experiments

is caused by small scale numerical instabilities of the order of L, as

suggested by Miller (1978),then fluctuations in the number of particles

per cell ought to have larger amplitudes in G5 than in R6.

Finally we would like to point out an expected, but unseen, numerical ef-

fect in model R1.

This integration has a very poor spatial resolution,with respect to other

integrations, and therefore a larger number of particles will be found .

in the same cell during the integration. Eq.(5.11) implies that forces

between particles in the same cell are smothed with respect the r^{-2}

interaction (but non-zero owing to eq.(5.15)), so these particles will

travel together in the same cell for sevral integration steps.

In the R1 integration this phenomenon would imply the presence of large
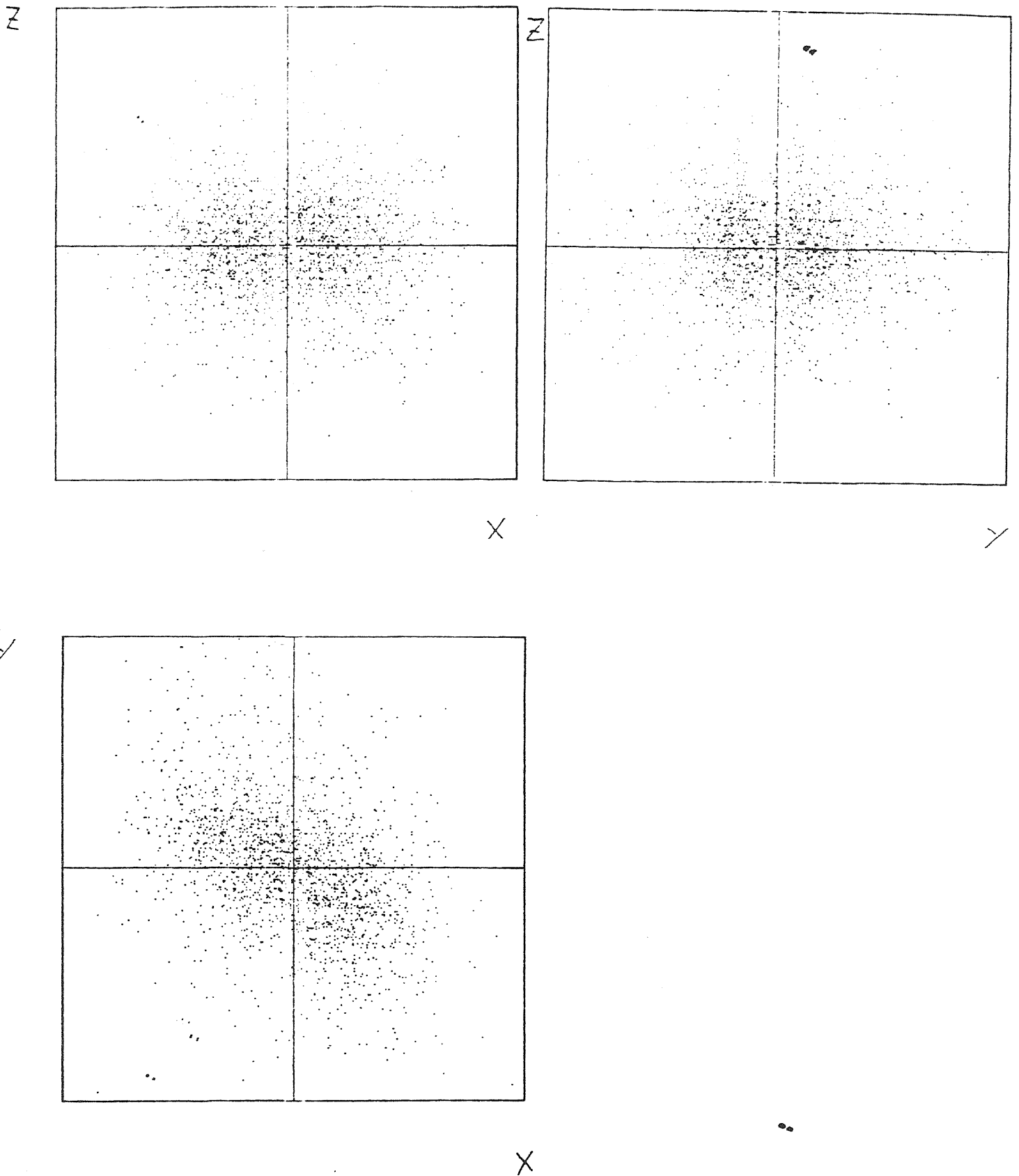
Fig.5.13 .Particle plots for model R1 in the x-y,x-z,y-z planes at t=3.
The box size is 32 Kpc.
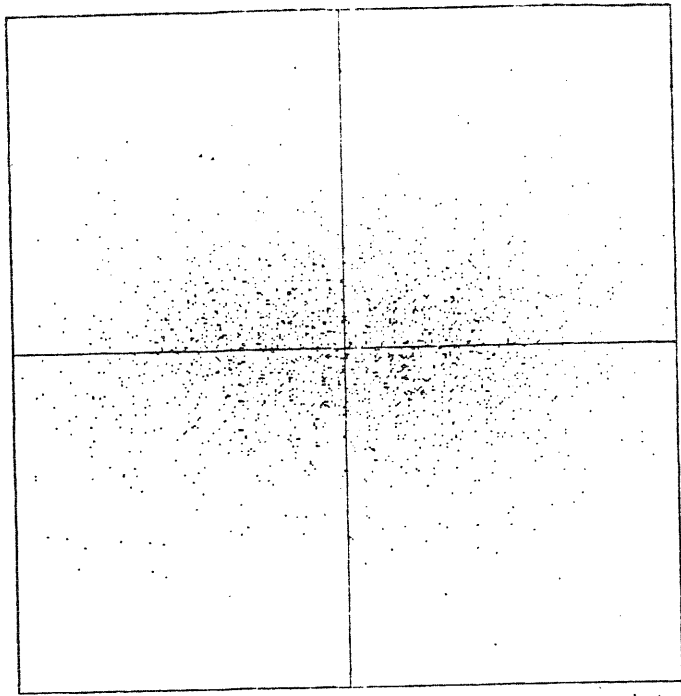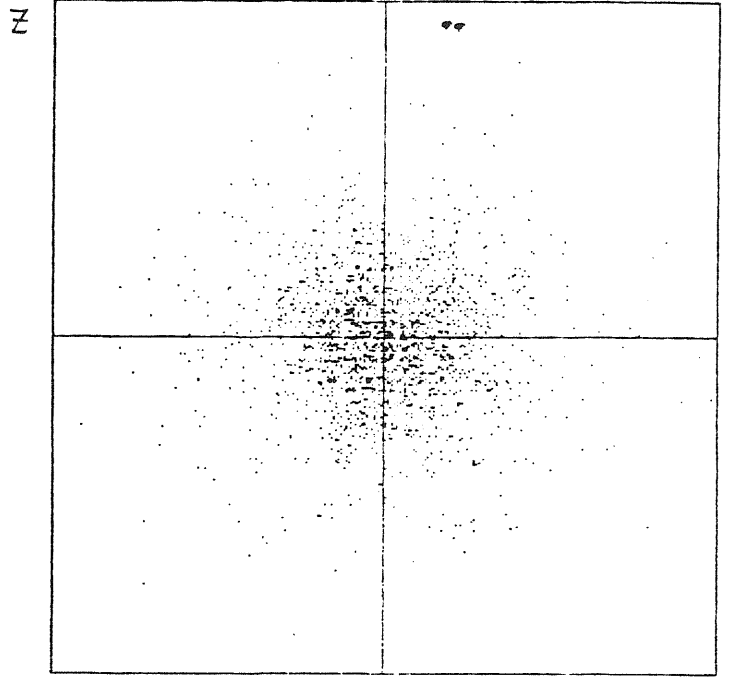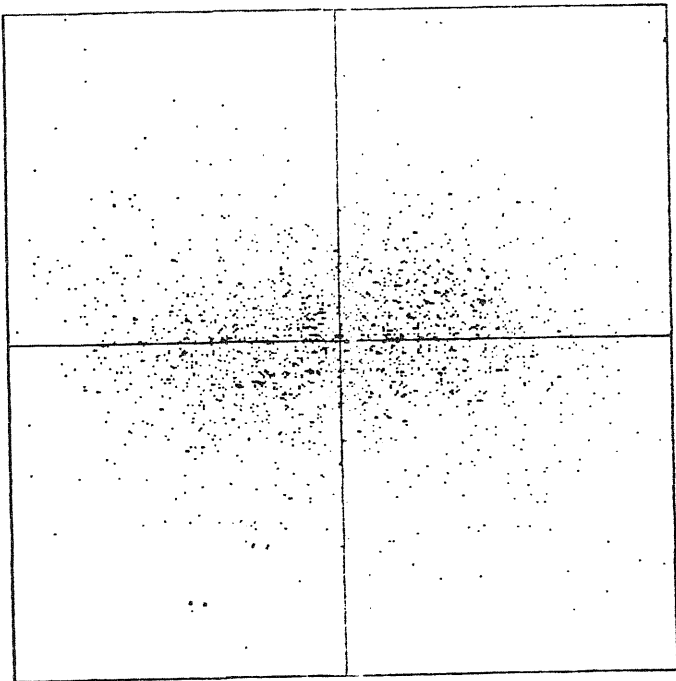
Fig. 5.14   Particle plots for model R2 in the x-y,x-z,y-z planes at t=3.
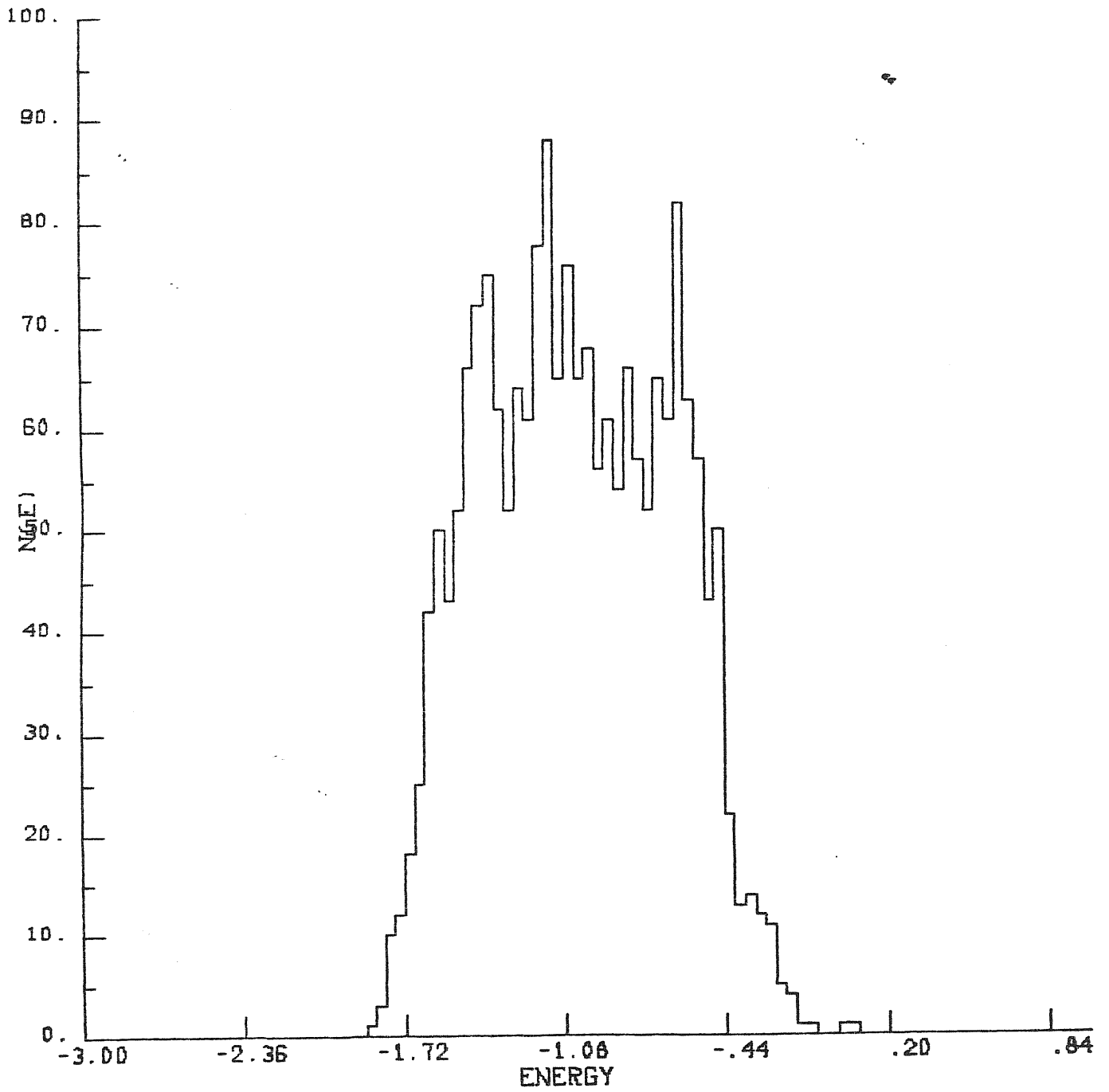
Fig. 5.15 Final energy histogram for model R1 at t=3. Units are the same of Fig.5.4a
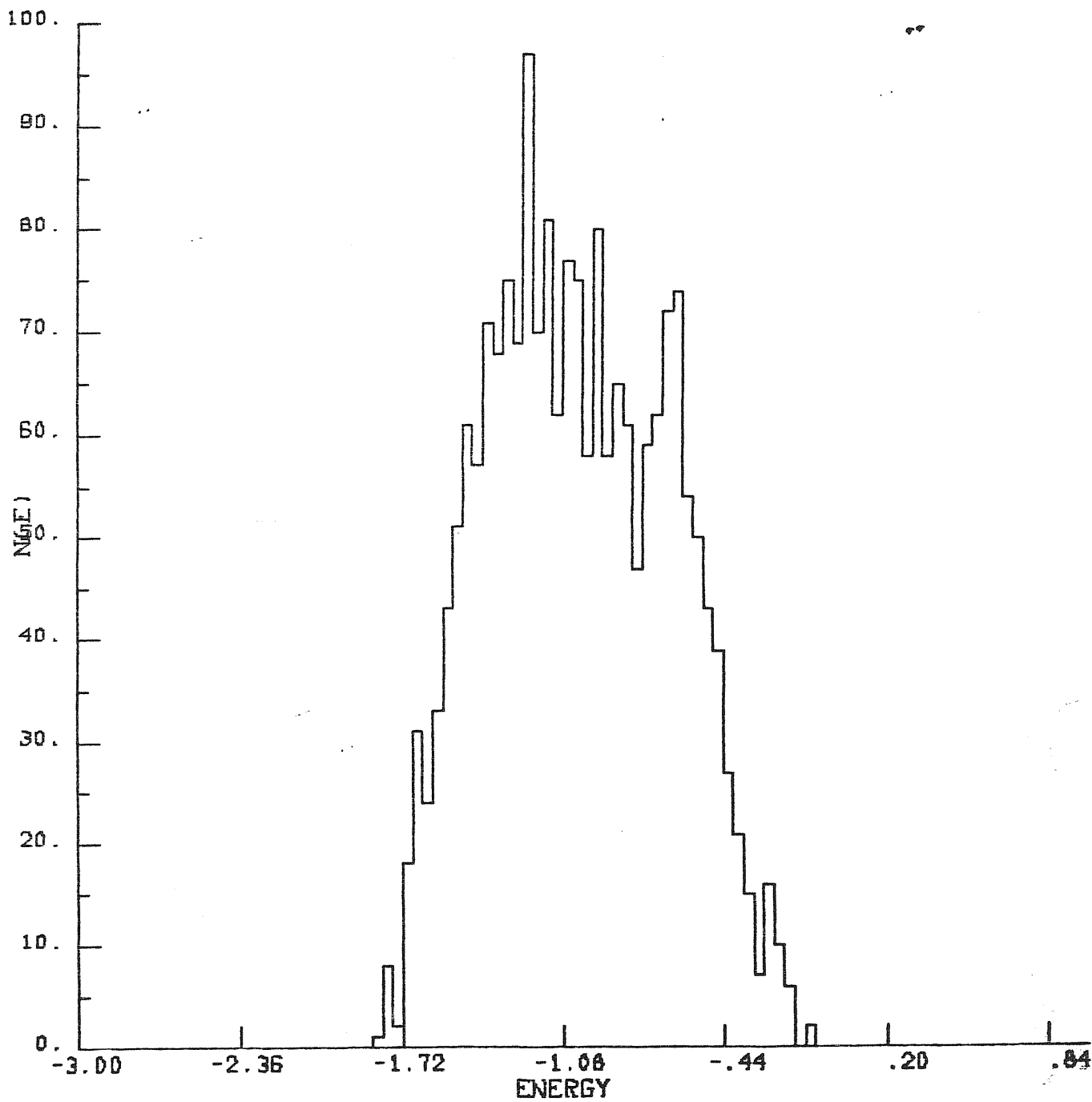
Fig. 5.16 Final energy histogram for model R2 at t=3. Units are the same of Fig.5.4a .
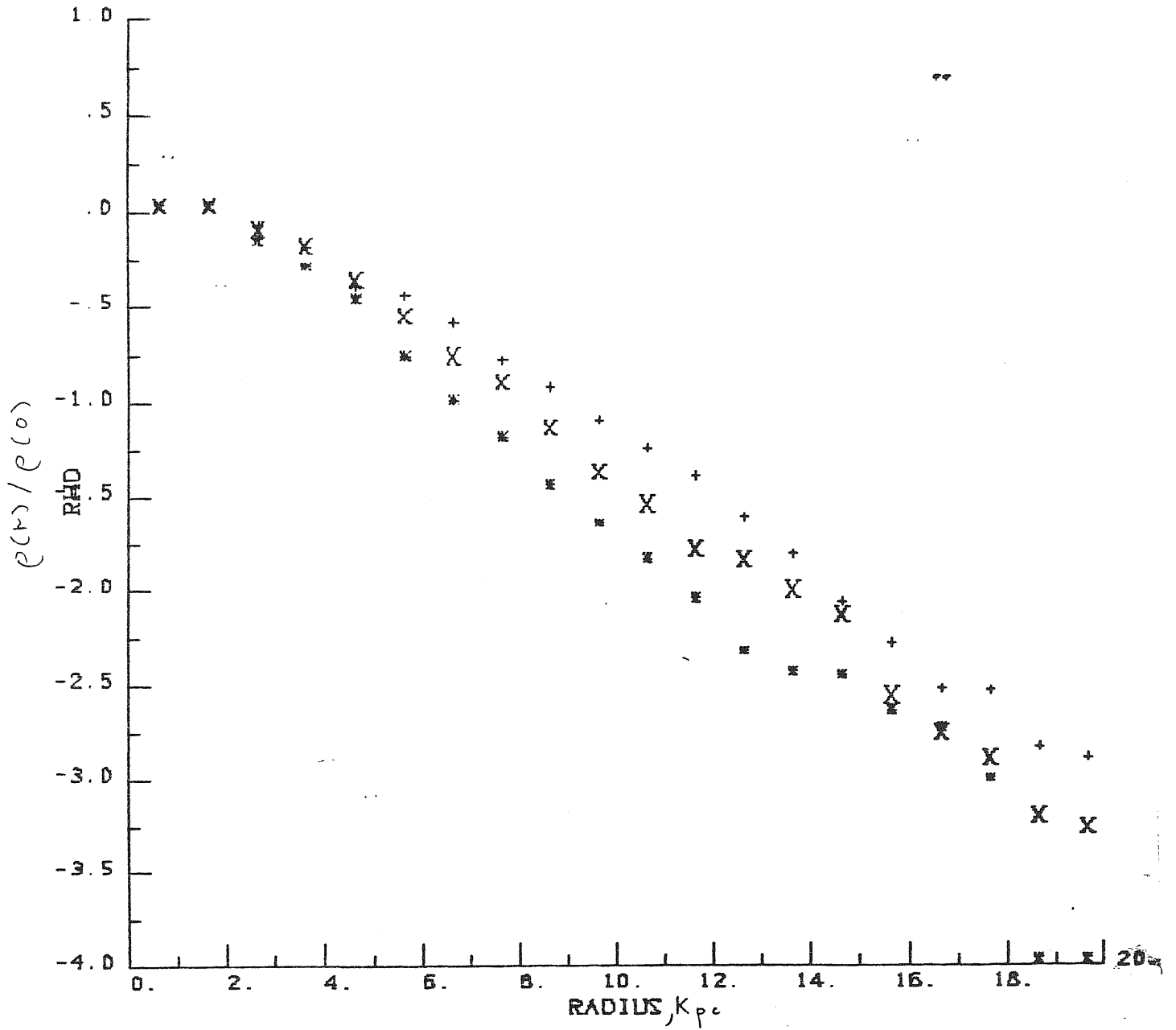
Fig. 5.17a Stellar density $\rho(r)$ as function of the radius r and the polar angle θ for model R2. Units are the same of Fig.5.8a.

Here is +: θ =90°, x: θ =60°, ✳: θ =45° .
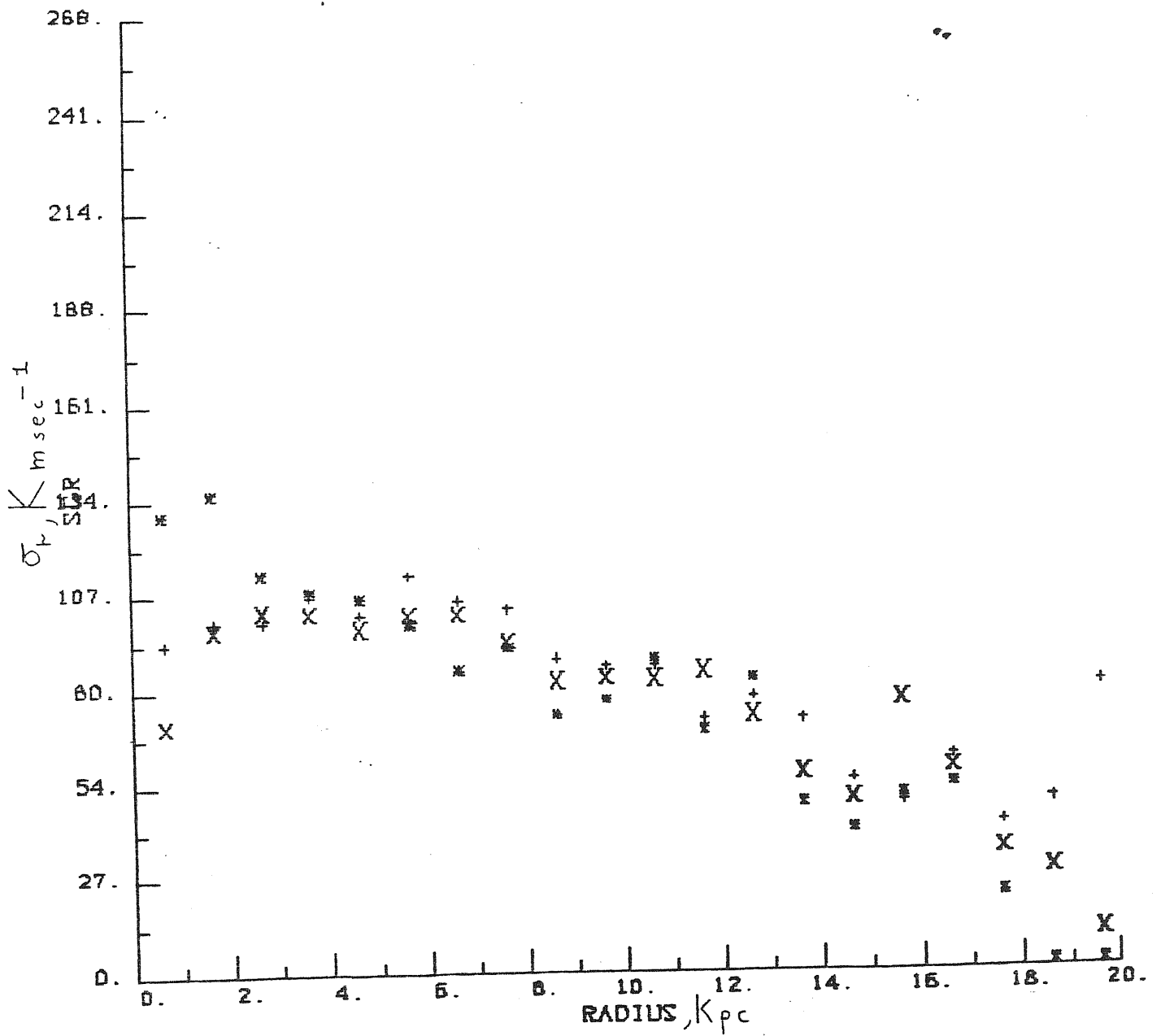
Fig. 5.17b Radial velocity dispersion σ_r as function of the radius and the polar

angle θ at t=3 for model R2. Units are the same of Fig.5.8b .
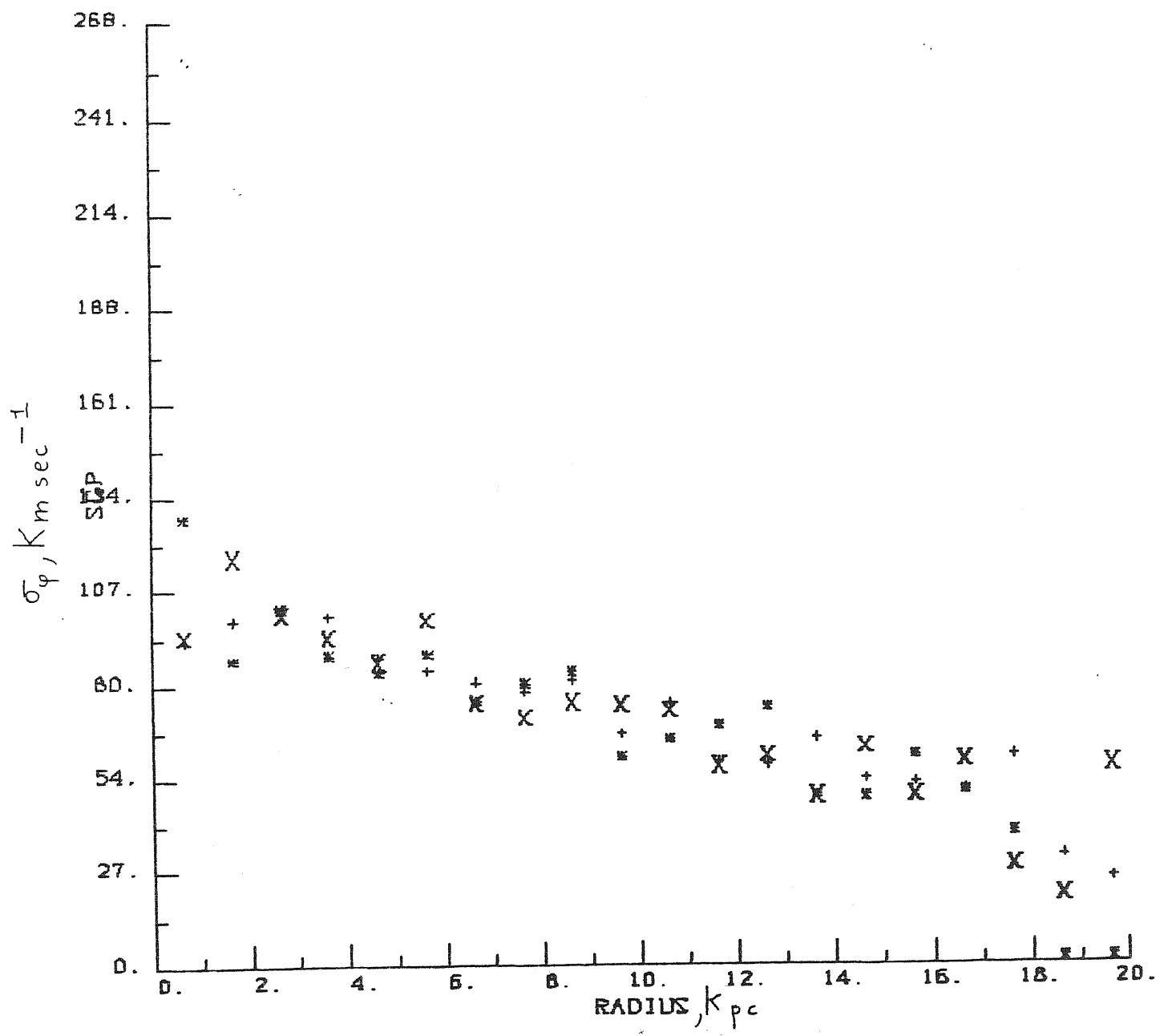
Fig.5.17c Azimuthal velocity dispersion σ_φ as function of the radius and the polar

angle θ at t=3 for model R2. Units are the same of Fig.5.8c .
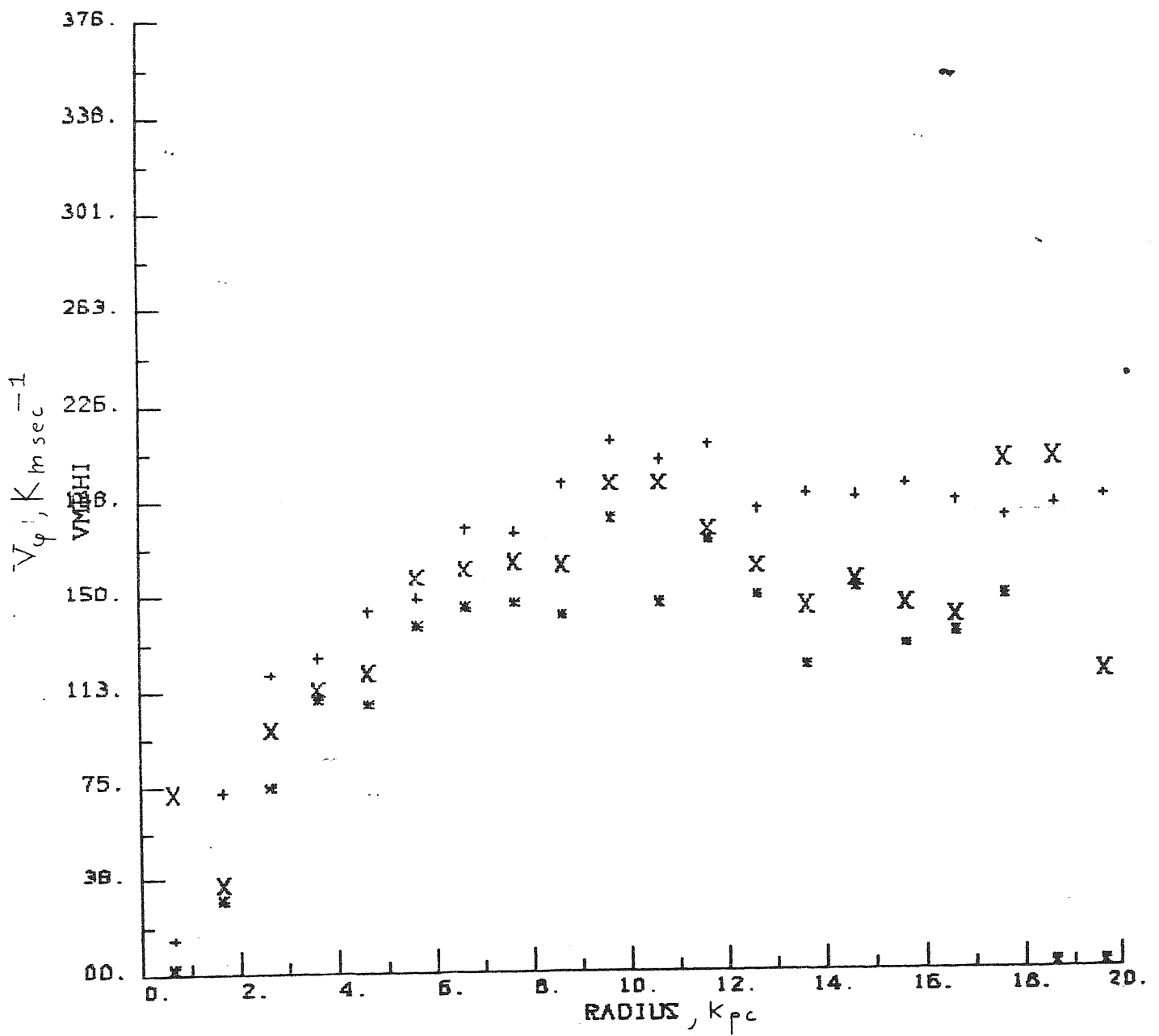
Fig. 5.17d   Rotation curve v_φ as function of the radius r and the polar angle at t=3 for model R2. Units are the same of Fig. 5.10d .
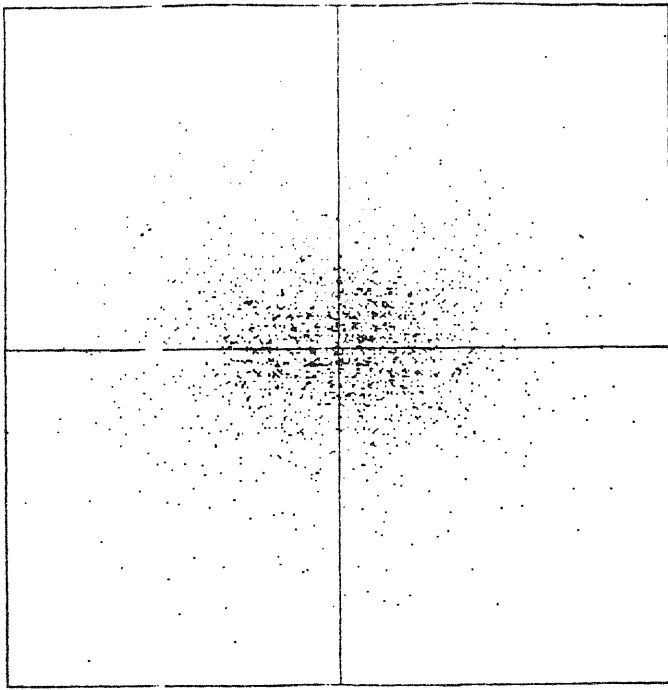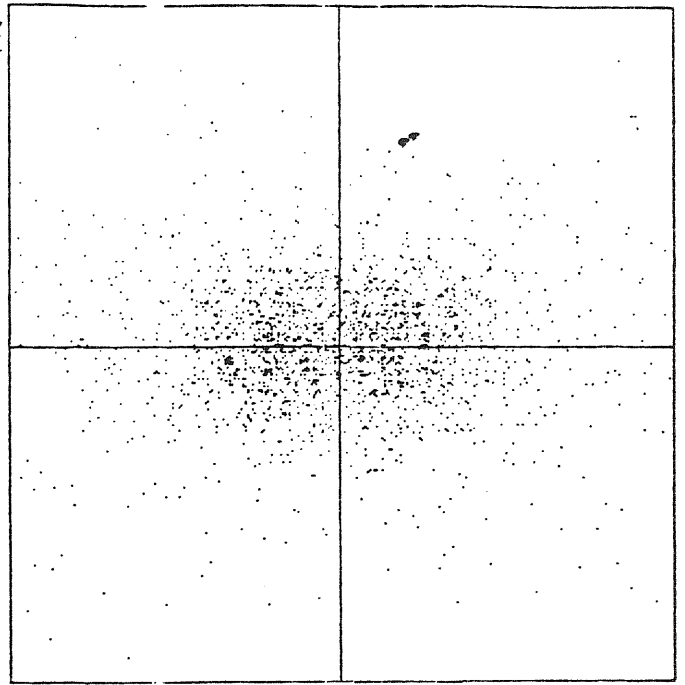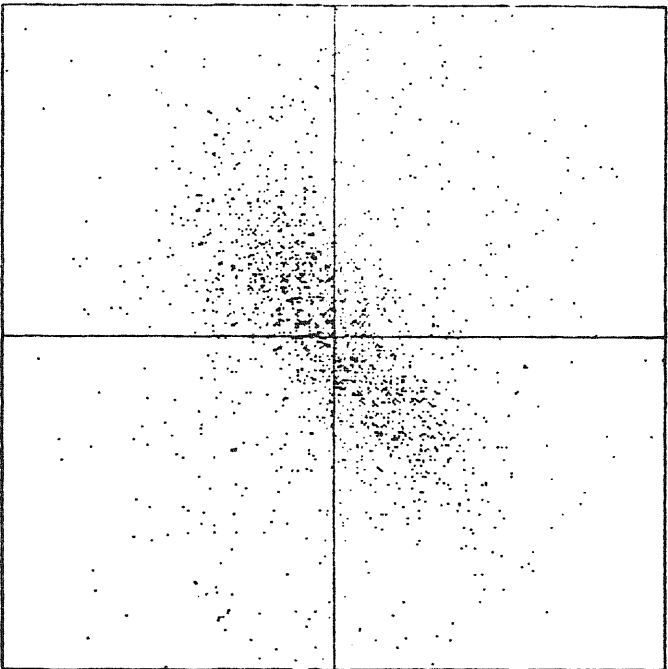
Fig. 5.18   Particle plots for model R6 in the x-y,x-z,y-z planes at t=3. The box size
is 32 Kpc.
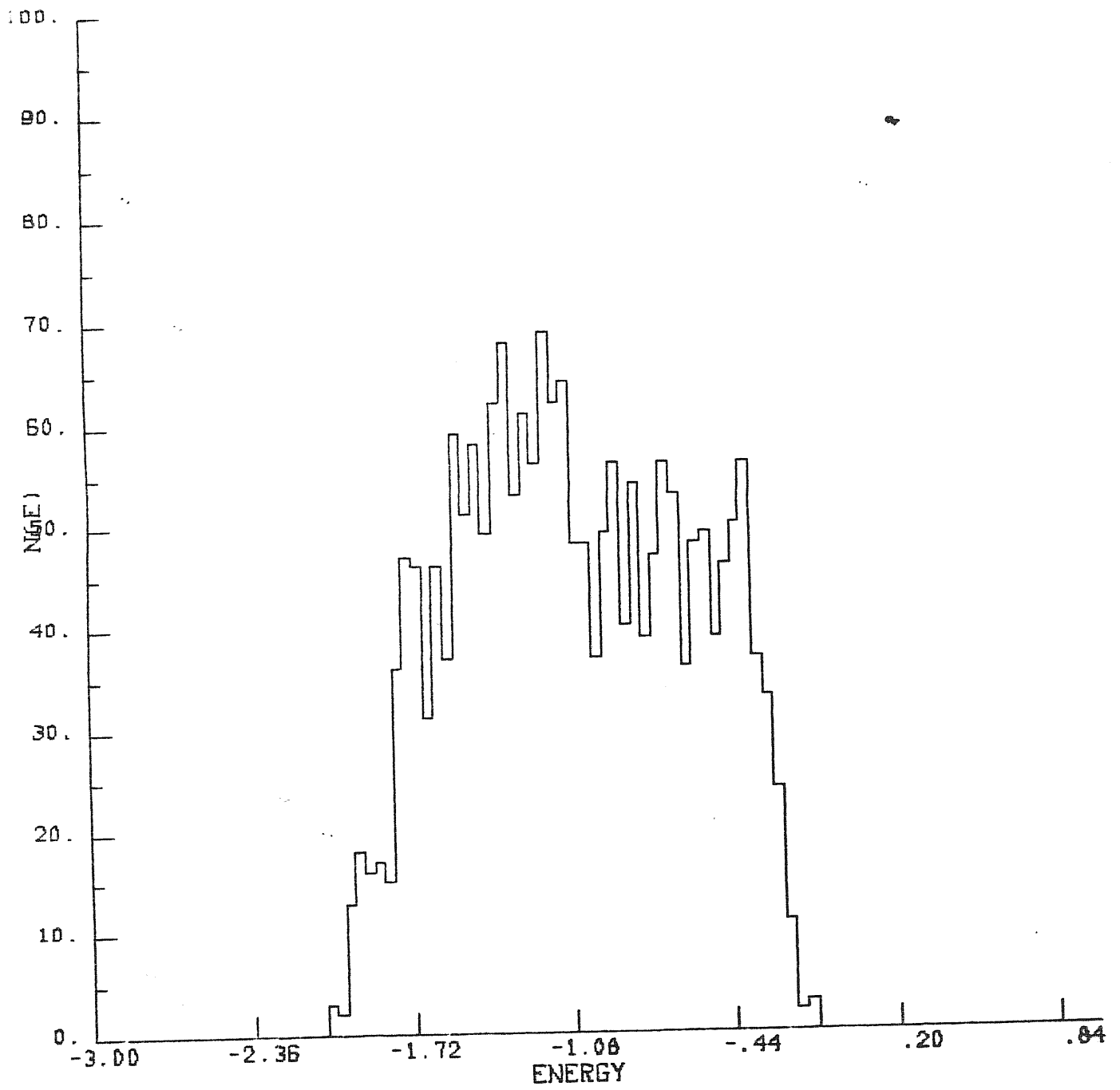
Fig. 5.19   Final energy histogram for model R6 at t=3. Units are the same of Fig.5.4a.
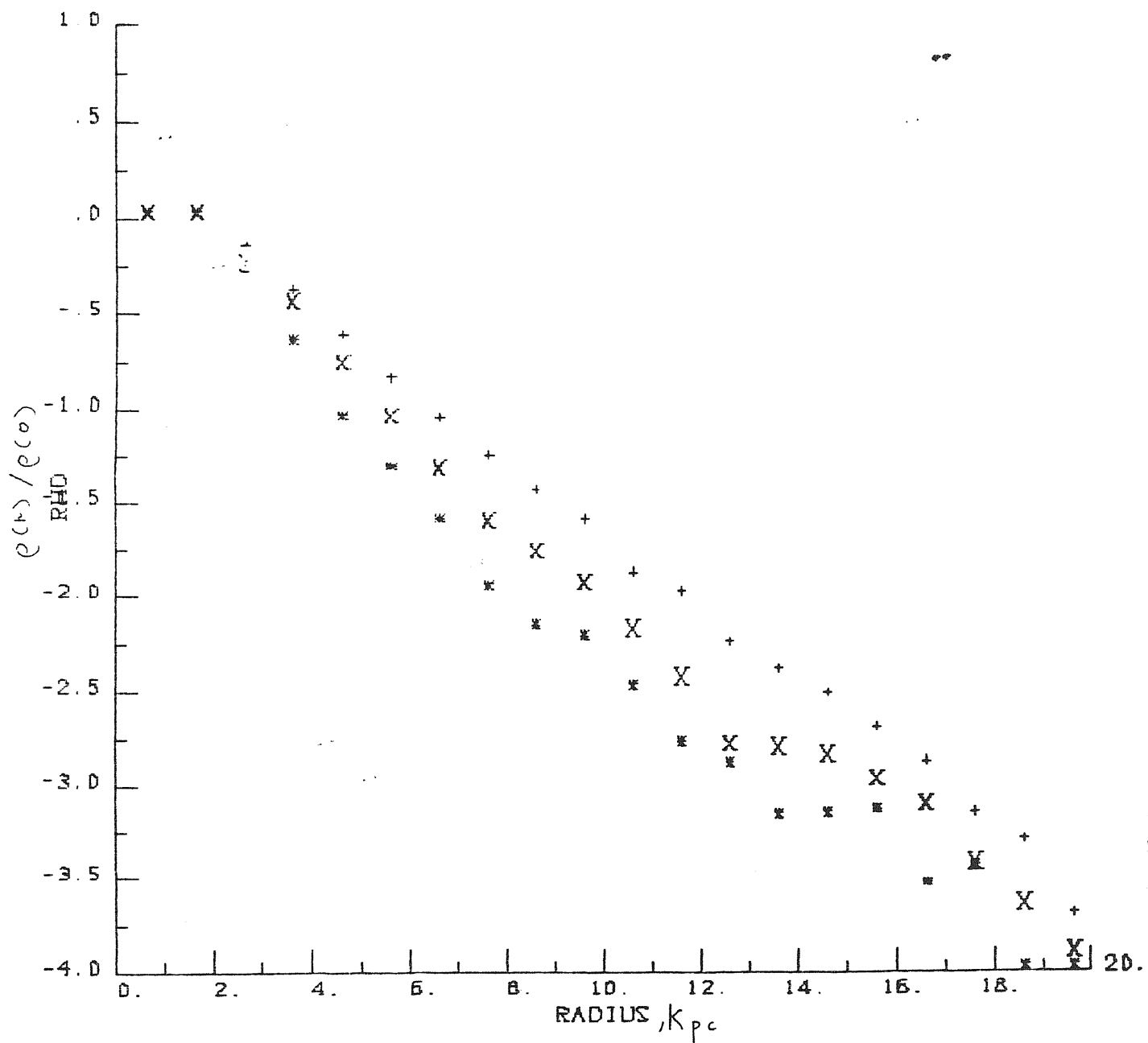
Fig. 5.20a The same as for Fig.5.17a, expect for model R6
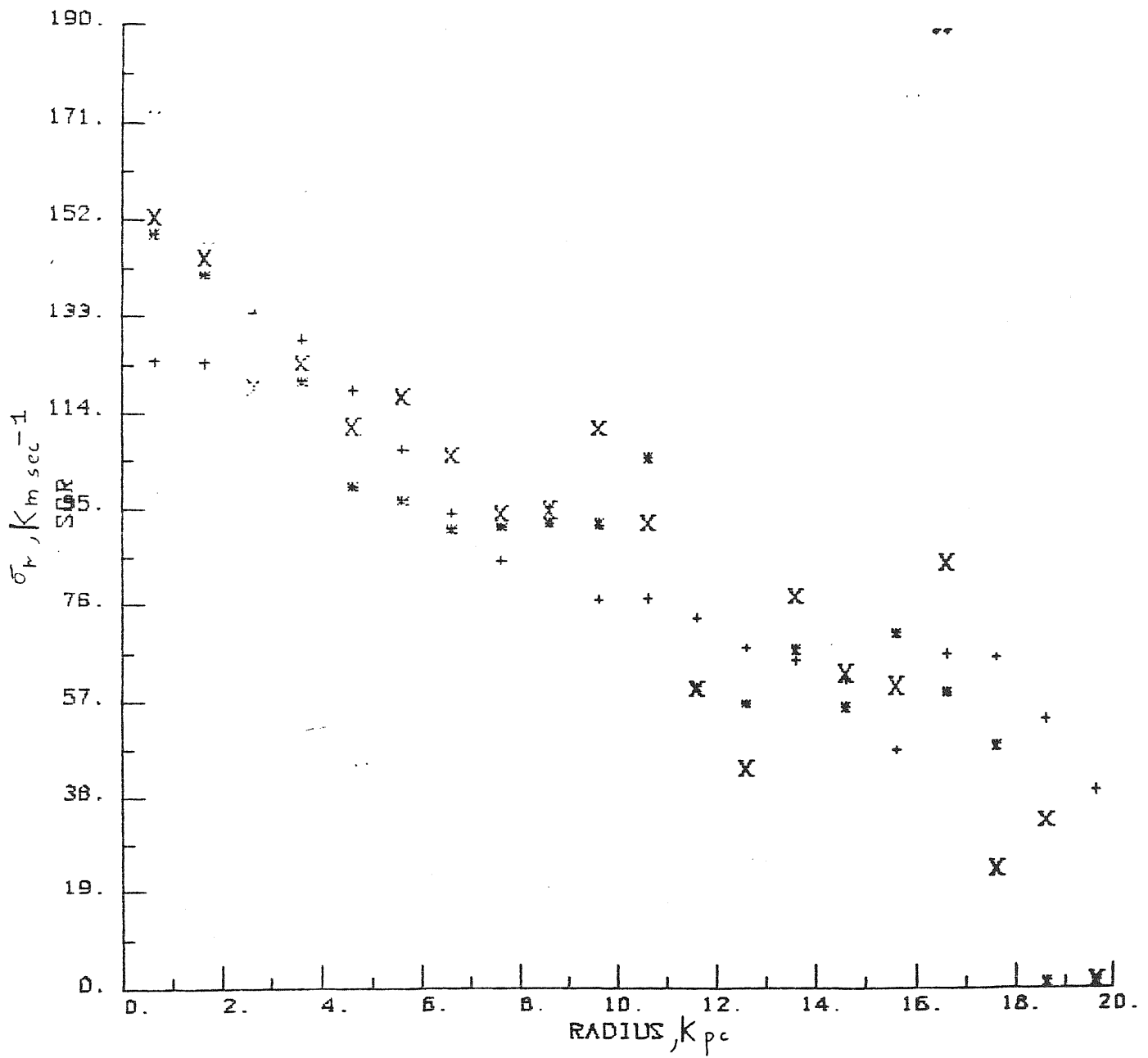
Fig. 5.20b   The same as for Fig.5.17b, expect for model R6.
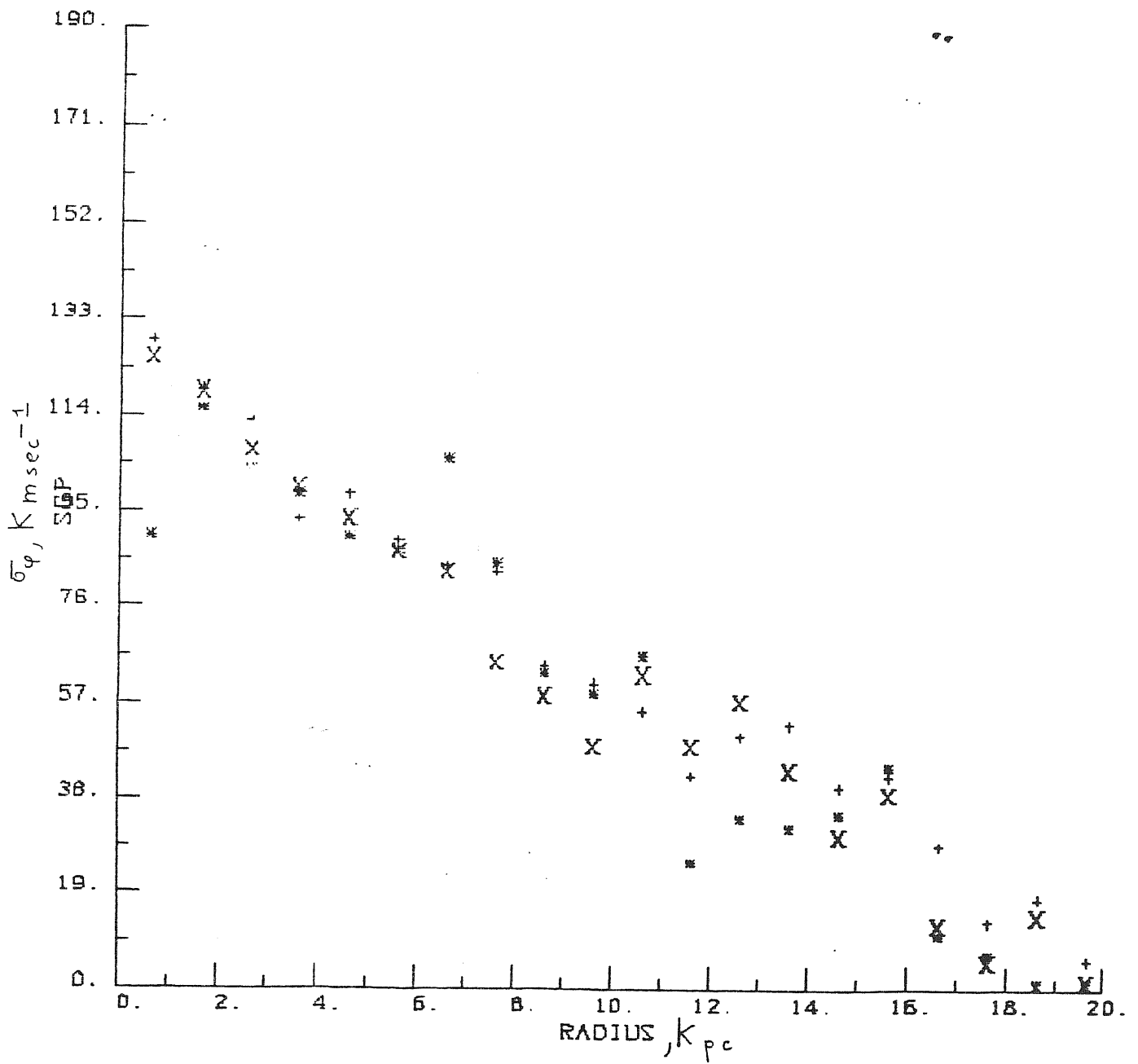
Fig. 5.20c   The same as for Fig.5.17c, expect for model R6 .
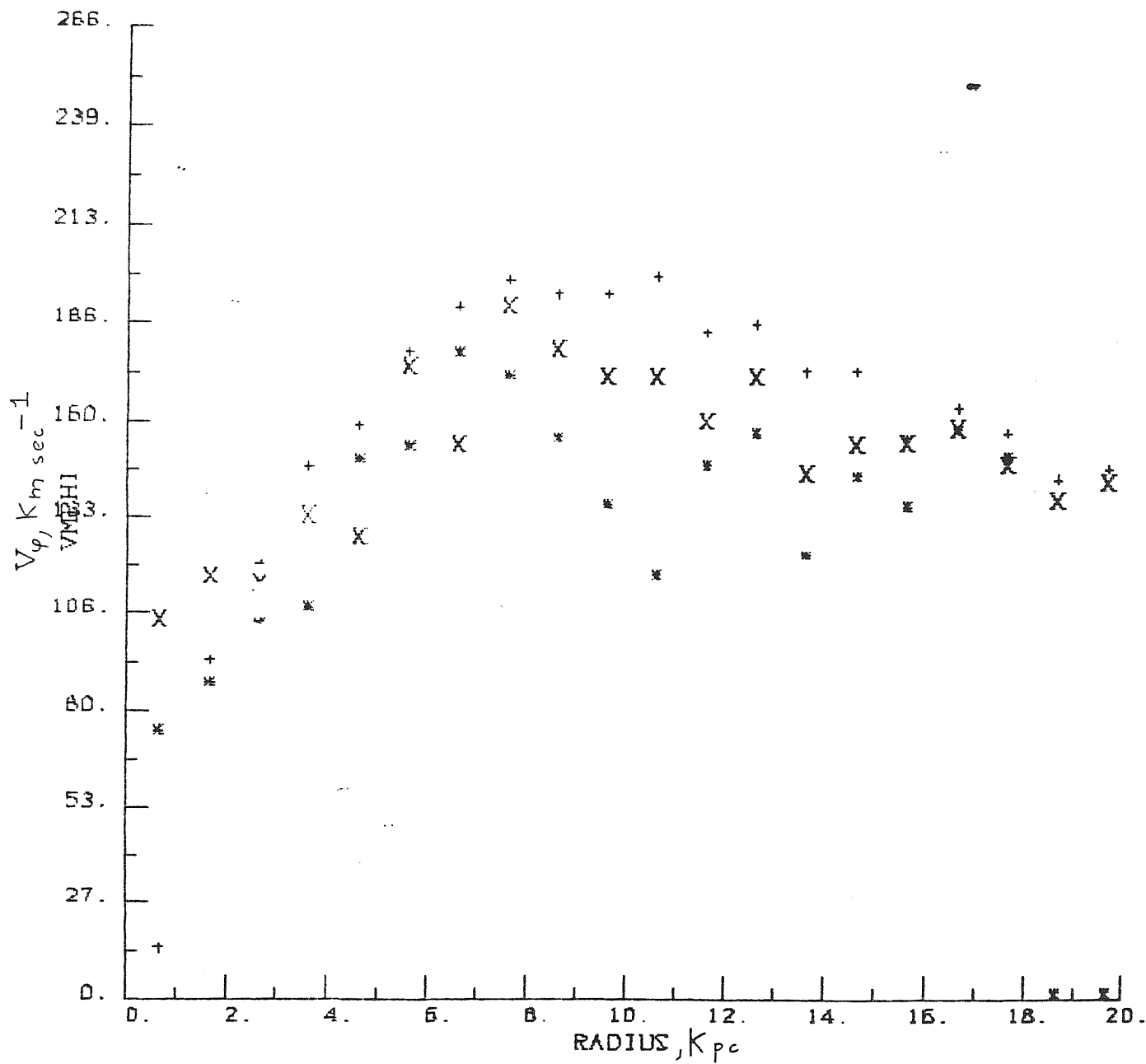
Fig. 5.20d   The same as for Fig.5.17d, expect for model R6 .

densities which would give rise to collapse and to the break-up of the system into several pieces.

This is not seen and a bar is even formed in the R1 case. The reason is that in models R (and also in G5) the field calculation has been changed (see eq.(5.24)).

c) N-body simulations for the collapse of an elliptical galaxy in the presence of a dark halo

The numerical integration for the collapse of a non-dissipative rotating system has finally been done in the presence of a dark halo.

The halo was not simulated by a fixed external potential but it has been left free to evolve in time under the action of its forces and those of the visible components.

Unfortunately at the moment of writing the thesis we have been able to perform only one integration of this kind (typically such a integration takes about 15 hrs of CPU time at the I.S.A.S. computer Gould MPX 32 3.2A, which has a computational speed of about $1 \text{Mfpsec}^{-1} = 10^6$ floating point operations per second).

The initial conditions for this integration are shown in Table III (for the sake of clarity we label as 'baryonic' the matter component in our simulation which is more concentrated and rotating with respect to the 'dark' component, however both of them behave in a collisionless way in

TABLE III

	R_I [a]	M [b]	R_I' [c]	α_r [d]	α_v [e]	N [f]	$T_r/|W|$ [g]	$T_c/|W|$ [h]
Dark matter	20	$1.8 \ 10^{12}$	16	0.1	0.33	$5.76 \ 10^4$	0.19	$2.5 \ 10^{-3}$
Baryons	10	2.10^{11}	8	0.866	0.2083	$6.4 \ 10^3$	$2.5 \ 10^{-3}$	5.10^{-3}

a) Initial radius in Kpc

b) Total mass in solar units

c) Initial radius in grid length units

d) Initial angular velocity in units of $\left(G \, M_{D,B} / R_{I_{D,B}}^3 \right)^{1/2}$

e) Cut-off velocity for the peculiar velocity distribution in units of $\left(G \, M_{D,B} / R_{I_{D,B}} \right)^{1/2}$

f) Number of particles used in the simulation

g) Initial ratio of the random kinetic energy to the total gravitational energy

h) Initial ratio of the rotational kinetic energy to the total potential energy

our simulation).

The initial conditions for the baryonic component are the same as in model R6

(the value of α_{r_β} is somewhat larger than the upper limit in eq.(5.7),

however the uncertainties in the theory allow us to take such a value).

The dark component has about the same initial $(T_r / |W| , T_c / |W|)$

ratios as model G3 and is 'dinamically' equivalent to it.

Fig.s 5.21,5.22 show the particle distributions in the x-y,x-z,y-z planes

for the baryonic and dark components (these particles have been chosen

with the same criterion used in the G models).

From Fig.5.22b it can be seen that at t=3 (time is in units of t_c =

$2\pi (R^3_{I_\beta} / G M_\beta)^{1/2}$) the bar mode is absent in the simulation, as

expected owing to the presence of the dark halo; it must be noted that

the halo is not bulge-like as in Hohl (1978) but has a radial extension

of the same order as the rotating component.

In Fig.s5.23 the stellar energy distribution is shown for the 'dark' par-

ticles. Fig.5.23a (t=2) is similar to Fig.5.23b (t=3) showing that

the dark component has achieved a steady-state by t=2. The two component

(core +halo) structure is characteristic of a collisonless non rotating

stellar system which has undergone violent relaxation.

These figures show also that the 'dark' particles have an energy distribution

with an extended tail toward low energies (see also Fig.s 5.5 for model

G3), this is due to the presence of the baryonic particles at the center

of the system, which increases the depth of the gravitational potential well

with respect the case where the baryonic component is absent.

In Fig.s 5.24 the stellar energy distribution is shown for the baryonic

particles.

These figures show that: a) at the beginning of the collapse the baryonic

particle quickly settle down to the low-energy staes fixed by the depth

of the dark matter potential wells (Fig.5.24a,t=0; Fig.5.24b,t=0.2);

b) the collapse of the dark halo produces an increases of the particle

velocities(Fig.5.24b; Fig.5.24c,t=0.4; see also Fig.5.25,5.26); c)

the baryonic component reaches a steady-state at t=2 (Fig.5.24c; Fig.

5.24D, t=2; Fig.5.24d, t=3).

The time evolution of the $\left(\frac{T_r}{|W|} , \frac{T_c}{|W|} \right)$ ratios is shown in Fig.s 5.25,5.26

for the dark and baryonic components.The characteristics of the time evo-

lution for the $T_r/|W|$ ratio have already been discussed for model G3.

Let us stress an interesting point: from Fig.5.26 there would seem to be

a secular conversion of rotational into random kinetic energy, this happens

at a very slow rate with respect to model G5 (Fig.5.12c) but it is

equally present. Of course the initial ratio $T_c/|W|$ for the baryonic

component satisfies the Ostriker and Peebles (1973) criterion and

the bar mode is absent in our simulation, however Fig.5.26 suggests that

in the integration there is a flow of angular momentum towards outer re-

gions on time scales comparable to the Hubble age ($H_o^{-1} \simeq 40$ in t_c units).

The behaviour of the mass density versus radius is shown in Fig.s 5.27a,b

at t=3 for the dark and baryonic components, these figures have been

calculated in the same manner as those of the G models.

From Fig.5.27b it can be   seen (and also from Fig.5.22b) that the bulk

of the baryonic matter in our simulation has collapsed to an unrealistic

final radius of the order of 4 Kpc (corresponding in Fig.5.27b to a

change in the slope of $\rho_b(r)$).

For the dark component the radial fall off is much more softer and is

$\rho_b(r) \propto r^{-3}$ between r=5 Kpc and r= 14 Kpc.

The behaviour of the velocity dispersions for the two matter components

is not shown here, since the collapse of the baryonic component at so

small radii has led to unphysical values for the central velocity dispersions.

These results show that in an integration of this kind a full range of

possible initial conditions (highest value of the $T_r/|w|$ ratio with

respect to the one considered here, highly inhomogeneous initial mass

distributions (Van Albada 1982), sheet-like initial configurations

(Aarseth and Binney 1978)) must be explored before we are able to find

those which produce realistic final configurations for the visible galaxy.

However the results of the integration stress a point already pointed out
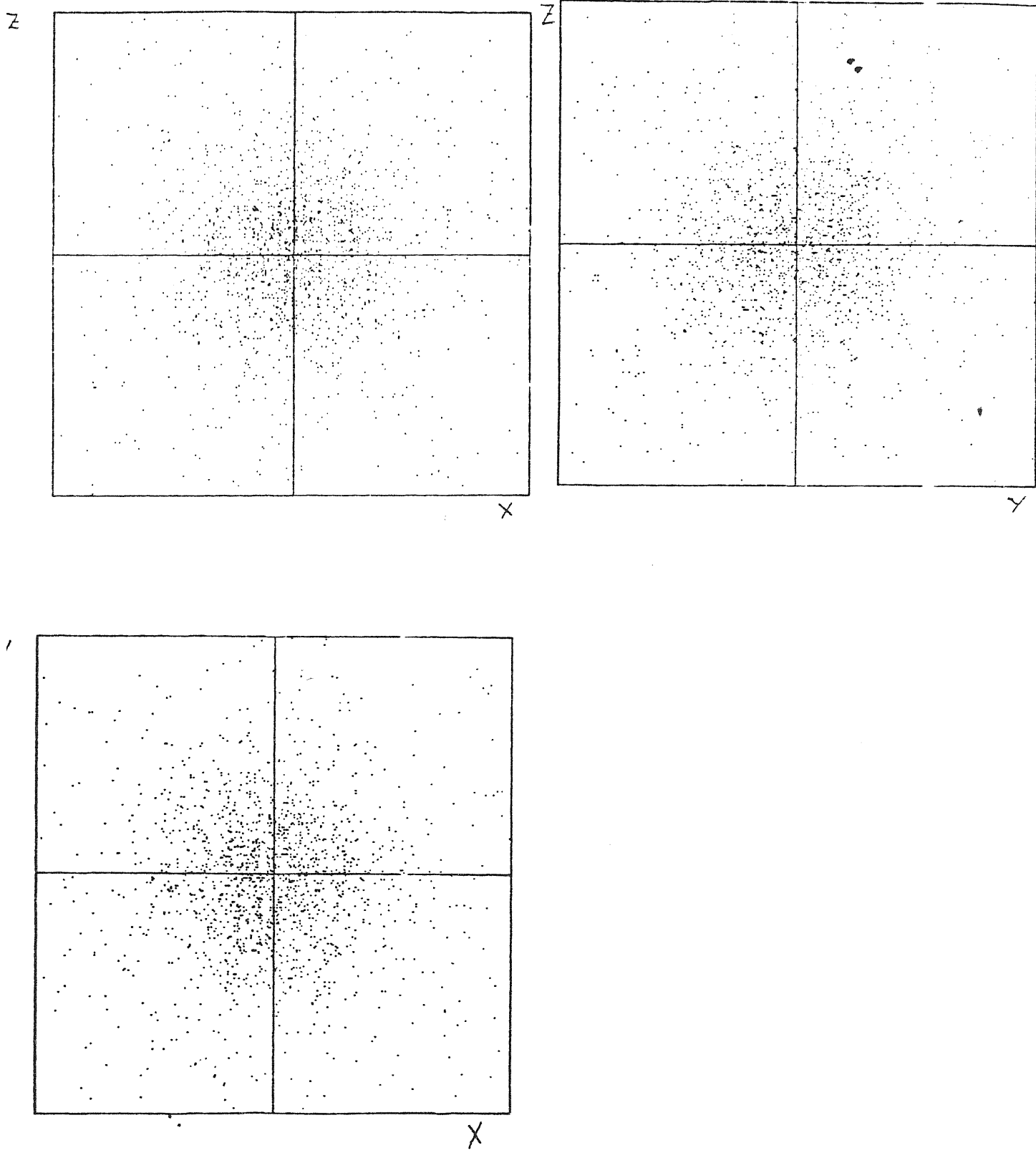
Fig. 5.21a Particle plots for the 'dark' particles in the x-y,x-z,y-z planes at t=2.
Time is in units of $t_c = 2\pi \left(R_{I_B}^3 / G M_B \right)^{-1/2}$. The box size is 32 Kpc.
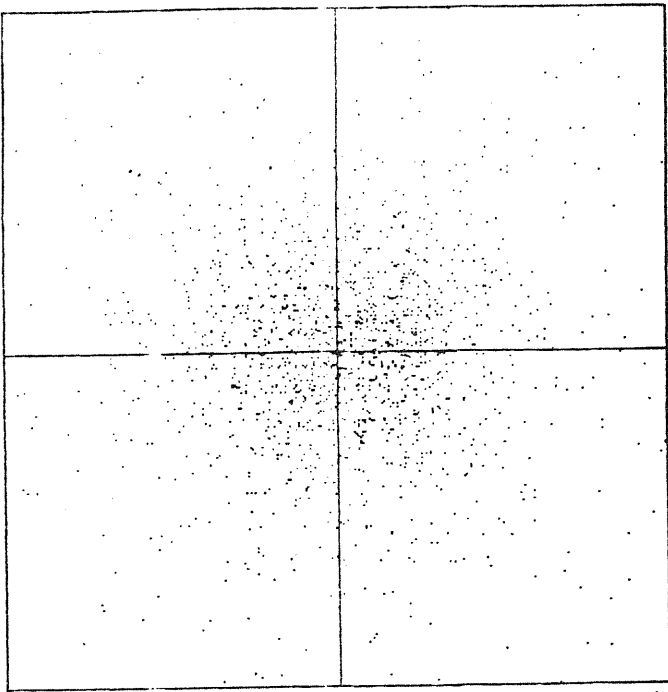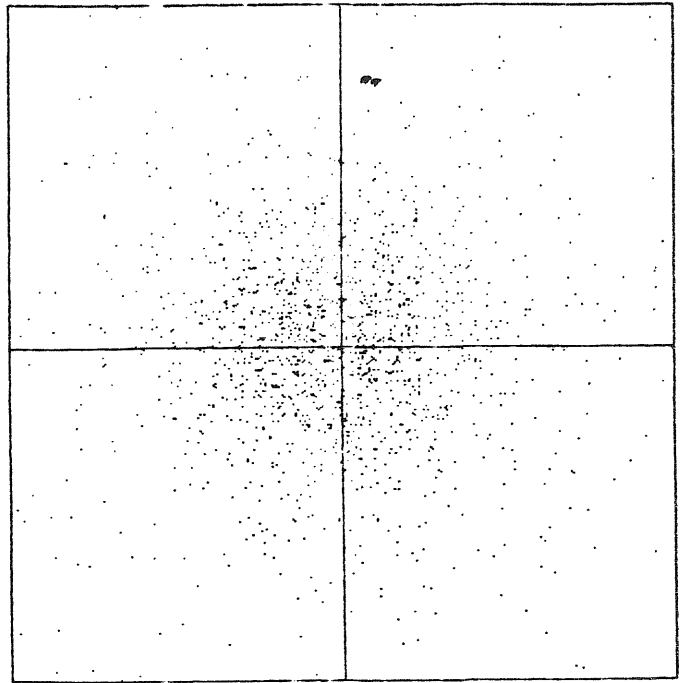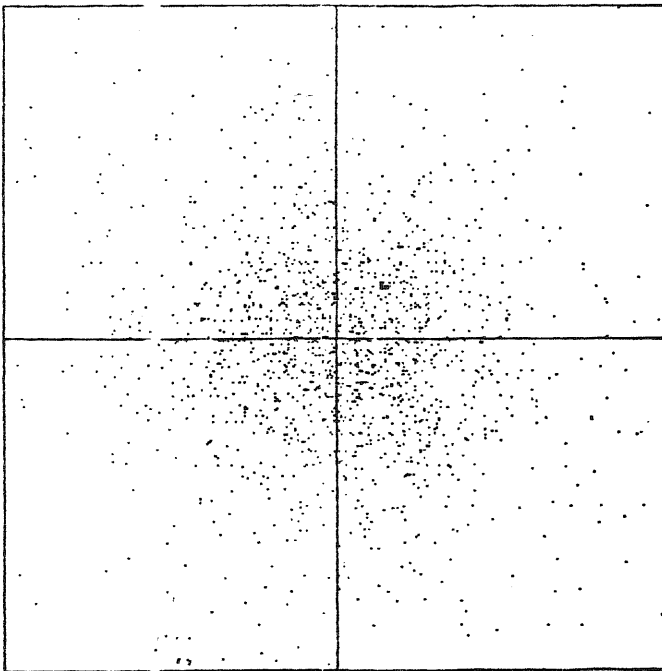
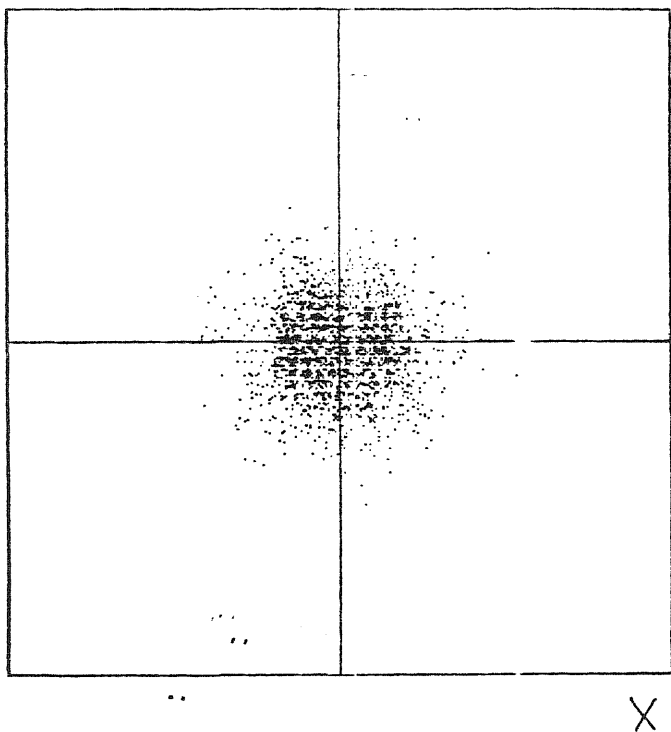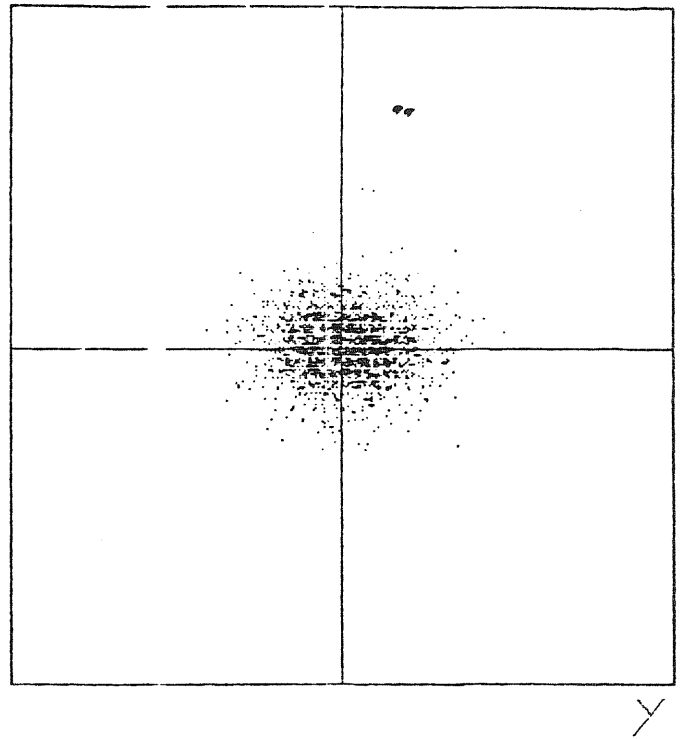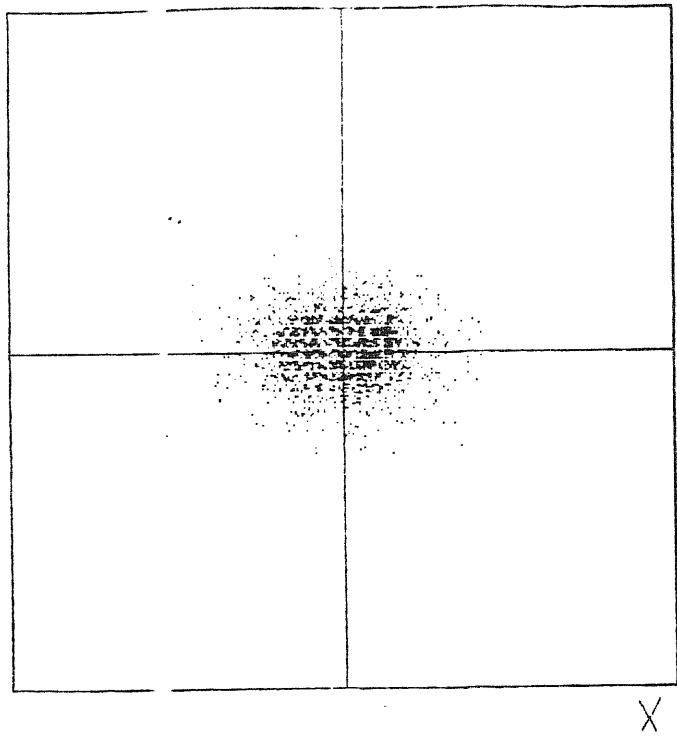Fig. 5.21b   The same as for fig.5.21a, expect for t=3.

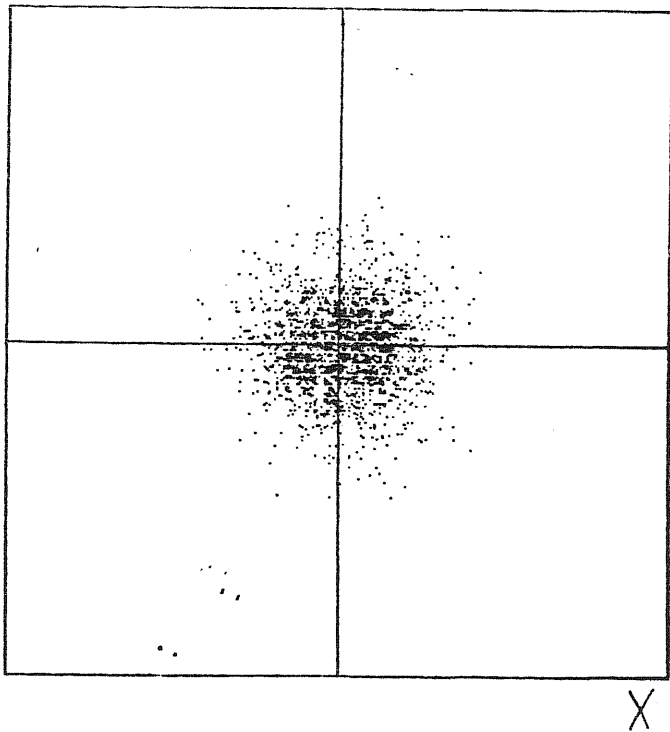**Fig. 5.22a** Particles plots for the 'baryonic' particles in the x-y,x-z,y-z planes at t=2. Units are the same of Fig.5.21a .
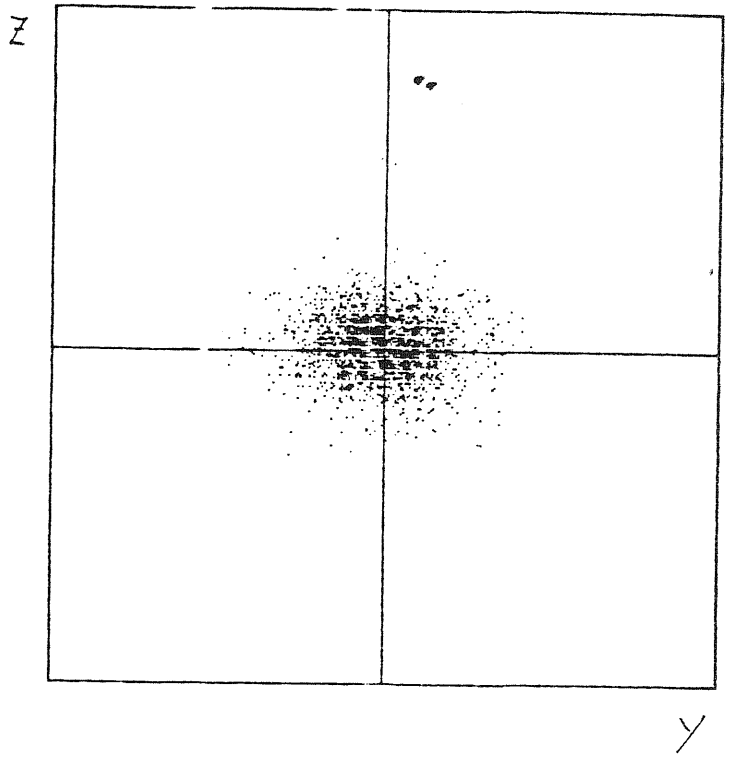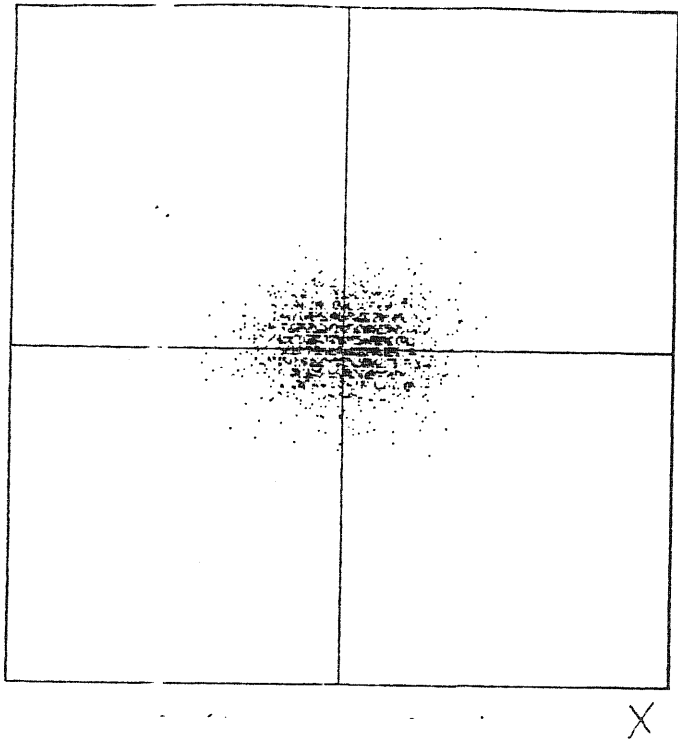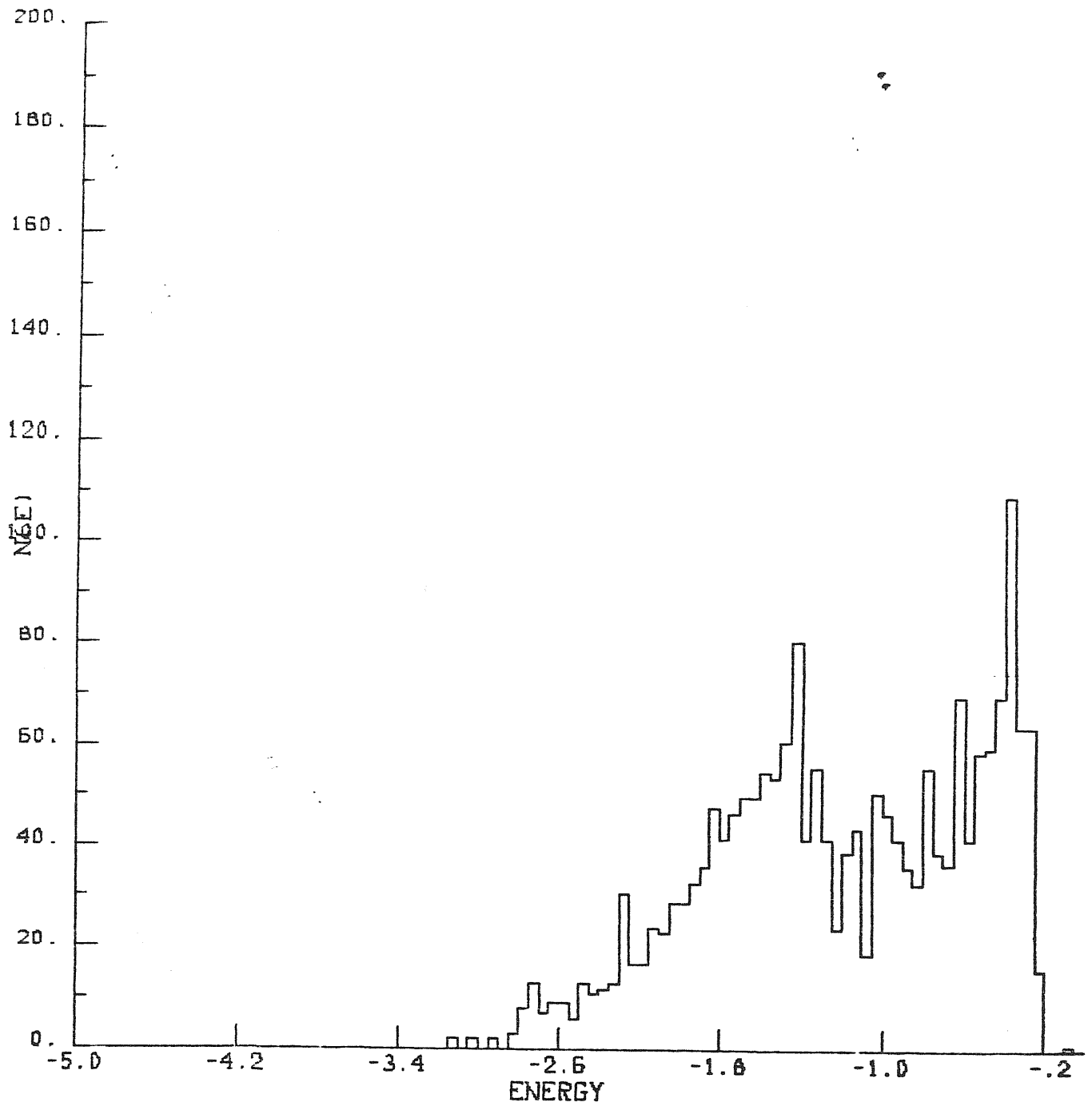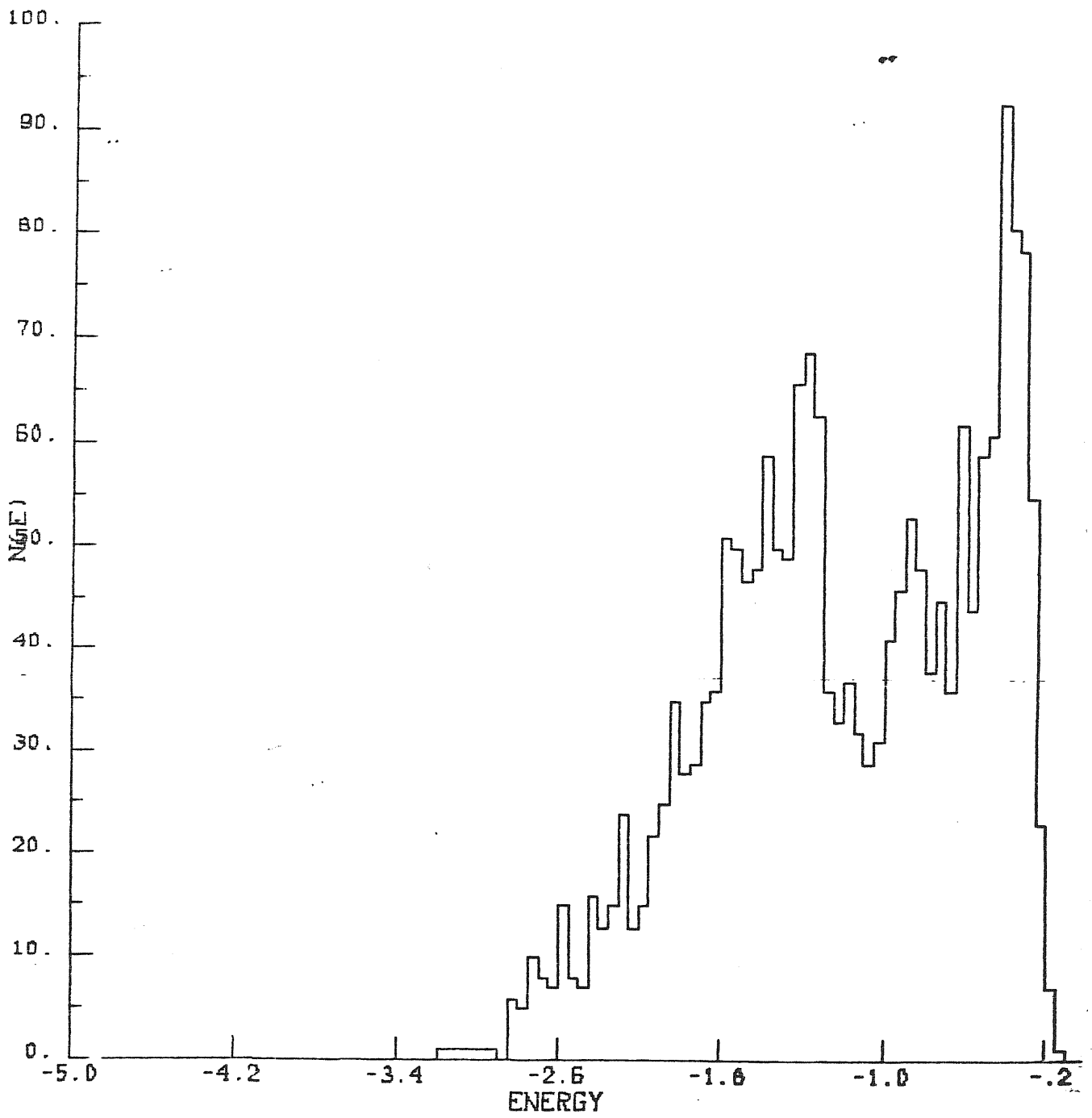
Fig. 5.22b   the same as for Fig.5.22a, expect for t=3.

<u>Fig. 5.23a</u>   .Energy histograms for the 'dark' particles at t=2 (time units are the same of Fig.5.21a). The abscissa are stellar energies in units of $G(M_D + M_B)/R_{I_D}$ R_{I_D} is the initial radius for the 'dark' particles. The ordinate is the number of particles in the energy interval of width $0.05\,G(M_D + M_B)/R_{I_D}$.

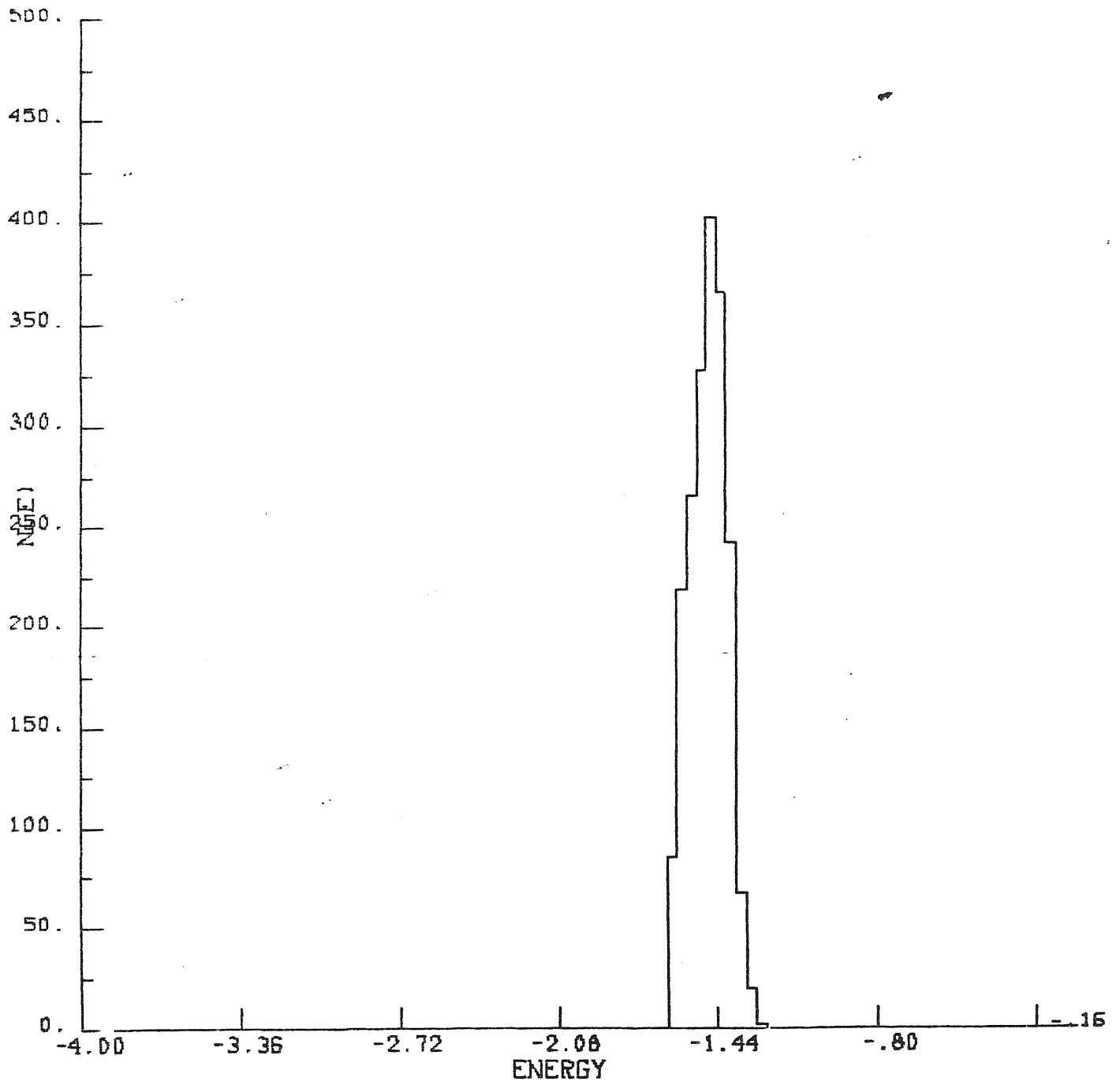Fig. 5.23b   The same as for Fig.5.23a, expect for t=3.

Fig. 5.24a   Energy histograms for the 'baryonic' particles at t=0. Units are the same of Fig. 5.23a .
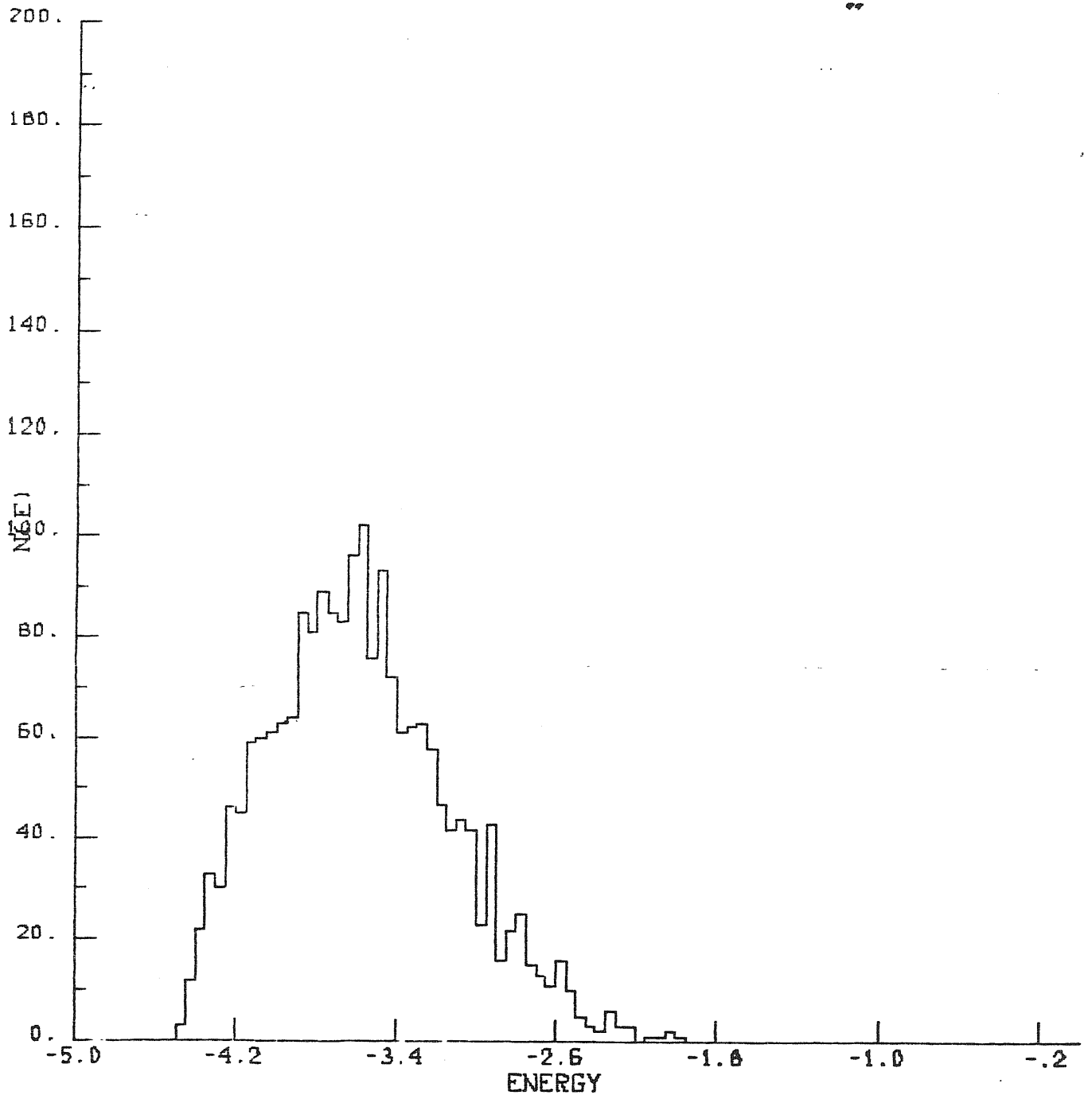
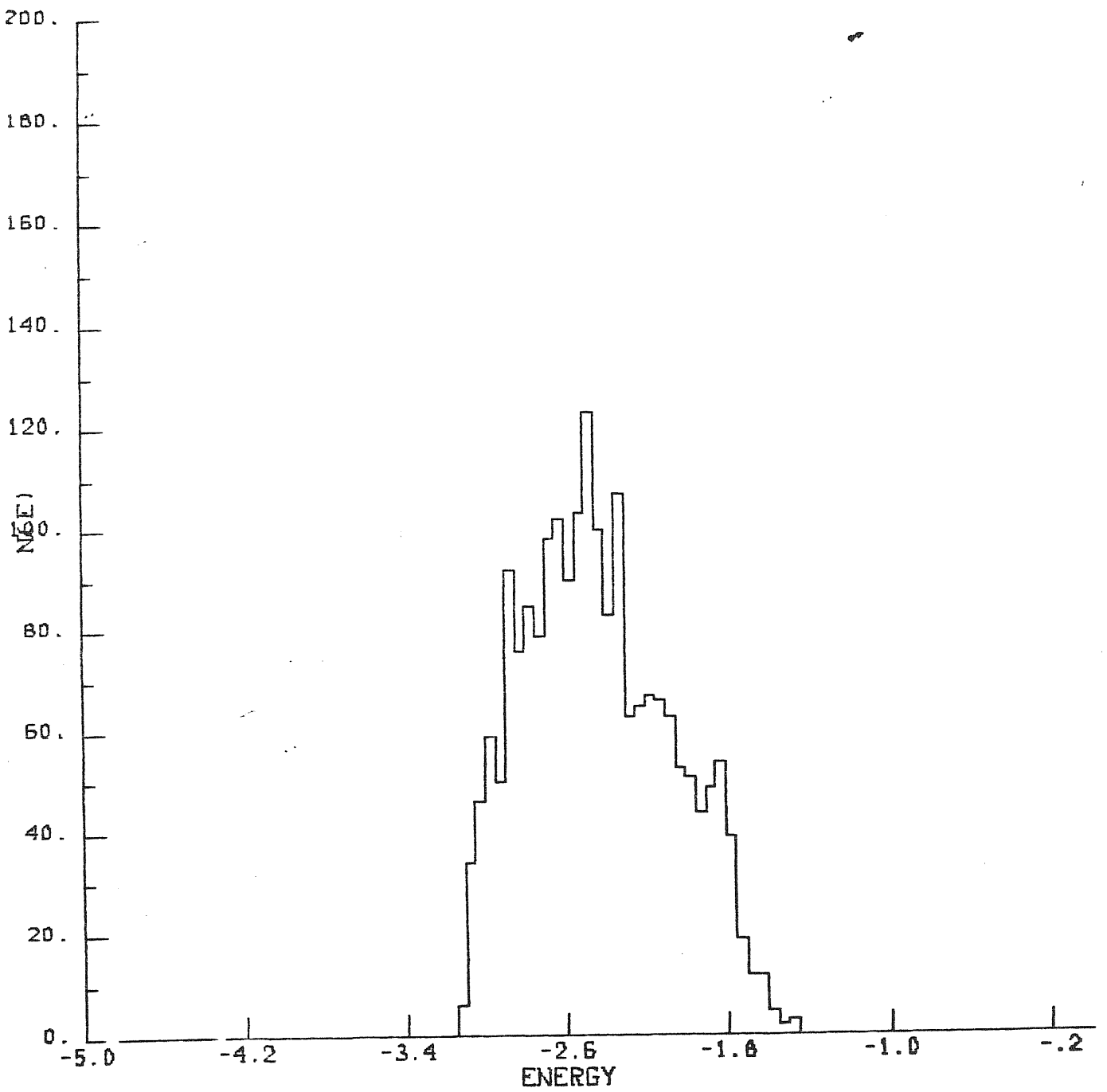Fig. 5.24b   The same as for Fig. 5.24a, expect for t=0.2 .

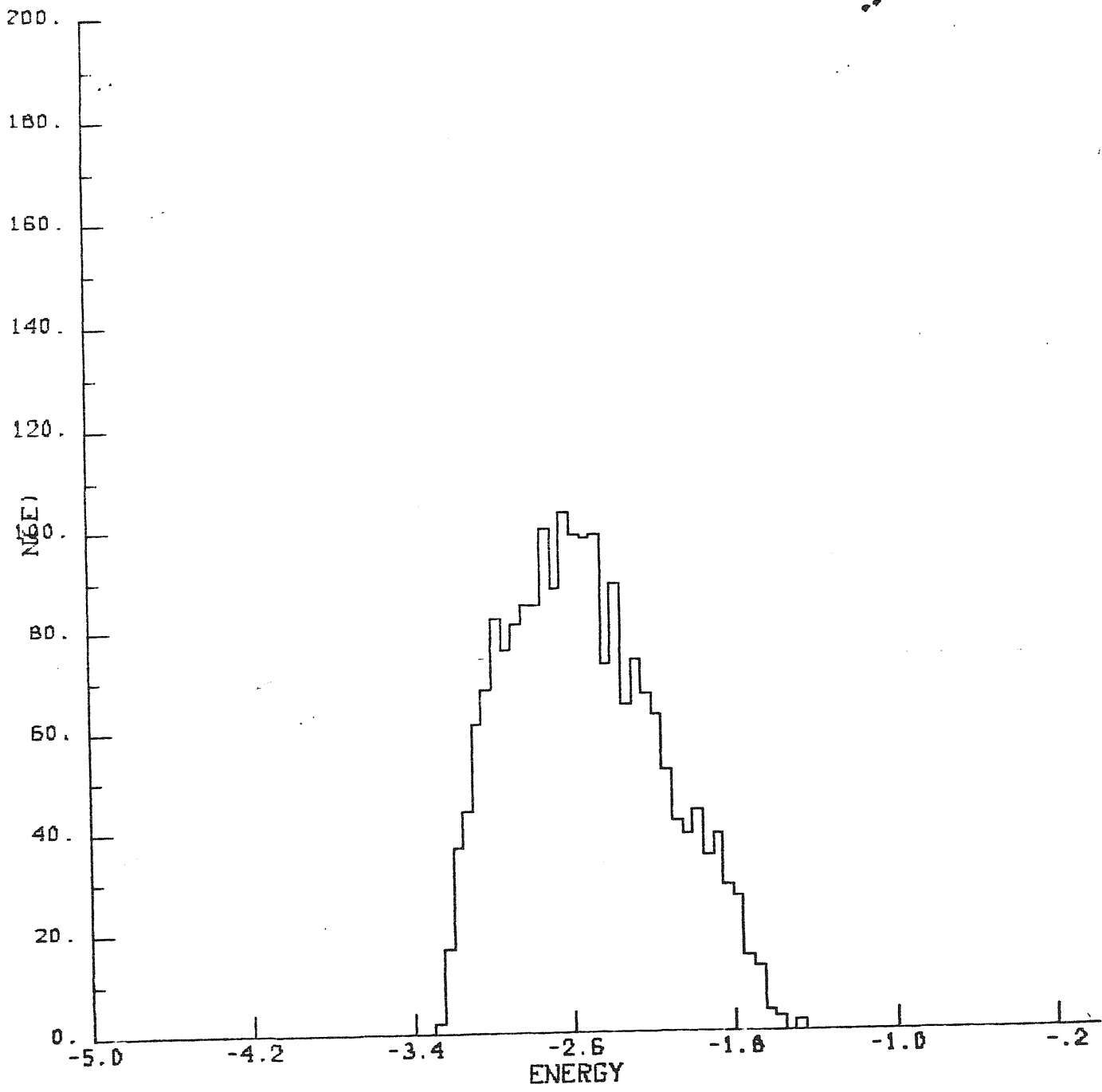**Fig. 5.24c**   The same as for Fig.5.24a, expect for t=0.4   .

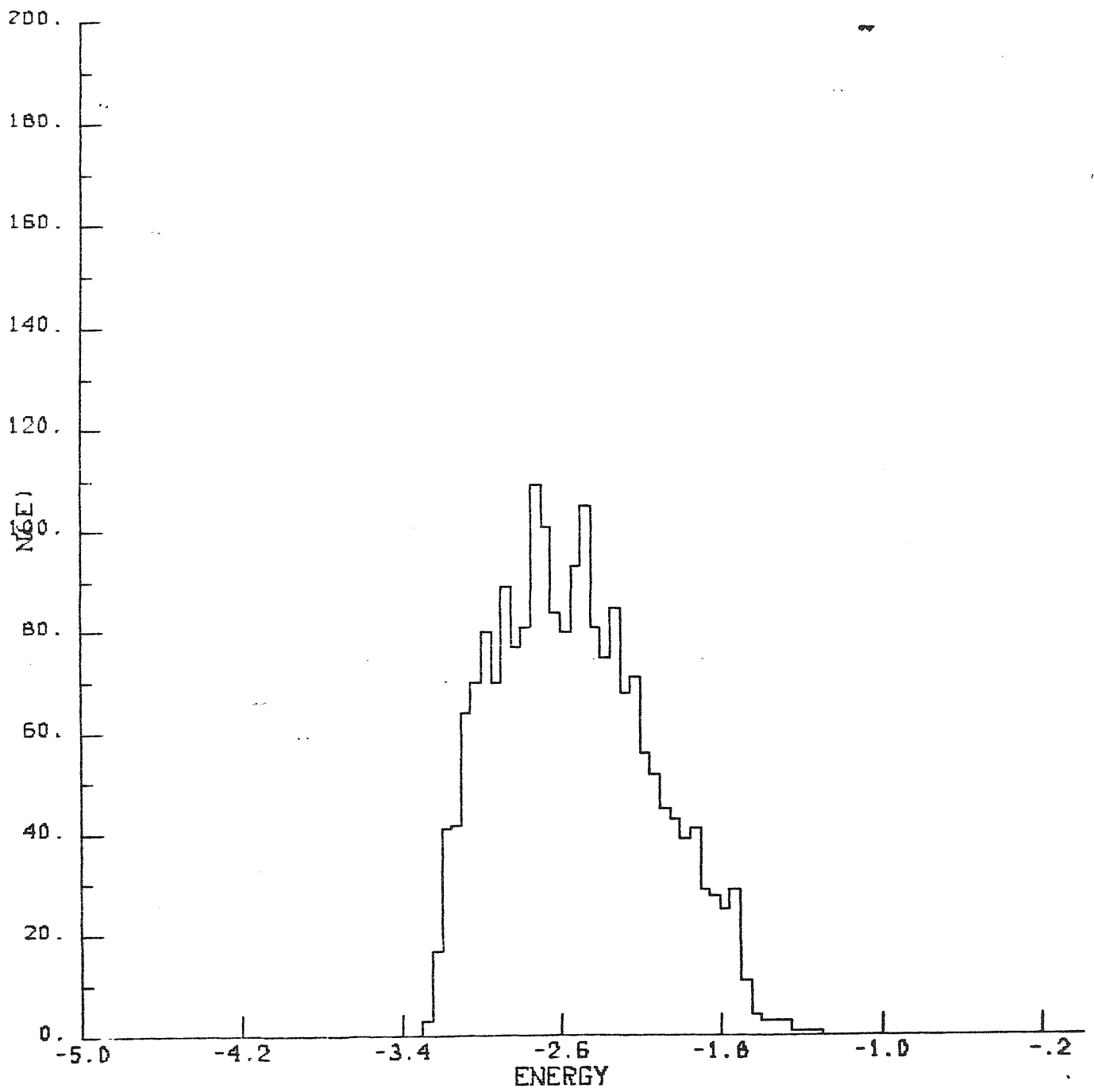Fig. 5.24d   The same as for Fig. 5.24a, expect for t=2.

Fig.5.24e   The same as for Fig. 5.24a, expect for t= 3.
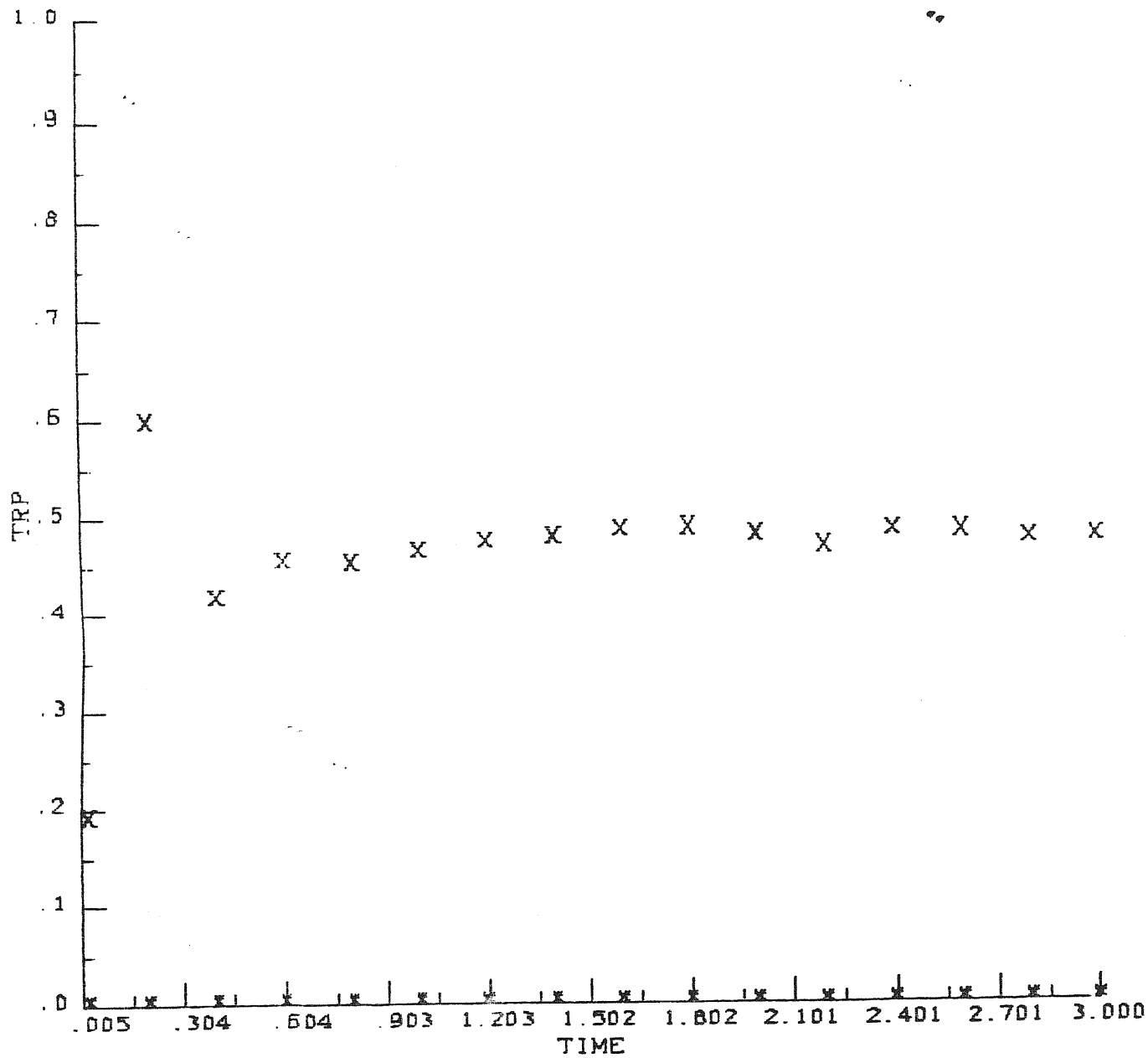
Fig. 5.25   Time evolution of the $(T_r/|w|,\ T_c/|w|\ )$ ratios for the 'dark'
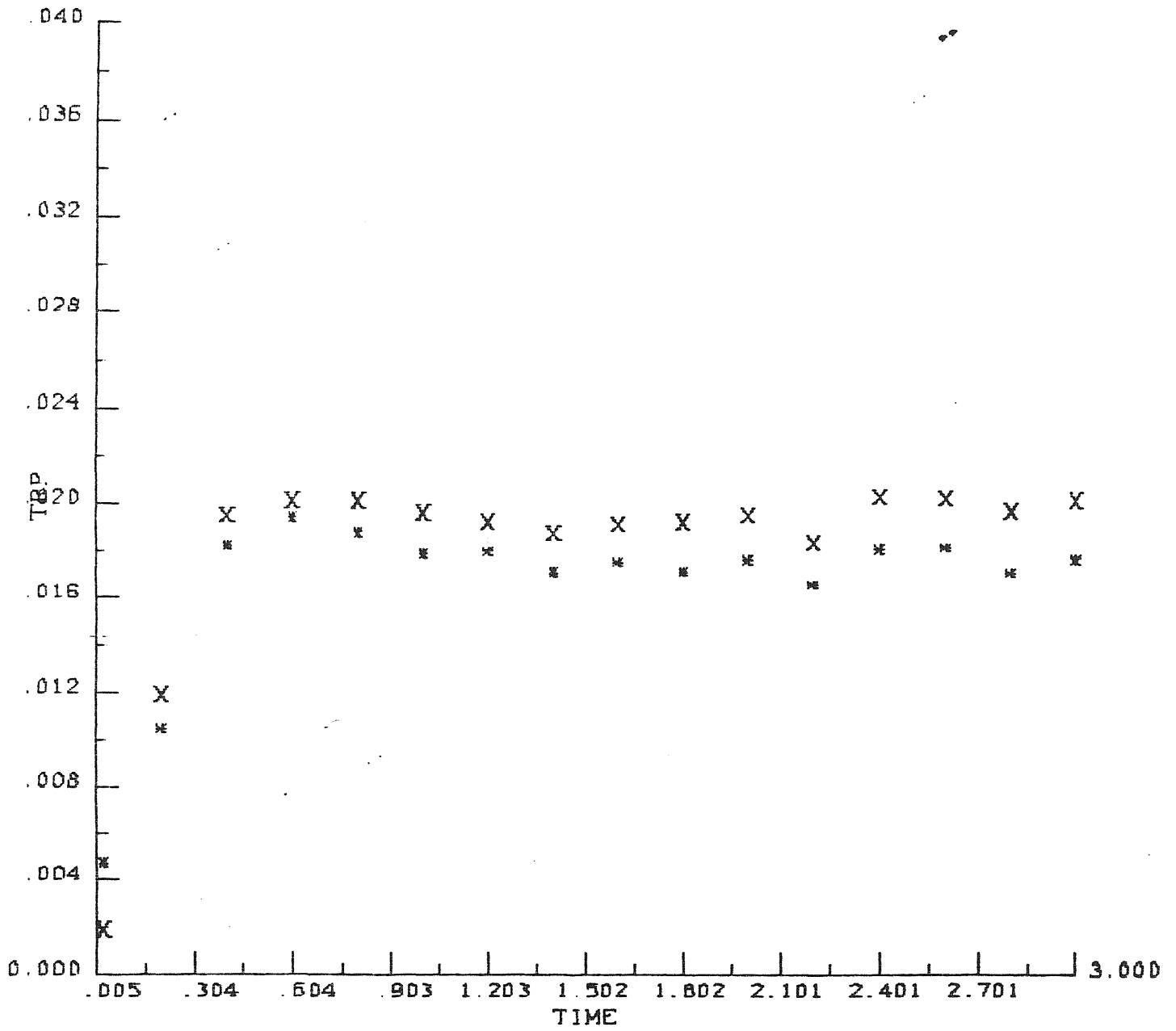particles. Here is $X : T_r/|w|, * : T_c/|w|$. Time is in t_c units.

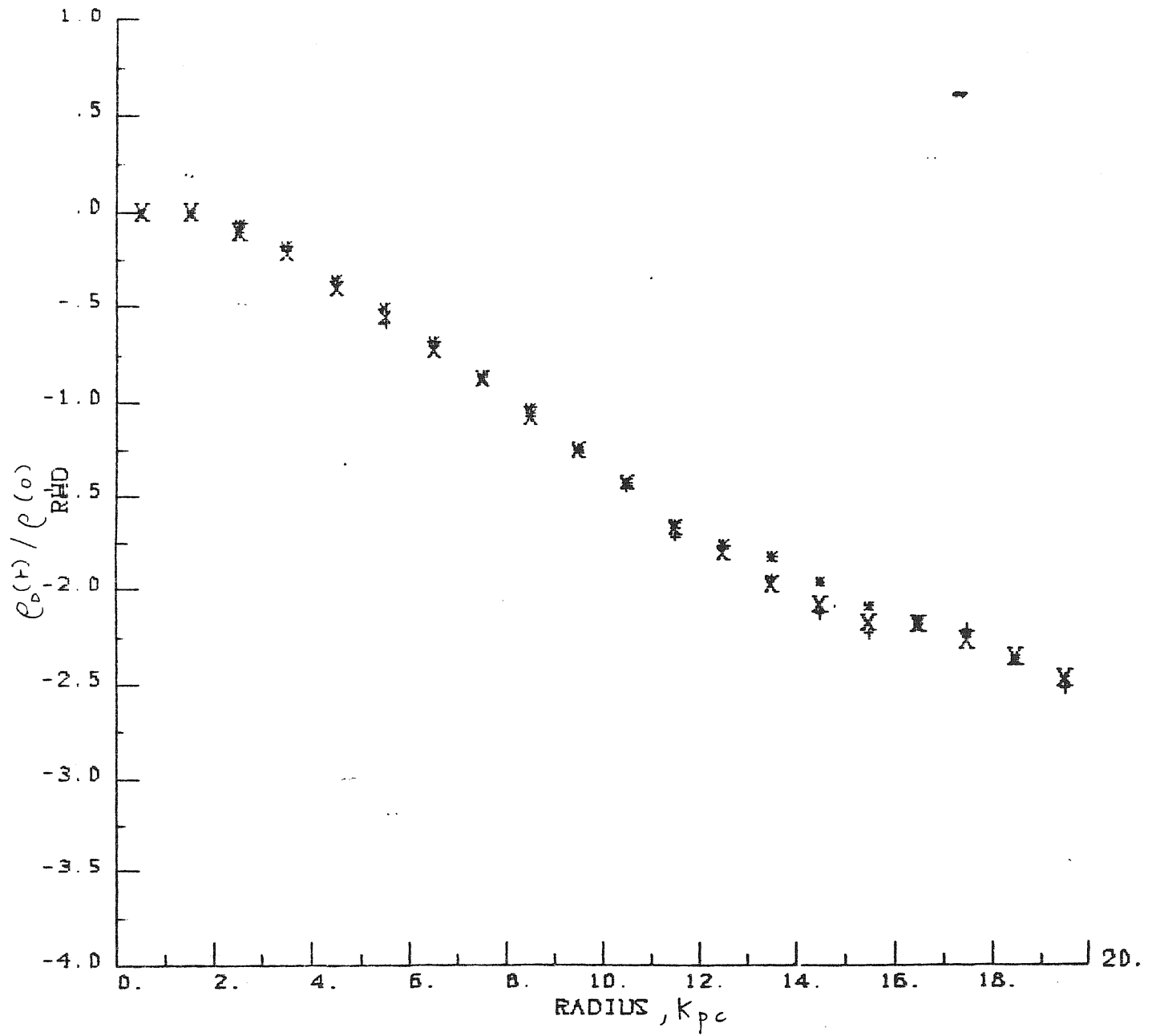Fig. 5.26   The same as for Fig.5.25, but for 'baryonic' particles.

Fig. 5.27a Stellar density $\rho(r)$ as function of the radius r and the polar angle Θ at t=3 for 'dark' particles.

Here is +: Θ =90°, x: Θ =60°, ✳: Θ =45°.
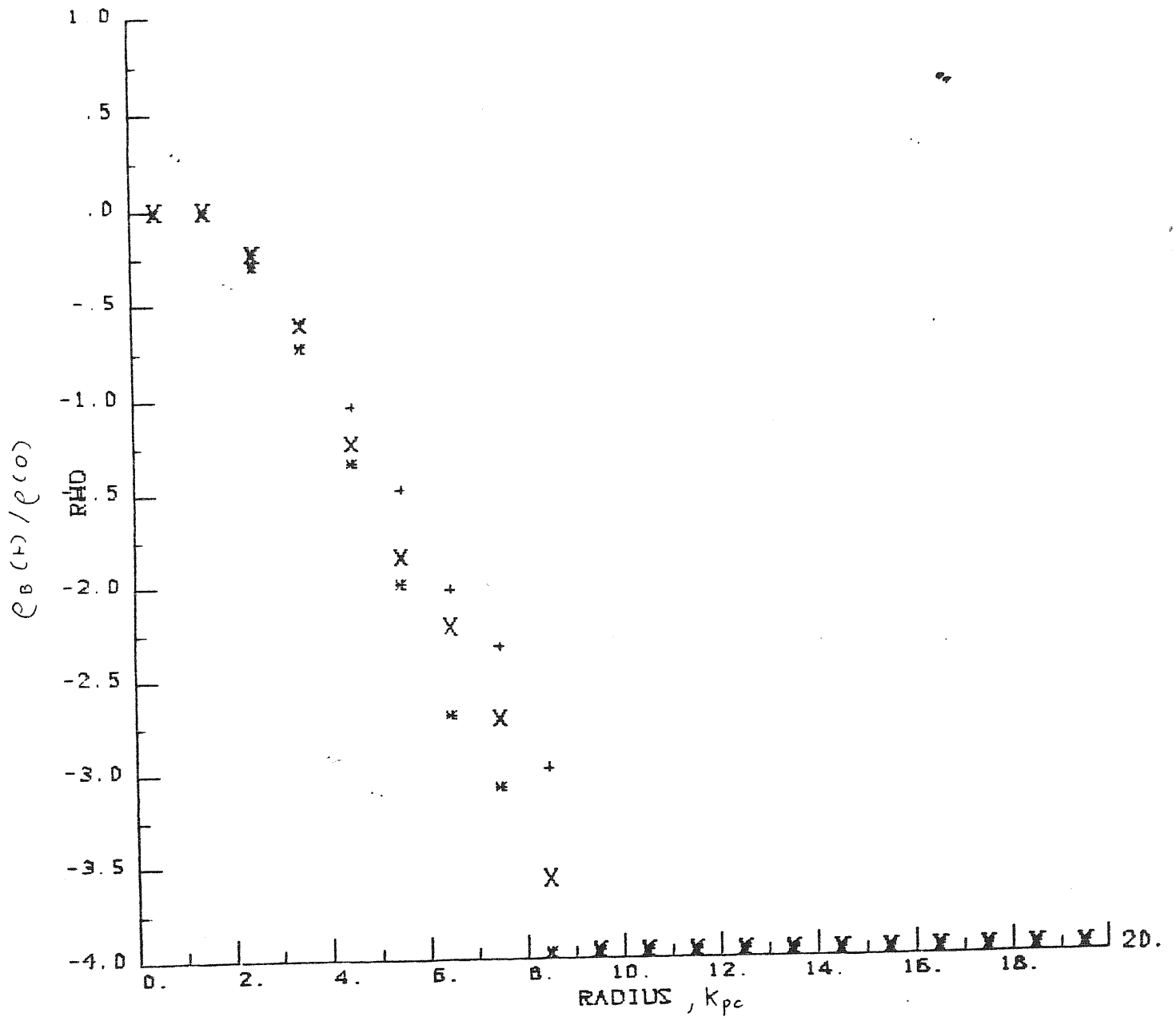
Fig. 5.27b The same as for Fig.5.27a, expect for baryonic particles.

in §IV.2: if elliptical galaxies are embedded in dark haloes, then the

observed mass-to-light ratio for giant elliptical galaxies at the

De Vaucoulers radius ($M/L_B \simeq$ 10h at $r_e \simeq 8h^{-1}$Kpc, see Fig.13 of

Kormendy 1982) which are of the same order as the ones for spiral galaxies

at the Holmberg radius, imply that elliptical galaxies must have   collapsed

by a factor 10 in radius; this does not agree with the observed low

rotation ($\lambda_e \simeq$ 0.07) which suggests that elliptical galaxies must have

collapsed by almost a factor two in radius.

This problem has to be explained by any theory of galaxy formation in the

presence of dark matter.

CONCLUSIONS

After presenting the results of my recent work, I would still like to point

out open questions whose countours are better defined also in the light

of the above outputs.

In the first part of the thesis I have studied the evolution of adiabatic

perturbations in a model gravitationally dominated by two species of colli-

sionless particles, photinos and neutrinos in the range of KeV and tens

of eV, respectively.

One important results which has emerged is that the clustering scale is

strongly sensitive to the value of the primordial spectral index n of the

perturbations. The clustering scale should coincide with the first scale

collapsing and reaching the non-linear regime.

A calculation of the MW background distortion in a photino+neutrino domi-

nated model is still in progress; according to preliminary results the

range of values taken by $\Delta T/T$ shows a strong dependence on the spectral

spectral index n; MW background observations can therefore be used to set

important limits on the fraction of X and ν in such mixture.

Indipendent analysis of the correlation functions and other clustering

data are likely to be produced by non-linear analysis shortly.

On such basis results for $\Delta T/T$ would prove useful tools either in deci-

ding the true nature of dark matter or in putting constraints on the abudan-

ce of massive collisionless quanta.

In chapter III we have seen that the computed small scale MW background

anisotropies are below the present observational limits in a photino-dominated

Universe. This is not the case in neutrino dominated models, unless galaxies

formed in recent epochs ($z \leq 2.5$). If such costraint will turn out to be

too restrictive photino dominated models should to be preferred.

N-body simulations for the collapse of a protogalaxy in the presence of

a dark halo are still a scarsely explored subject.

The natural outcome of chapter V is that numerical experiments for the

collapse of a protogalaxy which span different ranges of angular momenta

(and/or intial mass distributions) would clarify the importance of ini-

tial conditions in deciding, e.g., the final morphological type of the

galaxy.

The analysis of chapter V for low-resolution models outlines a further

interesting point.

Although not fully confirmed, dark matter might be present over dwarf gala-

xy mass scales. This raises the problem of performing numerical simulations

for the collapse of a protogalaxy, in the presence of a dark halo, consi-

dering how dark mass is distributed over internal smaller mass scales.

Actually, none of the techniques used so far in solving the gravitational

potential (Fast-Fourier-Transform) allow a better resolution than the minimum grid spacing. An improvement of the algorithm, as proposed by Eastwood et al. (1980), making use of an N-body code on small scales, would allow a better resolution.

The final outcome would be a direct answer to the possibility of having dark matter over dwarf galaxy scales as well as over scales of the size of internal galactic structures.

APPENDIX A . TIME EVOLUTION OF DENSITY PERTURBATIONS BEFORE RECOMBINATION

The equations for the gravitational field (A1), a collisionless particle

continuum (A2),and the matter-radiation set (A3), will be derived.

The present discussion is mostly taken from LSS; at some points it has

implemented using results taken from Peebles and Yu (1970),Bonometto and

Lucchin (1976).

A1. Gravitational field

In this epoch ($z \gg \Omega^{-1}$;z: redshift; Ω : present density parameter)

spatial curvature can be neglected. Let then (units with c=1 are taken)

$$ds^2 = dt^2 - a^2(t) \left[\delta_{\alpha\beta} - h_{\alpha\beta} \right] dx^\alpha dx^\beta \qquad \alpha,\beta = 1,2,3 \qquad (A1.1)$$

be the metric of the model of the Universe.Here a(t) is the scale factor,

x^α are orthonormal space coordinates.

The gravitational field equations

$$R_{ij} = 8\pi G \left[T_{ij} - \frac{1}{2} g_{ij} T \right] , \qquad (A1.2)$$

(R_{ij} :Ricci tensor; T_{ij} : stress-energy tensor; $T = g_{ij} T^{ij}$) will be used

to relate $h_{\alpha\beta}$ with small deviation of

$$T_{ij} = (\rho + p)\, v_i v_j - p\, g_{ij} \quad , \quad \left(v_i = \frac{dx_i}{ds} \right) \tag{A1.3}$$

from complete homogeneity. Clearly is

$$\begin{cases} v_i = (\gamma, \gamma\, v_\mu) \\[2mm] \gamma = (1 - v_\mu v^\mu)^{-1/2} \end{cases} \tag{A1.4}$$

in the gauge (A1.1), where v_μ are the components of the 'local' small

velocity field. For $v_\mu = 0$ is $T_{oo} = \rho$ (energy density), $T_{\alpha\alpha} = p$ (iso-

tropic pressure) and $T_{o\alpha} = 0$.

From the metric (A1.1) the Christoffel symbols

$$\begin{cases} \Gamma^o_{oi} = 0 \qquad \Gamma^\alpha_{oo} = 0 \\[2mm] \Gamma^o_{\alpha\beta} = \alpha\dot\alpha\,(\delta_{\alpha\beta} - h_{\alpha\beta}) - \frac{1}{\alpha^2}\,\dot h_{\alpha\beta} \\[2mm] \Gamma^\alpha_{o\beta} = -\frac{1}{2}\,\dot h_{\alpha\beta} + \delta_{\alpha\beta}\,\dot\alpha/\alpha \\[2mm] \Gamma^\gamma_{\alpha\beta} = \frac{1}{2}\left(h_{\alpha\gamma,\beta} + h_{\beta\gamma,\alpha} - h_{\alpha\beta,\gamma} \right) \\[2mm] \Gamma^j_{oj} = 3\dot\alpha/\alpha - \frac{1}{2}\,\dot h \qquad \Gamma^j_{\alpha j} = -\frac{1}{2}\,h_{,\alpha} \quad , \quad h = h_\alpha^\alpha \end{cases} \tag{A1.5}$$

can be derived. Owing to the well-known relation

$$R_{ij} = \Gamma^k_{ij,k} - \Gamma^k_{ik,j} + \Gamma^k_{ij}\,\Gamma^\ell_{k\ell} - \Gamma^k_{i\ell}\,\Gamma^\ell_{kj} \quad , \tag{A1.6}$$

the Ricci tensor components will then turn out to be (to the first order

in $h_{\alpha\beta}$)

$$R_{oo} = -3\frac{\ddot{a}}{a} + \frac{1}{2}\ddot{h} + \frac{\dot{a}}{a}\dot{h}$$

$$R_{o\alpha} = -\frac{1}{2}\dot{h}_{\alpha\beta,\beta} + \frac{1}{2}\dot{h}_{,\alpha}$$

$$R_{\alpha\beta} = a^2\left[\left(\frac{\ddot{a}}{a} + 2\frac{\dot{a}^2}{a^2}\right)(\delta_{\alpha\beta} - h_{\alpha\beta}) - \frac{3}{2}\frac{\dot{a}}{a}\dot{h}_{\alpha\beta} - \frac{1}{2}\frac{\dot{a}}{a}\dot{h}\,\delta_{\alpha\beta}\right.$$
$$\left. -\frac{1}{2}\ddot{h}_{\alpha\beta}\right] + R^{(3)}_{\alpha\beta}$$

$$R^{(3)}_{\alpha\beta} = \frac{1}{2}\left(h_{\alpha\beta,\gamma\gamma} + h_{,\alpha\beta} - h_{\alpha\gamma,\gamma\beta} - h_{\beta\gamma,\gamma\alpha}\right) . \tag{A1.7}$$

Replacing them in (A1.2) and taking the firs order terms we have

$$\frac{\ddot{h}}{2} + \frac{\dot{a}}{a}\dot{h} = 4\pi G\left[2 T_{oo} - T - \rho_b - 3 p_b\right]$$

$$\dot{h}_{,\alpha} - \dot{h}_{\alpha\beta,\beta} = 16\pi G T_{o\alpha} , \tag{A1.8}$$

here ρ_b and p_b are the background values of density and isotropic pressure; only scalar perturbations (depending just on $x_3 = x$ and t) will be considered. The evolution of the scale factor is given by

$$\dot{a}^2 = \frac{8\pi G}{3}\rho\, a^2(t) . \tag{A1.9}$$

A.2 Collisionless particles

For a collisionless particle continuum we define a distribution function

$f(\vec{x}, \vec{p}, t)$; the stress-energy tensor for this continuum will then

be (Lindquist 1966)

$$T^{ij} = \frac{1}{\sqrt{-g}} \int d^3p \; f \; p^i p^j / p^0 \quad . \tag{A2.1}$$

With the definition

$$P_\alpha = - p \; a(t) \, e \, \gamma_\alpha \; , \quad p^2 + p_0^2 = m^2 \; , \quad \gamma_\alpha \gamma^\alpha = 1 \tag{A2.2}$$

where γ_α are direction cosines and $e \simeq 1 - \frac{1}{2} h_{\mu\nu} \gamma^\mu \gamma^\nu$, eq.(A2.1)

becomes

$$T^{ij} = \left(1 + \frac{h}{2}\right) \int p^2 dp \, d\Omega \; \frac{p^i p^j}{p^0} \; f \left[1 - \frac{3}{2} h_{\mu\nu} \gamma^\mu \gamma^\nu\right] \quad . \tag{A2.3}$$

Let us suppose that the difference

$$f_1 = f - f_b \ll f_1 \tag{A2.4}$$

(f_b : background distribution); replacing $f = f_b + f_1$ in eq.(A2.3)

and keeping 0th and 1st order terms only, we have

$$
\begin{cases}
T^{00} = \int p_o \, p^2 dp \, d\Omega \left[f + f_b \left(\frac{h}{2} - \frac{3}{2} h_{\mu r} \gamma^{\mu} \gamma^{r} \right) \right] \\
\\
T^{0\alpha} = - \alpha(t) \int p^2 dp \, d\Omega \, \gamma^{\alpha} f_1
\end{cases}
\qquad \text{(A2.5)}
$$

Therefore if

$$
\delta = \frac{1}{\rho_b} \int p^2 dp \, p_o \, d\Omega \, f_1 = \frac{\Delta[T_{oo}]}{\rho_b}
\qquad \text{(A2.6)}
$$

then is $T^{00} = \rho_b (1 + \delta)$, δ is the fractional energy density.

From eq.(A2.3) it is found that

$$
T = m^2 \int p^2 \frac{dp}{p^o} \, d\Omega \, f \quad , \qquad \Delta[T] = m^2 \int p^2 \frac{dp}{p^o} \, f_1
\qquad \text{(A2.7)}
$$

The time evolution of f_1 is given by the relativistic collisionless

Boltzmann equation, in time orthogonal coordinates this equation reads

$$
\frac{\partial f}{\partial t} + \frac{\partial f}{\partial x^{\alpha}} \dot{x}^{\alpha} + \frac{\partial f}{\partial p^o} \dot{p}^o + \frac{\partial f}{\partial \gamma^{\alpha}} \dot{\gamma}^{\alpha} = 0 \quad .
\qquad \text{(A2.8)}
$$

* Hereafter the symbol $\Delta[\ ]$ means the difference of a quantity of its

  unperturbed value, i.e. $\Delta[f] = f - f_b$.

To the first order the last term can be neglected, $\dot{p}^o$ is given by the

geodesic equation $p_o\, \dot{p}^o = - p^2 \left(\dfrac{\dot{a}}{a} - \dfrac{1}{2} \dot{h}_{\alpha\beta}\, \gamma^{\alpha}\gamma^{\beta} \right)$, then eq.(A2.8)

becomes

$$\frac{\partial f_1}{\partial t} + \frac{p}{p^o}\, \frac{\gamma^{\alpha}}{a}\, \frac{\partial f_1}{\partial x^{\alpha}} - \frac{\partial f_b}{\partial p^o}\, \frac{p^2}{p^o} \left[\frac{\dot{a}}{a} - \frac{1}{2} \dot{h}_{\alpha\beta}\, \gamma^{\alpha}\gamma^{\beta} \right] = 0 . \qquad (A2.9)$$

The last equation completes the set of required equations to describe the

evolution of density perturbations in an expanding Universe for collisionless

particles.

A3. Matter and radiation

The main interaction between matter and radiation before recombination is

given by Thomson scattering of photons by nonrelativistic free electrons.

It can be shown (Peebles and Yu 1970) that the time evolution of the

radiation phase space distribution f is given by

$$\frac{\partial f}{\partial t} + \frac{\gamma^{\alpha}}{a}\, \frac{\partial f}{\partial x^{\alpha}} - p\, \frac{\partial f}{\partial p} \left(\frac{\dot{a}}{a} - \frac{1}{2} \dot{h}_{\alpha\beta}\, \gamma^{\alpha}\gamma^{\beta} \right) = t_c^{-1}(f_+ - f) , \qquad (A3.1)$$

here $t_c^{-1} = \sigma_T\, h_e(z)\, \chi(z)$, σ_T is the Thomson scattering cross

section, h_e the electron number density, x(z) the plasma ionization degree

and f_+ the scattered distribution into the beam; second order terms have

been neglected. A convenient variable is the fractional radiation brightness ι_{r},

defined as ($f = f_o + f_1$)

$$i_r (\theta, \varphi) = \frac{4\pi}{c_r} \int p^3 f_1 \, dp \quad , \qquad \text{(A3.2)}$$

here c_r is the background radiation density.

With the assumption that the scattering is isotropic in the local matter

rest frame the integration of eq.(A3.1) over $p^3 dp$ yields

$$\frac{\partial i_r}{\partial t} + \frac{\gamma_\alpha}{a} \frac{\partial i_r}{\partial x^\alpha} - 2 \gamma_\alpha \gamma_\beta \dot{h}_{\alpha\beta} = t_c^{-1} \left[\delta_r + 4 \gamma_\alpha v^\alpha - i_r \right] \quad , \qquad \text{(A3.3)}$$

here v^α is the matter velocity and δ_r is the radiation density contrast,

$$\delta_r = \int i_r \frac{d\Omega}{4\pi} \quad . \qquad \text{(A3.4)}$$

Multiplying eq.(A3.3) for γ_α and integrating over angles it is found

$$\frac{\partial f_\alpha}{\partial t} + \frac{1}{a} \frac{\partial \gamma_{\alpha\beta}}{\partial x^\beta} = t_c^{-1} \left[\frac{4}{3} v^\alpha - f \right] \quad , \qquad \text{(A3.5)}$$

where

$$f_\alpha = \int i_r \gamma_\alpha \frac{d\Omega}{4\pi} \qquad \text{(A3.6)}$$

is the radiation energy flux and

$$\eta_{\alpha\beta} = \int i_r \, \gamma_\alpha \gamma_\beta \, \frac{d\Omega}{4\pi} \quad . \tag{A3.7}$$

The equations for density and velocity matter can be obtained from the continuity and motion equations, one finds (LSS, §92)

$$\begin{cases} \dot{\delta}_m = \dfrac{\dot{h}}{2} - \dfrac{1}{a} \dfrac{\partial v^\alpha}{\partial x^\alpha} \\[4mm] \dfrac{\partial v^\alpha}{\partial t} + \dfrac{\dot{a}}{a} v^\alpha + \dfrac{v_s^2}{a} \dfrac{\partial \delta_m}{\partial x^\alpha} = \dfrac{1}{\eta} \left[\dfrac{3}{4} f_\alpha - v^\alpha \right] \end{cases} , \tag{A3.8}$$

where δ_m is the matter density contrast, v_s the sound velocity of

for neutral hydrogen, $\eta = \dfrac{3}{4} \dfrac{\rho_m}{\rho_r} t_c$ and ρ_m is the background matter

density.

In the limit $t_c \rightarrow 0$ the photon mean free path is much less than the

wavelength of the perturbation, matter and radiation behave

as a viscous fluid . In this regime the solution to eq.(A3.3) is, to the

first order in t_c ,

$$\begin{cases} i_r^{(1)} = i_r^{(0)} - t_c \left[\dot{\delta}_r + \dfrac{4\gamma_\alpha\gamma_\beta}{a} \dfrac{\partial v^\alpha}{\partial x^\beta} + 4\gamma_\alpha \dot{v}^\alpha - 2\gamma_\alpha\gamma_\beta \dot{h}_{\alpha\beta} + \dfrac{\gamma_\alpha}{a} \dfrac{\partial \delta_r}{\partial x^\alpha} \right] \\[4mm] \dot{i}_r^{(0)} = \delta_r + 4\gamma_\alpha v^\alpha \end{cases} , \tag{A3.9}$$

Then the full set of equations for matter and radiation is

$$\begin{cases} \dot{\delta}_r = \frac{2}{3}\dot{h} - \frac{1}{\alpha}\frac{\partial \mathcal{J}^\alpha}{\partial x^\alpha} \\[2mm] \dot{\delta}_m = \frac{\dot{h}}{2} - \frac{1}{\alpha}\frac{\partial \sigma^\alpha}{\partial x^\alpha} \\[2mm] \dot{\sigma}^\alpha + \frac{\dot{\alpha}}{\alpha}\sigma^\alpha = \frac{1}{\eta}\left[\frac{3}{4}\mathcal{J}_\alpha - \sigma^\alpha\right] \\[2mm] \dot{\mathcal{J}}^\alpha = t_c^{-1}\left[\frac{4}{3}\sigma^\alpha - \mathcal{J}_\alpha\right] - \frac{1}{3\alpha}\frac{\partial \delta_r}{\partial x^\alpha} \end{cases} \qquad \text{(A3.10)}$$

This set of equations is often referred to as the two-fluid model

(Bonometto and Lucchin 1976).

The $t_c = 0$ limit gives

$$\mathcal{J}_\alpha = \int i_r^{(0)} \gamma^\alpha \frac{d\Omega}{4\pi} = \frac{4}{3}\sigma^\alpha \quad , \quad \dot{\delta}_m = \frac{3}{4}\dot{\delta}_r \quad ; \qquad \text{(A3.11)}$$

then eq.s(A3.10) reduces to

$$\begin{cases} \dot{\delta}_r = \frac{2}{3}\dot{h} - \frac{4}{3}\frac{1}{\alpha}\frac{\partial \sigma^\alpha}{\partial x^\alpha} \\[3mm] \frac{d\sigma^\alpha}{dt} = -\frac{1}{4\alpha}\frac{\partial \delta_r}{\partial x^\alpha} \end{cases} \qquad \text{(A3.12)}$$

In the $t_c = 0$ limit matter and radiation behave as a single ideal fluid.

R E F E R E N C E S

Aaronson,M.,Mould,J.,Huchra,J.,1980,Ap.J.,237,655

Aaronson,M.,1983,Ap.J.,Lett.,194,543

Aarseth,S.J.,1972, in 'Gravitational N-Body Problems',(ed.M.Lecar,Reidel 1972

Aarseth,S.J.,Binney,J.,1978,M.N.R.A.S.,185,227

Aarseth,S.J.,Gott,J.R.,Turner,E.L.,1979,Ap.J.,228,664

Bahcall,N.,1974,Ap.J.,187,439

Bahcall,J.N.,et al.,1982,Ap.J.Lett.,258,1

Bahcall,J.N.,1984,Ap.J.,276,169

Barrow,J.D.,Silk,J.,1981,Ap.J.,250,432

Berman,R.H., et al.,1978,M.N.R.A.S.,185,861

Bertola,F.,Capaccioli,M.,1975,Ap.J.,200,439

Binney,J.,1976,M.N.R.A.S.,177,19

Binney,J.,1980,Phil.Trans.R.Soc.Lond.,A296,329

Birsdall,C.K.,Fuss,D.,1969,J.Comp.Phys.,3,494

Blumenthal,G.R.,Pagels,H.,Primack,J.R.,1982,Nature,299,37

Blumenthal,G.R.,Faber,S.M.,Primack,J.R.,Rees,M.J.,1984,Nature,311,517

Bond,J.R.,Efstathiou,G.,Silk,J.,1980,Phys.Rev.Lett.,45,1980

Bond,J.R.,Szalay,A.S.,1983,Ap.J.,274,433

Bond,J.R.,Efstathiou,G.,1984,preprint

Bond,J.R.,et al.,1984, in 'Formation and Evolution of Galaxies and
Galaxies and Large Scale Structures in tha Universe',(eds.Audouze,J. and
Tran Thanh Van,J.),1984
Bonometto,S.A.,Lucchin,F.,1976,Ap.J.,206,391
Bonometto,S.A.,et al.,1983a,Astr. and Ap.,123,118

Bonometto,S.A.,Caldara,A.,Lucchin,F.,1983b,Astr. and Ap.,126,377

Bonometto,S.A.,Lucchin,F.,Occhionero,F.,Vittorio,N.,1984,Astr. and Ap, in press

Bonometto,S.A.,Valdarnini,R.,1984,Phys.Lett.,103A,369

Bosma,A.,1981,A.J.,86,1825

Boughn,S.P.,et al.,1981,Ap.J.Lett.,250,15

Buneman,O.,1967,J.Comp.Phys.,1,517

Cabibbo,N.,Farrar,G.R.,Maiani,L.,1981,Phys.Lett.,105B, 155

Carnevali,P.,1983,Ap.J.,265,701

Carr,B.J.,1977,Astr. and Ap.,56,377

Carr,B.J.,1980,M.N.R.A.S.,181,669

Carter,D.,1978,M.N.R.A.S.,182,797

Centrella,J.,Mellott,A.L.,1983,Nature,305,196

Cheng,E.S.,et al.,1979,Ap.J.Lett.,232,139

Cohen,J.G.,1983,Ap.J.Lett.,270,241

Combers,F.,Sanders,R.H.,1981,Astr. and Ap.,96,164

Cowsik,R.,McClelland,J.,1972,Phys.Rev.Lett.,29,669

Cox,D.O.,Tucker,W.H.,1969,Ap.J.,157,1157

Davis,M.,Peebles,P.J.E.,1977,Ap.J.Suppl.,34,425

Davis,M.,Geller,M.J.,Huchra,J.,1978,Ap.J.,221,1

Davis,M.,et al.,1980,Ap.J.Lett.,238,113

Davis,M.,Peebles,P.J.E.,1983,Ap.J.,267,465

Davis,M.,et al.,1983,Ap.J.,266,41

Dekel,A.,1983,Ap.J.,264,373

De Vaucoulers,G.,1959,in Handbuch der Physik,vol.53,ed.S.Flügge

Doroshkevich,A.G.,1973,Sov.Astr.,16,896

Doroshkevich,A.G.,Shandarin,S.F.,1974,Sov.Astr.,18,24

Doroshkevich,A.G.,et al.,1978,M.N.R.A.S.,184,643

Doroshkevich,A.G.,Zel'dovich,Ya.B.,Sunyaev,R.A.,1978,Sov.Astr.,22,523

Doroshkevich,A.G.,et al.,1980,Sov.Astr.Lett.,6,252

Eastwood,J.W.,Brownrigg,D.R.K.,1979,J.Comp.Phys.,32,24

Eastwood,J.W.,et al.,1980,Comp.Phys.Comm.,19,215

Efstathiou,G.,Jones,B.J.T.,1979,M.N.R.A.S.,186,133

Efstathiou,G.,et al.,1980,M.N.R.A.S.,193,931

Efstathiou,G.,Eastwood,J.W.,1981,M.N.R.A.S.,194,503

Eggen,O.J.,Lynden-Bell,D.,Sandage,A.,Ap.J.,136,748

Einasto,J.,et al.,1980,M.N.R.A.S.,193,353

Ellis,J.,et al.,1984,preprint

Faber,S.M.,Jackson,R.E.,1976,Ap.J.,204,668

Faber,S.M.,1977,in 'The Evolution of Galaxies and Stellar Populations',
(eds; B.M.Tinsley and R.B.Larson), Yale University

Faber,S.M.,Gallagher,J.S.,1979,A.R.A.A.,17,135

Faber,S.M.,1982, in Astrophysical Cosmology (eds.Brück,H.,Coyne,G.,Longair,M.S.),
Pontifical Scientific Academy, Vatican,1982

Faber,S.M.,Lin,D.N.C.,1983,Ap.J.Lett.,266,217

Fall,M.S.,1975,M.N.R.A.S.,172,1p

Fall,M.S.,Efstathiou,G.,1980,M.N.R.A.S.,193,189

Field,G.B.,1972,A.R.A.A.,10,227

Frenk,C.S.,White,S.D.M.,Davis,M.,1983,Ap.J.,271,417

Gershtein,S.S.,Zel'dovich,Ya.B.,1966,JETP Lett.,4,174

Goldberg,H.,1983,Phys.Rev.Lett.,50,1419

Gott,J.R.,1973,Ap.J.,186,481

Gott,J.R.,et al.,1974,Ap.J.,194,543

Gott,J.R.,1975,Ap.J.,Ap.J.,201,296

Gott,J.R.,Thuan,T.X.,1976,Ap.J.,204,649

Gunn,J.E.,Gott,J.R.,1972,Ap.J.,176,1

Gunn,J.E.,1978,in Observational Cosmology,eds. A.Maeder,L.Martinet and G.A.Tamman,SAAS-FEE 1978

Henon,M.,1964,Ann.Ap.,27,83

Illingworth,G.,1977,Ap.J.Lett.,218,43

Illingworth,G.,1981,in The Structure and Evolution of Normal Galaxies,S.M. Fall and D.Lynden-Bell (eds.),Cambridge University Press,Cambridge

Kaiser,N.,1983,Ap.J.Lett.,273,17

Kashlinsky,A.,1982,M.N.R.A.S.,200,585

Kerr,F.J.,et al.,1965, in 'Stars and Stellar Systems',Chicago Univ. Press

King,I.R.,1966,A.J.,71,64

King,I.R.,Minkowski,R.,1972,Proc.I.A.U. Symp.,44,87

Kirshner,R.P.,et al.,1981,Ap.J.Lett.,248,57

Klypin,A.A.,Shandarin,S.F.,1983,M.N.R.A.S.,204,891

Kormendy,J.,1977,Ap.J.,218,333

Kormendy,J.,1982,in 'Morphology and Dynamics of Galaxies',SAAS-FEE 1982

Leach,R.W.,1981,Ap.J.,248,485
Lindquist,R.W.,1966,Ann.Phys.,37,487
Lynden-Bell,D.,1967,M.N.R.A.S.,136,101

Lyubimov,V.A.,et al.,1980,Phys.Lett.,94B,266

Marx,G.,Szalay,A.S.,1972,Proc. Neutrino 72,1,123

Mellott,A.L.,1983,Ap.J.,264,59

Miller,R.H.,1978,Ap.J.,223,122

Miller,R.H.,Smith,B.F.,1979,Ap.J.,227,407

Miller,R.H.,Smith,B.F.,1981,Ap.J.,244,467

Olive,K.A.,Turner,M.S.,1982,Phys.Rev.D,25,213

Ostriker,J.P.,Peebles,P.J.E.,1973,Ap.J.,186,467

Pagels,H.R.,Primack,J.R.,1982,Phys.Rev.Lett.,48,223

Partirdge,R.B.,1980,Phys.Scr.,21,614

Peebles,P.J.E.,1965,Ap.J.,142,1317

Peebles,P.J.E.,1969,Ap.J.,155,393

Peebles,P.J.E.,Yu,J.T.,1970,Ap.J.,162,815

Peebles,P.J.E.,Groth,E.J.,1976,Astr. and Ap.,53,131

Peebles,P.J.E.,1979,A.J.,84,730

Peebles,P.J.E.,1979a,in Physical Cosmology,Les Houches 1979

Peebles,P.J.E.,1980,The Large Scale Structure of the Universe,
Princeton University Press,Princeton

Peebles,P.J.E.,1981,Ap.J.,248,885

Peebles,P.J.E.,1982,Ap.J.,258,415

Peebles,P.J.E.,1984,Ap.J.,277,470

Press,W.H.,Schechter,P.L.,1974,Ap.J.,187,425

Preskill,J.,Wise,M.S.,Wilczeck,F.,1983,Phys.Lett.,120B,127

Prior,C.lecar,M.,1983,Ap.J.,269,513

Rees,M.J.,Ostriker,J.P.,1977,M.N.R.A.S.,179,541

Rees,M.J.,1978, in Observational Cosmology, SAAS-FEE 1978

Rood,H.J.,et al.,1972,Ap.J.,175,627

Rood,H.J.,1981,Rep.Prog.Phys.,44,1081

Rubin,V.C.,et al.,1978,Ap.J.,Lett.,225,107

Sandage,A.,et al.,1970,Ap.J.,160,831

Schechter,P.,Gunn,J.E.,1979,Ap.J.,229,472

Schimdt,M.,1959,Ap.J.,129,243

Schramm,D.N.,Steigman,G.,1981,Ap.J.,243,1

Shapiro,P.R.,Struck-Marcell,G.,Mellott,A.L.,1983,Ap.J.,275,413

Shukurov,A.M.,1980,Astrophysica,17,469

Silk,J.,1968,Ap.J.,151,459

Smoot,G.F.,Lubin,P.M.,1979,Ap.J.Lett.,234,83

Szalay,A.S.,Marx,G.,1976,Astr. and Ap.,49,437

Szymanski,M.,Jaroszynski,M.,1983,M.N.R.A.S.,205,91
Toomre,A.,1964,Ap.J.,139,1217
Tremaine,S.,Gunn,J.E.,1979,Phys.Rev.Lett.,42,407

Uson,J.M.,Wilkinson,D.T.,1984,Ap.J.Lett.,277,1

Valdarnini,R.,1984,SISSA preprint 48/83/A , to be published in Astr. and Ap.

Valdarnini,R.,Bonometto,S.A.,1984,SISSA preprint 54/84/A, submitted to Astr. and Ap.

Van Albada,T.S.,1982,M.N.R.A.S.,201,939

Van den Bergh,S.,1977,Vistas Astr.,21,71

Vittorio,N.,Silk,J.,1984, preprint

Wasserman,I.,1981,Ap.J.,248,1

Weinberg,S.,1972,'Gravitation and Cosmology',Wiley and Sons

Weinberg,S.,1982,in 'Astrophysical Cosmology', (eds.Brück,H.,Coyne,G.V., Longair,M.S.), Pontifical Scientific Academy, Vatican,1982

White,S.D.M.,1976,M.N.R.A.S.,177,717

White,S.D.M.,Rees,M.J.,1978,M.N.R.A.S.,183,341

White,S.D.M.,Silk,J.,1979,Ap.J.,231,1

White,S.D.M.,1982,in 'Morphology and Dynamics of Galaxies', SAAS-FEE 1982

Wilson,M.L.,Silk,J.,1981,Ap.J.,243,14
Witten,E.,1984,Phys.Rev.D,30,272
Yang,J.,et al.,1984,Ap.J., in press

Zel'dovich,Ya.B.,1970,Astr. and Ap.,5,84

Zel'dovich,Ya.B.,1972,M.N.R.A.S.,160,1p

Zel'dovich,Ya.B.,Sunyaev,R.A.,1972,Astr. and Ap.,20,189

Zel'dovich,Ya.B.,Sunyaev,R.A.,1980,Sov.Astr.Lett.,6,249